Models of Snow Distribution Patterns For Various Types of Sea Ice in the Canadian High Arctic.

By

John Iacozza

A Thesis
Submitted to the Faculty of Graduate Studies
in Partial Fulfillment of the Requirements
for the Degree of

MASTER OF ARTS

Centre for Earth Observation Science
Department of Geography
University of Manitoba
Winnipeg, Manitoba

THE UNIVERSITY OF MANITOBA

FACULTY OF GRADUATE STUDIES

*****

COPYRIGHT PERMISSION PAGE

MODELS OF SNOW DISTRIBUTION PATTERNS FOR VARIOUS TYPES OF SEA ICE IN THE CANADIAN HIGH ARCTIC

BY

JOHN IACOZZA

A Thesis/Practicum submitted to the Faculty of Graduate Studies of The University of Manitoba in partial fulfillment of the requirements of the degree

MASTER of ARTS

ABSTRACT

Extensive research has been conducted on the snow distribution patterns over terrestrial landscapes, while surprisingly little research has focused on the snow patterns over an icescape. Snow distribution over different types of sea ice (i.e. first-year, multiyear and rubble sea ice) has significant consequences on the physical, biological and climatological components of the marine cryosphere. The depth and distribution of snow controls much of the thermodynamic characteristics of the icescape, as well as the radiative exchanges between the atmosphere and ocean.

In this thesis, the distribution of snow over first-year (FYI), multiyear (MYI) and rubble (RI) sea ice were measured at 15 sites sampled during two years of field research in the Canadian Arctic. A geostatistical technique known as the variogram was used to model the statistical pattern of the snow distribution. The variogram examines the spatial continuity of a regionalized variable and how this continuity changes as a function of distance and direction. Results indicate that the variogram provided a good estimate of the type and change of spatial dependence on the snow depths over the various ice types. Over FYI, the regular smooth ice topography produced a periodicity in the snow drifts that was best estimated using a wave theoretical variogram in combination with a gaussian model. The more irregular ice topography characteristic of MYI and RI produced a more irregular snow drift pattern. The most appropriate models were a combination of the spherical and gaussian variogram models.

Geometric anisotropy was present in all 15 sites, indicating a directional trend in the spatial continuity of the snow distribution patterns which was attributed to the prevailing wind vector during depositional storm events.

These distribution models were used to estimate the spatial dispersion of the photosynthetically active radiation (PAR) transmittance through the snow and ice covers on the arctic oceans. This application of the models illustrated the importance of snow distribution on the transmittance of PAR. Plots of the transmittance for each ice type were produced.

ACKNOWLEDGMENTS

I would like to initially thank Dr. D.G. Barber for all his guidance and support in the last couple of years. I have learned considerably about my discipline and about myself these past years as a consequence of working under the tutelage of Dave. You have also provided me with arctic experience that can not be quantified. I would also like to thank D. Mosscrop for all his help with the various technical aspects of my thesis. His knowledge has saved me considerable of time and has help to broaden my skills immensely. Also, I must acknowledge and thank S. Drobot, T. Nichols and L. Misch (University of Waterloo) who have helped me considerably by being my Arctic field assistants in the two years of field work. Other members of C-ICE and CEOS, especially J. Yackel and J. Hanesiak, have assisted with my thesis preparation and production, along with some technical support and I recognize them for this help.

I would especially like to thank the individuals who critically examined this thesis and made it what it is, especially H. Welch, A. Catchpole and the two anonymous reviewers at ARCTIC journal.

Another group of individuals that needs to be acknowledged are those that provided data and equipment for my thesis and field work. I would like to thank Ross Brown (AES) and Arvids Silis (AES) for providing me with the climate data used in thesis, as well as D. Perovich for allowing me to use his light penetration model to provide an application of the models developed in this thesis. All the logistical support, in terms of lodging, food and equipment

provided by the staff at the Polar Continental Shelf Project and TFSS (Energy, Mines and Resources Canada) are greatly appreciated. Financial support has been provided by the previous agencies along with the Northern Studies Training Program (NSTP).

I wish to express my sincere thanks to all my friends in Winnipeg and outside whose advice and assistance aided considerably to the completion of this thesis. You know who you are. The emotional and mental support has not gone unnoticed. Without you, I don't know where I would be.

Lastly, I would like to deeply and sincerely thank my family, especially my parents for all their help in the past couple of years.

Table of Contents.

List of Figures.

List of Tables.

CHAPTER 1:

INTRODUCTION.

With the recent concern on climate change, focus has been directed towards the northern latitudes, where it is believed that increased greenhouse gases and global warming will have the most pronounced effect. In terms of snow, it is debatable as to whether atmospheric warming will cause a reduction or an increase in snowfall rate over the high latitudes (Schlesinger and Mitchell, 1987). Researchers do agree that the snow cover, along with the southern sea ice limits and climate of the high latitudes will be significantly affected by an increased CO_2 scenario.

In the scientific community, both the amount and distribution of snow on sea ice are important to our understanding of local, hemispheric and global processes. Due to the limited number of weather stations located in the north, there is a great deficit in our knowledge of the amount of snow that occurs in the Arctic, both locally and regionally. Because of the increased capability of differentiating ice types from synthetic aperture radar images, the snow distribution patterns over sea ice are obtainable (Barber et al., 1991). This knowledge of the distribution patterns will increase our understanding on the processes operating in the north.

Information sources on rates and distribution of snow on sea ice are spatially and temporally limited (usually point observations coinciding with

climate reporting stations). There are only four permanent weather stations located in the Arctic, and all of these stations are located on land. On sea ice, no permanent stations are set up that have measured the snow depth over an extended period of time. Although remote sensing has the potential to play a role in producing estimates of snow distribution there is as yet no operational method available using existing spaceborne platforms (Barber et al. 1993).

The importance of this area to the climatology, ecology and hydrology of the earth can not be overstated. However, researchers in these fields have surprisingly overlooked or even excluded this area from study. For instance, a variable routinely collected in the lower latitudes for decades such as precipitation amounts has only been collected in the Arctic since the 1950s and this record is incomplete at best. This is due in part by the harsh environment of the Arctic (i.e. low air temperatures and darkness for half a year) as well as logistic problems (i.e. transportation of materials and equipment). This lack of information or data is common in every aspect of the climatology, biology and hydrology of the north. It has only been in the last 40 years that researchers have begun looking at the north as an unique area in which processes operate on hemispheric and global scales (Barry, 1983). In the past decade, researchers have begun to fill some voids in the information on processes operating in the north.

The spatial and temporal extents of snow and sea ice in the Canadian Arctic are significant to our understanding of the processes operating in this region. Snow cover experiences the greatest fluctuations, both temporally and spatially, of all surface conditions. In the Arctic region, snow is a permanent and integral feature for over 9 months each year. For example, Resolute Bay, located in the eastern Northwest Territories, is snow covered for an average of 283 days in a year (French and Slaymaker, 1993). Snow cover exhibits a large

seasonal change in the northern hemisphere; snow varies from a maximum extent of 46.5 million km^2 in January to a minimum extent of 3.8 million km^2 in August (Robinson et al., 1993). There is also considerable year to year variability of snow cover in the northern hemisphere. Spatially, snow cover is the largest component of the marine cryosphere covering on average 23% of the northern hemispheric surface area in January; an area larger than that covered in the southern hemisphere. The marine cryosphere consists of the interactions between the ocean, sea ice and atmosphere (LeDrew and Barber, 1994).

Sea ice in the Arctic exhibits similar spatial and temporal ranges. In the Canadian Arctic, new sea ice begins to form in late September/early October and does not begin to break up until mid-June. Some ice in the Arctic region, however, remains for the entire year, comprising what is known as multiyear sea ice. It has been estimated that in the summer months, the minimum area covered by perennial or multiyear sea ice is $8x10^6$ km^2 (1.5% of the earth's surface), while the maximum area of multiyear and first-year sea ice cover in the winter months is $15x10^6$ km^2 (3% of the earth's surface), resulting in a seasonal variability factor of two (LeDrew et al., 1992). Compared to the southern hemisphere, the seasonal variation in sea ice for the northern hemisphere is not as great. In the Arctic ocean, the confined nature and high latitudes act in combination to produce a much larger perennial ice cover and the land surrounding the oceans restrict the distance the sea ice extends towards the equator in the winter months.

As well as a large temporal range, these features exhibit a great spatial variability. Figure 1.1 illustrates the large spatial extent of sea ice in northern Canada. It can be seen from this figure that the sea ice in winter extends southward into Hudson Bay and the North Atlantic Ocean, while in summer

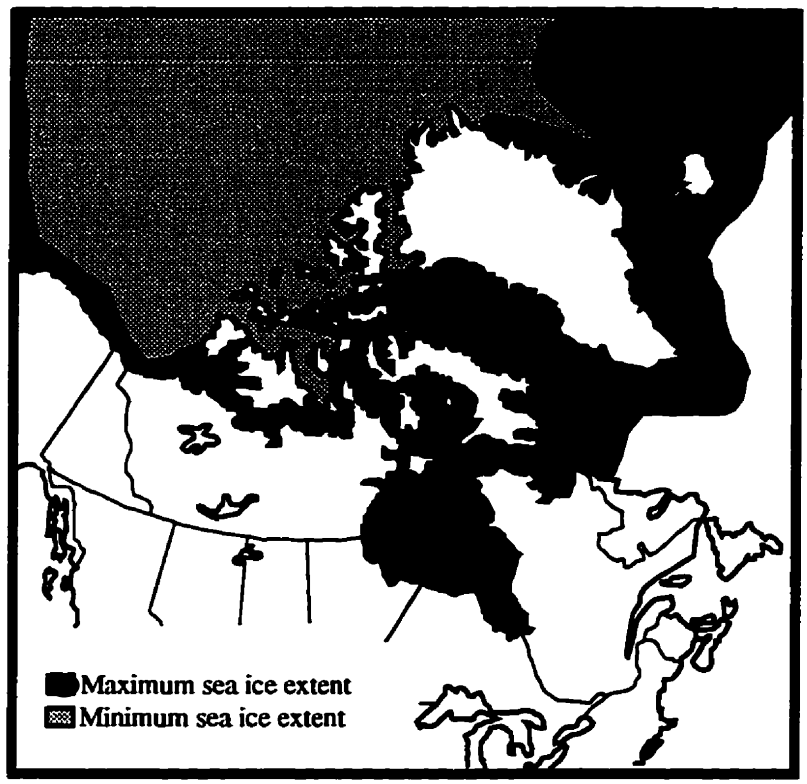

Figure 1.1. Minimum and Maximum sea ice extent for Canada (modified from French and Slaymaker, 1993).

covering a large portion of the ocean in the Arctic Archipelago. From passive microwave records that span the period from 1978 to 1995, it is suggested that the spatial extent of sea ice in the Arctic is decreasing by 2.7% per decade (Johannessen et al., 1995). The spatial and temporal scales at which snow and sea ice cover the waterways of the Arctic are extensive, however information on the impacts of these features is lacking.

The lack of snow and sea ice information in the north is best seen in the treatment of these two components in global climate models (GCMs). In the present models, the typical resolution is approximately 250 km^2. A

consequence of this low spatial resolution is that a significant portion of processes and landforms disappear or are eliminated (i.e. in most GCMs Lake Ontario does not exist in the model). Most significantly, the heterogeneity of the snow cover and sea ice, along with the impacts these have on the climate of the northern hemisphere, are eliminated. Instead, snow and sea ice are treated more as a homogeneous cover, with constant depths over several hundred kilometer sections. In the Arctic, snow and sea ice depths can vary within a few meters. Within several hundreds of kilometers of ocean, open water, young ice a few centimeters thick, first-year sea ice a meter thick, multiyear sea ice a few meters thick and pressure ridges up to tens of meters thick can all be present. The traditional view of snow and sea ice as an uniform sheet is inadequate to model many of the large scale geophysical processes operating in the north.

In a vast majority of global climate models, sea ice is treated as a motionless thermodynamic slab. In reality, sea ice is constantly deformed and transported by winds and ocean currents. In order to account for the freshwater input of a melting sea ice section as it moves out of the Arctic Ocean and its impacts on the climate, and to account for the thermodynamic impacts of open water or leads, the inclusion of ice motion is important in climate models. However, the computational requirements for a climate model with a sea ice component that includes motion may be too great and may limit the use of sea ice transport.

As with sea ice, serious shortcomings in the representation of snow in GCMs are also present. Snow exhibits large changes in the physical properties as it ages and undergoes metamorphism. These changes are both time- and temperature-dependent and need to be taken into account to sufficiently model the energy balance of the snow pack. Along with this, a multi-layer snowpack model is necessary. Within a snow pack, different layers exist that are

characterized by different values of snow properties which also have important consequences on the climate of the earth. Both of these processes must be properly represented in order to provide realistic simulations in GCMs, however most models do not incorporate them into their study.

Another weak area of the GCMs presently in use is the calculation of the mass budget of the snow in the polar regions. According to Randall et al. (1994) in the 14 GCMs investigated, the snow mass budget was determined by taking into account snowfall, melting and sublimation. In the northern Arctic region, one of the most, if not the most, significant contribution to the mass budget of snow is the transportation due to wind (i.e. saltation and suspension) during snow deposition in the direction of the predominant snow track. This aspect of the budget is not adequately dealt with in the GCMs and thus biases the snow mass budget of an area and the resulting modeling of climate change.

One of the main applications of GCMs is to predict the future climate with an increased atmospheric CO_2 concentration. There is a large discrepancy in the values obtained by different GCMs when the snow cover is modeled and this is primarily due to the treatment of the polar regions in these models (LeDrew, 1993). Temperature increases for an increased CO_2 scenario, for example, range from 5°C to 10°C globally. A major reason for this large variation in temperature increase is the modeling of snow cover and sea ice. The homogeneous snow covered area of the north in these models has considerable effects on the cloud and albedo responses to longwave and shortwave energy fluxes in the north, and these relationships are not modeled similarly for each GCM (Cess et al., 1991). Marshall et al. (1994) and Lynch-Stieglitz (1994) have concluded that in order to model the hydrological cycle accurately and thus increase GCM performance, snow cover must be treated appropriately.

There is also a large discrepancy between models in terms of the amount of snow cover in the Arctic region, which has implications on the surface albedo and therefore on the temperature of the region and planet. The direct effect of the snow (the shortwave snow radiative response) is not consistent between models, which causes various GCMs to produce dissimilar responses to carbon dioxide increases in the atmosphere (Cess et al., 1991). These models also have very different snow-climate feedbacks (between a warming climate and a decreasing snow cover). These feedbacks range from strongly positive to weakly negative (Cess et al., 1991). Without the adequate modeling of the snow and sea ice in the north, any findings of a GCM are subject to question and should be considered qualitative rather than quantitative. If the snow distribution patterns, as well as the magnitude of snow fall, can be estimated for areas in the northern hemisphere dominated by first-year, multiyear and rubble sea ice, climatic modelers can use this information to better model the northern regions in GCMs and more accurate estimations of the future climate can be approximated.

One area of hydrology that plays a particularly important role in the marine cryosphere is the snow catchment or the way precipitated snow distributes over various types of surfaces. Previous studies on snow catchments have primarily examined the patterns of snow distribution over terrestrial surfaces. Surprisingly, little or no systematic research has focused on the snow patterns over sea ice or an 'icescape'. The icescape is a term used to describe the portion of the landscape that is dominated by the presence of sea ice for the entire year or part of the year in which "a variety of processes [are] operating together in a coherent fashion" (LeDrew and Barber, 1994). The sea ice, which is a major component of the icescape, is an important element in the marine cryosphere. It acts as a barrier between the ocean and atmosphere,

restricting the movement of energy and mass between the two as well as regulating light penetration into the Arctic Ocean thereby affecting the marine ecosystem.

This sea ice is less permanent and more dynamic than a terrestrial landscape. In the Quaternary period, ice in general has advanced and retreated a number of times, while the positions of the landmasses have remained relatively constant in the same time period. Again, on an annual and seasonal basis, there is a great variation in the amount of sea ice in the northern hemisphere as compared to terrestrial surfaces.

In terms of snow catchment, the variables determining snow distribution vary between a terrestrial landscape and an icescape. For instance, vegetation on a terrestrial landscape significantly determines the snow distribution over an area (Elder et al., 1991; Evans et al., 1989; Golding and Swanson, 1986; Daugharty and Dickison, 1982; Patch, 1981). On an icescape, vegetation is absent and thus does not aid in determining the distribution of snow. Other variables such as topography (i.e. different ice types) and storm conditions (i.e. wind direction and precipitation) must play a more significant role in the snow distribution.

Information sources on rates and distribution of snow on sea ice are spatially and temporally limited. Very limited data sets exist that have physically sampled the snow depths over various types of sea ice. Although remote sensing technology has the potential to play a role in producing estimates of snow distribution, there is as of yet no operational method available using existing spaceborne platforms (Barber et al., 1993). Remote sensing techniques are able to delineate the presence or absence of snow cover, but are not able to quantify snow depth. Given these limitations, a modeling approach would be beneficial in understanding the nature of snow distribution

as a function of different types of sea ice catchments.

The main objectives of this thesis are to (i) determine the statistical patterns of snow distribution over various types of sea ice (including first-year ice, multiyear ice, and rubble ice) using data collected during the SIMMS '95 and the C-ICE '96 field experiments using variograms, and to (ii) apply the variogram models in the determination of the transmission of photosynthetically active radiation through the various ice catchments.

This thesis is divided into eight chapters. The first chapter is the introductory chapter, which introduces the problem being investigated in this thesis. Chapter 2 explores the significance of this research by examining the importance of the snow distribution over sea ice on the physical, biological and climatological components of the marine cryosphere. This is followed by the background chapter, or Chapter 3, which critically examines past models that have assessed the distribution patterns of snow over terrestrial surfaces. Chapter 3 also introduces the concepts of a variogram, kriging and a grey-level co-occurrence matrix and it examines the studies that have utilized these methods to model or differentiate the variables under investigation. Chapter 4 examines the data acquisition methods and introduces the field experiments used to collected the data for this thesis. Also, the remotely sensed data will be described in this chapter. In Chapter 5, I examine the results of the preliminary data analysis and provide a physical description of the ice catchments. The methods as well as the results and discussion of objectives i. and ii. are examined in Chapters 6 and 7 respectively. I conclude this thesis by reviewing the salient results of each of the chapters, reviewing the limitations of the research and thereby suggesting additional analysis within the field of study.

CHAPTER 2:

SIGNIFICANCE OF RESEARCH.

Snow catchment, or the way snow distributes over sea ice, has significant control on the physical, biological and climatological components of the marine cryosphere. This chapter will examine the affects of snow distribution over sea ice on these three components, as opposed to single snow depth values, and in the process will give a basis for the research conducted as part of this thesis. More specifically, the first section of this chapter will deal with the affects snow cover has on the ocean and sea ice growth and decay, through its low thermal conductivity. Following this, a description of how snow affects the energy budget component of the marine cryosphere is discussed, including the affects on albedo and sensible heat flux. The final section will discuss the consequences snow distribution has on the biology of the north, especially on the chlorophyll production and ringed seal habitat. Figure 2.1 illustrates the processes of the ocean-sea ice-atmosphere interface with particular reference to the control of snow distribution.

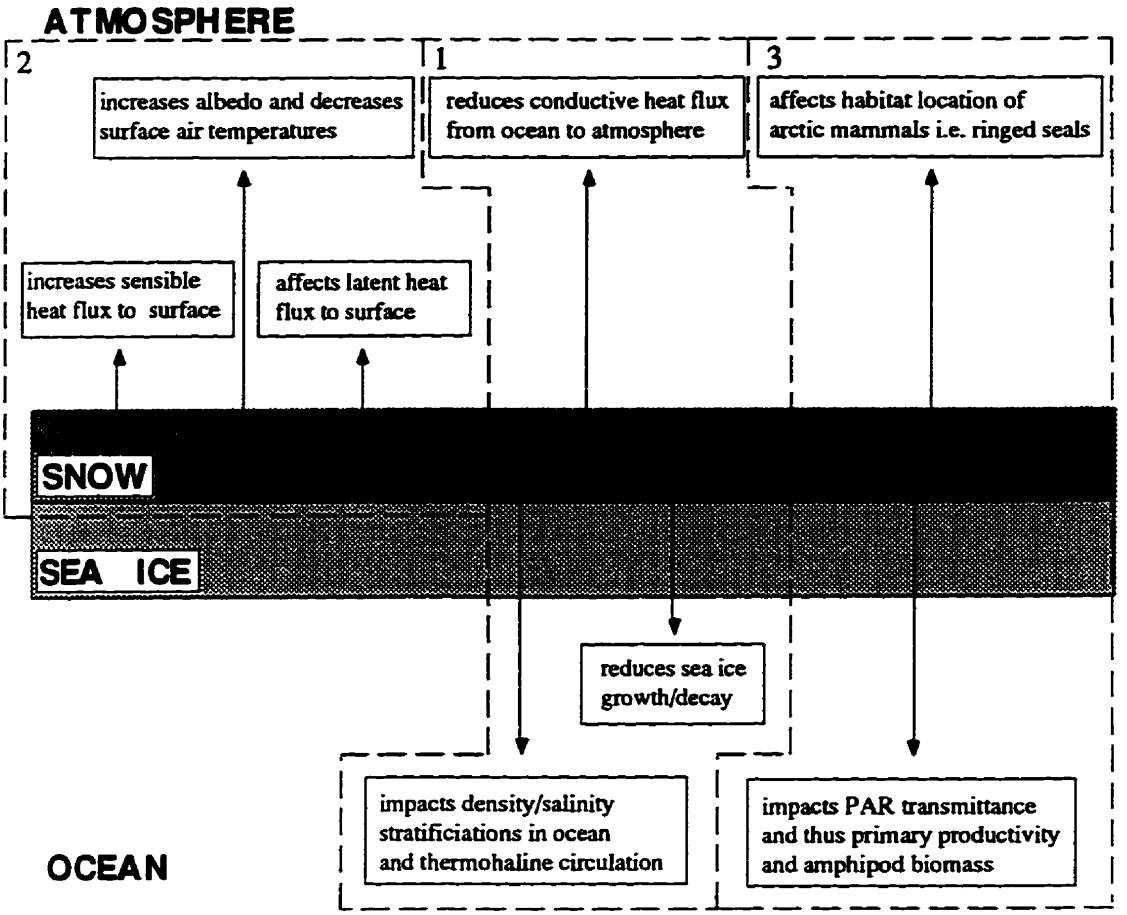

Figure 2.1. Schematic illustrating the significant control of snow catchment on the physical (1), energy budget (2) and biological (3) components of the marine cryosphere.

2.1 AFFECTS OF SNOW DISTRIBUTION ON OCEAN AND SEA ICE PROCESSES.

Snow depth and its distribution over sea ice affects the physical component of the marine cryosphere on three different levels; the control on the sea ice thickness due to the low thermal conductivity of snow, the influence of the snow cover on the ocean circulation, and the freshwater input into the ocean system with the melting of the snow cover (Figure 2.1).

2.1.1 Impacts of snow cover on ice physical properties.

Snow has one of the lowest thermal conductivities of any natural surface on earth. The value of the thermal conductivity varies but it is agreed that for a snow cover with a density of 250 kg m^{-3}, the average conductivity is 0.21×10^{-3} (Adams, 1981). This parameter is dependent on the temperature, density and microstructure of the snow cover (Langham, 1981). For instance, as the temperature of the snow pack increases, the thermal conductivity of snow decreases. The density of a snow pack has the opposite effect on thermal conductivity; the thermal conductivity also increases as the snow pack ages and the density increases

It has been estimated that the thermal conductivity of sea ice is roughly 8 to 10 times greater than that of snow (Kotlyakov and Grosswald, 1990; Eicken et al., 1995). Due to this low thermal conductivity, the snow acts as an insulating blanket for the sea ice. This insulating blanket helps to reduce the heat loss from the relatively warmer ocean to the cooler atmosphere in the winter season, thus keeping the sea ice relatively thin.

Maintaining an equilibrium thickness for sea ice is a critical component in the hemisphere sea ice mass balance (Maykut, 1978). Without a snow cover, more heat is conducted upward through the ice because the top of the sea ice is cooler than the bottom (Maykut, 1986). With the addition of snow, this barrier reduces the amount of heat conducted upward and less heat is transported from the ocean to the atmosphere. Thus, the ocean will remain relatively warm and will not promote bottom accretion of the sea ice in the winter. This will eventually lead to a thinner sea ice cover, as the surface is not able to produce additional sea ice (Eicken et al., 1995). Therefore, it could be concluded that

snow depth increasing over the sea ice will result in a net thinning of sea ice cover due to enhanced thermal insulation.

Based on this relationship between snow depth and ice thickness, the distribution of snow will affect the variation of ice growth in the area. An example of this is seen over multiyear sea ice. The low thermal conductivity associated with snow covered sea ice propagates the hummock-melt pond structure characteristic of multiyear sea ice. Generally, wind-blown snow will become deposited in the refrozen melt ponds, while being swept clear from the large rounded hummocks. The large depth of snow will result in thinner sea ice in melt ponds. Over hummocks, the lack of a deep snow layer will cause more heat to be lost from the warmer ocean and bottom ice growth will be promoted. These opposing affects result in thicker hummocks and thinner melt ponds.

The sensitivity of the conductive heat flux as a result of snow depth is dependent on the season, as well as the relative thickness. In winter, the conductive heat flux decreases much more rapidly with increasing snow depth (Figure 2.2). Although the same pattern is seen in spring, the extent of decrease in the heat flux is not as great. This is probably a product of a smaller temperature difference between the ice/ocean and the atmosphere. It would be expected that in the spring, the conductive heat flux between the ocean and the atmosphere would be smaller without a snow cover.

Ice thickness also contributes to the variation in the reduction of the conductive heat flux with respect to increasing snow depth. Figure 2.3 plots the conductive heat flux for 10 cm and 50 cm thick sea ice against increasing snow depth. It is apparent that young thin first-year sea ice is more sensitive to the snow depth impact on heat conduction (Maykut, 1986). Maykut (1986) found that for thin sea ice, the heat loss through the ice is more sensitive when the snow cover is thin, and thus sensitivity decreases as the snow depth increases.

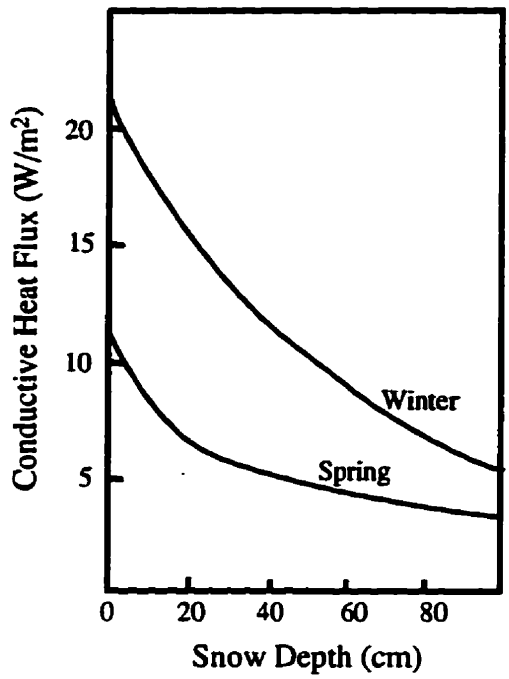

Figure 2.2. Effects of snow depth on heat conducted to the surface of multiyear sea ice during midwinter and spring (Maykut, 1989).

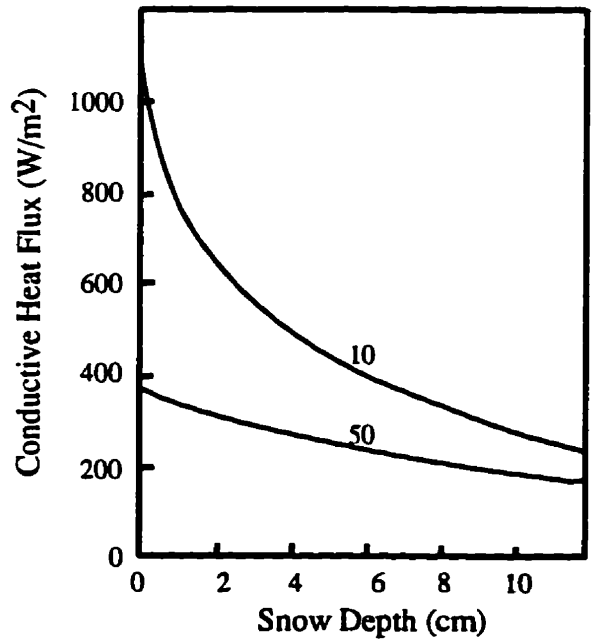

Figure 2.3. Effects of snow depth on heat conducted to the surface of young sea ice during midwinter. The bottom curve indicates 50 cm thick sea ice and the top line 10 cm thick sea ice (Maykut, 1986).

This pattern is also apparent for thicker sea ice, however the sensitivity is not quite as large. With a similar snow depth, thinner sea ice will lose more heat from the ocean to the atmosphere, than thicker sea ice. This will cause a thinner ice sheet to grow at a faster rate than thick sea ice.

Maykut and Untersteiner (1971) dispute the fact that the sea ice would become thinner with the addition of a snow cover. The experiment conduced by the authors found that for snow depths between 0 and 70 cm, the ice thickness remains relatively constant or unchanged, while for depths greater than 70 cm the ice thickness increases rapidly (Figure 2.4). This increase in sea ice thickness is caused by the submergence of the ice surface below ocean level due to a 'heavy' snow cover. This submerging will form slush ice at the surface

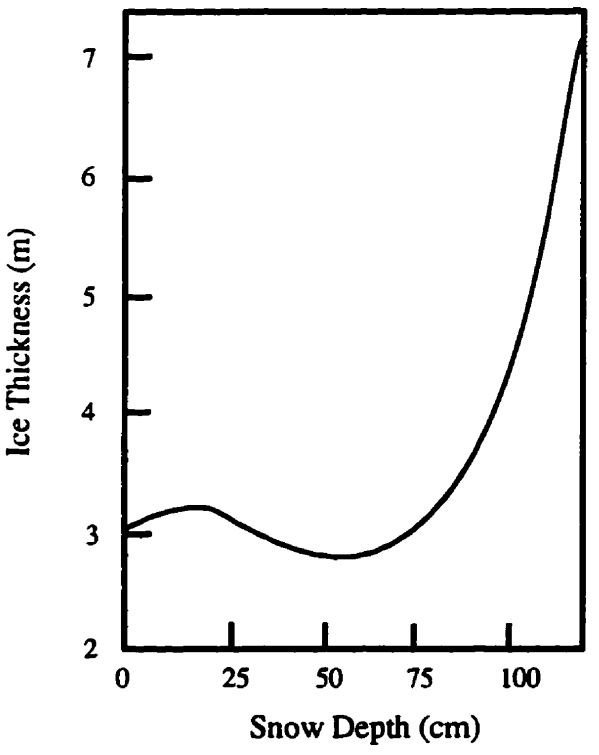

Figure 2.4. Average equilibrium thickness of Arctic sea ice as a function of maximum annual snow depth (after Maykut and Untersteiner, 1971).

which would offset the thermal insulation of the snow cover and cause an increase in the ice thickness (Flato and Brown, 1996). According to Maykut and Untersteiner (1971) this is one effect which promotes ice growth.

The snow also impacts the timing of the ice melt in the spring. Due to the addition of the snow layer to the system, this layer acts as a buffer reducing the heat gained by the snow/ice during the spring and the sea ice will take longer to melt in the spring/summer (Adams, 1981). The small thermal conductivity of the snow layer will reduce the heat gained by the sea ice in the spring season when the atmosphere is warmer than the ocean. Also, the high albedo of the snow causes more shortwave radiation to be reflected and not absorbed at the surface. Once snow melt begins, the albedo of the area decreases and more heat is gained to the system. (For a more complete description of the impacts of snow albedo see section 2.2.1.) As long as the sea ice is unexposed, the spring melt ponds or puddles will not form and surface ablation will progress slowly (Eicken et al., 1995).

Before the ice can ablate, the snow cover must have melted partially or completely, allowing the warmer spring atmosphere temperatures to penetrate the sea ice and cause melting. Also, Eicken et al. (1995) conclude that a thick snow cover will increase the chances for ice to survive the summer melting by restricting the downward heat flux. Therefore, the distribution of snow will result in different melting patterns on the surface and thus affect the amount of sea ice surviving the summer seasons, impacting the thermal and energy regimes of the north. The snow cover prolongs the break-up of the sea ice and delays the warming of the ocean. This will limit the heat gain to the ocean from the warmer atmosphere in the spring (Adams, 1981). Therefore, the addition of a snow cover to an existing sea ice layer causes a thinning of the sea ice, along with a delay in the ice melt during the spring thaw.

Contrary findings regarding the thinning and the prolongation of the melt of sea ice with a layer of snow have been found in the literature. The experiment conducted by Ledley (1991) corroborates the notion that the addition of snow on sea ice would cause the sea ice to become thinner. However, this experiment produced some findings that disagree with the prolonged period of ice melt. The author came to the conclusion that since snow acts as an insulator and keeps the sea ice relatively warm and thin during the winter, it would be easier to melt in the spring (Ledley, 1991). What is not taken into account by this model is that the albedo would decrease steadily as the melt period progresses. The albedo value in the Ledley (1991) study had a significant drop. According to Ledley (1991), "the general thinning of the sea ice is a result of the decreased amount of energy needed to warm and melt the snow...The ice then melts sooner and opens leads wider". With the addition of a snow layer, the warmer spring atmosphere would need to melt the snow layer prior to any melting of the sea ice. Sea ice ablation would occur at the surface, not at the interface between the sea ice and cool ocean. This would cause a prolonging of the melting of sea ice. Thus, in the literature, the affect of snow cover on the timing and melt of sea ice is disputed and not known with any certainty.

This control of snow cover on sea ice thickness has been shown to affect the interannual variability of ice thickness. Flato and Brown (1996) and Brown and Cote (1992) studying the Arctic, as well as Lytle and Ackley (1996) and Eicken et al. (1995) studying the Antarctic polar region, found that the annual variation in snow depth was the main factor affecting annual ice thickness variability. Sixty percent of the variance in the maximum ice thickness, according to a study by Brown and Cote (1992), could be explained by the insulating role of the snow cover. Annual snow depth variations alone

accounted for most of the variability illustrating the dominant affect of this insulating effect of snow depth.

The thickness of snow cover also affects the salinity and brine volumes of the sea ice. The thermal insulation of the snow cover causes ice growth to decrease and this decrease will diminish the initial salinity of newly formed layers (Eicken et al, 1995). The temperature of the ice is increased with a large snow cover, and this temperature increase will increase the brine volumes. Eicken et al. (1995) found brine volumes exceeding 80 parts per-thousand in the upper layers of sea ice. This change in brine volume ultimately affects the ice strength. The ice strength is inversely related to the brine volumes, therefore as brine volumes increase with an increasing snow cover, the strength of the sea ice is greatly reduced, impacting the large-scale behavior of the sea ice. The thermal properties of a snow cover affect the sea ice properties, most importantly, decreasing ice thickness in the polar oceans. The distribution patterns of the snow cover are the most important aspect affecting the variation in ice thickness.

2.1.2 Impacts of snow cover on the ocean circulation.

Thermohaline circulation is the vertical circulation in the ocean causing convective overturning and vertical mixing of the water. No research that has attempted to describe the thermohaline circulation has examined the snow cover impacts on this circulation; while little research has examined the relationship between sea ice and thermohaline circulation. Figure 2.5 shows a schematic of the idealized thermohaline circulation occurring in the world's ocean. Each autumn season, with the increased cooling of surface temperatures, sea ice begins to form over the Arctic Ocean. This growth

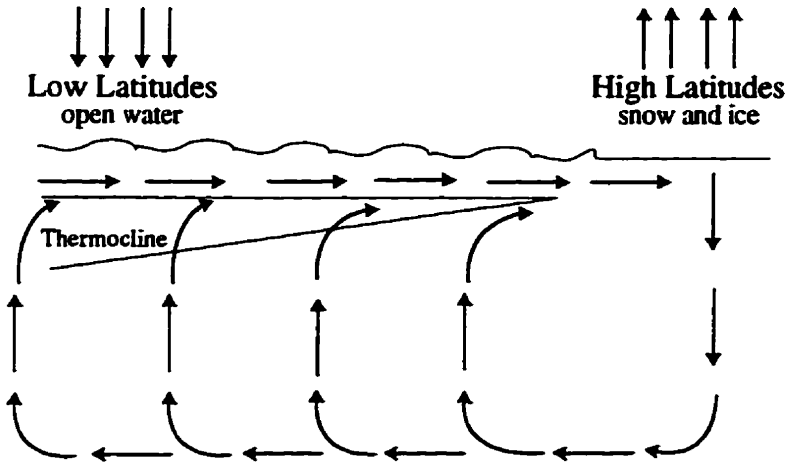

Figure 2.5. Schematic of the thermohaline circulation in the world's oceans, showing the importance of the snow and ice cover of the high latitudes.

increases the density and salinity of the sea water just beneath the sea ice in the northern latitudes by the expulsion of brine (i.e. a solution of salts) into the top layers of the oceans (Hibler and Zhang, 1995; Aagaard et al., 1985; Rundels, 1995). This water becomes what is known as deep water. The deep water sinks due to its greater density and salinity and is transported to the lower latitudes, initiating the thermohaline circulation. Aagaard and Carmack (1989) state that only a small amount of salinity stratification is required to generate and renew the production of deep water. As the water moves towards the equator, the increased shortwave radiation in the lower latitudes causes the water to become heated and the density decreases. This causes the water to ultimately rise to the surface and ascend through the thermocline, a region of the ocean that is marked by sharp density discontinuities in response to changes in temperature and salinity. The water cooled at the higher latitudes is replaced by warmer water from the lower latitudes which is transported along the surface of the oceans (McLellan, 1965). This circulation of oceanic water

from the high latitudes to the lower latitudes and back to the polar region is known as the thermohaline circulation.

This definition of the thermohaline circulation pattern described here is simplified but conveys the message that the snow and sea ice that form in the high latitudes are two of the principal mechanisms driving the thermohaline circulation of the oceans (Yang and Neelin, 1993). As was already stated, the ejection of brine from the bottom of the sea ice layer during growth controls the thermohaline circulation. Therefore, the variability of sea ice production in the high latitudes would impact the circulation pattern. Snow cover, a major factor in ice growth, would then also control the thermohaline conveyor belt. A thick snow cover would reduce the ice growth through its insulating properties and would reduce the expulsion of brine into the ocean below the ice layer. This in turn would restrict or diminish the production of deep water in the North Atlantic, which would ultimately impact the thermohaline circulation.

An impact related to the thermohaline circulation is the input of freshwater into the ocean as the sea ice melts. The expulsion of brine as sea ice grows causes the sea ice to become relatively 'fresh'. This fresh sea ice forms in one location and is transported out of the Arctic into the north Atlantic where it melts forming a freshwater layer at the surface. This layer at the surface may moderate deep convection in the Atlantic and affect the global conveyor belt circulation which is important for the northward transportation of oceanic heat.

2.1.3 Freshwater input of snow cover.

In the present literature dealing with the snow cover on sea ice, not much literature exists that describes the impact the freshwater input has on the physical component of the marine cryosphere. What is known about the freshwater input due to snow and sea ice melt is that a freshwater layer forms on the sea ice. The layer is composed on water formed during snow melt that has not been able to drain through the sea ice into the underlying ocean. This layer inhibits mechanical stirring by the wind and thus the absorbed shortwave radiation within the freshwater and ice layer remains at the surface (Lewis, 1982). This heat storage results in quicker sea ice ablation at the surface.

It has been postulated that the development of the Arctic halocline (area of the Arctic ocean that marks that boundary between fresh polar water and salty water and exhibits large vertical gradients in salinity) is dependent on the input of freshwater into the Arctic ocean either by atmospheric precipitation and/or runoff from the landmasses (Kotlyakov and Grosswald, 1990). However, no quantitative evidence is available that would confirm that the development of the Arctic halocline is a function of the input of freshwater due to precipitation in the form of snow. This lack of evidence does not disclaim the hypothesis, yet it can not be taken as a definite impact of snow on the physical component of the marine cryosphere.

Little additional information is known about the freshwater input into the oceans once the snow and ice melt in the high latitudes. What impact does this addition of freshwater have on the marine life, ocean circulation and the basic properties of the oceans, such as salinity and density? What impact does snow distribution have on the production of melt ponds on multiyear sea ice? This aspect of northern hydrology has not been examined and no literature exists

that even attempts to discuss this situation. It can be postulated that the freshwater input would decrease the salinity and density of the oceans, but what impact does this have on the ocean circulation of the northern hemisphere and the world? Research needs to be conducted on this aspect of the northern snow and ice cover.

2.2 AFFECT OF SNOW DISTRIBUTION ON CLIMATOLOGICAL PROCESSES.

Due to logistical and temperature constraints on the acquisition of data, most of the work on the energy budget of the marine cryosphere in the polar regions is done using modeled studies. Little research has been conducted in the High Arctic examining the radiation and energy balance. In situ studies have been conducted as part of the SIMMS field program, focusing on tower based flux measurements (Barber et al., 1995; Derksen, 1995; DeAbreu et al., 1994) The following sections describing the impacts of snow distribution on surface air temperature and surface energy exchanges come from studies that have modeled the Arctic energy balance. Snow distribution impacts the radiative and surface energy fluxes between the ocean and atmosphere (Figure 2.1).

2.2.1 Impact of snow cover on radiative fluxes.

Studies have found that there is a general decrease in the surface air temperatures as snow thickness over sea ice increases in the Arctic region (Ledley, 1991; 1993; Maykut, 1978). This general trend in surface air temperature can be attributed to an increase in surface albedo from the snow and a decrease in exchange of heat from the ocean to the atmosphere with

increased snow thickness. The increase in surface albedo with additional snow cover was shown to be the primary factor in decreasing the surface temperature (Ledley, 1991).

Albedo is defined as the ratio of outgoing or reflected shortwave radiation to incoming shortwave radiation and is either presented as a percentage or as a decimal. This value is the fundamental component in the computation of the total shortwave radiation absorbed at the surface, according to the equation $I_o=(1-\alpha)F_r$, where I_o is the amount of absorbed shortwave radiation, α is the albedo of the surface, and F_r is the amount of incoming shortwave radiation.

Snow has the highest albedo value of all natural surfaces but this value varies with age, contaminants in the snow, and other factors (Berry, 1981; Langham, 1981). Generally, freshly fallen snow has the highest albedo value and as the snow ages and contaminants collect in the snow, the albedo decreases. Table 2.1 lists the albedo values for snow and different natural surfaces, including different age classes of snow. The absolute values listed in this table can be debated and are only representative of the different surfaces.

But what should be noted are the relative albedo values for these different surfaces. It can be seen from these values that old snow (snow that has undergone metamorphism and densification in which the crystal structure of the snow particle has been altered) has a higher albedo than the sea ice which it covers in the Canadian High Arctic. With the initial deposition of snow, the albedo of the surface doubles in value, therefore the surface absorbs approximately half of the incident shortwave radiation it had previously absorbed. This high albedo of snow cover brings about a reduction in the shortwave radiation that is absorbed at the surface. This reduction in absorbed shortwave radiation will alter the surface temperature of the area.

Table 2.1. Albedo values for different natural surfaces (adapted from Kotlyakov and Grosswald, 1990).

Surface	Albedo (%)
fresh snow	75-95
old snow	40-70
sea ice	30-40
water	5-30

According to Ledley (1991), when snow was added to sea ice in an experiment, the thermal properties of the snow layer (albedo, thermal conductivity, volumetric specific heat and volumetric heat of fusion) caused temperatures to decrease and an overall cooling of the surface occurred. This author states that the cooling begins with the formation of the sea ice and the addition of a snow layer increases the albedo and further decreases air temperatures (Ledley, 1991). The high albedo associated with snow causes more shortwave radiation to be reflected away from the surface to the upper atmosphere. This loss of shortwave radiation results in less radiation being utilized for heating the atmosphere which ultimately leads to cooler temperatures.

The albedo of the snow cover produces a positive feedback within the marine cryosphere; the snow cover increases the amount of shortwave radiation reflected, causing a cooling of the atmosphere. This cooling results in the preservation or enhancement of the snow cover and sea ice, which further enhances the reflection of shortwave radiation and so on. This feedback is broken once the input of shortwave radiation increases in the spring causing snow and ice melt to occur and the albedo of the snow decreases to a point that it no longer promotes the reduction in temperature.

The albedo of a snow surface is not directly dependent on the snow

thickness. Prior to initial snowfall, the albedo of the ice surface will be quite low, within the range of 30%-40% (Table 2.1). With the initial deposition of a few centimeters of snow, the albedo increases to a maximum value of over 90%. This albedo will remain at a relatively high value, or increase slightly, with any additional deposition of snow. The increase is not due to the snow thickness, rather the physical properties of the new snow cover (i.e. less compaction) will impact the albedo and the surface temperatures. Over young sea ice, Maykut (1978) found that the largest decrease in surface temperatures occurs with the deposition of the first few centimeters of snow. On a climatological basis, the initial deposition of snow will have the greatest impact on the temperature of the surface, while additional snow will only promote a small increase in albedo value and thus a slight addiational reduction in surface temperature.

Although the distribution of snow does not directly impact the surface albedo, it will indirectly impact the surface temperatures. As the snow distributes within a region of sea ice, the distribution pattern indirectly causes an increase in surface albedo and a decrease in absorbed solar radiation. This reduction causes a delay in the break-up or melt of the sea ice found below the snow cover (Tucker et al., 1992). In the late spring/early summer, the shortwave radiation reaching the earth increases in the northern latitudes. However, the presence of the snow cover causes a vast majority of that incoming radiation to be reflected back to space, only allowing the surface to absorb very little of the incoming radiation. An area with a thick snow cover will generally survive longer into the summer, causing the surface albedo to become larger than areas with a thin snow cover. This high albedo will again cause more solar radiation to be reflected from the surface and the temperatures will cool.

The second dominant parameter in the impact of snow distribution on surface air temperatures is the conductive heat flux. The conductive heat flux is

the amount of heat that is conducted from the ocean, through the sea ice and snow layers, to the atmosphere. As was already discussed, the thermal conductivity of snow is much lower than that of sea ice, therefore a snow layer over sea ice will reduce the amount of heat conducted to the atmosphere. This conductivity is also dependent on the depth of snow cover; the heat flux through the snow layer is inversely proportional to the snow cover thickness. A thick snow cover will decrease the conductive heat flux substantially over the ice in the polar regions (Lytle and Ackley, 1996; Ledley, 1993; Maykut 1978). Lytle and Ackley (1996) found that the conductive heat flux decreased by approximately 50% with the doubling of snow thickness. Therefore, when snow is thick, less heat is conducted through the snow and ice into the atmosphere and this keeps the temperatures colder at the surface.

The distribution of snow and its influence on the conductive heat flux also regulate the climate by affecting the amount of open water and leads in the summer season. The lead fraction has been shown to influence the surface air temperatures greatly in the polar regions (Ledley, 1988). The reduced conductive heat flux associated with a thicker snow cover will result in less sea ice ablation in the spring melt season. This will produce a greater area that is covered with sea ice and less open water will be present. Ledley (1988) showed that at the end of the summer season, a small decrease in the lead fraction can have a dramatic effect on the climate by reducing the energy exchange between the ocean and atmosphere and thus reducing the surface air temperature by 1.0°K in the north polar region.

2.2.2 Impact of snow thickness on sensible and latent heat fluxes.

The effect of varying amounts of snow is not restricted to surface air temperature, but also affects the surface energy fluxes. The most important of these fluxes in the polar regions is the sensible heat flux. Sensible heat is the heat exchanged between two surfaces that can be detected by humans. This heat is transported between two layers of materials as a result of temperature dissimilarities encountered between the two surfaces. The sensible heat flux is the predominate mode for heat transfer from the ocean to the sea ice, from the sea ice to the snow layer and finally from the snow cover to the colder atmosphere. The snow cover distribution over sea ice is a primary determinant in increasing the sensible heat flux from the atmosphere to the surface on occasions when the atmosphere is warmer than the snow. This increase in the downward sensible heat flux is a product of the snow distribution impacts on the surface albedo, as well as on the open water and lead fraction.

Because the sensible heat flux is a result of temperature gradients, the decrease in surface temperature caused by a thicker snow layer will also impact this heat flux. Ledley (1991) found that the addition of a snow layer resulted in an increased sensible heat flux from the atmosphere to the surface in the high latitudes, as well as at all latitudes. The finding would suggest that a snow cover facilitates the transportation of heat from the atmosphere to the surface (the surface has a gain in heat, while there is a loss by the atmosphere). The increase in the downward flux of the sensible heat is in response to the change in the absorbed solar radiation caused by the increase in albedo. The sensible heat flux reacts to the reduction in shortwave radiation by increasing the transfer of energy from the atmosphere to the snow surface. This reaction reduces the cooling at the surface and at the same time cools the atmosphere.

The snow distribution patterns on rough sea ice will affect the sensible heat flux in the area. For instance, within a hummock-melt pond area, snow will tend to accumulate on the lee side of the hummock, covering a great portion of the melt pond. This snow pattern will affect the spatial pattern of the sensible heat flux. On the snow free hummock (or a hummock with a generally thinner snow cover) heat will be moved from the sea ice to the atmosphere because of the lack of snow cover to prohibit this. On the snow covered melt pond, the snow will cause a downward flux of heat. Thus the spatial pattern of snow is important in calculating the sensible heat loss or gain at the surface.

Again, the snow distribution over sea ice will result in areas having a larger albedo in the spring season. Areas with a thick snow cover will not completely melt, or will take longer to melt, and this snow layer will keep the albedo at high values. These high albedos will cause a reduction in the absorption of solar radiation and thus an increase in the downward sensible heat flux.

The relationship between open water and leads and the snow thickness also impacts the sensible heat flux. In present conditions, Ledley (1988) found that the sensible heat flux in leads has a significant affect on the total surface energy exchange and can be one to two orders of magnitude greater than the flux from the sea ice to the atmosphere. Thick snow cover will reduce the amount of open water and leads present in the Arctic Ocean. When the two months of ice-free conditions were replaced with ice cover in the study by Ledley (1988), the colder surface temperatures associated with the additional ice increased the temperature difference between the ocean and the atmosphere and thus increased the downward sensible heat flux. Therefore, when the snow layer is thick, it acts to maintain a large temperature gradient between the warm ice and cold snow surface, which in turn causes an increase

in the downward sensible heat flux.

The other energy exchanges at the surface (i.e. the latent heat flux and net longwave radiation) are also affected by the snow distribution, but to a lesser extent. These two energy exchanges respond to the snow distribution in similar ways as the sensible heat flux, but the magnitudes are smaller (Ledley, 1993; 1991; Maykut, 1978). Over snow-covered sea ice, the latent heat flux is small in winter because of the low water carrying capacity of cold air. Variations in snow cover will only produce small changes in the magnitude of the heat flux, as compared to the sensible heat flux. The greatest change in latent heat flux is observed during the melt season. Latent heat, which is a product of phase changes in a substance, will increase when the snow and ice layers begin to melt. The snow cover is a large sink for latent heat because of the large amounts of energy needed for the phase change during melt, thus the snow distribution will strongly influence this flux. With a thick snow cover, this melt will take longer and may not be complete, therefore reducing the flux.

The snow distribution will also impact the snow surface roughness associated with different ice types. Over FYI, it is expected that the snow surface will be essentially flat, with little variation of snow thickness. On the other hand, a sea ice type such as multi-year ice will have a greater roughness due to the underlying topography and the wind-induced drifting. A more even surface will reduce the turbulence and vertical transfer of heat from the surface, while a more uneven surface will cause the transfer of heat to increase (Davies, 1994). These different snow distributions will impact the air-ice drag coefficients, which effect the bulk transfer coefficients for sensible and latent heat flux. In summary, the impacts of snow distribution on the annual presence of sea ice as well as on the surface air temperature impact the energy exchanges at the surface, especially the sensible heat flux.

2.3 AFFECT OF SNOW DISTRIBUTION ON BIOLOGICAL PROCESSES.

There are two main impacts the snow distribution over sea ice has on the biology of the north (Figure 2.1). The first impact deals with the consequence of snow distribution on the primary productivity of the oceans. The second effect deals with the habitat location of Arctic mammals and their dependence on snow distribution and ice consolidation.

2.3.1 Impacts of snow cover on the primary productivity.

One of the most widely studied ecological impacts of snow distribution in the north is the affect the distribution patterns have on the sub-ice (epontic) primary productivity of the oceans. In recent studies, researchers have concluded that the surface light, which is primarily determined by the amount of snow cover over the sea ice, is one of the major factors controlling the primary productivity in the oceans (Welch and Bergmann, 1989; Welch, 1991). Ecologically, the epontic primary producers have evolved to take advantage of the historical climatologies of snow and ice thickness distributions.

The control by the snow cover on the penetration of photosynthetically active radiation (400 nm to 700 nm) is primarily due to the fact that the percentage of visible light transmitted through snow is less than that transmitted through sea ice (Figure 2.6). For example, the percentage of photosynthetically active radiation, or PAR, transmitted through a 10 cm snow pack is only 4%, compared to a 90% transmission rate for the same thickness of first-year sea ice. For snow, this value significantly drops to 0.1% as the snow depth increases to approximately 30 cm, while for sea ice the transmission rate is

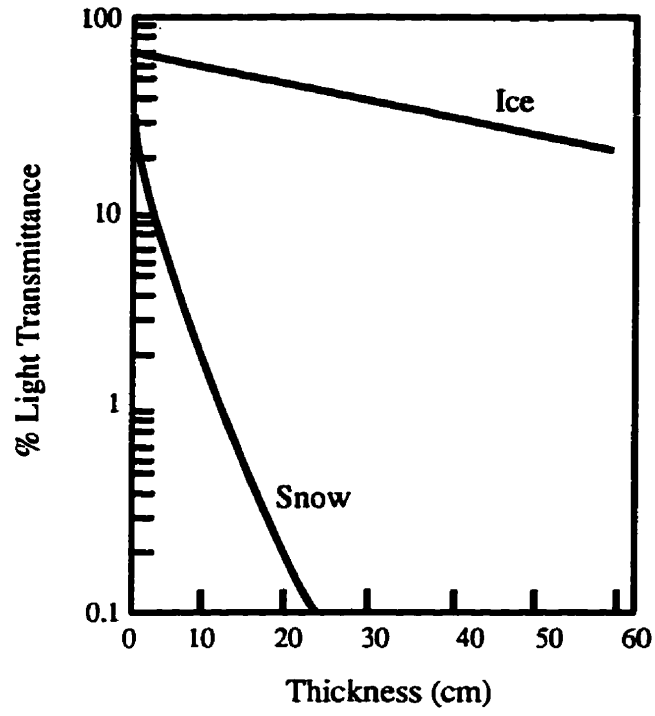

Figure 2.6. Percentage of light transmittance as a function of substrate thickness (after Welch, 1991). This figure shows that a greater amount of light is transmitted through sea ice at any thickness, as compared to snow.

approximately 40% when the ice thickness approaches 30 cm (Welch, 1991). This illustrates the fact that the PAR transmittance through snow and sea ice are not level, but the percentage decreases more rapidly for increasing snow thicknesses than ice thicknesses. Thus the PAR penetration is determined primarily by the snow distribution.

PAR penetration into water is important for the development of algae in the world's ocean. Using a pigment known as chlorophyll, algae utilize and convert light into food that aids in the development of the algae. Because of this relationship between snow depth and light transmittance, the amount of algae growth is controlled primarily by the snow cover. In studies, authors found that the distribution of ice algae is a log function of the overlying snow cover (Welch,

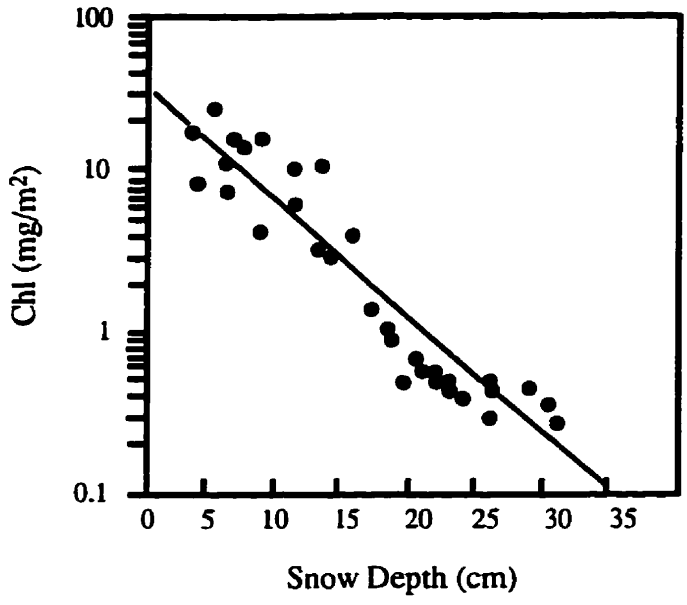

Figure 2.7. Ice algal chlorophyll concentration as a function of overlying snow depth (Welch, 1991).

1991; Welch et al., 1991; Welch and Bergmann, 1989). This relationship between chlorophyll and snow depth can be best described by a negative log-linear function. Figure 2.7 illustrates this relationship and shows that when the snow depth increases, the log function of chlorophyll production in the algae decreases. This exponential relationship between chlorophyll and snow cover suggests that the spatial distribution of snow on sea ice will greatly impact the spatial distribution of chlorophyll production in the ocean.

Because the change in PAR penetration through snow is exponential, generalizing about the amount of snow cover on sea ice will underestimate the amount of light penetration into the Arctic oceans. A uniform snow cover (e.g. 10 cm) over an area composed of first-year sea ice will allow more penetration of PAR than a drifted snow cover containing the same volume of snow. This will have implications on the estimated amount of primary productivity in the

oceans. In order to obtain a more realistic and accurate estimation of the primary productivity in the north, the snow distribution patterns must be known. Therefore, the snow distribution patterns over sea ice affect the amount of PAR penetrating through the snow and ice pack into the oceans and indirectly affect the amount of primary productivity occurring in the oceans.

Snow depth also impacts the amphipod biomass growth in the Arctic waterways. Two of the most important factors controlling the amount of PAR available for amphipod growth, as well as phytoplankton growth in the oceans of the high latitudes are the distribution and thickness of the snow and sea ice (Eicken et al. 1994). (Amphipod is a large order of marine crustaceans, which is a major food source to higher order Arctic mammals and fish.) In the early spring, studies have shown that the total amphipod biomass in the northern latitudes is negatively correlated with snow cover (Figure 2.8) (Pike and Welch, 1990). Later in the spring season, the opposite effect was observed, with total biomass positively correlated with snow depth. Pike and Welch (1990) explain this reversal of correlation between biomass and snow depth using the relationship between algae and snow depth. They state that "since [the] sub-ice amphipods consume ice algae, their distribution is probably related to the abundance of their food source" (Pike and Welch, 1990). In the early spring, the snow cover inhibits algae production, due to the lack of PAR penetrating through the thick snow cover, causing the amphipod biomass to decrease. As the spring season progresses, the snow cover decreases due to melting. This allows more light to penetrate through the snow and sea ice promoting algae growth. This growth then allows the amphipod biomass to increase in the late spring; the food source for the amphipods increases which in turn causes an increase in the amphipod community.

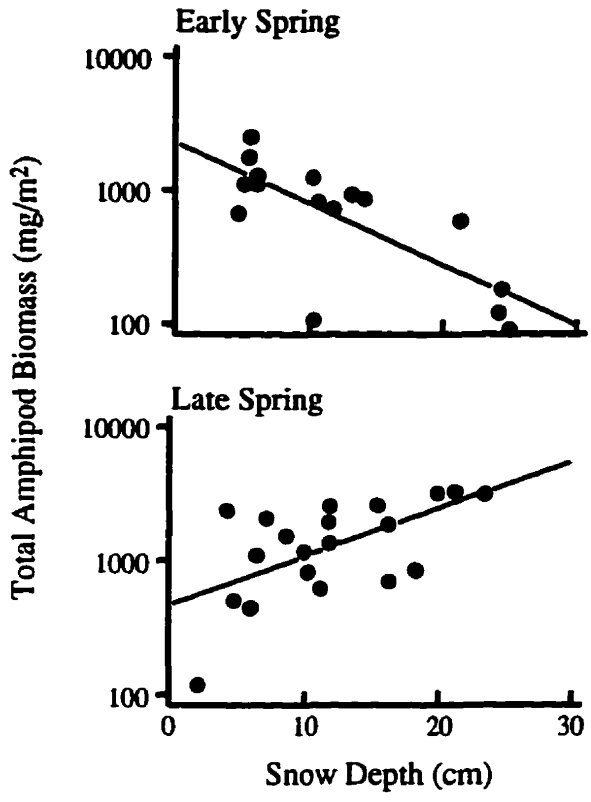

Figure 2.8. Relationship between total amphipod biomass and snow depth (Pike and Welch, 1990).

Thus as illustrated, the snow distribution patterns, or the relative change of snow depth in one location versus another, has major implications on the light penetration. This not only controls the primary productivity, but also the amphipod biomass in the oceans. Because of the major control of snow on algae and amphipod communities, the snow distribution patterns must be known in order to acquire more accurate and realistic estimations of the amphipod biomass.

2.3.2 Impacts of snow cover on habitat location of Arctic mammals.

During the polar winter, most of the Arctic mammals and birds migrate out of areas dominated by the presence of snow and sea ice into areas of open water or to the south. However, the ringed seal (*Phoca hispida*) is one of a few mammals that remains in areas that have a permanent snow and sea ice cover. The way the snow distributes over the sea ice is important for the ringed seal in the sense that this distribution pattern, along with sea ice thickness and deformation structures, will help to determine the location of the seal's breathing holes, as well as their birthing and resting lairs (McLaren, 1958; Smith and Stirling, 1975; Hammill and Smith, 1989: 1991).

Ringed seal breathing holes are excavated in newly formed sea ice in the autumn near to hummock ice or refrozen cracks and in fast ice during the winter months. Lairs are constructed as soon as there is sufficient snow to form a lair roof (Furgal et al., 1996). These subnivean lairs are located in areas where deformation structures (such as ridges or uplifted ice pieces) in the ice sheet have resulted in stable snow drifts forming in close proximity to the structure. Hammill and Smith (1989) found that the abundance of lairs increased as snow depth increased and the consolidation time of the ice was later. In locations with flat ice, such as first-year ice floes, the distribution of snow is relatively constant, therefore snow drifts of considerable height do not form (Smith, 1987). This distribution of snow is therefore not conducive to ringed seal habitat location and few, if any lairs are found in these locations.

These lairs, as well as being used for birthing and resting, are used as protective structures from predators (i.e. polar bears and arctic fox) and the cold atmospheric temperatures. The snow roof will insulate the structure underneath it from the cold atmosphere through the low thermal conductivity of snow.

Therefore, the snow distribution patterns over sea ice, in particular ridged sea ice, will govern the location of the ringed seal habitat in the winter months. In trying to estimate or locate the suitable habitat for ringed seal lairs, the snow distribution patterns, as well as the presence of deformation structures, must be known for the study site.

The snow distribution patterns also play an indirect role on the habitat location of the polar bear (*Ursus maritimus*) and the arctic fox. Polar bears feed almost exclusively on the ringed seal, therefore these mammals will locate in areas where the ringed seal maintains its lairs (Welch, 1991). The snow distribution on sea ice and its consequences on the snow depth influence the success rate of polar bear predation on the ringed seal lairs. Hammill and Smith (1991) found that as the snow depth increases, the success rate of polar bear predation attempts decreases. Polar bears generally pounce on the roof of the lair to gain access to the occupant(s) of the lair. With increased snow depth on the roof of the lair, polar bears increase the predation effort but success decreases (Furgal et al., 1996). Ringed seals have a greater chance of sensing the polar bear attack through a thicker snow cover prior to the entrance of the polar bear. Arctic foxes, another significant predator of the ringed seal, generally excavate through the lair at an angle to gain access to the occupant(s). The polar bear and arctic fox rely on the ringed seal as a major food source, therefore their habitat location is dependent directly on the location of the ringed seal. Thus, the snow drift dependency of the ringed seal habitat further determines the location in which the polar bears and arctic foxes will be found.

The patterns of snow distribution over sea ice in the Canadian High Arctic have significant consequences on the physical, climatological and

biological components of the marine cryosphere. Snow reduces the thickness of sea ice and prolongs the timing of the ice melt. The thermohaline circulation, important to the patterns of ocean circulation, is influenced by the snow cover in the high latitudes. However, even though snow research has been conducted in the high latitudes for a significant period of time, little is known about what impacts the freshwater from snow and ice melt has on the marine cryosphere. The high albedo of snow impacts the energy balance of the high latitudes. This causes a decrease in air temperatures which results in changes to other components of the energy balance, especially the sensible heat flux. It can thus be seen that there is a great need for research on the patterns of snow distribution over sea ice in the Canadian High Arctic since the impacts of these patterns influence all aspects of the northern system. The biology of the high latitudes is dependent on the snow distribution patterns over sea ice. The amount of chlorophyll produced in the Arctic waters is contingent on the depth of snow cover on the sea ice, while Arctic mammals require sufficient snow depths in order to construct habitats and survive in the Arctic.

Generalizing the amount of snow on sea ice is not adequate if understanding these components in the marine cryosphere is to evolve and become complete. The only way a complete understanding of the physical, biological and climatological nature of the north, and the earth as a whole, can be achieved is with a knowledge of the snow distribution patterns. Because of the lack of stations collecting snow data in the north, and the inability of remote sensing to obtain snow measurements, these distribution patterns need to be modeled. The next chapter will introduce the concepts of the variogram and grey-level co-occurrence matrix methods used in this thesis, as well as providing a general background on the snow distribution, including previous models.

CHAPTER 3:

BACKGROUND.

This chapter provides a general background on snow distribution and the modeling of this distribution on terrestrial surfaces. The first section discusses the spatial and temporal distributions of snowfall in the Canadian Arctic. Past models of snow distribution found in the literature are critically examined in the second section of this chapter. Following this, a general review of the uses of geostatistics and the grey-level co-occurrence matrix is presented.

3.1 MAGNITUDE AND DISTRIBUTION OF SNOWFALL IN THE CANADIAN ARCTIC.

3.1.1. Temporal distribution of precipitation at Resolute.

This section of describes the temporal precipitation patterns observed at Resolute for a time period extending from 1971 to 1995.

The precipitation amounts recorded at the Resolute weather station are summarized in Figure 3.1 for a 25 year period (1971-1995 inclusive) on a annual and seasonal basis. The dominant period of snowfall in this region is in the late summer and the autumn seasons with approximately 50% of the total precipitation. This dominance of precipitation is due to the movement of a large number of storms in the area during this time period. These storms will deposit

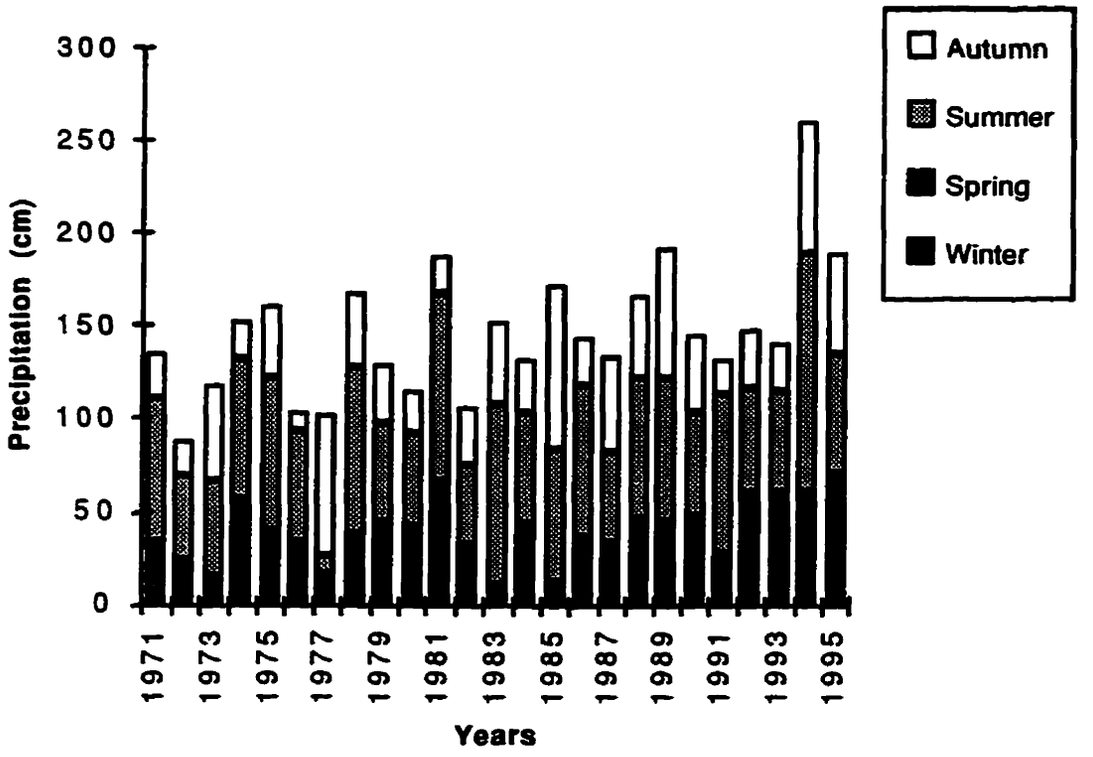

Figure 3.1. Precipitation amounts recorded at the Resolute weather station from 1971 to 1995. Graph illustrates that seasonal component of precipitation amounts. Autumn was defined as occurring from September to October, summer from June to August, spring from April to May, and winter from November to March.

a great amount of snow on the sea ice that is already present or is beginning to form. In comparison, the winter and spring seasons in the Arctic produce less snowfall.

The distribution of snow in the Arctic is a by-product of this temporal precipitation distribution. In the autumn months, when the sea ice is beginning to form, a considerable amount of snow falls to the surface due to the high frequency of storm events. The snowfall is distributed by the winds of that storm and eventually settle on the surface. This will form a distribution pattern that is distinct for the ice type and location. With the advancement of an additional

storm, new snow falls and is distributed on the surface by the winds associated with the new storm. The horizontal velocity component of the storm causes the trajectories of the falling snow to become oriented in a particular direction. This will result in snow drift formations many times greater than the areal snow cover. Eventually this snow will settle and form a new surface topography. The addition of a new snow cover distributed on the surface will change the characteristics of the surface and thus will change the characteristics of distribution for a subsequent snowfall. Thus, the distribution patterns of snow are predominantly formed in the months with the most storm events (i.e. late summer/early autumn).

3.1.2. Mechanisms for snow distribution.

The mechanisms responsible for snow distribution or snow drifting in the Canadian Arctic are primarily wind speed and direction near the surface of the earth, as well as the mode of mass transport. Wind speed and direction will determine the direction and the proportion of loose snow on the surface that will move. As was previously stated, the nature of the wind speed and direction occurring during storm events will primarily determine the variability of snow depth on the sea ice. More specifically the wind closest to the surface will impact the patterns most strongly.

The wind flow near the surface of the snow is usually turbulent because of the frictional drag exerted on the air by the surface. The snow patterns on the surface will usually reflect this turbulent flow (McKay and Gray, 1981). In short, where the turbulent wind speed accelerates, erosion of the fallen snow will occur, transporting the snow and depositing it forming drifts and banks in areas where the speeds decelerate. This deceleration is a product of the high

aerodynamic roughness associated with the surface. Therefore snow drift depths tend to be greatest where the greatest deceleration of wind speed occur (i.e. leeward of zones with high aerodynamic roughness).

This pattern is seen over the sea ice in the Arctic. Large flat areas, such as smooth first-year sea ice, will have large fetches and the least resistance to airflow because of the lack of obstacles. This area will thus have high wind speeds during storm events, promoting the erosion and transport of snow particles. This will produce small snow drifts, such as sastrugi. Once the winds reach the boundary between first-year sea ice and other ice types that are more irregular in terms of topography (i.e. multiyear or rubble sea ice), wind speeds generally decrease. This deceleration of wind will result in the deposition of snow. This pattern continues in the multiyear and rubble ice areas, where high wind speeds over flatter areas (i.e. melt ponds) will erode the snow and deposit it when the wind decelerates once it comes into contact with hummocks. This process is the primary reason why snow depths are greater in the areas dominated by the more irregular ice types.

Wind speed and its implications on snow drifting is also controlled by the thickness of the boundary layer at the earth's surface. The boundary layer is defined as the zone in which the wind speed increases from zero at the earth's surface to its geostrophic value at some distance above the ground. The thickness of this layer is controlled primarily by the surface roughness. Over rough terrain, the boundary layer is thick and wind speeds increase relatively quickly with height producing large velocity gradients (Kind, 1981). These large gradients will result in the movement of loose snow particles and thus drifting of snow will occur.

Another feature associated with rough terrain and snow drifting are separation bubbles. Over a smooth terrain, streamlines of wind are generally

parallel. When these wind streamlines come into contact with an obstacle they tend to converge and form separation bubbles behind the obstacle, relative to the wind direction (Kind, 1981). These separation bubbles have low wind velocities and small shear stress resulting in the formation of snow drifts and limiting the erosion of these drifts. At the surface, the shear stress tends to be relatively high, eroding the snow around the base of the obstacle. This pattern is commonly seen in the Arctic around large uplifted ice pieces. Kind (1981) and McKay and Gray (1981) provide a more complete explanation of the physics behind snow transport.

Wind direction also plays an important role in the formation of snow drifts. When the wind during a particular storm event is from a single direction, snow drifts tend to be the greatest and oriented in that direction. If the storm event has several changes in wind direction associated with it, the snow drifts tend to be less pronounced.

The mode of transport is another important aspect when considering the physics of snow distribution. The primary mode of transport for snow is by saltation. Figure 3.2 illustrates the process and trajectory of a saltating snow particle. Saltation is the process by which a snow particle is initially lifted from the surface at a steep angle and carried in the downwind direction by the aerodynamic drag forces (Kind, 1986). Constantly under the influence of gravity, the particle will eventually 'splash' back to the surface, terminating its trajectory. The descent to the bed is more gradual than the initial lift. The splash back to the surface causes most of the momentum associated with the impacting particle to be dissipated into the snow surface. This displacement may result in other particles being ejected and thus continuing the saltation process.

The rate of transport by the saltation process is driven by the ability of the

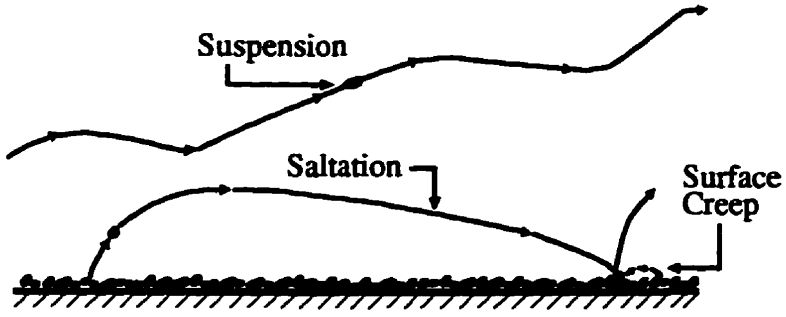

Figure 3.2. Schematic illustrating the three modes of snow transport; saltation, suspension and surface creep. Saltation is the predominant mode of snow transport in the Arctic. (modified from Kind, 1990).

wind to exert shear stress on the snow surface (Kind, 1986). Shear stress is produced by velocity gradients in the boundary layer and reaches a maximum value at the earth's surface, decreasing gradually with height. The ability of wind to exert shear stress increases as the wind speed increases. Thus, with a greater wind speed, more particles will be involved in the saltation process. The saltation of snow particles further modifies the wind velocity profile by increasing the effective roughness of the snow surface (Kind, 1986).

In wind tunnel experiments, it was concluded that the mean saltation length and thickness decreased with increasing snow particle diameter and decreasing wind speed (Kind, 1986). In the same experiment, it was also found that the mean diameter of the snow particle decreased only slightly with increasing height. Increasing wind speed thus also causes an increase in the length of the saltation trajectories and the particles will retain greater horizontal velocities.

Two other modes of transport, surface creep and suspension act to transport snow particles. However, these modes are not as dominant as saltation for the transport and deposition of snow in the Arctic. Figure 3.2 illustrates all three modes of transport. Surface creep occurs when the saltating

particle impacts the surface. The impact will cause larger particles to be 'nudged' small distances in the flow direction, not actually leaving the snow surface. Particles too large for saltation will creep along the surface in the manner described here and do not acquire any appreciable height above the surface. Light small snow particles can be transported by suspension. In this third mode of transport, the particles are suspended and airborne in the turbulent flow causing them to be carried to relatively greater heights and distances than saltation or surface creep. These three modes of transport, while not proportional in terms of dominance of snow transport, work in tandem and not separately.

In order for the snow particle to be transported, certain conditions must first be met. Primarily, the particle will only move in saltation once the wind speed becomes sufficiently high to exceed the resisting forces due to gravity and cohesion on the surface, known as the threshold velocity. The threshold velocity is dependent on the shape, size and weight of the snow particle, as well as on the magnitude of the cohesive forces. As the size of the snow particle increases, the velocity required to move the particle increases.

On a snow surface, the cohesive forces are those forces formed when snow particles tend to stick to one another. These forces tend to be the dominant factor in determining the threshold wind speed (Kind, 1990). They can develop as soon as the particle reaches the surface and are dependent on time, temperature and other factors (Kind, 1986). At temperatures below approximately 2°C the cohesive forces become negligible and thus snow particles are more readily available for transport via saltation. The threshold velocity increases once the snow becomes wet, aged or wind-hardened because strong inter-particle cohesive forces bond the snow particles together making them less likely to move.

In the Canadian Arctic, snow distribution occurs primarily through saltation on the surface during periods of storm events that pass through the area. Modeling this distribution pattern is difficult due to these factors, but many approaches have been attempted. The next section of this chapter will examine these modeling attempts.

3.2 PREVIOUS MODELS OF SNOW DISTRIBUTION.

The modeling of snow distribution over various landscape features has been extensively studied in the literature. Most studies have focused on, but are not exclusive to, the distribution patterns in alpine environments for the purpose of modeling snow melt runoff. It is deemed important by both the scientific and commercial industries to have an educated forecast as to the amount of runoff occurring when snow melts. This basic product of the spring season is fundamental to most snow distribution models.

Models of snow distribution can be classified as either deterministic or statistically-based models. Computer-based models examine the problem of snow distribution using complex computer sub-routines to delineate different components of the snow cover, such as snowfall, densification and snow melt. Empirical models use various statistical methods to define the distribution patterns over the landscape. These models examine the relationship between various features of the landscape and snow distribution, including vegetation and topography. This section of the thesis examines in greater detail the two categories of snow distribution models that have been developed in the scientific literature.

3.2.1 Deterministic models.

In the past decade, computers have been utilized more by researchers to estimate the snow distribution patterns over terrestrial surfaces. A number of computer models exist in the literature (Brun et al., 1994; Ujihashi et al., 1994; Blöschl et al., 1991; Schroeter et al., 1991; Sambles et al., 1990; Schroeter and Whiteley, 1987; 1986; Rachner and Matthäus, 1986). These computer-based, or deterministic, models generally estimate the snow distribution patterns as part of or as a variable leading to the estimation of melt runoff in a terrestrial environment.

A similar feature of these deterministic models is that all use a number of computer sub-routines to estimate the amount and pattern of snow distribution. These computer sub-routine models use measured climatic variables such as wind speed, direction and air temperature as the input variables in the model as opposed to any hydrological variables, such as snow depth or density. The subroutines use these input variables to evaluate whether net ablation or net accumulation occurs in the study area.

Another similarity between deterministic models is the segmentation of the study area into blocks or cells. Generally, the area under investigation is divided into blocks based on similar topographical/land cover types and then similar cells are grouped according to meteorological similarities. For instance, the snow accumulation-ablation model (SAAM) used by Schroeter and Whiteley (1987) and Schroeter et al. (1991) divide the catchment area into 'equivalent accumulation blocks', or EAB for short. Each block represents a homogenous land cover type and blocks within similar climatic zones are grouped together. The EABs are further subdivided into a number of cells, each having a capacity height. This capacity height "denotes the maximum depth of

snow that can be stored in the cell during full drifting snow conditions." (Schroeter and Whiteley, 1987). This parameter varies depending on the cell and the land use type of the EAB. Other models, such as the program SNOW developed by Rachner and Matthäus (1986), use hydrological and meteorological features of the study area to divide the region. The digital model, SNOMO (snow model) developed by Sambles et al. (1990) divides the study area based also on topographical and vegetation features.

The various deterministic models differ primarily in the methodology or structure used by the researcher. The sub-routines that simulate the ablation or accumulation of the snow cover vary from model to model. The SNOMO model is based on the conductive energy-budget equation. This equation is used to calculate whether net ablation or net accumulation occur in the various cells, as well as the quantity of the change. This ablation/accumulation determines the distribution patterns of the cells and eventually of the entire study area.

The sub-routines and equations involved in the SNOW model are much more complicated than those for the SNOMO model. The SNOW model utilizes the radiative and conductive energy-balance equations, along with equations that describe the topographical features of the area (Rachner and Matthäus, 1986). This results in a number of sub-routines and equations that must be executed prior to any calculation of a distribution pattern. The intense division of the snow pack in the SAAM model results in complicated and unique sub-routines. The model examines the initial deposition and erosion of snow within all cells of the snow pack, as well as the redistribution of the snow cover due to erosion caused by wind. Snow may move from one cell to another depending on whether accumulation or ablation occurs within the EAB. This characteristic of constant change within each EAB adds to the complexity of the model. Therefore, it can be seen that although a number of computer-based models

have been developed to model the snow distribution patterns, either as a direct output or as some variable utilized for further outputs, the models differ significantly in their structure and equations. To say that one model is more accurate or reliable than another would not be possible since a number of factors differ between models, such as application and general use.

In relation to the work being carried out by this researcher, these various deterministic models of snow distribution are not adequate to model the snow distribution patterns over an icescape. A major difficulty with using deterministic models for snow distribution is that a complete knowledge and understanding of the processes operating on a landscape, either terrestrial or ice, is required. However processes operating on an icescape are only presently being studied and understood, thus making any deterministic model inadequate for modeling the snow distribution patterns.

These models are also of a predictive nature; that is that they are used to predict the snow distribution patterns over terrestrial surfaces with only climatic information. This is not possible in the present study because the snow distribution patterns over sea ice have never been statistically examined in the past. Snow distribution patterns over terrestrial surfaces have been statistically examined in the literature for a number of years, and these deterministic models are used in conjunction with the existing statistical examination. Also, all the computer models studied do not retain the spatial information contained within the data set. The spatial information is seen as one of the important properties in modeling the snow distribution patterns over an icescape. Prior to any deterministic models being developed for an icescape, the patterns must be statistically surveyed.

3.2.2 Statistical or empirical-based models.

While a number of computer-based models to study the snow distribution patterns over terrestrial surfaces have recently appeared in the literature, a vast majority of the studies utilize classical statistics to estimate this phenomenon. Most studies have surveyed the snow distribution patterns over terrestrial surfaces using regression analysis and/or correlation matrices (Elder et al., 1991; Evans et al., 1989; Golding and Swanson, 1986; Daugharty and Dickinson, 1982; Hamilton and Lahey, 1982; Patch, 1981; Steffen and Müller, 1977). In these studies, snow depth or snow distribution was the primary output. These studies all attempt to predict the snow depth given a certain topographical feature, land cover type and/or vegetation pattern.

The methodologies in these studies are very similar. Snow depth for different land cover types (such as forests, fields, ditches, etc.) or topographic feature (i.e. slope, elevation and aspect) is first measured. The next step is to use regression analysis and correlation matrices, either alone or in combination, to model the relationship statistically between snow depth and other variables such as elevation, vegetation, and/or slope. Using the coefficients derived from the analysis, snow depth can be predicted and modeled for different land cover types and elevation. However, most of these studies have one weakness; they do not include atmospheric or climatic variables in their modeling of snow distribution. These variables have been shown to be important in the distribution of snow over a terrestrial surface (Kind, 1986; McKay and Gray, 1981).

Other studies utilize various other statistical methods to model the snow distribution patterns. One commonly used method in the literature is the areal distribution curves (ADCs) (Burckard et al., 1991; Dickinson and Whitely, 1972).

ADCs are used to summarize the areal distribution of the snow cover and define the state of the snow cover at a specific time (Goodison, 1981). ADCs are "constructed by ordering the depths [and water equivalent] and calculating the cumulative percent of observations that equal or exceed each depth" (Burkard et al., 1991). The plotted curves of the cumulative frequency distributions of the occurrences of a given snow cover property are the areal distribution curves. Coefficients of variation are used to characterize the curves and these parameters are compared for different areas as well as different dates. These curves are then used as inputs into models that calculate distribution, such as SAAM, or can be used to characterize snow patterns for catchments that are in the same geographical area with limited snow measurements (Burkard et al., 1991).

Donald et al. (1995) calculated ADCs for various land cover types and then used a collection of these curves in the form of a snow cover depletion curve (SDC). The SDC was used to develop a distributed snow cover representation for areas that are largely affected by land cover types. ADCs become a point on the SDC, which summarize the percent areal coverage of the snow pack as it increases in average depth (Donald et al., 1995). An important feature of an ADC is the underlying frequency distribution. The slope of an ADC appears constant within a given vegetation type, implying that the variability around the mean depth remains constant as the snow cover changes (Donald et al., 1995). A large disadvantage of the computation of ADCs is that intensive sampling programs, in terms of both time and expense, are needed to quantify the snow distribution patterns.

Another statistical technique widely used in the literature to characterize the snow distribution pattern is the probability density function (pdf). The pdf is defined as "the probability of encountering at a randomly chosen point a snow

depth value between z and z+dz, divided by the width of the sampling interval" (Eicken et al., 1994). In other words, the pdf is the relative frequency of occurrence for a specific thickness value within the thickness bin z to z+dz. The pdf is obtained by dividing the width of the bin for all bins to be considered. When this function is plotted against snow thickness, a curve is obtained. This curve represents the snow distribution of the area being studied. The pdf is completed for different land cover types or ice types, in the case of Eicken et al. (1994), and the curves are compared and analyzed. The curves will differ depending on the spatial and temporal scales.

This method has also been used to model the thickness distribution of snow over sea ice in Antarctica (Massom et al., 1997; Worby et al., 1996; Lange and Eicken, 1991). Lange and Eicken (1991) divided the ice floes measured into classes based on the physical description of the floes. The snow type was then modeled for each class and the different pdfs were compared and analyzed for normality and thickness ranges and maximum values. Worby et al. (1996) used pdfs to compare the snow thickness measurements of three independent data sets, while Massom et al. (1997) used the same method to compare snow thickness measured 'in situ' and 'in transit'.

One of the first methods used to model the distribution of snow was used by Kuz'min (1960). This researcher characterized the snow distribution over an area composed of many different topographical features and types of vegetation. The method utilizes a curve that expresses the relative frequency of the snow depth and was called a curve of probability distribution. The exceedance probability for different intervals of the snow depth is plotted against the modal coefficient of the snow cover (Kuz'min, 1960). This curve is determined by the arithmetic mean, coefficient of variation and skewness. Again, these curves vary for different catchment areas and characterize a

specific area in both space and time.

What is evident and common in all statistical models in the literature is that all models do not retain the spatial information within the data set. Regression analysis and the various other forms of statistics employed by snow modelers are all based on the classical form of statistics. This form of statistics has as a premise that the snow depths at various distances are independent and randomly distributed. Thus the models do not include information about the spatial relationship between the sample points. Due to the dependence of snow depth on location, another form of statistics is required to model the spatial distribution of snow depth over sea ice. Geostatistics, a more recent form of statistics, is a prime candidate for the modeling of snow distribution because of its retention of the spatial information in the snow pack.

One study found in the literature on modeling snow distribution retains the spatial information within the data set. Burn and Ray (1989) used geostatistics to model the water equivalent of a basin's snow pack from point measurements. Data collected from a terrestrial catchment area in Manitoba was analyzed using variograms as well as kriging. These researchers produced a variogram that statistically characterized the snow depth of the catchment area under study. This information, according to the researchers, could be used in the kriging process to produce a map of the snow depths. This study was the only study that used a geostatistical technique to characterize the snow distribution patterns. Problems with spatial resolution of data limited the accuracy and reliability of the results. However, this study illustrated the potential of the variogram for examining snow distribution patterns. The next section will examine the uses of this method in other scientific disciplines.

3.3 PARALLEL USES OF GEOSTATISTICS AND GLCM METHODS.

This section will review the uses of the two research methods used in this thesis, the variogram and the grey-level co-occurrence matrix.

3.3.1 Geostatistics and Variograms.

As already stated, previous models on snow distribution have examined the spatial distribution of snow over various types of landscapes without retaining the spatial information contained within the data itself. This information, or more accurately the idea that the snow depth values located at closer locations will be more similar than snow depth values located at widely spaced locations, is seen as one of the important factors in the modeling of the spatial distribution of snow. Geostatistics, a deviation from or branch of classical statistics, retains the spatial organization contained in the data set and attempts to detect, model and estimate any spatial patterns present. The location of the measured snow depth, relative to the location of other measurements is retained in the statistics that comprise geostatistics. The variogram, more specifically, calculates the spatial continuity of the variable in question and utilizes the spatial information in the calculation of the semivariance.

Geostatistics, and more specifically variograms, were originally designed and applied to the field of mining geology. However, in the past two decades, variograms have been used in a wide range of scientific fields; including biology, pedology, hydrology and remote sensing. This section of the thesis will examine the applications of geostatistics and variograms within these fields.

GEOLOGY

The principal application of variograms, since its conception, was in the field of mining geology. Matheron (1963) developed the 'new' statistical theory known as geostatistics to evaluate the distribution of ore-grades in a deposit. In order to retrieve a mineral in an ore-body economically, the direction in which the specific ore-body or grade flows is required, along with its size and position in space. Variograms allow for the determination of the size of the ore-body. An example of the application of variograms to reserve estimations is in Champigny and Armstrong (1993). This study reviews the use of geostatistics and its effectiveness for estimating gold reserves. Findings indicate that while the application of geostatistics is limited in the gold mining community, it has the potential to improve significantly the estimation of global and local gold reserves.

Norrish and Blackwell (1987) described the implementation of geostatistics for grade estimation of a copper/molybdenum ore body. Conclusions from this study imply that there are considerable advantages in using the geostatistical method for calculating a mineral ore-body. The use of the variogram in ore deposit modeling becomes difficult if the deposits have complex distributions (Pan, 1995).

Variograms have also been applied to the fields of petroleum estimation, marine geophysics and hydrogeology. Hohn (1988) found that a similar process to that being used to estimate ore-bodies is being used to estimate the petroleum reserves in different parts of the world. Herzfeld (1993) and Carr and Glass (1989) used the variogram to classify sea floor and maximum earthquake ground motion, respectively. Both of these studies were the first attempts at the utilization of the variogram to marine geophysics and showed that this technique can be applied successfully to the respective fields.

A significant amount of work has been conducted in the application of geostatistics within the field of hydrogeology or geohydrology. A review of the applications in geohydrology has been completed by ASCE (1990). Delhomme (1979) provided one of the earliest uses. This study mapped spatial variables within the field of geohydrology, including transmissivity and piezometric heads. Other applications within geohydrology include the simulation of hydrogeological variables, as well as the management of ground water systems. In this last example, geostatistics were used to eliminate or reduce the parameter uncertainty in ground water management models, as well as in the analysis of the modeled results. Ahmed et al. (1995) used variograms to study various hydrogeological parameters for an aquifer. It was evident that any geostatistical analysis should be done on an aquifer that has been divided into a number of zones. The application of the variogram to the numerous fields in geology is extensive as indicated in the above summary. For a more complete examination of the applications, see Journel and Huijbregts (1978) and Hohn (1988).

PEDOLOGY

The spatial variability of soil properties has been quantified in the literature using the variogram. Burgess and Webster (1980) were among the earliest to apply the variogram and associated kriging methods to soil properties. This study used the semivariogram successfully to model and map the variability of sodium content, stoniness and thickness of cover loam for two areas in the United Kingdom. The study was intended to introduce the application of the variograms and other geostatistical methods to modeling and mapping soil characteristics.

Later studies have expanded on the application of geostatistics with

respect to pedology. Studies by Oliver and Webster (1986; 1987) are two such studies. Oliver and Webster (1986) described the practical application of the variogram for quantitatively representing the spatial variability of soil properties along with describing the physical nature of the theoretical variogram models through various case studies. This study, along with Burgess and Webster (1980) are considered introductory studies for soil scientists in the application of the variogram.

Another study by Oliver and Webster (1987) and ones by Halvorson et al. (1995) and Jackson and Caldwell (1993) are prime examples of the applications of the variogram. The spatial variability of various soil properties, including stone, sand, clay and mottling, were modeled from data collected at Wyre Forest in England. Results examined the spatial scales and scale of variation for these properties and concluded that the upper limit of spatial dependence was no more than 60 m (Oliver and Webster, 1987). Oliver and Webster (1987) concluded that future sampling must occur at intervals less than 20m in order to capture most, if not all, of the spatial variability of soil properties in Wyre Forest.

Halvorson et al. (1995) used the variogram to analyze the spatial characteristics of resource islands in the soil under Big Sagebrush in the intermountain western USA. The researchers concluded that spatial dependence existed for all individual soil variables examined, including inorganic nitrogen concentrations, soil microbial biomass and water-soluble soil (Halvorson et al., 1995). The ensembles of variables were also correlated spatially and systematically within the landscape. The study by Jackson and Caldwell (1993) used variograms to quantify the scale and variability of various soil nutrients with emphasis around perennial plants. The researchers found that autocorrelation existed at spatial scales less than 1 m for each of the

nutrients studied, implying that individual plants with roots a meter or so apart encounter the same soil variability as occurs across the entire plot (Jackson and Caldwell, 1993). The application of the variogram and other geostatistical techniques to pedology is relatively new. However, the literature is promising and illustrates the effective use of these methods to model the soil properties in a number of areas.

BIOLOGY

Apart from geology, variograms have also been used most extensively in biological disciplines, namely botany, virology and zoology. One of the prime applications of variograms in the biological literature is to estimate and map the density of plant communities. One example of this is a study by Donald (1994), which used the variogram, as well as kriging, to map the population density of Canada thistle shoot density, as well as the root growth at progressively greater depths. Another study used these geostatistical techniques to examine the quantitative traits (i.e. heading date and summer growth) of perennial ryegrass in France. The variograms modeled for heading date and summer growth were then used to map the occurrence of these traits in France. These two studies show that the variogram can be used successfully to map the population of different plant species along with their traits in different regions of the globe.

Variograms have also been applied to the study of pathogens or viruses found in different plant species in order to develop a method of treatment or avoidance. Chellemi et al. (1988) studied the use of variogram in evaluating the spatial patterns of soil-borne plant pathogens. The modeled variograms indicated that the aggregation of inoculum was not homogeneous, but varied with direction, a concept known as anisotropy (see section 6.1.2 for a more complete description of anisotropy). Lecoustre et al. (1989) found a similar

result for the spatial pattern of African cassava mosaic virus. This anisotropy was attributed to the prevailing wind direction. In a study by Schotzko and Smith (1991), the modeled variogram for the spatial distribution of Russian wheat aphid revealed that the distributions of this pathogen on wheat and oats are unique. Also, the variograms illustrated the notion that the distributions varied as the population and dispersion changed.

The spatial distribution patterns of insect pathogens have also been examined using variograms. In a study by Schotzko and O'Keeffe (1989), the spatial structures of *L. hesperus* adults and nymphs in lentil fields were modeled using variograms. As in the previous study, the variograms revealed unique structures for both types of pathogens. These distribution patterns varied as the season progressed and population densities changed. Midgarden et al. (1993) applied the variogram in a similar fashion to characterize the spatial pattern of western corn rootworm adults. The application of the variogram to the analysis of pathogens is predominant in the biological literature and has met with some great success.

The third biological discipline that have used the variogram with some success is the modeling and mapping of marine and terrestrial animal populations. The analysis of the spatial distribution of fish stocks and other aquatic animals has been extensively studied using variograms. One of the first studies to examine the applicability of geostatistics in fish surveys was Guillard et al. (1992). This study provided a preliminary look at the application of the variogram in fish stocks. Other studies followed that also used survey data to model the spatial distribution of certain fish and brachyuran species (Pelletier and Parma, 1994; Petitgas, 1993; González-Gurriarán et al., 1993).

A number of studies have applied the variogram method to examine the spatial variability of terrestrial animal populations. Kemp et al. (1989) modeled

the distribution of rangeland grasshopper species. These variograms for the patterns of dispersion were then used to map the spatial variability and associated risk hazard of these species. Another study utilized variograms and kriging to model and map the population densities of gypsy moth species (Liebhold et al., 1991). As with the previous study, these patterns could be used to assess the risk hazard of these species.

In the study by Villard and Maurer (1996) the variogram was used to examine the spatial pattern of two species of wood warblers. This study is an excellent example of the use of the variogram in biology. The wood warbler species have been declining in the continental US. Villard and Maurer (1996) used geostatistics to analyze the spatial and temporal patterns of population change in these species. This study is a prime example at the use of geostatistics to study and monitor the declining species in all parts of the world.

The application of the variogram to biological fields have flourished in the recent years and is a good illustration of the potential uses of this method to other disciplines. As seen in the last examples, the variogram can be utilized beyond the modeling of the spatial patterns of biological populations; it can also be used to examine the risk assessment and population changes in declining species, both aquatic and terrestrial.

HYDROLOGY

In the recent decade, variograms have been applied to the field of hydrology to examine the spatial variability of precipitation and evapotranspiration in a number of different terrain types. Burn and Ray (1989) was one of the first studies to apply the variogram to snow data. This study presented a modeling framework that was used to estimate the water equivalent of a basin's snow pack from snow course data in Manitoba. The variogram was

a major component in this framework. The result of this study indicated that while the study area was quite large, findings were skewed based on this fact. However, the authors concluded that the variogram and kriging methods could be successfully applied to the modeling and mapping of snow pack data. Another study by Hosang and Dettwiler (1991) explore the possibility of the use of variograms, plus regression analysis, to model the spatial distribution of water equivalent. This study used a much smaller catchment area, compared to the study by Burn and Ray (1989). Again, the results indicated that the variogram and kriging can be used effectively to map the snow water equivalence.

Liquid precipitation distribution has also been examined using variograms. de Montmollin et al. (1980) applied the variogram to evaluate precipitation distribution over a large area in western Switzerland. This study examined the elevation and precipitation relationship and used the variogram to estimate and map precipitation using elevation data. A similar study, conducted by Philips et al. (1992) used variogram analysis to model the spatial distribution patterns of precipitation across mountainous terrain. These models could then be used in agricultural and natural resource management models to estimate other hydrological processes and soil moisture. As with the previous study, the effects of elevation and topography were incorporated in the modeling of precipitation estimates.

Apart from precipitation, the spatial distribution estimates of evapotranspiration has also been modeled using the variogram. Martinez-Cob and Cuenca (1992) modeled the spatial correlation between evapotranspiration and elevation using multivariate geostatistics, namely the cross-variograms. Experimental variograms, both cross- and direct-variograms were adequate and accounted for a majority of the variance. This reveals that the variogram

method is accurate for the modeling of evapotranspiration. The use of the variogram modeling in hydrology to model various hydrological processes is recent and the literature indicates that this method can be accurately applied to other processes.

REMOTE SENSING

One of the most recent and promising applications of the variograms is in the field of remote sensing. In this field, the variogram represents the spatial dependence among pixel values. Variograms have been applied to a number of remote sensing products, from aerial photos to satellite images. Sommerfeld et al. (1994) compared the variograms for snow melt flow calculated from data obtained using lysimeters on slopes in a lake basin to surface brightness obtained from aerial photos. Both variograms calculated from lysimeter and aerial photo data suggest the spatial pattern of meltwater flow was approximately 6 m. This result indicates that aerial photos can be used to model the spatial variability of a certain phenomenon using variograms.

The variogram method has also been applied to study the spatial pattern of several terrain features using satellite imagery. Cohen et al. (1990) evaluated the potential of using variograms to model and distinguish stands having different canopy structures. This study used SPOT HRV panchromatic and Landsat TM data of the pacific northwest region of the US. The researchers concluded that while variograms may provide fairly accurate estimates of stand structure parameters, they can not evaluate the patterns in stand structure.

Woodcock et al (1988) had better results using remotely sensed images for three different kinds of environment: forest, agricultural and urban/suburban. The data was acquired from the Thematic Mapper or Thematic Mapper Simulator. Variograms were able to model the different spatial patterns

characteristic of the different environment type (i.e. the periodicity caused by the crop rows in agricultural fields).

In another study by Curran (1988), the variogram was shown to adequately model the spatial variability of a number of features derived from airborne multispectral scanner imagery of northern England. Despite the somewhat contradictory findings, the application of variograms to remote sensing in the literature illustrates the potential in this field for this method to model the spatial patterns on the earth. This application will save considerable time and expense. It will also allow researchers to examine the spatial patterns of different variables that may not have been examined otherwise due to a number of factors.

3.3.2 Grey-level co-occurrence matrix.

Grey-level co-occurrence matrices have been shown in the literature to accurately segregate sea ice classes within a radar image. This section of Chapter 3 will examine the past uses of the GLCM method, both in the field of sea ice classification as well as terrain classification from remotely sensed data.

In the past decade, the classification of sea ice types from satellite radar imagery using the GLCM method has received considerable attention by a number of researchers. One of the earliest studies looked at developing a digital procedure to identify the ice types in SAR imagery in an attempt to automate the segmentation of SAR data using texture analysis (Holmes et al, 1984). They concluded that two types of ice, first-year and multiyear sea ice can be segmented based only on texture without *a priori* knowledge of the location of the ice. This study however only incorporated one texture statistic in the discrimination analysis resulting in less than acceptable overall accuracies.

The use of a single texture measure was due to the computational and technological costs involved.

With the development of computing technology, as well as the advancement in the knowledge on GLCMs, the discrimination of ice types has involved a number of texture measures applied to a number of SAR images. Two of the main researchers in GLCM use in ice classification, D.G. Barber and E.F. LeDrew, used a combination of five texture measures to classify ice type (Barber and LeDrew, 1989; 1991; Barber et al. 1991). They found that for a complete discrimination of ice types, all five measures calculated at contrasting orientations and interpixel sampling distances is needed (Barber and LeDrew, 1989). However, this would not be feasible for an automated ice classification scenario, due to the large time requirement needed to compute the statistics. A reduction in computation time will result in a slight decrease in classification accuracy. Barber et al. (1991) found that with a certain pair of measures, the accuracies were in excess of 80%. The authors noted that these accuracies were 'universal' due to the limitations of the two images used (Barber et al.. 1991). Shokr (1989; 1991) found similar results, but suggested that the combination of gray tone and texture may be more accurate for the classification. Therefore GLCMs have a great potential for the discrimination of ice types.

Other research disputes the claim of GLCMs to be the best method for ice classification. One study by Nystuen and Garcia (1992) found that first-order measures alone (i.e. variance, range, mean, standard deviation, etc.) were at least as effective in the classification of ice types as second-order GLCM statistics. This finding supported the conclusions of other studies (Shuchman et al., 1989; Holt et al., 1989).

While a great deal of research has been conducted on the development

of a sea ice classification algorithm based on the GLCM, the classification of terrain types from radar images using this method has also flourished in the recent past. This application was one of the earliest in the literature. Weszka et al. (1976) compared the GLCM method to two other methods for the classification of two sets of terrain samples. They concluded that the grey level method (i.e. GLCM) perform as well or better than the other methods studied (Weszka et al., 1976). Ulaby et al. (1986) found similar results, suggesting that second-order spatial statistics give better results than first-order statistics for the classification of land-use, with classification accuracies in excess of 80%. In the same study, the tonal measures out performed texture measures in the classification of forest-cover. GLCMs have been used with great success in the classification of not only sea ice types but also terrain features and types.

This chapter has provided a general background on the theory and methodology used in this thesis. The first section of this chapter examined the physics behind the snow distribution mechanisms operating over sea ice. A preliminary examination of the seasonal precipitation patterns in the Resolute, NWT area was included in this section. The next section provided a critical examination of previous models used in the literature to estimate snow distribution, mainly on terrestrial surfaces. Both computer-based and empirical models were examined. The final section provided a background to the utilization of two methods essential to this thesis, the geostatistical technique and the grey-level co-occurrence matrix method. The use of these methods in other disciplines was examined to illustrate the suitability of these methods to the present study. The next chapter examines the data acquistion methods used in the field experiments.

CHAPTER 4:

DATA ACQUISITION.

This chapter will examine the field research techniques utilized by this author in the Arctic during the 1995 and 1996 sampling campaigns. Following this description, the remotely sensed data used in objective two will be examined and a brief background regarding the acquisition of the data will be introduced.

4.1 FIELD EXPERIMENTS.

Data utilized to study and model the snow distribution patterns over sea ice has been acquired during two years of Arctic research carried out by this author. In 1995, research was carried out as part of the Seasonal Sea Ice Monitoring and Modeling Site (SIMMS) field project. The following year, the research was part of the Collaborative-Interdisciplinary Cryospheric Experiment (C-ICE). This section of the thesis will give brief descriptions of both these projects, and the methodology used to collect the relevant data. Also, additional data that has been provided by other sources will be described in this section of the thesis.

4.1.1 SIMMS 1995 Field Experiment.

Data for this thesis was initially collected during the SIMMS field experiment conducted in the spring of 1995. SIMMS was a multiyear, interdisciplinary research project initiated in 1990 by the Earth Observation Laboratory (EOL) of the Institute for Space and Terrestrial Science (ISTS/University of Waterloo). This field experiment primarily conducted research on the sea ice located in the Eastern Canadian High Arctic. Research was conducted from 1990 to 1995 during the spring seasons. The primary objective of the SIMMS field experiment was to characterize the physical and energetic processes operating within the marine cryosphere with each individual project examining a different aspect of the process (Barber et al., 1995a). At the present time, there is a large void in the knowledge and understanding of the systems and feedbacks occurring in the polar regions and how these processes affect the climate and hydrology on the polar scale as well as on a global scale. This project provided the surface data needed to develop an understanding of the processes operating on an icescape. In 1995, the SIMMS field experiment was located just east of Lowther Island on the sea ice located in Barrow Strait (Figure 4.1). The base camp was located at approximately 74°35'N and 97°23'W.

During the 1995 field experiment, snow thickness data was collected over both multiyear and first-year sea ice in order to model the snow distribution patterns. The method used to collect this data was based on a stratified random sampling scheme. This method of data collection has been extensively used by researchers studying the snow distribution patterns over terrestrial surfaces and is considered the best method available to collect snow depth data (Blöschl et al., 1991; Elder et al., 1991; Adams, 1976; Steffuhn and Dyck, 1973). In this

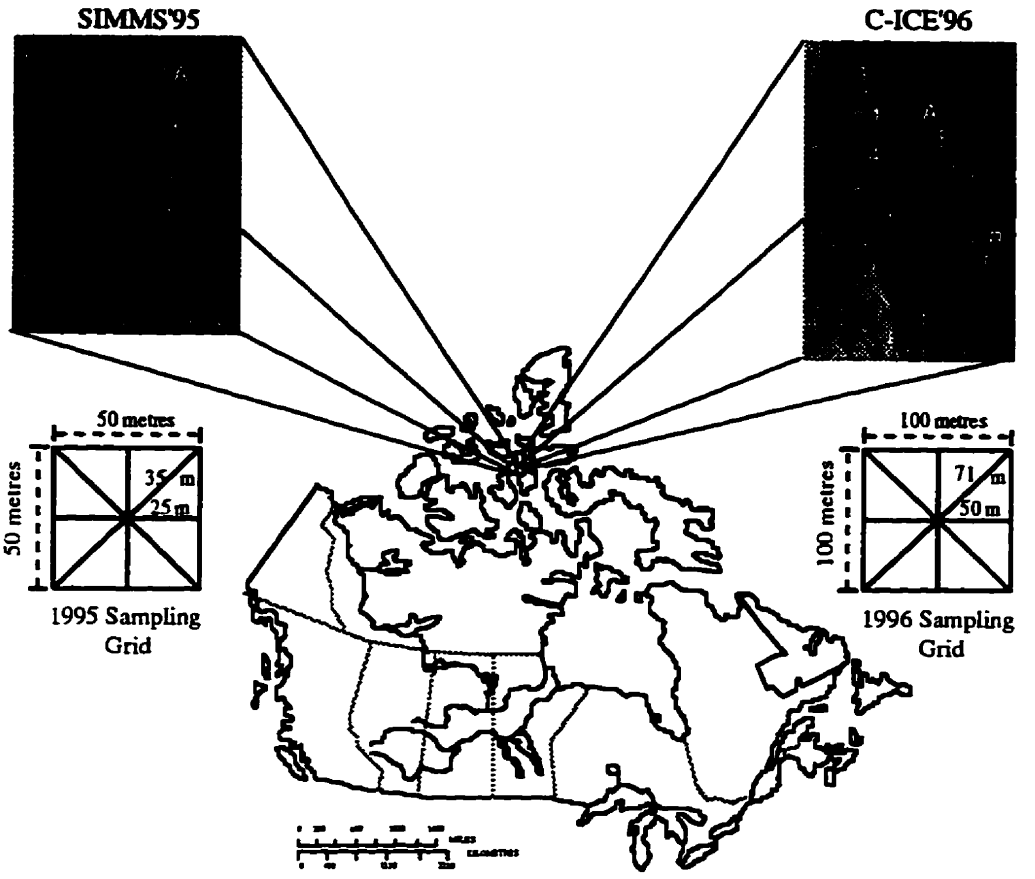

Figure 4.1. Location of the SIMMS'95 and C-ICE'96 field experiments and sampling sites. Inserts illustrate the sampling grids used during the two field experiments.

type of sampling method, the population is considered heterogeneous and is divided into a number of distinct homogeneous sub-populations. This separation is based on one or a combination of variables. Following this stratification, each stratum can be sampled using a simple random sampling scheme, where specific sites can be randomly selected within each stratum. The population for this field experiment was comprised of the snow covered sea ice of Barrow Strait. This population is divided into strata or sub-populations based on the type of sea ice that makes up each unit (i.e. first-year, and multiyear).

A stratified sampling regime makes the assumption that "snow variability is distributed somewhat uniformly throughout each stratum (Steffuhn and Dyck, 1973). This is a reasonable assumption for the Arctic region because the processes operating within each ice type, in terms of snow distribution (i.e. wind speed and direction), would be similar. Elder et al. (1991) states that a stratified random sampling scheme is favored over a random sample because a gain in precision is obtained when a population varies spatially and a stratified random sample is used. This relationship introduces into the sample, the relevant sources of variability that occur in the population and thus reduces or eliminates any sources of sampling error (Singleton et al., 1993). Also, by stratifying the area, the number of samples required is reduced.

During SIMMS'95, three sites were sampled on the first-year ice, and one site on the multiyear sea ice during a period between April 28 and May 7 (day 118 to day 127). Figure 4.1 shows the locations of each site, and Table 4.1 lists the latitude and longitude co-ordinates of the sampling sites, as well as the dates of acquisition. These sites were located a sufficient distance (greater than 1 km) away from the boundary between the two ice types. This was done in order to remove any affects the other ice type may exhibit on the one under

Table 4.1. Co-ordinates of the snow sites sampled during the 1995 SIMMS field program. The acronyms under ice type, FYI and MYI represent first-year and multiyear sea ice, respectively.

Site No.	Ice Type	Co-ordinates	Date Completed
1	FYI	N 74°34'36.7" W 96°49'28.0"	April 28, 1995
2	FYI	N 74°35'41.6" W 96°49'39.3"	May 6, 1995
3	MYI	N 74°36'53.4" W 96°46'16.4"	May 7, 1995
4	FYI	N 74°32'42.5" W 96°49'39.6"	May 7, 1995

study, for example causing a change in wind direction and speed, during a storm event. Each site was approximately 50 m x 50 m in area.

At each site snow depth and sea ice elevation, as well as the co-ordinates of the area were measured. Snow depth and ice elevation measurements were carried out in eight directions (north, south, east, west, northeast, northwest, southeast, southwest) each originating from a center point (Figure 4.1). The transects for the cardinal directions (north, south, east, west) were approximately 25 m in length, while the other directions were sampled for 35 m. Snow depth was measured using a snow probe that was graduated in increments of 5 cm, with an uncertainty of 1 cm. These measurements were taken every 2 m, originating in the center of the sampling area. Ice thickness was measured at the center of the sampling grid by manually drilling through the ice. Elevation of the ice surface was also measured at a sampling distance of 2 m. These measurements began at 5 m from the center of the sampling area because of visual limitations resulting from the use of the transit. Table 4.2 gives a complete list of the variables measured along with the instruments used to measure the variables.

Table 4.2. List of the variables measured at the snow sampling sites, including the instruments used to collect the data. Also, the climatology variables collected at various meteorological stations within the area are listed along with the instruments used to collect these variables.

	Variable	Units	Instrument
Snow Catchment variables	snow depth	cm	graduated snow probe
	snow density	g • cm-3	100 cc snow sampler
	ice thickness	cm	auger
	elevation	cm	transit, ruler
	GPS location		Trimble Scout Master GPS
Climatology variables	air temperature	°C	thermocouple sensors
	wind speed	ms-1	anemometers
	wind direction	°	microvane

The ice surface topography was determined using a complex method. First, the ice underneath the tripod that was positioned in the center of the sampling grid and used to establish the directions of sampling, was manually drilled and measured with a tape measure. This value, called the tripod thickness in this chapter, was used as a reference value. Due to the time and logistical constraints, the ice could not be directly measured at every sampling point. A more indirect method was used. The height of the transit above the snow surface was measured and the snow and ice thickness values measured underneath the tripod were added to this value. This value is called the tripod value and varies from site to site. At each sampling point, the snow depth as well as the height of this point (above the snow surface) relative to the tripod was measured. This latter value was determined using a transit and ruler positioned at the top of the surface at each sampling point. The ice thickness underneath the sampling point was determined by subtracting the value at the sampling point (snow thickness + height) from the tripod value. Figure 4.2 gives a schematic that represents the methodology used to determine the ice surface roughness. Therefore, at each sampling point a value that represents the height of the ice above a reference value is obtained. These values can then be compared and surface topography can be determined.

The method described above makes the assumption that the bottom of the ice at each site is level. Generally, this is not the case, but for the purpose of this study this assumption is acceptable. The bottom topography of the ice is of no importance to the distribution of snow on the top of the ice layer. The ice thickness values noted throughout this chapter, except for the values measured under the tripod are thus relative, not absolute terms, and are not intended to quantify the ice thickness.

Ice surface topography measurements were not completed for the first-

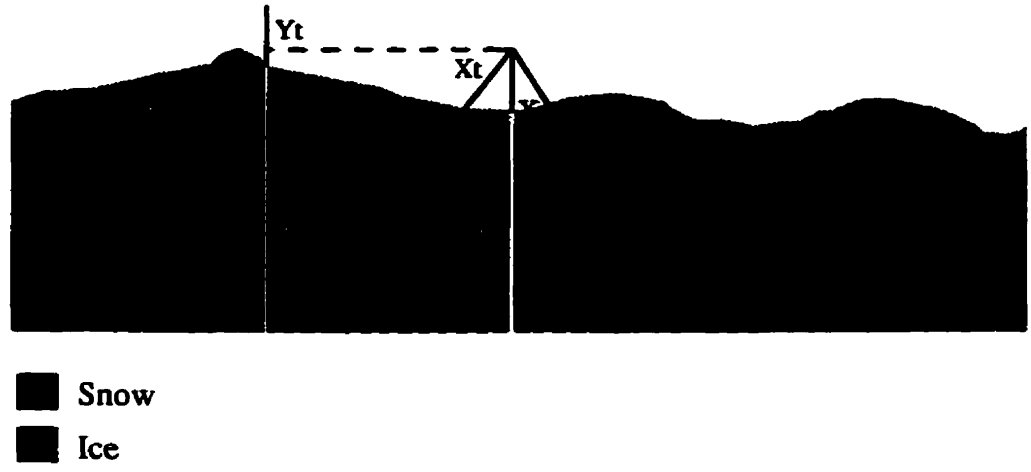

Figure 4.2. Schematic illustrating method for obtaining ice surface roughness values for each sampling point. Xt is the height of the tripod, Xs and Ys are the snow thicknesses for the center point and the sampling point respectively, Xi and Yi are the ice thicknesses for the center point and the sampling point respectively, and Yt is the height of the sampling point relative to the transit.

year ice sites. For this type of sea ice, it was assumed that the ice surface topography did not vary within the sampling grids, but rather remained relatively uniform. Therefore, the ice thickness under the sampling points for these grids was assumed to be the same to that underneath the tripod.

Other variables collected during the SIMMS field experiments by other researchers will be utilized in this thesis. These variables include atmospheric data such as precipitation, wind speed, and wind direction and were collected at meteorological sites located in close proximity to the sampling grid, as well as the meteorological station located at Resolute Bay. (For a more complete description of how these variables were collected, refer to Derksen, 1995.) Table 4.2 also includes a list of these variables including the measurement units and the instruments used to collect the data.

4.1.2 C-ICE 1996 Field Experiment.

The primary data for this thesis was collected during the Collaborative Interdisciplinary Cryospheric Experiment (C-ICE). C-ICE is a multi-disciplinary research project developed in 1996 by the Center for Earth Observation Science (CEOS) at the University of Manitoba. Its primary research mandate is to characterize the physical and geophysical properties and processes that occur due to the atmospheric-cryospheric-hydrospheric interactions. As with the SIMMS experiment, there are a number of different research projects occurring under the umbrella of C-ICE. Each individual project shares the primary research mandate as their underlying goals. In 1996, research was conducted on the sea ice located in Wellington Channel, northeast of Resolute Bay, Northwest Territories. Figure 4.1 shows the location of the study area. The base camp for C-ICE'96 was located at approximately 74°04'N and 93°23'W.

A similar sampling method was utilized by this researcher during the spring of 1996, however certain aspects of the procedure were modified to give a more accurate picture of the snow distribution patterns. As in 1995, a stratified random sampling scheme was adopted to select the sampling sites. During 1996, five FYI sites, four MYI sites, and two RI sites were chosen and studied from May 12 to May 28 (day 133 to day 149). The locations of these sites are shown in Figure 4.1. Table 4.3 lists the latitude and longitude co-ordinates of the specific sites. Each sampling site was enlarged, compared to 1995, to include an area of 100 m x 100 m (Figure 4.1). The transects for the cardinal directions were sampled for approximately 50 m, while the transects for the other directions were approximately 71 m in length. The sampling method was identical, measuring the variables in eight directions, however the distance between sampling points was reduced to 1 m due to the snow drift conditions in

Table 4.3. The co-ordinates for the sites sampled during the 1996 C-ICE field program. The acronyms FYI , MYI and RI, represent first-year, multiyear, and rubble sea ice, respectively.

Site No.	Ice Type	Co-ordinates	Date Completed
1	FYI	N 75°04'16.9" W 93°22'28.5"	May 10, 1996
2	MYI	N 75°06'48.8" W 93°22'33.8"	May 12, 1996
3	FYI	N 75°05'43.7" W 93°24'08.8"	May 13, 1996
4	RI	N 75°05'27.9" W 93°19'24.9"	May 14, 1996
5	FYI	N 75°03'39.7" W 93°23'31.4"	May 17, 1996
6	MYI	N 75°03'38.9" W 93°17'18.6"	May 18, 1996
7	FYI	N 75°04'43.0" W 93°24'18.1"	May 22, 1996
8	MYI	N 75°04'20.8" W 93°17'00.8"	May 24, 1996
9	MYI	N 75°05'00.3" W 93°18'11.9"	May 25, 1996
10	RI	N 75°03'21.0" W 93°16'06.1"	May 27, 1996
11	FYI	N 74°58'52.6" W 93°23'10.8"	May 28, 1996

this area during this time period. Elevation measurements were taken at every 1 m and began at 3 m from the tripod, again due to visual limitations. All other aspects of the data collection were similar to the 1995 method.

4.2 REMOTELY SENSED DATA.

The remotely sensed data, used primarily in the second objective of this thesis, consists of synthetic aperture radar (SAR) images acquired from the European Space Agency's (ESA) European Remote Sensing (ERS) satellites. The ESA's remote sensing program consisted of two satellites, both containing

a set of active microwave remote sensing instruments, including SAR. The first satellite was launched in July of 1991, followed by the launch of the second satellite in April of 1995. At present, only ERS-2 is operational. The 1995 and 1996 SAR data set consisted of images taken using ERS-1.

4.2.1 Description of Synthetic Aperture Radar.

SAR is the preferred remote sensing instrument available to study the polar regions as well as the world's oceans. Active microwave instruments, such as SAR, remotely sense the earth's surface by sending out a pulse and observing how these pulse signals interact with various objects on the ground. SAR is an imaging system because it converts the backscatter energy into digital values that can be displayed as an image. Because the instrument senses the radar backscatter which it had originally sent out, SAR is not dependent on sunlight conditions and is thus capable of imaging the earth during the polar night. The wavelengths used by SAR instruments pass relatively unaffected through cloud cover, thus it is not dependent on the absence of cloud cover for imaging. These two properties of active microwave instruments, in particular SAR, makes this instrument able to image the earth's surface regardless of the weather conditions.

The amount of backscatter observed by the antenna of the SAR instrument depends primarily on the dielectric properties of the surface, as well as the SAR system parameters. Dry snow, common in the Arctic, has temperatures less than 0°C and thus no free water is present in the snow pack. This type of snow is composed of a combination of air and ice particles; each having a different dielectric value associated with it. The dielectric constant defines the ability of a substance to conduct electrical energy. Each substance

on earth will have a dielectric value association with it, however the value for a particular material is specific for the wavelength used in remote sensing.

Because of the heterogeneous nature of both snow and sea ice, a complex dielectric model is required. This model will incorporate all the different particles in defining the dielectric value for the medium. Air has a constant value of one, while the dielectric constant for ice is higher at approximately 3.2. The combination of these two constant values, depending on the proportion of each in the snow pack, results in the dry snow pack having a complex dielectric constant between 1.2 and 2.0 for snow densities between 0.1 and 0.5 g/cm^3 (Hallikainen and Ulaby, 1986). This constant value will affect the microwave response properties of snow covered sea ice.

The dielectric properties of sea ice is a function of the volumes of different water phases present, as well as the relative proportion of brine. As with snow, the proportions of ice and air determine the dielectric constant. The more air present, the lower the constant value. However, sea ice is also composed of brine, a concentration of salts. While the relative proportion or brine to water and air is low, the high dielectric value for brine (approximately 80) significantly influences the dielectric constant for sea ice. For saline first-year sea ice, Kovacs and Morey (1978) reported a typical dielectric value of 4.6. As the ice ages and the brine is expelled during the melt seasons, the dielectric value decreases to 3.7 (Kovacs and Morey, 1978). The dielectric constant value for sea ice is a combination of the proportions of ice, air and most importantly brine.

The backscatter return from an area composed of snow covered sea ice is defined by the scattering mixing model, which is the sum of surface scattering along with volume scattering within the snow pack and ice layer. The fresnel reflection coefficient is a measure of the amount of radiation that is reflected at the interface between two mediums, and is used to quantify the dielectric

dissimilarity between two surfaces. It is computed as a complex ratio of the dielectric properties of the two materials creating the interface. Because of the small dissimilarity between the air and snow, the emitted microwave energy from the SAR instrument will not 'see' a boundary and will not distinguish between the two materials resulting in no scattering. Thus, surface scattering at the air/snow interface is negligible in the Arctic because for dry snow, the dielectric dissimilarity between the air and snow is small. In fact, the only time snow has an impact on the radar return is during the late spring/summer period when the snow becomes wet, or free water is present in the snow layer. At the boundary between the snow and ice, the dielectric mismatch between these materials is quite large, resulting in surface scattering. The occurrence of surface scattering is dependent on the dielectric properties of the materials composing the interface.

The primary determinant for the amount of surface scattering is surface roughness. Smooth surfaces will reflect most of the incoming signal at the same angle as the incidence angle away from the radar antenna, according to Snell's law. This reflection will diminish the radar return and will cause the specific feature to appear dark on a SAR image. For instance, a very smooth first-year sea ice area is dark on SAR imagery because it reflects the radar signal away from the satellite. The smoother the ice, or surface, the darker the ice will appear. For a surface to be considered smooth, the rayleigh criterion must be met. This criterion is defined as:

$$R = \frac{\lambda}{8\cos\theta} \qquad (4.1)$$

where λ is the wavelength and θ is the incidence angle. It states that the surface variation in the direction of the incoming radar must be less than 1/8 the

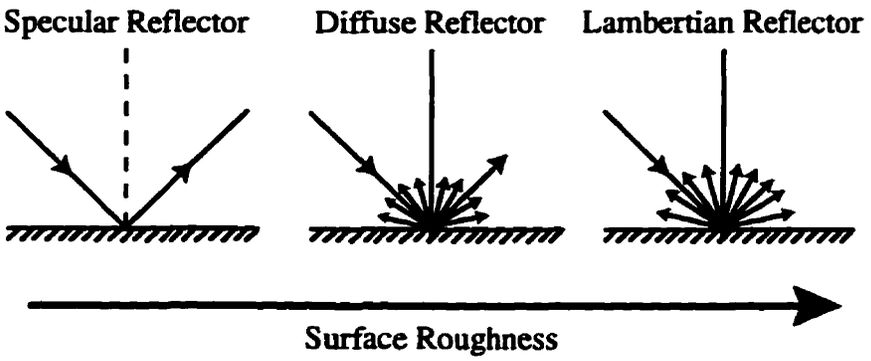

Figure 4.3. Schematic illustrating the reflection of incoming radiation as the surface roughness varies. For a smooth surface, the reflection will be specular, while for a rougher surface lambertian reflection dominates.

value of the radar's wavelength to be considered smooth. Such a surface will act as a specular reflector (Figure 4.3). As the surface variation becomes greater than 1/8 the wavelength, the surface becomes lighter on the SAR image. A rougher surface, such as rubble ice, will cause the radar signal to be reflected in all directions and returns a significant portion of the incident energy to the radar antenna, acting as a diffuse reflector (Figure 4.3). The incident energy may also bounce again off other objects (i.e. other ice pieces) and thereby redirect the signal back towards the satellite. The amount of backscatter received by the SAR is predominantly determined by the type of surface scattering occurring.

Volume scattering in the snow and ice packs strongly determine the amount of backscatter. Volume scattering coefficients used to quantify the volume scattering in a snow and ice volume, are based on a presumed dielectric mixing model. This coefficient is dependent on the number density (or the number of scatters per unit volume) and the ice and water inclusion scattering components. In short, the incoming microwave energy is strongly scattered by the snow and water particles in the snow volume and the ice and

water particles, along with brine inclusions, in the ice pack. This scattering is dependent on the size of the crystals relative to the wavelength of the instrument. In sea ice, the volume scattering is dependent on the geometric form and distribution of the ice crystals (Morey et al., 1984). As the wavelength of the signal approaches the size of the particles, the scattering will increase. Scattering decreases if the wavelength is greater than the crystal size (Heacock and Lewis, 1989). This scattering is further complicated in multiyear sea ice by the presence of enlarged pockets. As the ice melts in the previous melt seasons, the brine pockets are replaced with air/gas pockets. If these pockets are on scales similar to those of the emitted wavelengths, they can act as volume scatters. Therefore, the scattering of the incoming energy from SAR is a combination of volume scattering of the snow layer, surface scattering at the snow/ice interface and the volume scattering within the ice layer. The combination of the various components of scattering will produce a specific amount of backscatter that is unique to the surface conditions.

Scattering on sea ice is primarily a function of the ice type. Figure 4.4 illustrates the difference in scattering for the three ice types studied in this thesis. First-year sea ice is more saline than multiyear sea ice. This highly saline material results in a high loss of incoming energy at the surface layers. This means that most of the incoming radar pulse is scattered at the surface, with little penetration. Thus, for first-year sea ice, the backscatter of the radar pulse is controlled primarily by the roughness of the upper ice surface, with a limited contribution by volume scattering. On the other hand, multiyear sea ice has a low brine concentration due to the flushing of the brine in the previous melt season. This low brine in the upper layers of the sea ice results in a much greater penetration of the radar signal. The radar signal can thus interact with the internal inhomogeneities present in the sea ice, resulting in

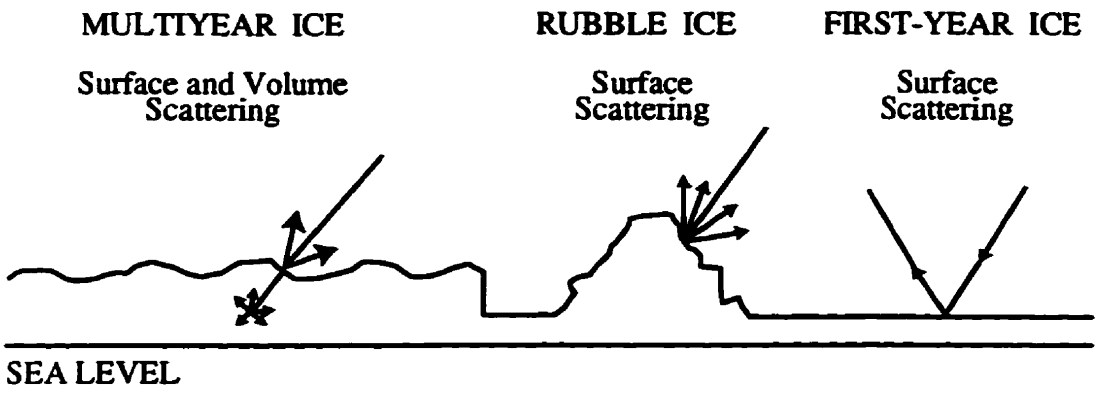

Figure 4.4. Schematic showing the interactions between radar and different types of sea ice. For multi-year sea ice, the scattering involves both surface and volume, while for rubble and first-year sea ice scattering is predominantly at the surface (modified from Massom, 1991).

a greater amount of volume scattering. The scattering in multiyear sea ice is influenced by both surface and volume scattering.

Various system parameters associated with the SAR instrument being used also affect the amount of backscatter. These parameters include frequency, polarization and incidence angle (Barber et al., 1991). If the frequency of the system is decreased, the dielectric mismatch between surfaces is also decreased and the scattering from the snow pack will be small. Most of the scattering will occur at the snow/ice interface (Heacock and Lewis, 1989). Polarization of the system determine the plane orientation in which the antenna receives and transmits energy. In a study by Kong et al. (1980), the results indicated that the two like-polarized backscatter coefficients (horizontal-horizontal and vertical-vertical) respond differently with increasing snow depth. In active microwave systems, the incidence angle or view angle is very sensitive to changes because it furnishes both the illumination and backscattering angles (Heacock and Lewis, 1989). The scattering, both surface and volume, along

with the system parameters will determine the amount of active microwave return.

4.2.2 ERS Satellites.

The ERS satellites are devoted to remote sensing the earth's surface from a polar orbit. Both satellites have a sun-synchronous, polar, near-circular orbit, with a mean altitude of 785 km and an inclination of 98.5°. This orbit brings the satellites over the polar regions where they are able to 'see' most of the world as the earth rotates underneath. The repeat period for ERS-1 and ERS-2 is 35 days. During the C-ICE'96 field experiment, ERS-1 and ERS-2 were operating in a tandem phase, with ERS-2 24 hours behind. Overpass times for the C-ICE'96 field sites were approximately 22:30 local time for ascending passes and 13:30 local time for descending passes.

The SAR instruments carried on board both satellites operate at C-Band frequency with a polarization of vertical-vertical. The frequency of the SAR instrument is 5.3 GHz with a wavelength of 5.66 cm. The ERS SAR is a 10 m by 1 m rectangular antenna aligned with the satellite's flight path direction. The instrument looks to the side (20.4° to the right of nadir) and this enhances terrain variation observed by the satellite. The pulse sent out by the instrument decreases 15.5 MHz in frequency during the pulse duration. An area on the ground approximately the shape of an oval about 100 km long and several kilometers wide is illuminated by the pulse. The SAR antenna monitors the backscatter returns and the resulting composite signal is down converted to a more convenient frequency and compared to both the reference and quadrature functions.

Images obtained from ERS SAR were processed at the Alaska SAR

Facility (ASF) located at the Geophysical Institute, University of Alaska, Fairbanks. ASF can downlink SAR images for a region that is approximately a circle of radius 3000 km centered at Fairbanks. Each SAR image covers a 100 km x 100 km area. Full-resolution images processed at ASF have a pixel sampling of 12.5 m and a resolution of 30 m. Low resolution SAR images are generated from a simple 8x8 pixel average of the full resolution imagery. The pixel sampling of low-resolution images is 100 m with a resolution of 240 m.

This chapter discussed the surveying methods, as well as the remotely sensed imagery acquired during the two years of field experiments conducted by the author in the Canadian Arctic. The first two sections briefly introduced the two field experiments conducted in the spring of 1995 and 1996. As well, in these sections the methods used to collect the surface data, namely snow and ice thickness, were discussed. The following section briefly examined the science behind the synthetic aperture radar imagery used in the second objective of this thesis. The satellite used to acquire the data was also introduced in this section. The next chapter will conduct preliminary analysis on the data collected.

CHAPTER 5:

PRELIMINARY DATA ANALYSIS.

Chapter 5 of the thesis contains the preliminary analysis of the snow and ice thickness data obtained during the two field experiments. It examines the average snow depth and ice thickness for the different ice catchments. While this is important for the methods used, the snow distribution patterns are important for the understanding of the processes operating in the marine cryosphere. The first section discusses the physical characteristics of the ice catchments, including ice thickness and surface roughness of the various ice classes used in this study. Following the physical description of ice catchments, a preliminary data analysis of the snow depth values for different ice catchments is presented.

In this chapter, the sites sampled during the C-ICE'96 field program are abbreviated with the name of the ice type followed by the site number of that ice type. For instance, if the second first-year ice site sampled is being referred to, the site will be abbreviated FYI02. The same procedure was used for the SIMMS'95 sampling sites, however an 'S' was added at the beginning of the abbreviation to differentiate these sites from those sampled during the following year.

5.1 PHYSICAL DESCRIPTION OF ICE CATCHMENTS.

This section of Chapter 5 will briefly describe the physical characteristics (i.e. consolidation times, ice thickness and surface topography) of the three sea ice catchments used to study the snow distribution patterns. The icescape during both SIMMS'95 and C-ICE'96 field projects provided a large variety of ice types, all within close proximity to the base camp. In 1995, large multiyear floes were present along with first-year sea ice that consolidated at different times. All three ice types were present in 1996, with a large abundance of each type within a 20 km radius.

5.1.1 Consolidation of Sea Ice.

Consolidation times for first-year sea ice were derived from ice concentration composites produced for the eastern Arctic and supplied by the Canadian Ice Services (CIS) branch of the Atmospheric Environment Service (AES). For the purpose of this study, first-year sea ice is considered consolidated when the total concentration in the area of study is greater than or equal to five tenths. Weekly charts were studied and the consolidation date was determined by comparing the weekly charts.

The first-year sea ice present in both 1995 and 1996 consolidated at approximately similar times. In 1995, the first-year ice in Barrow Strait between Lowther and Griffith Islands consolidated between 13 October and 20 October, 1994. The following year, the composites indicated that the ice in Wellington Channel consolidated between 26 October and 02 November, 1995. Typically, the ice in the channel consolidates in a step-wise fashion, with the northern areas consolidating first. The major ridge running east-west in the 1995 field

experiment probably developed between 02 December 1994 and 01 January, 1995 according to the ice composites.

The areas of multiyear sea ice present in both years were composed of multiyear ice (ice that survived two or more years of melt) and second-year ice (ice that survived one melt season). The thicker multiyear ice sites were probably formed a number of years prior to sampling, being composed primarily of truly multiyear sea ice. The thinner ice sites were probably composed of second-year ice, thus consolidating the year prior to sampling, as was suggested by Barber et al. (1995b.). This ice must have been transported to the field sites from locations farther north, drifting down in the summer and early autumn months, prior to consolidation of first-year ice. These floes then would become entrapped within the first-year once consolidation began. The icescape of both sampling years was comprised of similar ice types, however the ice types were considerably different in terms of surface roughness.

5.1.2 Ice Surface Roughness.

Snow depth measurements were obtained on three different ice type catchments; first-year, multiyear, and rubble sea ice. First-year sea ice sites were composed of relatively flat, smooth sea ice that consolidated in the previous autumn season. Figure 5.1 illustrates the relatively uniform surface topography of an FYI site, including a photograph of the site, as well as measured transects of snow and ice thickness. The variances and standard deviations associated with the sites, and for the overall ice type, were small indicating the uniform topography associated with this ice catchment (Table 5.1). This topography would present a smooth surface to falling or drifting snow, which is not very effective in the entrainment of snow. The snow drifting forms

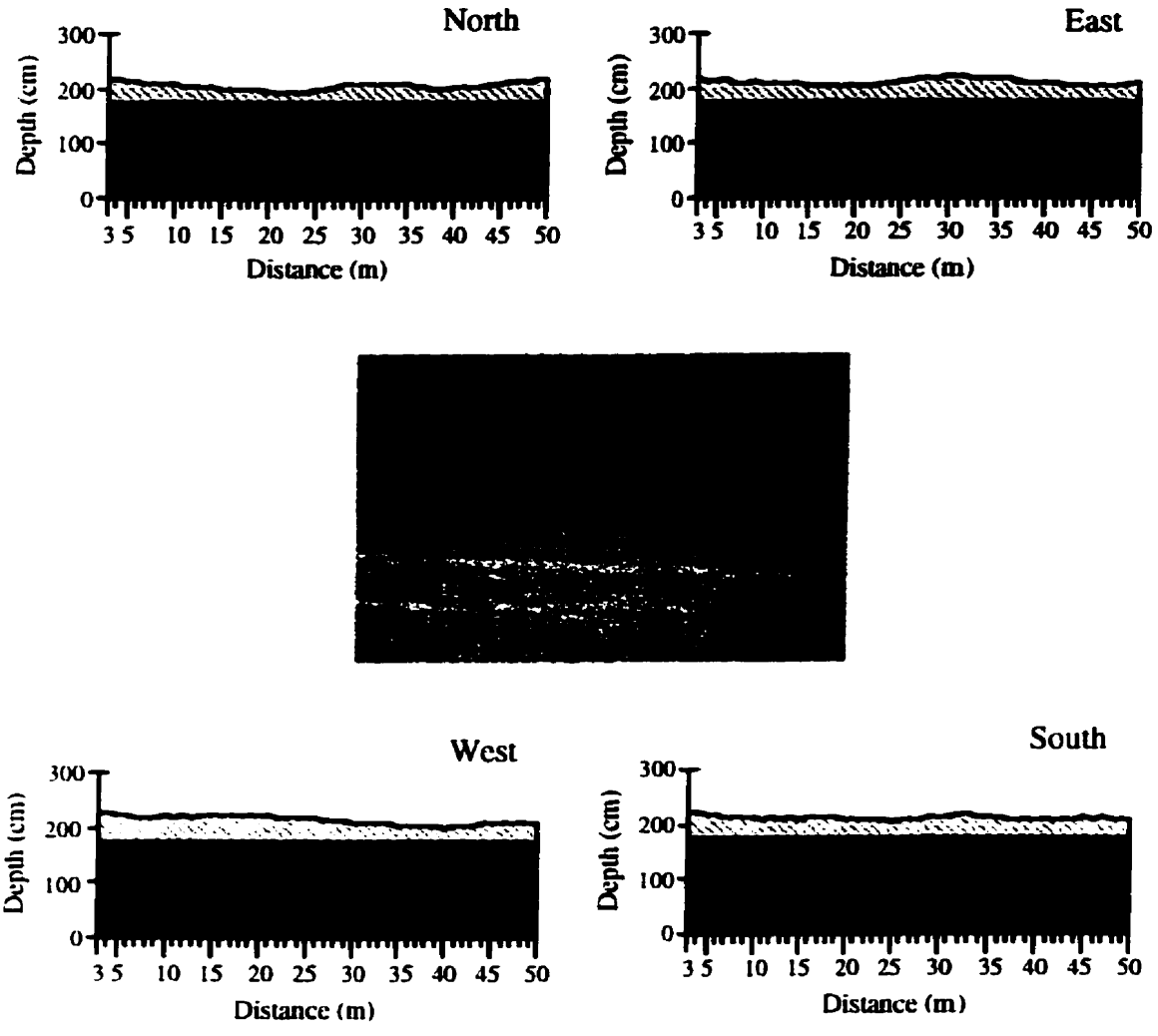

Figure 5.1. Transects for the four cardinal directions for a FYI site (FYI03), illustrating the variation in ice surface topography and the associated snow distribution. The photograph in the center shows the relatively smooth ice surface.

observed on first-year sea ice are comprised mainly of surface dunes and/or sastrugi.

Generally first-year sea ice is less than 200 cm in thickness. The three sites sampled in 1995, as well as three sites sampled in 1996 were composed of sea ice that was less than 200 cm thick, averaging approximately 178 cm (Table 5.1). The two other FYI sites sampled in 1996 had ice thicknesses

Table 5.1. Average tripod ice thicknesses for the three different ice catchments sampled during the two years of study.

	FYI	MYI	RI	SFYI	SMYI
mean (cm)	187.4	269.3	305.1	175.0	291.7
stnd. dev.	16.9	48.5	65.7	11.0	27.4
number of sites	5	4	2	3	1

Notes: i.Sites sampled during 1995 were differentiated from other sites by an addition of 'S' to the ice type.
ii. Stnd. dev. represents the standard deviation for the ice type.

measured under the tripod of over 200 cm. This could be explained by the fact that these sites had lower than average snow cover under the tripod, as well as throughout the sampling grid (Table A2). This lower snow cover would have provided less insulation for the consolidating ice during freeze-up, allowing more heat to be lost from the warmer ocean to the cooler atmosphere, and thus producing a thicker snow cover.

The second type of ice catchment studied in this thesis was comprised of multiyear sea ice. For the purposes of this study, multiyear sea ice is defined as sea ice that has a hummock/melt pond structure and has survived at least one melt season. Therefore, this ice catchment contained both second-year and multiyear types of sea ice.

Figure 5.2 illustrates the variation in the ice thickness in a multiyear sea ice site, including a photograph of a site on this catchment type and the snow and ice transects. Comparing this figure to Figure 5.1 for an FYI site, it is noticeable that the ice surface topography is more irregular in this ice catchment. This finding is further substantiated by an examination of the ice topography values.

The standard deviations of the ice surface topography values for the four

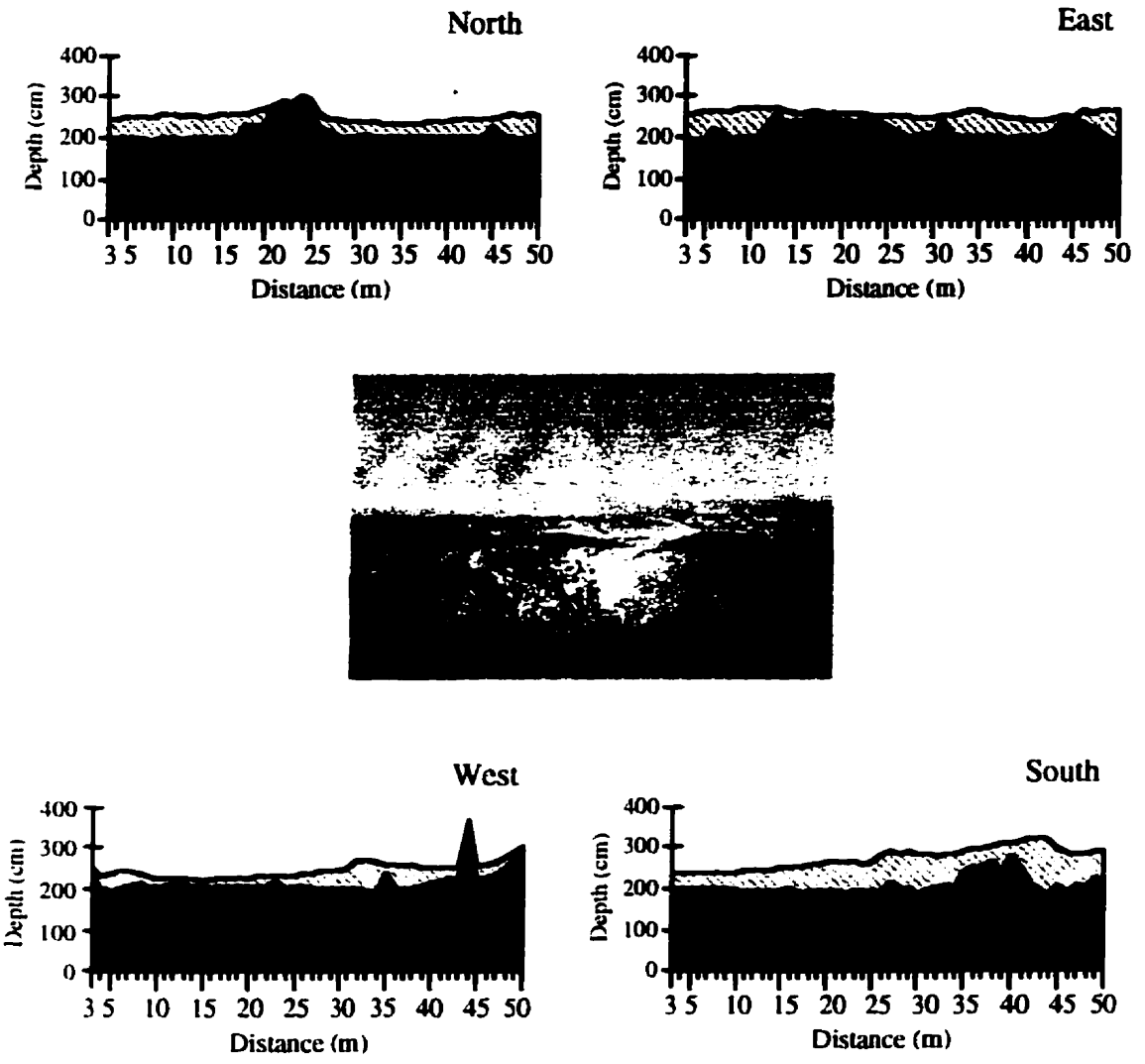

Figure 5.2. Transects for the four cardinal directions for an MYI site (MYI02), illustrating the variation in ice surface topography and the associated snow distribution. The photograph in the center shows the hummocky surface topography.

sites sampled in 1996 and the one site in 1995 indicate that the surface ice topography of the multiyear ice catchment was more irregular than first-year sea ice, as was expected (Table 5.2). The undulating topography formed by the alternating hummocks and melt ponds would produce a more irregular ice

Table 5.2. Average ice surface topography values for multiyear and rubble sea ice sites. Sites sampled during 1995 were differentiated from other sites by an addition of 'S' to the ice type. (Surface topography was not measured at the individual sampling points for first-year ice sites.)

	MYI	RI	SMYI
mean (cm)	269.3	305.1	291.7
standard deviation	48.5	65.7	27.4
minimum (cm)	178.2	163.5	250.0
maximum (cm)	464.0	492.5	374.5
number of samples	2433	931	116

surface and thus have implications on the snow distributions. Drifting snow was the principal snow forms observed on this ice catchment.

Multiyear sea ice is generally greater than 200 cm in thickness. The ice thickness measured under the tripod substantiated this claim (Table 5.3). However, one site (MYI02) had a tripod ice thickness less than 200 cm. This could have been due to the placement of the tripod. For this thesis, the ice thickness values were determined by measuring the ice under the melt ponds. Site MYI02 had melt ponds with a thick snow cover, therefore producing a thinner ice cover under the tripod.

From Table 5.2 it is evident that the multiyear ice catchment sites were more irregular in 1996 than in 1995. This irregularity was concluded from the larger standard deviation values in the multiyear sites sampled during 1996. Generally, the hummocks were larger and higher and the melt ponds deeper in 1996. This would suggest that sea ice growth was greater in the autumn season and/or ablation was less in the spring and summer periods. Both of these factors, either alone or in combination, would control the sea ice thickness observed during the sampling dates.

Table 5.3. Sea ice thickness measured in the center of the sampling grid under the tripod (tripod ice thickness).

	Ice Type	Site Number	Ice Thickness (cm)
SIMMS'95	FYI	1	175
		2	186
		3	165
	MYI	1	275
C-ICE'96	FYI	1	181
		2	206
		3	174
		4	203
		5	186
	MYI	1	266
		2	195
		3	246
		4	299
	RI	1	247
		2	400

Rubble sea ice is the final ice catchment type examined in this thesis. This ice catchment consisted of large uplifted ice pieces that extended beyond the surface of the snow. These large pieces were uplifted when two ice sheets consolidated and collided during ice drifting. The large ice pieces act as obstacles, being able to entrain snow and forming drifts around the pieces, in a similar way to that in which hummocks entrain snow in multiyear ice catchments. Figure 5.3 contains a photograph of a rubble ice site, as well as the transects of snow and ice, illustrating the irregular surface topography of this catchment type.

In this study, the rubble ice sites had a greater tripod ice thickness than both MYI and FYI catchments (Tables 5.1 and 5.3). This is to be expected because the collision of the ice sheets would produce the greater ice thicknesses. Ice would become piled up in the collision zone and would

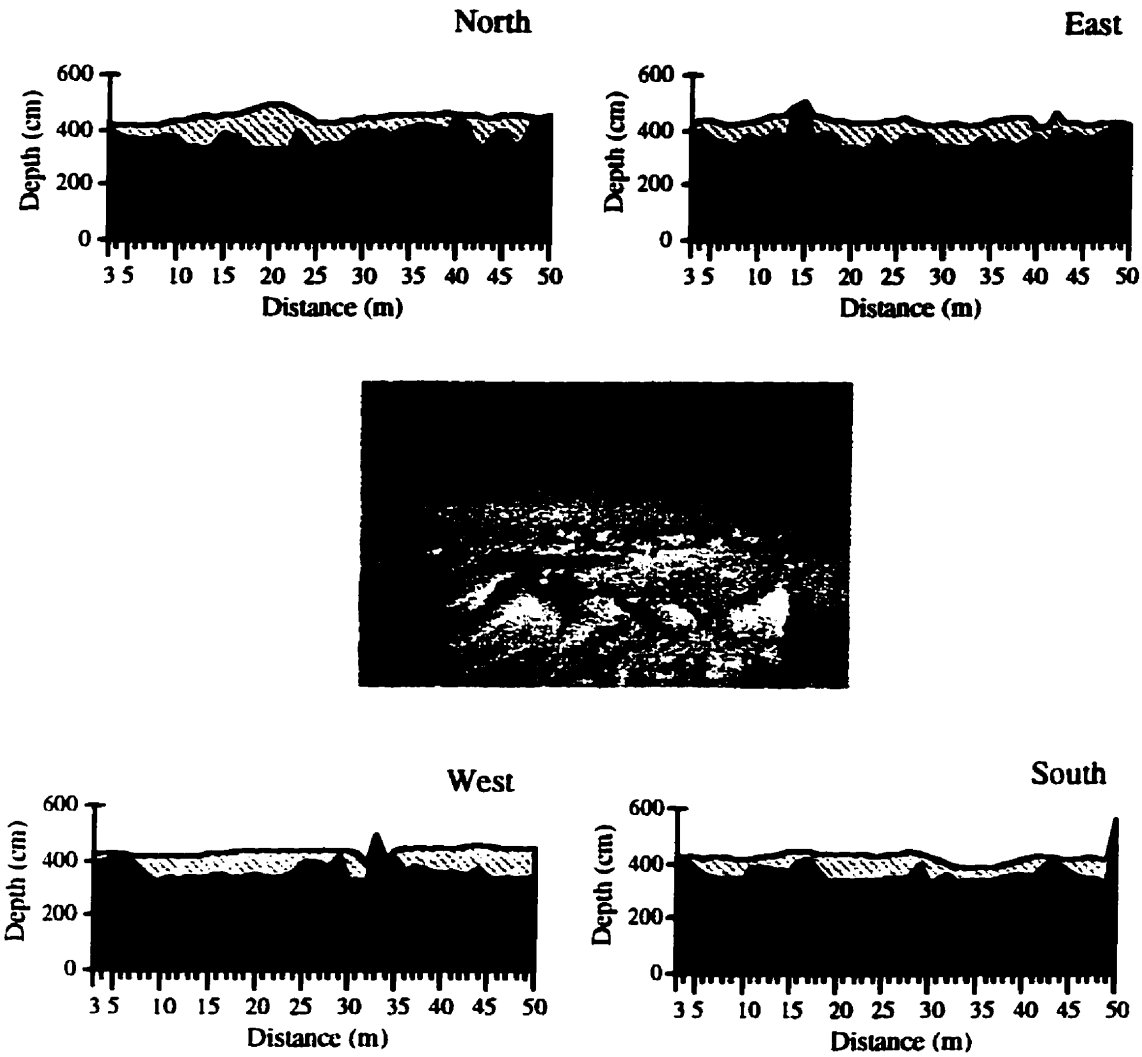

Figure 5.3. Transects for the four cardinal directions for an RI site (RI02), illustrating the variation in ice surface topography and the associated snow distribution. The photograph in the center shows the irregular ice surface.

consolidate into one large thick mass.

The standard deviations for the rubble sea ice sites show that the surface ice topography of this ice type is more irregular than the previous two catchments described (Table 5.2). This more irregular topography would suggest that this ice type would produce more snow drifts than MYI and FYI.

Observations made during the field projects indicated that the principal snow form on this ice catchment was drifted snow. The three ice catchments presented above have a specific surface topography that was more irregular than the previous one. This topographic factor strongly influenced the snow distribution patterns for the individual catchment.

The variation in surface topography was greater for the second rubble site sampled. The standard deviation in the values for this site was greater, indicating the larger variation. Generally, the site contained larger uplifted ice pieces and thus produced a larger variation in surface topography. These larger ice pieces would impact the snow drifting between sites. It is expected that because of this larger variation in surface topography, the second rubble site would produce greater drifting of snow. The variation in surface topography between ice types has great impacts on the thickness of snow drifts encountered over the three ice catchments studied.

5.2 EXPLORATORY DATA ANALYSIS.

Preliminary data analysis was conducted on the snow depth measurements, to identify the similarities and differences between ice types, as well as to test for normality in the data sets. Table 5.4 summarizes the measurements of snow depth for the ice types sampled in the two years. (Appendix A. lists the statistics for each individual site sampled, along with the corresponding histograms.) The results show that the mean snow depth amounts to roughly one fifth of the mean ice thickness, independent of ice type. A similar result was obtained by Worby et al. (1996). This study found that the mean snow depth over sea ice in the Antarctic was approximately 0.3 times the mean sea ice thickness.

Table 5.4. Snow depth descriptive statistics for first-year, multiyear and rubble sea ice sites, collected during the two years of sampling. Sites sampled during 1995 were differentiated from other sites by an addition of 'S' to the ice type.

	FYI	MYI	RI	S FYI	S MYI
mean (cm)	29.3	35.5	53.3	23.6	21.6
stnd. dev.	9.5	20.2	33.7	21.0	16.9
min (cm)	4.0	0.0	1.0	2.0	0.0
max. (cm)	58.0	131.0	165.0	110.0	67.0
no. of samples	2445	1938	270	486	117

Note: Stnd. dev. represents the standard deviation for the ice type, min. and max. represent the minimum and maximum snow depth value measured for the ice type, respectively, and no. of samples represents the number of samples measured for the ice type.

The snow thickness distributions over first-year sea ice for the 1995 and 1996 field projects show that more than 90% of the snow depths were less than 50 cm (Figure 5.4). This shallow snow cover corroborates the assumption that snow is generally blown free on smooth first-year sea ice, producing a thin snow cover and forming dunes and/or sastrugi. The patterns shown in Figure 5.4 indicate that different patterns in the snow depths existed for the two years.

In 1996, the majority of snow thickness values were between 20-40 cm, while in 1995 the snow was generally thinner with most values falling between 0-20 cm. This pattern is also evident in the mean snow thickness values. The sites measured in 1996 had a thicker average snow cover than the sites sampled in the previous year (Table 5.4). Because the 1996 measurements were made roughly one month later than those in 1995, the deeper snow in 1996 might reflect the longer period available for snow accumulation.

On multiyear sea ice, the snow thickness distributions for both years of

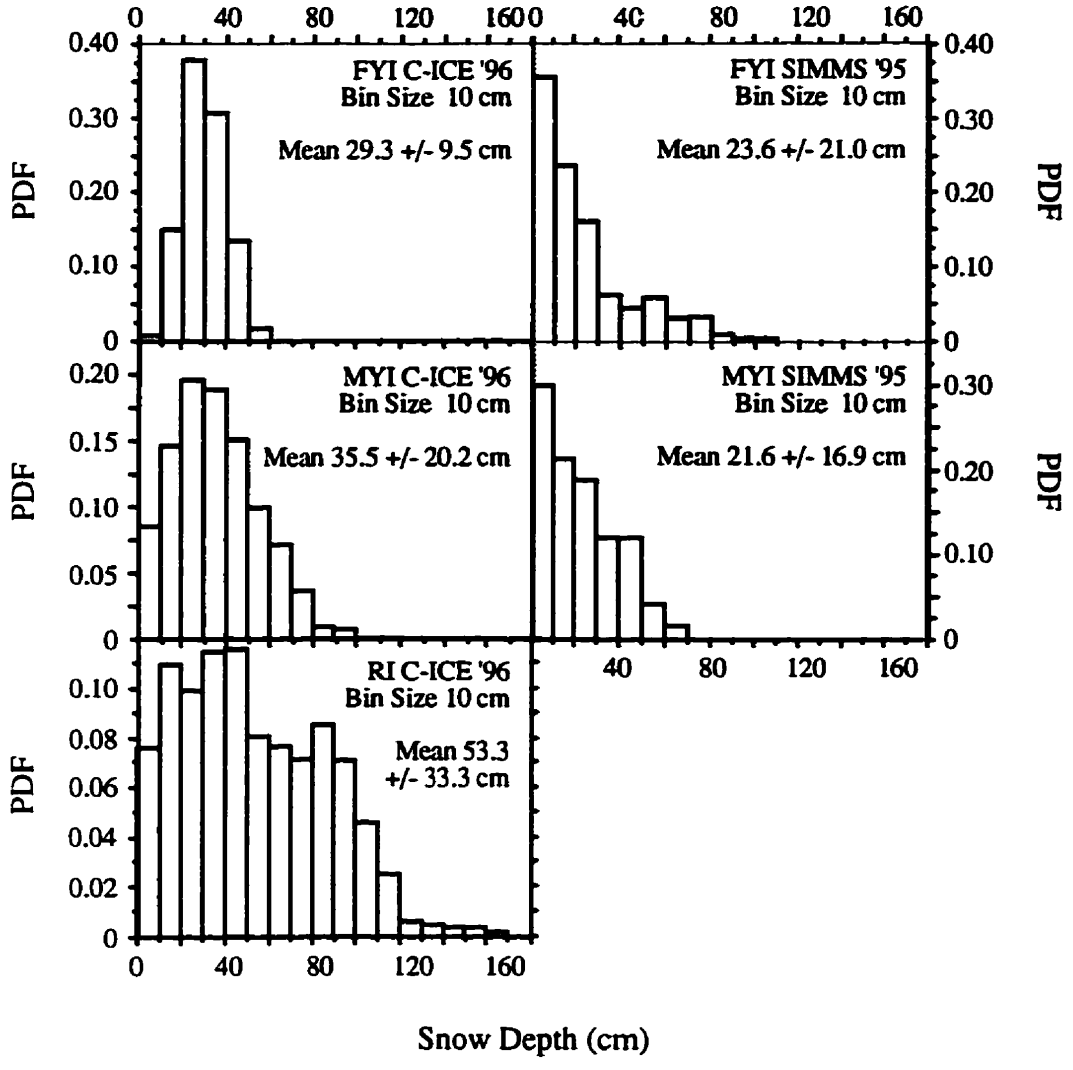

Figure 5.4. Probability density distributions for snow depth acquired during the SIMMS'95 and C-ICE'96 field projects. Each bar represents the probability that a particular depth will fall in that bin.

study had between 95% and 100% of the measurements with less than 80 cm snow depth (Figure 5.4). This value is greater than that obtained for FYI suggesting that this type of ice retained and drifted snow to a greater depth.

This finding reflects the more irregular topography associated with this ice catchment.

Patterns in the snow thickness distributions for the two years were similar to those derived for the first-year ice category; mean depth was greater in 1996 (Table 5.4). Also, most of the snow measurements made in 1996 were between 20-50 cm, while for 1995 the 0-20 cm category contained the most snow thickness measurements (Figure 5.4). Also, in 1996 the MYI sites had some measurements greater than 80 cm (roughly 5%) while in 1995 no measurements were greater than 70 cm. This pattern again suggests that more snow was present in 1996, which could be a product of later sampling.

The snow thickness distributions for the rubble sites show that 97% of the measurements were less than 120 cm (Figure 5.4). This range of snow thickness measurements is larger than the range for both first-year and multiyear sea ice for 1995 and 1996. This finding substantiates the claim that the more irregular topography associated with the rubble ice sites will produce drifts with greater thickness. No measurements were made in 1995 on this type of ice catchment, therefore no comparisons between years can be made.

The finding that snow depth and variation in snow thickness increases as the ice roughness increases (Table 5.4) corroborates the findings by Crocker (1992), Perovich et al. (1988) and Tucker et al. (1987). These studies found that snow thickness was significantly greater on rubble sea ice that on first-year ice. There was a greater distribution of snow depths over the rougher surfaces because the larger local variations in snow thicknesses are a result of wind-induced drift and a rough ice surface topography. Thus, snow depth distributions can act as a good delineator for ice types (Perovich et al., 1988).

Several reasons exist to explain the ranking of snow thickness with respect to ice types. The irregular ice topography associated with the rubble ice

is able to capture and retain a greater amount of snow than the other two topographies; the smaller rounded hummocks associated with MYI and the smooth, flat ice of FYI. In the rougher ice topographies, obstacles projecting into the path of the predominant wind direction will cause snow to accumulate around the obstacles. Over a flat surface, such as that found in the FYI sites, no obstacle to air flow are present and the depth variations are due to dune formations. A second factor is that for rubble and multiyear sea ice, a platform to catch the snow has been present for the entire season, while for first-year sea ice the platform to catch snow would first have had to develop in the autumn, subsequent to the initial snow fall. Tucker et al. (1987) also hypothesized that this difference in snow depth may be due to a loss by sublimation on first-year sea ice. Because FYI is generally much thinner than multiyear sea ice, especially in the autumn months, more heat is conducted through the ice from the warmer ocean, thus making the overlying snow cover more susceptible to loss by sublimation.

The data collected during the SIMMS'95 field experiment shows the opposite trend in snow thickness. The mean and standard deviations for the ice types studied in 1995 indicate that snow depth was greater on FYI than on MYI (Table 5.4). This reversal in the rankings of snow thickness with respect to ice classes was likely due to the fact that the third FYI site (SFYI03) was sampled south of a major ridge subsequent to a major storm event in the area. The combination of the storm and the ridge would have deposited a large amount of snow on the site. This finding is substantiated by the fact that SFYI03 had twice as much snow as SFYI02 and four times as much as SFYI01 (Table A1.).

Along with identifying the snow depth variation over the ice catchments, exploratory data analysis was also completed in order to test for normality within the data sets. Normality needs to be determined in order for variography to be

calculated on the data. Two measures of normality, the skewness and kurtosis statistics, are used to describe the deviation of the data set from a normal distribution. A distribution that has a tail end that extends to larger values than that of the normal distribution is said to be positively skewed. A negatively skewed population has a tail end that extends to smaller values. Kurtosis describes the width of the sampling distribution, relative to a normal distribution. If the distribution is narrower than a normal distribution, then positive kurtosis is occurring. Negative kurtosis represents a distribution that is wider than a normal distribution. For a normal distribution, the skewness statistic is equal to 0 and the kurtosis statistic is equal to 3.0. Normal probability plots can also be used to examine the normality of the data. If the data is normally distributed, the probability plot will produce a straight line.

When examining the statistics for normality (Table 5.5), as well as the normal probability plots (Appendix A) , most of the estimates for the distribution patterns were sufficiently close to a normal distribution to allow for parametric analysis. Two sites sampled in 1996 stood out as being slightly non-normal. FYI04 and MYI03 were both positively skewed and had moderately high kurtosis values (Table 5.5). The probability plots for these two sites also illustrate the slightly non-normal distribution for these sites. Because of the predominance of normality in the other sites samples and because variograms are robust to normality assumptions, working with the natural units of the observations, rather than transforming prior to analysis, was justified. The normality of the data sets suggests that variography can be applied to model the spatial structures of the snow distributions over the three sea ice catchments.

Table 5.5. Skewness (skew.) and kurtosis (kurt.) statistics for the individual sites. Sites sampled during 1995 were differentiated from other sites by an addition of 'S' to the ice type.

	FYI01	FYI02	FYI03	FYI04	FYI05	SFYI1	SFYI2	SFYI3
skew.	0.518	0.329	0.051	1.123	0.157	1.009	0.704	0.074
kurt.	3.173	3.035	2.493	4.542	2.437	3.406	4.1016	2.754

	MYI01	MYI02	MYI03	MYI04	SMY1		RI01	RI02
skew	0.673	0.412	0.924	0.368	0.662		0.911	0.046
kurt.	3.035	3.242	4.483	2.510	2.605		3.904	2.615

This chapter presented the preliminary analysis of the ice and snow thickness measurements made during the SIMMS'95 and C-ICE'96 field experiments. In terms of the icescape, preliminary analysis showed that the ice surface topography was more irregular for rubble sea ice. First-year sea ice was found to be the least irregular ice type studies, as was expected. This ice topography has implications on the snow thickness values measured over the three ice catchments. Data analysis showed that the more irregular the ice surface topography, the greater the thickness of the snow drifts. Also, a comparison of the snow thickness between the years was made. It was concluded from this comparison that the 1996 sites had a greater thickness of snow, compared to 1995 and this was attributed to a later sampling program. The exploratory data analysis is important to understand fully the snow distribution patterns modeled in the next section of this thesis. The next chapter discusses the methods and results for modeling the snow distribution patterns.

CHAPTER 6:

MODELING SNOW DISTRIBUTION.

This chapter introduces the methodology and results of the first objective of this thesis, the modeling of the snow distribution patterns over sea ice. In terms of physical interactions, the snow distribution patterns, as opposed to the snow depth, are the more important factor and more difficult component to attain. The first section will describe the geostatistical technique known as the variogram, including its definition, construction and analysis. The following section will present the result of the modeling, as well as addressing the relevant findings. Section 6.3 will describe the wind analysis conducted to investigate the anisotropy present in the data.

6.1 VARIOGRAPHY.

This section will examine the geostatistical technique known as the variogram. Section 3.3 in Chapter 3 gave a general background of this technique along with its previous uses in different fields of science. Chapter 6 will more specifically survey the theoretical principles and modeling of the experimental variograms from a snow distribution point of view.

6.1.1 Definition of Geostatistics and Variogram.

Geostatistics, in the form it is known today, is a branch of statistics developed in the early 1950s that emphasizes location within areal distributions. The main basis for the development of this 'new' technique was for the spatial analysis of mining ore deposits (Clark, 1979). Geostatistical methods utilize three functions for summarizing spatial continuity. The variogram, one of these functions, is the most traditional choice used by geostatistians because it is a very powerful tool with which to analyze the structure of the spatial patterns.

A major difference between geostatistics and classical statistics is that the former allows variance to be a function of the inter-sample distance and statistical parameters are computed by taking successive differences instead of deviation from a universal mean as in the latter. The fundamental advantage of geostatistics over classical statistics is that the new statistical technique not only emphasizes the description of spatial data, as in classical statistics, but more importantly emphasizes the distribution of the same spatial data set (Carr and Glass, 1989). Geostatistics has as a basic premise that values closer together are more correlated than values farther apart, which is absent is classical statistical modeling. Classical statistics is based on random independent variables and assumes zero spatial continuity in the data set. This form of statistics does not utilize any information of the actual sample positions or the relationships between the samples in the modeling of the phenomena in question.

Another advantage of geostatistics over classical statistics is the requirements of the sampling design. Classical sampling methods are not able to work with autocorrelated data and therefore the main purpose of sampling

programs is to avoid spatial correlations. In geostatistics, sampling becomes less restrictive because there is no need to avoid autocorrelations.

Geostatistics, and especially the variogram, is based on the concept of stationarity. Stationarity makes the assumption that the values in the data set represent the same statistical population. This concept is required to ensure that the spatial correlation may be modeled with an appropriate function. In short, under the hypothesis of stationarity, both the variogram and the covariance, another geostatistical tool, are adequate to estimate the spatial continuity and correlation between regionalized variables (Pannatier, 1996).

In order for variography to be statistically valid, the intrinsic hypothesis must be satisfied. This hypothesis makes the assumption that the difference in the variable under study must be consistent, rather than constant over the area of study (Royle et al., 1980). Mathematically, the two conditions of the intrinsic hypothesis are:

$$E[z(x)-z(x+h)]=0 \tag{6.1}$$

$$\begin{aligned} \mathrm{var}[z(x)-z(x+h)] &= E[z(x)-z(x+h)^2] \\ &= 2\gamma(h) \end{aligned} \tag{6.2}$$

These conditions state that the expected differences between values separated by a distance is zero (6.1) and that the variance of the difference depends on h (McBratney and Webster, 1986). When these two conditions are met, the observations are said to be "on an intrinsically stationary process" (Cressie, 1989) and thus the semivariances can be estimated and the variogram can be used to characterize the spatial continuity within the data set.

Second order stationarity denotes the existence of the intrinsic hypothesis, but the intrinsic hypothesis does not imply that second-order

stationarity exists (Journel and Huijbregts, 1978). This should be kept in mind when applying geostatistics to various data sets. With the acceptance of only the intrinsic hypothesis and the second-order stationarity, only the variogram can be used to model the spatial continuity of the data. When an experimental variogram is modeled using a model that does not reach a plateau, which indicates that the underlying random function does not meet the requirements for second-order stationarity (Pannatier, 1996).

In definition, a variogram is a geostatistical technique that examines the spatial continuity of a regionalized variable and how this continuity changes as a function of distance and direction. Spatial continuity is simply the assumption that the closer two sampling points are, the more similar the values will be. Any random variable that is distributed in both time and/or space is considered to be a regionalized variable.

A regionalized variable can be thought of as having a structural and erratic aspect (Pannatier, 1996). The structural aspect is related to the overall distribution of the natural phenomena, while the erratic aspect is related to the local behavior of the natural phenomena. Therefore, any analysis of the natural phenomena must take into account both of these aspects. The variogram, and geostatistics as a whole, take these dual aspects into account using a random function in which the regionalized variable is considered a particular realization of the random function. The random function is a set of random variables whose dependence on each other is determined using a probabilistic mechanism (Pannatier, 1996). This mechanism takes both the random and structured aspects into account by assuming that the variable [z(x)] is random at a local scale, but is related to another variable [z(x+h)] some distance (h) away by a correlation representing the spatial structure of the natural phenomena.

The variogram describes the expected difference in value between pairs

of samples with a given relative orientation. Computation of a variogram involves plotting the relationship between the semivariance ($\gamma(h)$) and the distance vector or lag distance (h). The semivariance can be defined as one-half of the variance of the difference between points separated by a distance h, or:

$$\gamma(h) = \frac{1}{2N}\sum_{i=1}^{N}(x_i - x_{i+j})^2 \qquad (6.3)$$

where $\gamma(h)$ is the semivariance, X_i is the measured sample value at point i, $X_{(i+j)}$ is the measured sample value at point i+j where j is the change in distance and N is the number of observations. Production of the semivariance involves repeating the procedure for all intervals or ranges of the lag distance (h).

The lag distance vector is defined as the separation distance between two points within a data set. In a regularly spaced or pseudo-regular grid, the lag spacing is the sampling spacing or intervals. For an irregular grid, the initial lag spacing should be an estimate of the average spacing between sampling points (Isaaks and Srivastava, 1989). Associated with this lag distance is the lag tolerance. This tolerance is a value selected so that any points within this tolerance value are accepted for the computation of semivariance of a directional variogram. It is common to choose a lag tolerance value that is half of the lag spacing or distance.

When the semivariance statistic is plotted against the distance vector, certain features of parameters are displayed on the variogram. One parameter of the variogram is the range (a). As the separation distance between the pairs of data points increases, the variogram or the semivariance also increases. Eventually an increase in the distance will no longer produce an increase in the

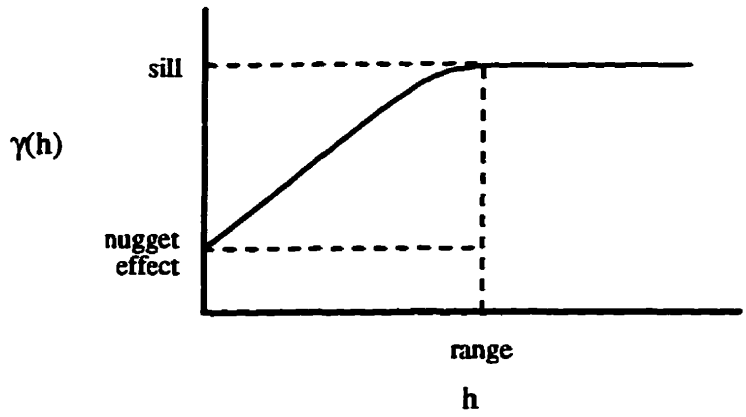

Figure 6.1. Idealized variogram illustrating the three basic variogram parameters: the nugget, the sill and the range.

semivariance and the variogram reaches a plateau (Figure 6.1). The distance at which the variogram reaches this plateau is called the range. In other words, the entire range of the sample variability (or a major portion of this variability) should be encountered within a distance equivalent to this range. Beyond the range, the samples are no longer correlated and are independent. The second parameter is related to the range and is known as the sill (c). The sill is the value at which the variogram levels off or stabilizes (Figure 6.1), and is theoretically equivalent to the sample variance. The shape of the overall variogram, along with the sill and range aids the researcher in determining if the pattern of spread is random or spatially dependent.

A third parameter that is shown on a variogram is known as the nugget effect (Figure 6.1). Ideally, when the separation distance is zero, the semivariance between two points is also zero. At extremely small distances, the sample values may be quite dissimilar. This jump from a value of 0 at the origin to the semivariance at extremely small separation distances is known as the nugget effect (Isaaks and Srivastava, 1989).

The nugget effect represents unexplained or random variance in the data set. A non-zero value may be caused by two factors; errors in sampling by the researcher, and the presence of a very small scale structured component whose range is much less than the sampling interval. It is important to identify the nugget effect in the model because the difference between the sill value and nugget value represents the total amount of variance that can be modeled as spatial dependence from the data set (Rossi et al., 1992).

An additional principal feature or property of the variogram is its bi-directional nature. A variogram calculated for any particular direction will be identical to the variogram calculated in the opposite direction (Clark, 1979). Therefore, when modeling the spatial continuity for a variogram calculated in the north direction, for instance, the spatial continuity can be described as occurring in the north-south direction.

6.1.2 Variogram Construction.

H-Scatterplots

The first step in examining and modeling the spatial continuity of a data set is the production of an h-scatterplot. An h-scatterplot is simply defined as "a plot of the pairs of all data values separated by a common lag" (Rossi et al., 1992). Therefore, different h-scatterplots are constructed for different lag distances studied, as well as for different directions.

The shape of the clouds of points in a given h-scatterplot is indicative of the continuous nature of the data. A cloud centered around the x=y line of the graph, or the 45-degree line passing through the origin, indicates that the sample points are very similar. A wider and more diffuse cloud would suggest that the points are less similar. As the lag distance increases between h-

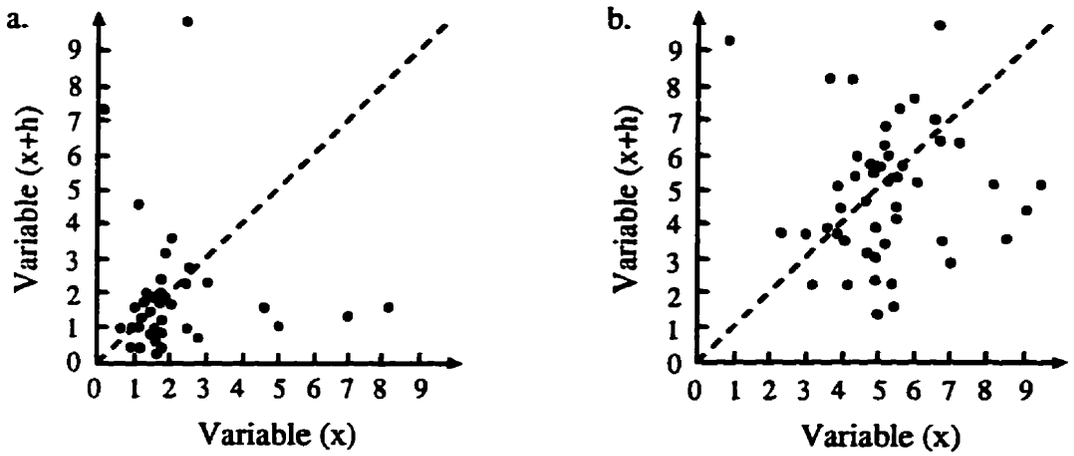

Figure 6.2. Examples of h-scatterplots illustrating the butterfly-wing shape (a.) and a more symmetric h-scatterplot (b.).

scatterplots, it is expected that the cloud of points becomes more diffuse or wider since the basic idea behind spatial continuity is that as the distance increases between sampling points, the points become less similar.

The shape of individual and successive h-scatterplots are also important for variogram construction and analysis. If individual h-scatterplots display a 'butterfly-wing' shape then the spatial continuity of the data set(s) can not be summarized accurately with a single number (Figure 6.2). The spatial continuity can only be summarized with a single number if the shape of the cloud is symmetric.

The succession of h-scatterplots provides a check for stationarity. If such a succession shows that the center of the cloud of points departs from the diagonal line, then the random function representing the studied phenomena can not be considered stationary (Pannatier, 1996). Therefore, prior to any variogram construction and analysis, the h-scatterplots must be constructed and

analyzed.

There are two major advantages to constructing an h-scatterplot prior to any variogram analysis. The first advantage is that in the h-scatterplot, outliers or points that are outside the cloud, are quite visible. These outliers can be investigated prior to any further analysis for errors in data entry and other human errors that may have occurred prior to the plotting of an h-scatterplot. If these points were retained in the data set without any investigation, they could have produced erroneous results in the modeling of the spatial continuity of the data set, resulting in variogram estimates that do not reflect the continuity. Another advantage is that distinct and different populations are also visible in the h-scatterplot as separate clouds of points. These distinct populations may not appear in the analysis of the raw data using such techniques as the histogram. If not detected, these populations may also cause an inaccurate modeling of the variogram.

H-scatterplots, while providing a different view of the data, are not able to precisely summarize the spatial continuity within the data set, therefore variograms must be constructed and analyzed in order to model this continuity. The first step in variogram construction and analysis is the production of omnidirectional variograms for the data set, followed by directional variogram construction.

Omnidirectional Variograms.

Before omnidirectional and directional variograms are described, a few terms must be explained. An experimental variogram is one that is constructed from the data set used by the researcher. This variogram is defined by a finite geometric field. This variogram is in turn an approximation of the theoretical variogram. A theoretical variogram is defined by an infinite number of pairs

over an infinite field which can never be computed. It consists of a number of models that are used alone or in combination to model the experimental variogram. This variogram, as its name suggests, is theoretical in nature, and is used to simplify the spatial continuity found in the data set and the experimental variograms.

An omnidirectional variogram is usually the initial step in variography. This variogram is an average of all pairs within the data set, not dependent on the direction or orientation between pairs (Isaaks and Srivastava, 1989). The lag measure is only scalar since the direction of the lag distance is not important in the construction of the omnidirectional variogram.

The main purpose of this variogram is to determine the appropriate distance parameters (i.e. lag distance and lag tolerance) that will be used in the development and production of the directional variograms. Due to the large number of sample points used in the omnidirectional variogram, this variogram will be the most appropriate to determine the distance parameters.

The primary advantage of the omnidirectional variogram is that it can serve as an early warning for erratic directional variograms. If the omnidirectional variogram is disorderly and disorganized, then the directional variograms will also be erratic. If this occurs the researcher must examine the reasons for this erraticness and attempt to remove it from the variogram. One way to identify the reason for the disorganized variogram is to examine the h-scatterplots and maps of the locations of erratic points to determine whether this is the product of data entry or if the points are accurate and actually do represent the spatial continuity of the data set. When the omnidirectional variogram displays a clear structure, then the next step will be to produce a directional variograms that will describe any anisotropy that may be present in the data.

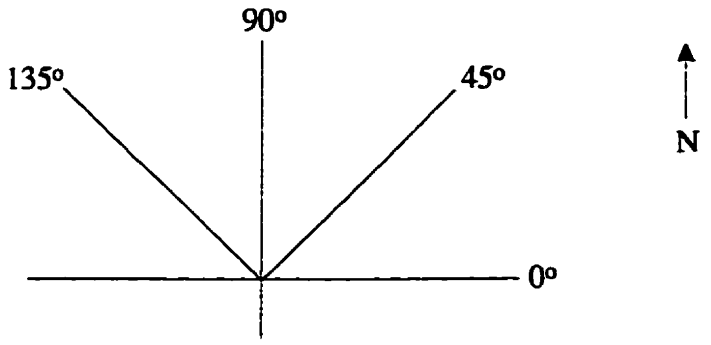

Figure 6.3. Direction convention used for variogram analysis.

Directional Variograms.

Directional variograms are similar to omnidirectional variogram except that the lag distance is a vector not a scalar measurement; it has a magnitude as well as a directional component. Variogram construction for this type of variogram involves calculating the semivariance statistics for a certain lag in a specific direction. Directional variograms are usually constructed for 0°, 45°, 90° and 135° orientations. In geostatistics, the directional convention most commonly used, and that used in this thesis is east-west which represents the 0° direction. (Figure 6.3). Associated with the directional component are the angular and lag tolerances. Angular tolerance can be viewed as a window that allows data pairs located within an allowable deviation from the specific direction to be included in the variogram under construction (Isaaks and Srivastava, 1989). Again, lag tolerance allows a sufficient number of data pairs to produce a clear variogram. These values can be determined from the omnidirectional variogram, and allows pairs that are not exactly in the lag distance and direction to be included in the variogram analysis.

When directional variograms are produced for different directions, the

major and minor axes of anisotropy can be identified. Anisotropy is defined as occurring when the range and/or sill values are not consistent in all directions and thus the variability is not solely dependent on the distance between the two sampling points but also on the direction (Cressie, 1993). In most cases information exists about the natural phenomenon studies that would suggest the direction of the axis of anisotropy. For snow distribution, this information might be knowledge of the prevailing wind direction during storm events or the underlying ice surface topography. Information such as this should be studied before variograms are constructed to aid in anisotropy axis identification.

Two types of anisotropy exist: i.) geometric anisotropy where the range changes with direction and the sill remains relatively constant; and ii.) zonal anisotropy where the sill changes with direction but the range remains constant. Geometrical anisotropy can be considered equivalent to an elliptical shaped zone, where the zones are stretched in the directions of the maximum range and the data values are highly correlated in this direction (Rossi et al., 1992). Zonal anisotropy is symptomatic of different directions or zones expressing different degrees of overall spatial continuity. When the four directional variograms exhibit different sill values, the spatial variability is greater in the direction with the greater sill value. However, pure zonal anisotropy is not commonly found using real world data. When zonal anisotropy occurs, it is typically found in combination with geometric anisotropy, so that both the sill and range vary with different directions.

In analyzing anisotropy from sample variograms which show changes in range and/or sill with direction, the first step is to identify the anisotropy axes. This identification of anisotropy axes is done by experimentally determining the "directions corresponding to the minimum and maximum range or the minimum and maximum sill in the case of the zonal anisotropy" (Isaaks and Srivastava,

1989). Qualitative information, such as the orientation of winds or other features, can be helpful in determining the axes of anisotropy. Also h-scatterplots and contour maps of the data set may be useful in the determination of the axis of anisotropy. These plots may show the axes of anisotropy in a graphical way, which may be more obvious to the researcher.

When comparing different directional variograms for different locations, standardization may become necessary. One way to standardize the variogram is to divide each variogram value by the overall sample variance, so that each value is equal to the sample variance. This will allow the researcher to compare different directional variograms for different locations and different years even though they may contain dissimilar measurement units and/or levels of spatial variability (Rossi et al., 1992). Standardization was completed in this thesis to compare variograms for the different years and the different ice catchments.

Two rules apply to the construction of the experimental variograms. The first rule states that it is only appropriate to plot values of semivariance for approximately one half of the sampling width (Journel and Huijbregts, 1978). This rule is necessary because the semivariance for any lag distance greater than one half of the sampling width only measures the variance at the boundary of the sampling grid or space. This rule allows for the variogram to be "representative of the whole sampling space" (Liebhold et al., 1993). The second rule deals with the number of values used to compute the semivariance for a particular lag. It has been estimated that in order to maintain statistical reliability in the variance calculation, a minimum of 30-50 pairs of samples should be used to calculate the semivariance (Journel and Huijbregts, 1978). With the adherence of these two simple rules, the calculated or experimental variogram will be statistically credible for modeling and describing the spatial

continuity of the regionalized variable in question.

6.1.3 Variogram Analysis.

One of the most important steps in defining the spatial autocorrelation in the data set is modeling the experimental variogram to produce a theoretical variogram. This modeling is done in order to make inferences or draw conclusions about the whole area of study from the sampled sites. The process of modeling involves determining from the plot of semivariance against lag distance the appropriate variogram model(s) to summarize the spatial continuity of the data set. The principal components of the variogram, namely the sill, range and nugget effect, are incorporated in the models to produce a theoretical model that is specific to the data set. These theoretical models allow the researcher to adequately define the spatial autocorrelation present in the data set, without examining or incorporating every minor oscillation present in the variogram plot.

In some cases of spatial continuity in natural phenomena, the variogram may lack any structure (i.e.. does not reach a sill at a prescribed range). The absence of structure represents a pure nugget effect model. The nugget effect model signifies that there is an absence of any spatial continuity within the data set, and the variance between different lag spacing is nearly identical. The nugget effect behavior is shown in the variogram plot as a horizontal line that runs through the sample points (Figure 6.4). Due to the fact that this model indicates a lack of spatial continuity in the data set, the nugget model is not considered a true theoretical model.

Several theoretical models exist which define the experimental variogram. The experimental models can be divided using two criteria;

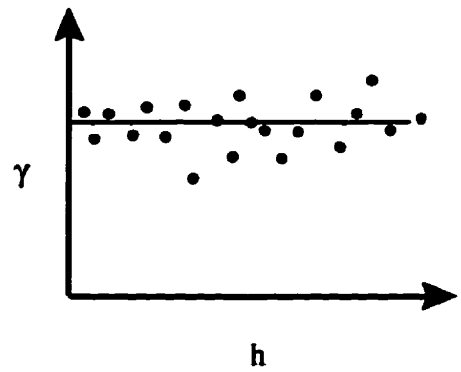

Figure 6.4. Variogram that lacks any structure and modelled using the nugget effect behaviour. The modelled theorectical variogram represents a flat horizontal line that goes through the data points.

i.) the presence or absence of a sill, and ii.) the behavior of the variogram at the origin. For the purposes of this research, the models will be divided into two classes, models that reach a sill, known as transition models, and models that do not reach a sill, known as unbounded models.

Transition Models:

i. Spherical Model. The model most commonly used in the literature, especially mining geology, to model the experimental variogram is known as the spherical model. This model is considered the 'ideal' variogram model because it has a well defined sill and the range is easily interpreted. The mathematical equation describing this model is:

$$\gamma(h) = \begin{cases} 0 & h = 0 \\ c_0 + c\left[\frac{3}{2}\left(\frac{h}{a}\right) - \frac{1}{2}\left(\frac{h}{a}\right)^3\right] & 0 < h \le a \\ c_0 + c & h > a \end{cases} \qquad (6.4)$$

where c_o is the nugget value, c is the sill and a is the range. As was already stated, this variogram model reaches a sill at a specific range, and its behavior at the origin is linear, indicating good continuity (Figure 6.5). This linear behavior suggests that a progressive decrease of spatial dependence of the variable occurs when the distance between them decreases. For separation distance greater than the range, the semivariance is equal to the sample variance of the data set. Beyond this value no further increase in semivariance is observed and the spatial correlation is equal to zero. When a nugget effect occurs in the variogram, the sill value is the difference between the nugget effect and the value at which the variogram flattens.

ii. Exponential Model. A second theoretical model that is used often in the literature is the exponential model. Like the spherical model, the exponential model is linear at the origin. However, unlike the spherical model, this model rises more steeply and then flattens out more gradually, as well as approaching the sill asymptotically. Therefore the semivariance increases with increasing separation distance for all h values. As the model is characterized by a gradual approach to the sill, the practical range is defined as the distance at which the variogram value is 95% of the sill (Isaaks and Srivastava, 1989). The equation for this model is:

$$\gamma(h) = \begin{cases} 0 & h = 0 \\ c_o + c\left[1 - \exp\left(\frac{-3h}{a}\right)\right] & h \neq 0 \end{cases} \qquad (6.5)$$

where c_o represents the nugget value, c represents the sill and a represents the range (Figure 6.5).

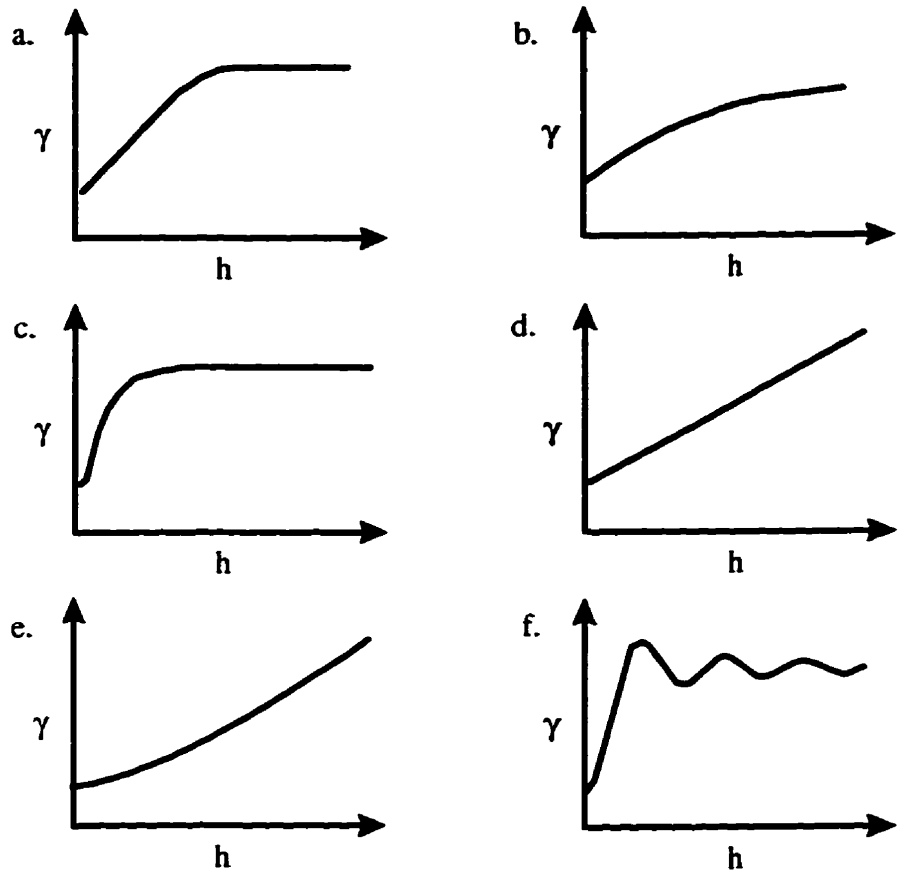

Figure 6.5. Variogram theoretical models: a. spherical model, b. exponential model, c. gaussian model, d. linear model, e. power model and f. wave (hole-effect) model. The first three models are considered transition models because they reach a sill, while the other three model do not reach a sill and are classified as unbounded models.

iii. Gaussian Model. The third theoretical variogram model that reaches a sill is called the gaussian model. This model is not used as extensively to model the spatial continuity as the two previously described models. The equation representing this model is:

$$\gamma(h) = \begin{cases} 0 & h = 0 \\ c_o + c\left[1 - \exp\left(\frac{-3h^2}{a^2}\right)\right] & h \neq 0 \end{cases} \qquad (6.6)$$

where c_o is the nugget value, c is the sill and a is the range. The gaussian model, like the exponential model, reaches its sill asymptotically and the practical range has the same definition as the range for the exponential model. The difference between this model and the previously described models is that this model is parabolic near the origin indicating perfect continuity (Figure 6.5). The gaussian model expresses a rather smooth spatial variation of the variables. This model is generally used to model extremely continuous variables and should only be utilized whenever the parabolic shape of the estimated variogram at the origin is justified given the physical nature of the variable.

Unbounded Models:

i. Linear Model. The simplest theoretical variogram model that does not reach a sill is known as the linear model. This model applies when the spatial variability observed for a variable keeps increasing linearly with distance and never levels off, as shown in Figure 6.5. Its shape near the origin comes close to that of the spherical and exponential models, but unlike the spherical and exponential models, it never reaches a sill. Its standardized equation is:

$$\gamma(h) = \begin{cases} 0 & h = 0 \\ c_o + b_l h & h \neq 0 \end{cases} \qquad (6.7)$$

where c_o is the nugget value, and b_l is the slope of the line.

ii. Power Model. An extension of the linear model is the power model. This model can be defined by the equation:

$$\gamma(h) = \begin{cases} 0 & h = 0 \\ c_o + b_p h^{\lambda} & h \neq 0 \end{cases} \qquad (6.8)$$

where c_o is the nugget value, b_p is the slope of the line, and λ is the power coefficient . As with the linear model, the power model does not reach a sill, but increases non-linearly with increasing separation distance (Figure 6.5). Values of λ are between 0 and 2. When λ is less than or equal to 1, the model is linear at small separation distances, resembling the spherical and exponential models, however, when λ is greater than 1 the model is parabolic near the origin, resembling the gaussian model. This model is rarely applied to experimental variograms in the literature (Hohn, 1988).

iii. Wave (or Hole-Effect) Model. The final theoretical model used to model the experimental variogram is known as the wave or hole-effect model. This model suggests that the variogram does not increase monotonically with increasing separation distance, but oscillates around the sill as the distance increases. It can be defined using the equation:

$$\gamma(h) = \begin{cases} 0 & h = 0 \\ c_o + c\left[1 - a\sin\left(\frac{h}{a}\right)/h\right] & h \neq 0 \end{cases} \qquad (6.9)$$

where c_o is the nugget value, c is the sill and a is the range. The wave model suggests that a periodicity or cyclicity of the spatial autocorrelation exists within the data set, and that samples separated by larger separation distance may be more similar than those with smaller separation distances. The periodicity results in a wave-like pattern as shown in Figure 6.5. The distance to the first maximum can be interpreted as the average width of the snow drifts zones and

the distance to the first minimum as the average distance between snow drifts zones. The wave model should only be used when periodicity is likely within the data set because of the nature of the regionalized variable under study. In the literature, the wave model is generally found nested with other models particularly the spherical model.

It should be noted that these basic models may be combined to produce more complex models, which more accurately describe the spatial autocorrelation found in the data set. The new complex model is a combination of several simple theoretical models, such that $\gamma^*(h) = \gamma_1(h) + \gamma_2(h)$, where $\gamma^*(h)$ is the overall complex model, $\gamma_1(h)$ is the first model and $\gamma_2(h)$ is the second model. Different models may be incorporated, with each model describing a different feature of the variogram. For instance, if the variogram is parabolic near the origin but does not have a sill, then the combination of the gaussian and linear models could be used.

In using a combination of theoretical models to model the experimental variogram, the sill and range values must first be determined. The overall sill and range value for the model will be a product of the sill and range values for each model used in the combination. If another model was added to the overall model, then the range for the complex model must be a combination of the two range values. However, there is a limit to the number of basic models that should be used to describe the experimental variogram. It is suggested by Isaaks and Srivastava (1989) that while the combination of three or more models may capture every curve and kink in the variogram, these complicated models do not lead to estimate more accurately the spatial continuity than simpler models. Therefore, only two or three models should be combined to model the experimental variogram.

In modeling the experimental variogram using the theoretical models it is

important to realize that at large values of h or separation distance, fewer sample pairs are available to calculate the semivariance. This will cause the variogram to be generally erratic at large values of h (Miesch, 1975). This erratic behavior will produce negative slopes between points. These slopes may or may not be indicative of a periodicity in the data, and only knowledge about the variable in question and the experience of the researcher with variograms will be able to distinguish or determine the relative importance of the negative slopes.

The appropriateness of the combination of models for modeling snow distribution patterns over sea ice was determined using an indicative goodness of fit (IGF) measure. This measure, developed by Pannatier (1996), is based on a least square estimation and is defined as:

$$IGF = \frac{1}{N} \sum_{k=1}^{N} \sum_{i=0}^{n(k)} \frac{P(i)}{\sum_{j=0}^{n(k)} P(j)} \bullet \frac{D(k)}{d(i)} \bullet \left[\frac{\gamma(i) - \hat{\gamma}(i)}{\sigma^2} \right]^2 \qquad (6.10)$$

where N is the number of directional variograms, n(k) is the number of lags relative to variogram k, D(k) is the maximum distance relative to variogram k, P(i) is the number of pairs for lag i of variogram k, d(i) is the mean pair distance for lag i of variogram k, $\gamma(i)$ is the experimental measure of spatial continuity for lag i, (i) is the modeled measure of spatial continuity for d(i), and s^2 is the variance of the data for the variogram. A value close to zero indicates a good fit. This goodness of fit measure is standardized so that values for different variograms, using different models can be compared.

6.2 RESULTS AND DISCUSSION.

6.2.1 H-Scatterplots.

H-scatterplots are identified as the first step in variogram analysis. In this study, h-scatterplots were computed for each site at each lag distance. Appendix B shows the h-scatterplots computed for each site at three lag distances. The succession of h-scatterplots for each site shows that as lag distance increases, the shape of the cloud becomes more diffuse or wider. This progression of cloud shape was to be expected because the general principle of spatial continuity is that points closer together are on average more similar than those farther apart. As points become more dissimilar, the cloud of the h-scatterplot should become more diffuse.

In comparing the h-scatterplots for each ice type an interesting point becomes evident. Firstly, it is apparent that the cloud of points is more symmetric for FYI types (Figure 6.6). This is probably a product of the fact that this ice type had the smallest range in snow depth values, as well as the lowest variance, and therefore points located 1 m apart (lag=1) are more likely to be equal in values.

The pattern of h-scatterplots also provides a check for stationarity. Because the center of the cloud of points does not depart from the diagonal line in each site (Figure 6.6 and Appendix B), the random function representing the snow distribution can be considered stationary. Thus, variography can be done on the data to model the snow distribution patterns.

The shape of the individual h-scatterplots also suggests that variography can be completed on the data sets. As stated previously, if the shape of the h-scatterplot cloud of points is 'butterfly-wing' shape (Figure 6.2), then the spatial

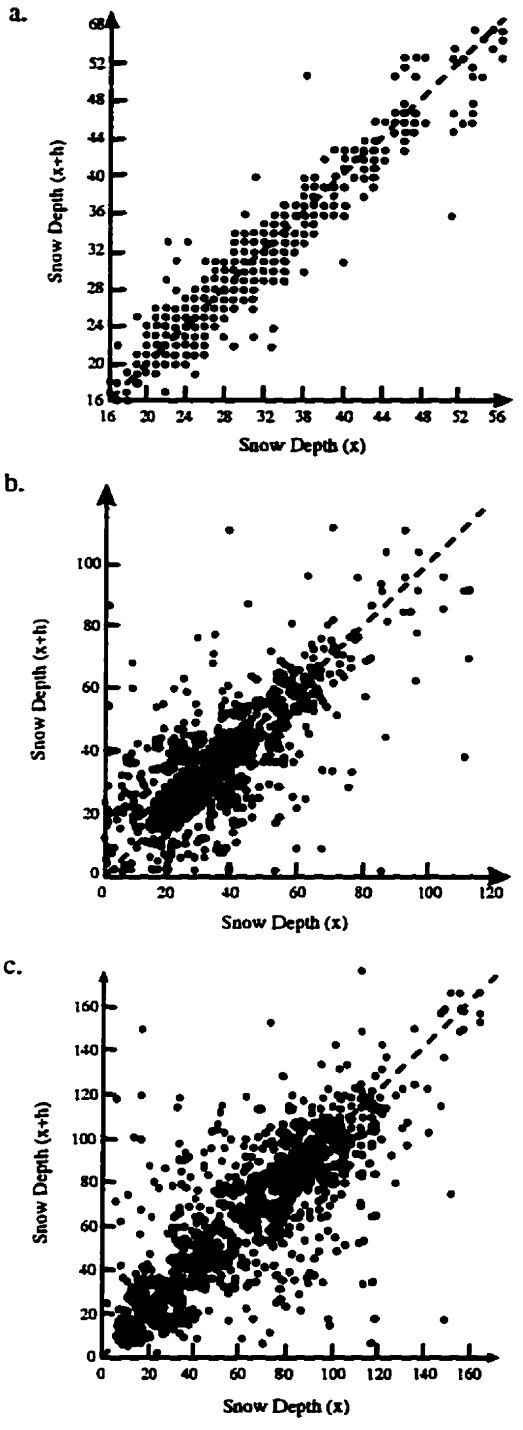

Figure 6.6. H-scatterplots produced for a site sampled over the three different ice catchments at a lag of 1; a. FYI04, b. MYI03 and c. RI02.

continuity of the studied phenomena can not be summarized with a single number, such as a variogram. The h-scatterplots produced for each site (Appendix B) do not exhibit this 'butterfly-wing' shape but are more symmetric. Therefore, a single number will adequately summarize the spatial continuity of the data sets.

Besides justifying the adequacy of the variogram in modeling the snow distribution, h-scatterplots also serve as a tool to predict any aspects of the data that may cause inaccurate modeling results (i.e. outliers and distinct populations). The h-scatterplots produced for the sampled sites show that no outliers or distinct populations are present in the data sets. Therefore, there are no reasons to expect erroneous results with the modeling of the spatial continuity using a variogram.

While h-scatterplots are able to detect any problems that may occur with modeling the spatial phenomenon under study, as well as justifying the use of the variogram, they are not powerful enough to precisely summarize the spatial continuity within the data set. In order to summarize the spatial continuity, variograms, namely the omnidirectional and directional variograms, must be constructed and analyzed.

6.2.2 Omnidirectional Variograms.

The omnidirectional variograms produced for the three different ice catchments displayed different patterns. For the FYI sites the gaussian theoretical model was fit to the experimental variograms. (Appendix C contains the omnidirectional variograms for each site sampled on FYI.) The gaussian model indicates that as separation distance increases between snow depths at small lags, the semivariance or amount of spatial correlation remains relatively

similar. However, at some lag distance, the semivariance values between separation distances increases, indicating that the spatial correlation is decreasing. This pattern continues until a certain lag is reached where the semivariance approaches the sample variance or the sill of the variogram (i.e. range). An example of the gaussian model fit to a first-year sea ice site (FYI05) is:

$$\gamma(h) = \begin{cases} 0 & h = 0 \\ 0.07 + 1.10\left[1 - \exp\left(\frac{-3(h)^2}{(25.92)^2}\right)\right] & h \neq 0 \end{cases} \qquad (6.11)$$

where 0.07 represents the nugget variance, 1.10 the sill value and 25.92 the range (Figure 6.7).

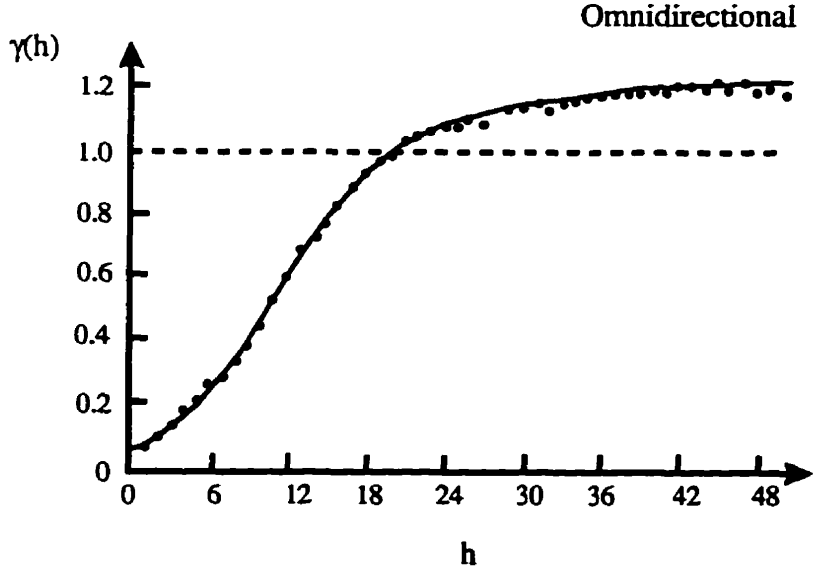

Figure 6.7. Omnidirectional variogram produced for FYI05. The line represents the theoretical variogram model and the points the experimental variogram.

Table 6.1. Variogram parameter values for FYI, MYI and RI omnidirectional variograms. IGF represents indicative goodness of fit values.

	FYI 1	FYI 2	FYI 3	FYI 4	FYI 5	SFYI 1	SFYI 2	SFYI 3
model	gaussian	gaussian	gaussian	gaussian	gaussian	gaussian	gaussian	gaussian
nugget	0.17	0.18	0.11	0.05	0.07	0.07	0.13	0.16
range	10.92	7.45	14.98	14.94	25.92	10.15	17.76	18.40
sill	0.89	0.86	1.00	1.00	1.10	1.02	0.95	0.86
IGF	1.29e-2	3.45e-3	1.00e-2	4.21e-3	1.17e-3	1.28e-2	2.91e-2	1.23e-2
	MYI 1	MYI 2	MYI 3	MYI 4	SMYI 1		RI 1	RI 2
model	spherical	spherical	spherical	spherical	spherical		spherical	spherical
nugget	0.29	0.10	0.37	0.11	0.03		0.30	0.17
range	4.98	14.43	24.09	15.49	14.88		35.18	15.45
sill	0.71	0.88	0.68	0.93	1.01		0.85	0.90
IGF	5.88e-3	9.26e-3	2.09e-2	7.02e-3	1.95e-2		3.56e-3	1.30e-2

Note: SMYI denotes first-year sea ice and multiyear sea ice sites sampled during SIMMS'95.

Table 6.1 lists the parameter values for the six FYI omnidirectional variograms. The range value indicated the separation distance at which the majority, if not all of the variability would be accounted for within the data set. There was considerable variation between the sites, with ranges varying from 7.4 m to 25.9 m (Table 6.1). This could be due to the passage of winds over the sampling areas between sampling dates. The additional winds would produce additional drifting as well as further developing drifts that already exist in the overall sampling area and thus increasing the range values for the models.

Nugget values indicate the percentage of the variability in the data set that can not be modeled using the separation distance. For the FYI sites, the nugget values suggesting that less than 20% of the variability in the data set could not be accounted for using this model (Table 6.1). Due to the low measurement errors associated with the method of snow depth sampling, the variability that could not be accounted for was solely attributed to the

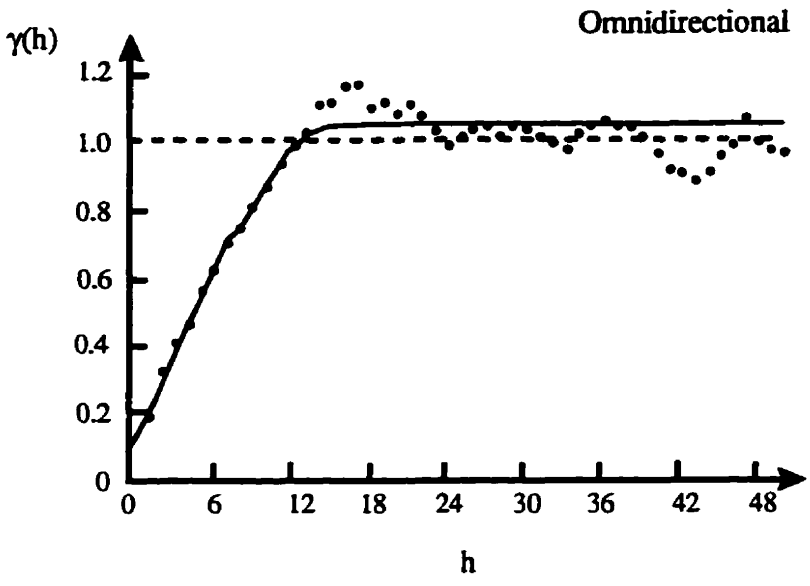

Figure 6.8. Omnidirectional variogram produced for MYI04. The line represents the theoretical variogram model and the points the experimental variogram.

phenomenon of micro-regularization or micro-distribution within the sampling site (i.e. snow drifts that were less than 1 m in distance and hence missed with the sampling scheme). These values were extremely low (much lower than half of the sill value) and suggest that these models are an excellent representation of the spatial continuity in the snow patterns.

The spherical theoretical model was used to model the MYI omnidirectional variograms. Figure 6.8 shows the omnidirectional variogram (theoretical and experimental) for site MYI04, while the other omnidirectional variograms are contained in Appendix C. The theoretical variogram model associated with the spherical model was defined as:

$$\gamma(h)=\begin{cases}0 & h=0\\ 0.11+0.93\left[\frac{3}{2}\left(\frac{h}{15.49}\right)-\frac{1}{2}\left(\frac{h}{15.49}\right)^3\right] & 0<h\le a\\ 0.11+0.93 & h>a\end{cases} \quad (6.12)$$

where the nugget variance is 0.11, the sill is 0.93 and the range is 15.49. This model indicates that for all the sites the snow depth changes rather uniformly as the lag distance increases. Again, this only occurs until at a certain lag where the semivariance value is equal to the sample variance and no spatial dependence is present.

Range values varied from 4.98 m to 24.09 m (Table 6.1), indicating that for multiyear sea ice, points separated up to a distance of 24 m will exhibit some spatial dependence. The spread of range values is similar to the spread for the FYI sites, indicating that for both types of sea ice, spatial dependence varies over a large range. This large range in values was attributed once again to the passing of storms over the sampling site during the sampling years. This is shown in the fact that the range values increase as each successive site was sampled.

The nugget values for the MYI sites ranged from 0.03 to 0.37 (Table 6.1). Since the nugget values were less than half of the standardized sample variance, these values suggest that the models used to represent the omnidirectional variograms for the five MYI sites were an appropriate modeled representation of the statistical pattern of the snow distribution on these sites. These values were greater than those for FYI sites, indicating an increase in the point-to-point variation and may suggest greater spatial autocorrelation at distances less than 1 m. Larger nugget values were expected because of the heterogeneous nature of the ice topography in MYI locations.

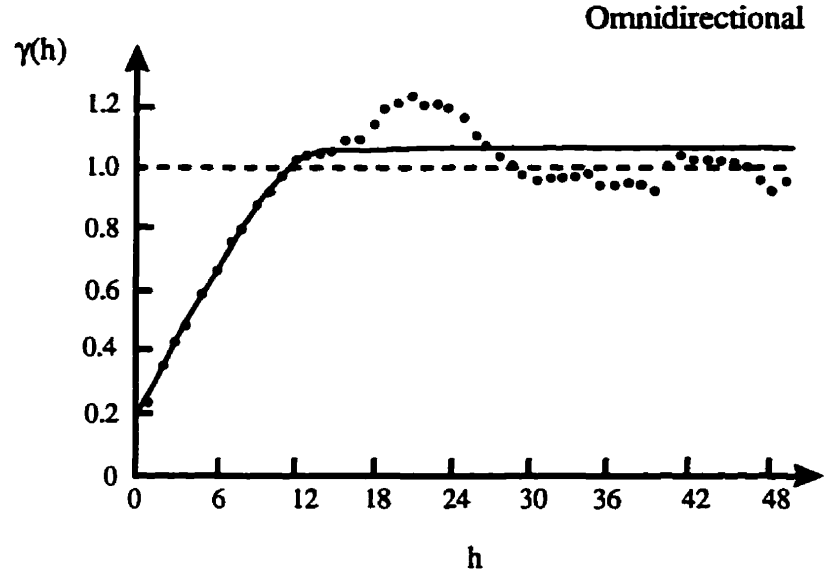

Figure 6.9. Omnidirectional variogram produced for RI02. The line represents the theoretical variogram model and the points the experimental variogram.

Only two sites were sampled over rubble sea ice (RI). As with the MYI sites, the omnidirectional variograms for the RI sites were best modeled using a spherical model, suggesting that points closer together are more similar and the spatial correlation decreases linearly as the lag distance increases (Figure 6.9). The experimental variogram model for RI01 was modeled by:

$$\gamma(h)=\begin{cases}0 & h=0\\ 0.17+0.90\left[\frac{3}{2}\left(\frac{h}{15.45}\right)-\frac{1}{2}\left(\frac{h}{15.45}\right)^3\right] & 0<h\le a\\ 0.17+0.90 & h>a\end{cases} \qquad (6.13)$$

where 0.17 represents the nugget variance, 15.45 the range and 0.90 the sill value.

The range values for the two rubble sites, RI01 and RI02 were 15.45 m and 35.18 m, respectively (Table 6.1). A larger range value indicated that observed values for snow depth on rubble sea ice are influenced by other values of snow depth over greater distances than are values for snow depth on FYI and MYI sites, which have smaller ranges. The larger range values for rubble ice was to be expected because of the greater irregular ice topography associated with the RI sites. This ice topography will cause the wind blown snow to catch and form snow drifts greater than those seen over first-year and even the classical hummock/melt pond structure of multiyear sea ice.

The nugget values associated with these two sites suggests that these models explained between 70% and 83% of the total variation in the two rubble sites (Table 6.1). As with the other two ice types, these values were less than half of the sill values thus signifying that the models used are appropriate for this ice type. The ice topography of rubble ice is similar to MYI sites, in that it will cause some patterns that are smaller than the sampling distance used, and thus cause the omnidirectional variograms to exhibit similar nugget values.

The indicative goodness of fit measures for the models for all the sites indicate that the models chosen were appropriate. For all three catchments, the IGF values ranged from 3.45e-03 to 2.91e-02. These low values can be considered very close to zero and thus indicating a good fit between the model, or combination of models, and the experimental variograms. Using other models resulted in an increase in the IGF values and thus a worse fit for the experimental variograms. This would suggest that the models could only be used of one specific ice type and not another.

One of the primary advantages of the omnidirectional variogram is that it can serve an early warning for erratic and unpredictable directional variograms. The well behaved nature of the omnidirectional variograms for the 15 sites

suggests that the directional variograms should also exhibit the same well behaved pattern.

6.2.3 Directional Variograms.

The directional variograms for the 8 FYI sites exhibited a combination of two kinds of spatial structures, the first structure modeled by a wave (hole-effect) model and the second structure modeled with a gaussian model. Figure 6.10 shows the theoretical and experimental directional variograms for FYI01. (Appendix D contains the directional variogram for the other FYI sites.) The smooth ice topography associated with first-year sea ice, combined with the predominant wind direction, produced a regular snow drift pattern. This periodicity is best defined using the wave model. The gaussian model is incorporated into the overall FYI model because as the separation distance increases at small lags, the snow depths are similar and only after a certain separation distance does this spatial correlation decrease. The variation of drift patterns between sites, i.e. the variation in the length of drifts, as well as the superposition of drift patterns caused by different directional trends, would affect the semivariance at small distances and thus the gaussian component in the complex models.

In a wave model, the distance to the first minima and maxima can be interpreted as the average distance between the snowdrifts and the average width of the snow drifts respectively. Table 6.2 lists the minima and maxima values for each direction for each FYI site sampled. The results suggest that the snow drifts on first-year sea ice were quite large, averaging over 30 m for the distance and between 15 m and 37 m for the width. The direction of the largest maximum and minimum values (highlighted in Table 6.2) can be interpreted as

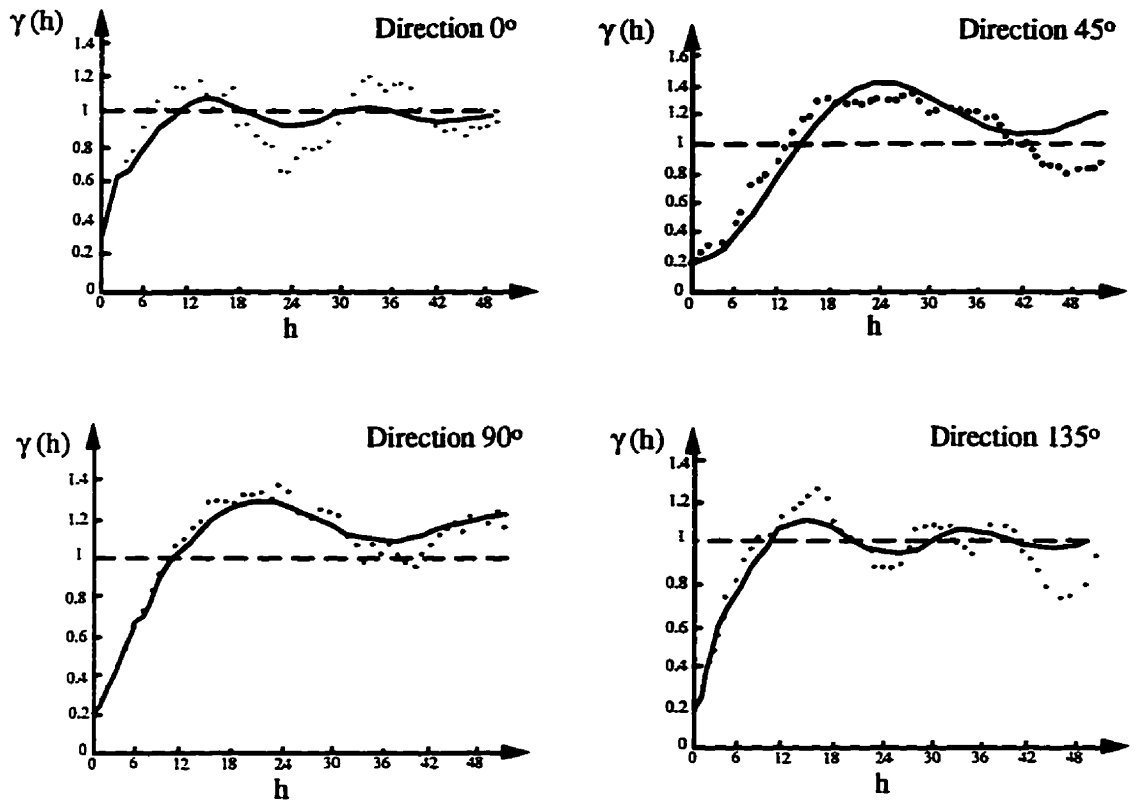

Figure 6.10. Directional variograms produced for FYI01. The line represents the theoretical variogram model and the points the experimental variogram.

Table 6.2. Minima and maxima values for directional FYI wave variogram models.

		0°	45°	90°	135°
FYI01	maxima	24	**41**	37	25
	minima	14	**26**	23	15
FYI02	maxima	12	15	**26**	20
	minima	7	9	**15**	12
FYI03	maxima	38	24	29	**41**
	minima	23	16	17	**24**
FYI04	maxima	**46**	37	14	35
	minima	**26**	21	10	20
FYI05	maxima	23	40	50	**>50**
	minima	13	25	30	**37**
SFYI01	maxima	**>30**	22	21	>30
	minima	**20**	12	13	24
SFYI02	maxima	>30	**>30**	24	24
	minima	22	**24**	16	14
SFYI03	maxima	12	28	26	**>30**
	minima	8	16	16	**24**

representing the direction in which the snow drifts are oriented. The results suggested that the orientation varied between sites.

All the directional variograms had strong spatial dependence with very limited random variation. This strong spatial dependence is illustrated by the low nugget values listed in Table 6.3. The nugget values were less than 0.27, indicating that the combination of the gaussian model and the wave (hole-effect) model accounts for more than 70% of the variability in the snow depths over first-year sea ice. These low values would suggest that the scale of sampling closely matched the spatial variation of the snow depth, and future in situ sampling over first-year sea ice should continue at a 1 m sampling interval.

There was considerable difference in the sill values when comparing the different directional variograms for an individual site suggesting the presence of zonal anisotropy (Table 6.3). The variograms indicate that the spatial variability in the 45° and 90° directions is greater than that for the 0° and 135° directions. This type of anisotropy is most likely caused by prevailing or predominant wind direction during storm events and ice topography. Section 6.3 will examine the relationship between the wind track and direction of anisotropy more concisely.

The FYI sites also exhibited a large variation in the range values between sites and within sites at different directions (Table 6.3). The greatest spatial range (51.6 m) was found at site FYI05, while FYI02 had a minimum range of 5.6 m. As with the sill value, site FYI05 had the largest spread of range values (43.9 m) for the four directions. This large spread of range values for site FYI05 would be due to the fact that this site consisted of sea ice that consolidated much later than sea ice for the other sites. The lack of agreement between sites could be attributed to winds that passed through the sampling area at the time of the study.

Table 6.3. Variogram parameter values for FYI directional variograms. IGF represents indicative goodness of fit values.

	FYI1		FYI2		FYI3		FYI4		FYI 5		SFYI1		SFYI2		SFYI3	
model	gaus.	wave	gaus.	wave	gaus.	wave	gaus.	wave	gaus.	wave	gaus.	wave	gaus.	wave	gaus.	wave
nugget	0.08		0.23		0.01		0.04		0.1		0.1		0.18		0.02	
range	27	3.1	4.2	1.4	11	5	15	5.9	4.8	2.9	9.2	2.1	10	2.5	7.2	3.6
sill	0.49	0.43	0.4	0.42	0.52	0.53	0.47	0.8	0.31	0.18	0.49	0.78	0.32	0.75	0.32	0.73
IGF	2.4e-02		1.3e-02		3.6e-2		2.7e-2		1.2e-2		7.7e-3		2.2e-1		1.2e-1	

	FYI1		FYI2		FYI3		FYI4		FYI 5		SFYI1		SFYI2		SFYI3	
model	gaus.	wave	gaus.	wave	gaus.	wave	gaus.	wave	gaus.	wave	gaus.	wave	gaus.	wave	gaus.	wave
nugget	0.19		0.22		0.05		0.07		0.1		0.04		0.08		0	
range	15.1	5.4	10	2	39	3.2	7.6	4.7	47	4.6	16.6	1.4	24.6	2.6	8.6	1.9
sill	0.5	0.51	0.5	0.42	0.54	0.65	0.37	0.64	0.89	0.55	0.95	0.24	0.38	0.61	0.41	0.59
IGF	2.5e-2		1.4e-2		1.3e-2		3.1e-2		8.8e-3		6.4e-4		3.5e-2		6.4e-2	

	FYI1		FYI2		FYI3		FYI4		FYI 5		SFYI1		SFYI2		SFYI3	
model	gaus.	wave	gaus.	wave	gaus.	wave	gaus.	wave	gaus.	wave	gaus.	wave	gaus.	wave	gaus.	wave
nugget	0.18		0.13		0.27		0		0.04		0.02		0.02		0	
range	9.7	4.7	4.2	3.3	10	3.7	45	2	26	6.8	16.	1.4	24	1.6	5.8	1.7
sill	0.53	0.46	0.34	0.58	0.2	0.54	0.67	0.54	0.5	0.9	0.62	0.27	0.33	0.58	0.28	0.85
IGF	7.6e-3		8.8e-4		1.9e-2		1.8e-2		7.3e-3		2.2e-2		6.1e-2		6.3e-2	

	FYI1		FYI2		FYI3		FYI4		FYI 5		SFYI1		SFYI2		SFYI3	
model	gaus.	wave	gaus.	wave	gaus.	wave	gaus.	wave	gaus.	wave	gaus.	wave	gaus.	wave	gaus.	wave
nugget	0.1		0.13		0.07		0.01		0.07		0.03		0.13		0	
range	5.3	3.2	4.4	2.6	9.7	5.3	9	4.5	12	8.4	5.8	2.7	8.1	1.6	8.6	2.9
sill	0.5	0.41	0.48	0.45	0.3	0.9	0.7	0.49	0.36	0.89	0.3	0.99	0.23	0.86	0.31	0.71
IGF	1.5e-2		7.1e-5		7.3e-2		7.6e-3		2.0e-3		2.9e-3		3.0e-2		6.5e-2	
aniso.	0.29		0.47		0.32		0.26		0.15		0.47		0.38		0.64	

Note: 1. SFYI denotes sites sampled during the SIMMS'95 field experiment.
2. gaus. represents a gaussian model.

When comparing the different directions for each site with respect to the range values, it becomes evident that each site exhibits geometric anisotropy. There was actually no reason to assume that the snow distribution patterns would exhibit the same behavior in every direction, i.e. be isotropic; anisotropy is consistent with the main underlying physical process of the prevailing or predominant wind direction and its implication on the snow distribution.

The degree of geometric anisotropy located within each site was measured by the anisotropy ratio, which is equal to the range of the variogram in the direction producing the shortest range divided by the range in the direction with the longest range. The more dissimilar the ratio is from one, the stronger the geometric anisotropy. Each site had a ratio that was much lower than one, ranging from 0.64 (SFYI03) to 0.15 (FYI05), suggesting a directional trend in the data. The long axis of anisotropy, or the direction with the longest range, characterizes the predominant wind direction and also exhibits the greatest spatial dependence. The direction of the geometric anisotropy for the eight FYI sites varied between 0° and 90°, with a majority of sites having the long axis of anisotropy oriented in the 45° direction. This would suggest that the prevailing wind direction is oriented in this direction (see Section 6.3).

The MYI experimental directional variograms were best modeled using two spatial structures; a combination of the spherical and gaussian models (Figure 6.11 illustrates the combination of the two models for MYI03, while Appendix D contains the directional variograms for the other sites.). The linear behavior at small lag distances suggests that as the lag distance increases, the semivariance values also increase. This would indicate the appropriateness of the spherical model. As the lag distances increase, the experimental variogram approaches the sill asymptotically, suggesting that the gaussian model should be incorporated into the theoretical variogram model for snow distribution on

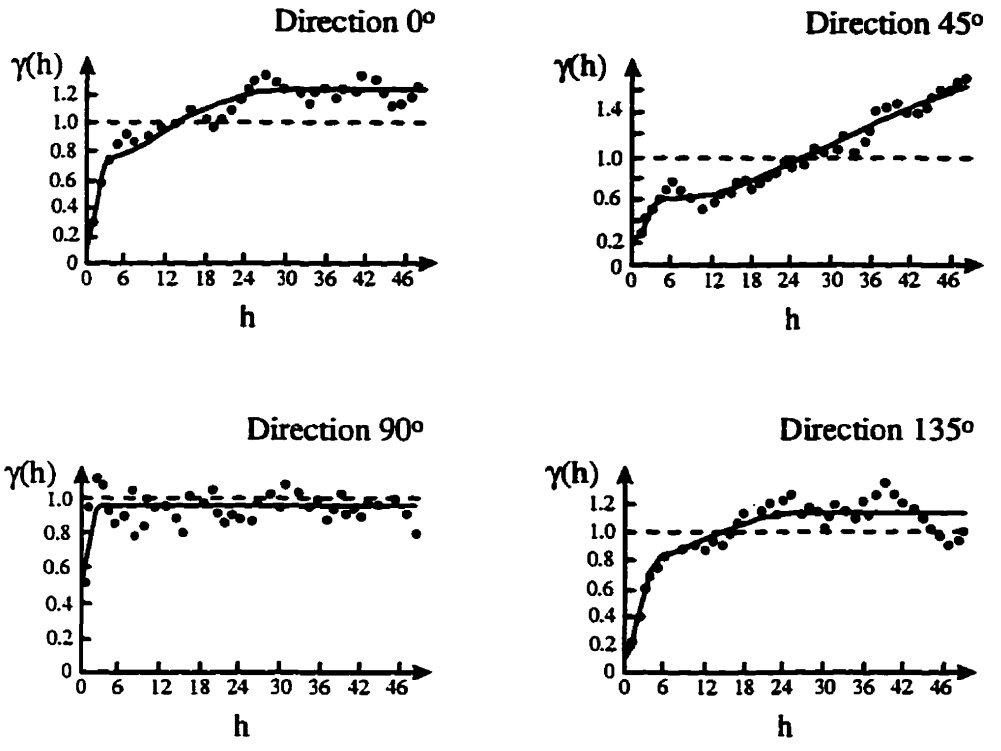

Figure 6.11. Directional variograms produced for MYI03. The line represents the theoretical variogram model and the points the experimental variogram.

multiyear sea ice.

For the SIMMS site (SMYI01), the best theoretical model is a single gaussian model. This singularity in modeling may be due to the fact that the sampling interval for this site was 2 m, therefore eliminating half of the semivariance values from the variogram. The linear behavior at the origin may be incorporated into the gaussian model, due to the absence of values at small lags.

The five MYI sample sites exhibited different directional variograms than those of the FYI sites. This variation in variogram models between first-year and multiyear sites, is probably due to the irregular topography of multiyear sea ice.

On MYI, snow drift patterns are less periodic, compared to those on FYI. This irregularity in snow drifts results in modeling the experimental variogram using a theoretical model other than a wave (hole-effect) model.

There was also significant difference in the sill values when the directional variograms were compared within each site. Only MYI01 showed little difference in the sill values related to direction, indicating the absence of any zonal anisotropy at this site. The other four sites had differences in sill values that ranged from 0.37 for SMYI01 to 1.28 for MYI03, suggesting the presence of zonal anisotropy in some degree. Again, this anisotropy was probably caused by the prevailing or predominant wind direction.

When comparing the five sites, the variation of range values was large, varying from 6.4 m for SMYI01 to 116 m for MYI03 (Table 6.4). This variation suggests that the range of spatial continuity varies significantly between sites, which again could be due to the fact that winds occurred between sampling dates. Another factor contributing to this variation is the different ice topographies associated with this ice class. The five MYI sites exhibited a great variation in the ice topography, thus affecting the distribution patterns and in terms of the variogram, the range of the theoretical models.

In general, the range values are greater for MYI sites when compared to the FYI sites. These larger ranges would indicate that the values for snow depth in MYI sites are influenced by other values of snow depth over a greater distance than are values of snow depth in FYI sites. The larger ranges for MYI are to be expected since the ice topography will facilitate greater drifts, in terms of both depth and length, in the MYI sites and because the ice topography on multiyear will also provide an underlying autocorrelation in the catchment dynamics.

Table 6.4. Variogram parameter values for MYI and RI directional variograms. IGF represents indicative goodness of fit values.

	MYI1		MYI2		MYI3		MYI4		SMYI		RI 1	RI 2
model	spher.	gaus.	spher.	gaus.	spher.	gaus.	spher.	gaus.	gaus.		gaus.	gaus.
nugget	0.30		0.07		0.05		0.21		0.08		0.54	0.20
range	2.5	4.0	7.5	56.0	4.0	27.	3.4	11.5	9.5		23.5	12.5
sill	0.31	0.44	0.53	1.10	0.68	0.52	0.31	0.51	1.03		0.47	0.98
IGF	1.8e-2		1.8e-2		9.8e-3		3.4e-2		3.1e-2		1.6e-2	8.2e-2

	MYI1		MYI2		MYI3		MYI4		SMYI		RI 1	RI 2
model	spher.	gaus.	spher.	gaus.	spher.	gaus.	spher.	gaus.	gaus.		gaus.	gaus.
nugget	0.34		0.20		0.19		0.08		0.08		0.27	0.32
range	15.1	5.4	10	2	39	3.2	7.6	4.7	47		29.0	23.4
sill	0.28	0.40	0.57	0.47	0.40	1.49	0.46	0.64	0.88		1.04	0.74
IGF	1.10e-2		1.8e-2		1.5e-2		3.9e-2		8.2e-2		9.1e-3	4.3e-2

	MYI1		MYI2		MYI3		MYI4		SMYI		RI 1	RI 2
model	spher.	gaus.	spher.	gaus.	spher.	gaus.	spher.	gaus.	gaus.		gaus.	gaus.
nugget	0.30		0.19		0.34		0.00		0.10		0.33	0.40
range	4.5	29.0	6.5	8.0	2.5	3.0	19.0	97.0	8.4		31.5	9.5
sill	0.55	0.17	0.61	0.20	0.30	0.31	0.90	0.49	1.04		1.03	0.59
IGF	1.1e-02		1.4e-01		1.1e-2		1.6e--2		1.8e-2		1.9e-2	2.8e-2

	MYI1		MYI2		MYI3		MYI4		SMYI		RI 1	RI 2
model	spher.	gaus.	spher.	gaus.	spher.	gaus.	spher.	gaus.	gaus.		gaus.	gaus.
nugget	0.30		0.12		0.03		0.13		0.00		0.47	0.21
range	4.0	13.1	8.0	24.3	6.0	26.5	6.0	23.6	10.6		41.8	11.4
sill	0.50	0.27	0.54	0.46	0.75	0.39	0.42	0.60	1.25		0.78	1.00
IGF	1.2e-2		1.0e-2		1.4e-2		9.9e-3		1.7e-1		2.9e-2	6.2e-2
aniso.	0.19		0.28		0.07		0.13		0.60		0.56	0.41

Note: 1. SMYI denotes sites sampled during the SIMMS'95 field experiment.
2. spher. represents a spherical model and gaus. represents a gaussian model.

All five MYI sites exhibited some degree of geometric anisotropy, ranging from 0.07 to 0.23. These values are much lower than those for the FYI sites, suggesting that the MYI sites contain a greater degree of anisotropy, or in other words, the degree with which the ranges varied was significantly greater for the MYI sites. The directional component of the geometric anisotropy for the MYI sites was similar to the FYI sites, varying between 0° and 90°. This would also further suggest that the predominant wind track in MYI sites was oriented 45°. See section 6.3 for an examination of wind directions in the Resolute area.

The nugget values for the various MYI sites suggest that a significant amount of variation in the snow distribution patterns can be accounted for by the theoretical complex models developed from the experimental data. The values were less than 0.35, suggesting that more than 65% of the variability associated with this distribution was explained by the spatial structure (Table 6.4). As with sampling on first-year sea ice, any further sampling of the snow distribution on multiyear sea ice should continue at an interval of 1 m.

The data suggests that the local discontinuity, measured by the nugget effect, was slightly greater for MYI than for the FYI sites. The greater nugget effect for MYI was to be expected because the irregular ice topography characteristic of the MYI sites would more likely produce snow drifts that may be less than 1 m, and thus more likely to be omitted from the sampling.

The distribution of snow was different on rubble sea ice than was observed on multiyear and first-year sea ice. The experimental variograms for the two rubble sea ice sites sampled during the C-ICE 96 field experiment can best be modeled using a single gaussian model (Figure 6.12 and Appendix D). This singular model is probably a result of the greater fluctuation in snow depth as the separation distance increases caused by the more irregular topography associated with rubble sea ice.

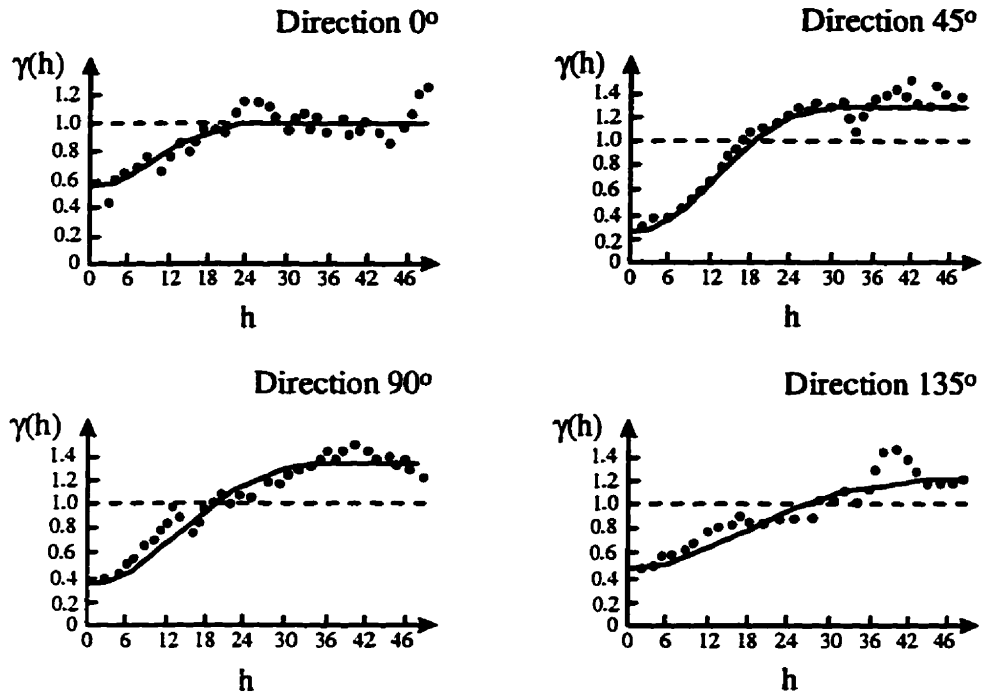

Figure 6.12. Directional variograms produced for RI01. The line represents the theoretical variogram model and the points the experimental variogram.

Zonal anisotropy is also present in these two sites. The difference in sill values between directions for these sites was 0.57 for RI01 and 0.41 for RI02. These values indicate that the zonal anisotropy for the first rubble ice site was greater than the anisotropy for the second site.

When comparing these two sites with the one MYI site that was sampled in 1995 it can be seen that the ranges were greater for the RI sites. This can be attributed to the more irregular topography associated with the rubble ice that would produce large snow drifts and the distribution patterns would be more spatially correlated over a larger distance.

The two rubble ice sites also exhibited geometric anisotropy. The ratio for geometric anisotropy suggests that this anisotropy was significant, with

values of 0.57 and 0.41 for the two sites respectively. The geometric anisotropy is greater for the second site because of the greater irregular ice topography found in this site. The directional component of the geometric anisotropy in the rubble ice sites varies depending on the site; the directional component is 135° for the first rubble site and 45° for the second site. This difference in direction could be due to the impact the topography of the ice type had on the prevailing wind direction.

As was expected, the nugget values for the rubble ice sites were large indicating a lower percentage of variation being explained by the models. The nugget values ranged from 0.2 to 0.54 (Table 6.4), suggesting that only between 50% and 80% of the variation can be modeled with the theoretical variograms used in this study. The large nugget values indicate that micro-structures, or drifts that are less than the sampling interval of 1 m, were frequent in the sites and missed within the data set. Therefore, a sampling interval less than 1 m should be used for future in situ sampling of the snow distribution patterns on rubble sea ice.

The indicative goodness of fit measures for the models for all the sites indicate that the models chosen were appropriate. For all three catchments, the IGF values ranged from 9e-03 to 8e-02. These low values can be considered very close to zero and thus indicating a good fit between the model, or combination of models, and the experimental variograms. Using other models resulted in an increase in the IGF values and thus a worse fit for the experimental variograms. This would suggest that the models could only be used of one specific ice type and not another. For example, the low IGF value for the combination of the wave and gaussian model on FYI indicates that this combination of models best represents FYI and that other models, such as a combination of a spherical and gaussian models (as in the MYI sites) will not

adequately model the FYI variograms.

The models for the three different ice types were also chosen based on the ice topographic influence on the snow distribution. On smooth first-year sea ice, for instance, the harmonic snow pattern formed on the ice is best modeled using a wave model. The more irregular ice topography associated with multiyear and to a greater extent rubble sea ice, produced snow distribution patterns that were more random and best reflected a spherical model, either alone as in the case of rubble ice, or in combination as in the multiyear-year sites.

Ice topography will influence the anisotropic orientation of the snow drift features. Over first-year sea ice, the smooth ice will not impact the orientation as much as the wind direction. Over the two other ice classes, the topography will influence the anisotropy direction to a greater extent. The hummocks/ice pieces will be able to catch blowing or drifting snow, thus producing snow drifts deeper than the flat first-year sea ice. The irregular topography will result in snow drifting in a particular direction, oriented with the wind direction.

6.3 Wind Direction Analysis.

To link the direction of geometric anisotropy found in the variogram models of snow distribution with wind direction, an analysis of the prevailing wind direction during storm events occurring at Resolute over the past 25 years was conducted. For this study, only the direction of winds occurring during storm events was analyzed. It is only this wind direction that affects the direction of snow drifting in the Arctic.

Climatological data, namely precipitation amounts, wind speed and direction measured at the Resolute weather station were obtained from the

Atmospheric Environment Service (AES). These climatic variables were routinely collected for the period from1971 to 1995. Precipitation amounts were collected on a daily basis, while wind speed and direction were hourly data.

In order to compute the prevailing wind direction during storm events, daily averages of both wind speed and direction were initially calculated. For days without precipitation, the wind speed and wind direction values were eliminated from the analysis. A total of 2597 days in the 25 year period were used in this analysis. Thus, the calculation of the predominant wind direction was done by taking the average of the wind directions for the days with precipitation. Analysis was conducted for a 25-year time period, as well as on a decadal, yearly, and seasonal basis.

The 25-year analysis showed that the predominant wind direction for the Resolute weather station was 13°, with a standard deviation of 81° (Table 6.5). This finding agreed with the direction of anisotropy calculated from the variogram analysis. The direction of anisotropy calculated for the FYI and MYI sites varied between 0° and 90°. The wind direction during the storm events fell within this range. Thus, it can be stated that the direction of anisotropy for the variogram models of snow distribution is a product of the predominant wind direction during storm events.

The large standard deviation associated with the wind direction indicates that when low pressure cells pass over the area, the wind direction varied. This variation in wind direction would ultimately impact the overall distribution of snow on the ice catchments. Drifting within the sampling sites would not closely reflect the varying direction of the wind. Therefore, snow drifts would not be distinguishable within the data set. This would cause the direction of anisotropy to vary, and thus accounts for the variation measured at the sites.

Table 6.5. Average wind speed and wind direction during storm events measured at the Resolute weather station. Values in brackets repesent the standard deviation associated with the variable. The final row in this table represents the 25 year average of the variable.

Year	Wind Speed (km/hr) Yearly Average	Decadal Average	Wind Direction (°) Yearly Average	Decadal Average
1971	25.4 (13.2)		10 (83)	
1972	23.5 (11.5)		17 (78)	
1973	26.4 (12.8)		18 (83)	
1974	23.0 (11.2)		22 (80)	
1975	19.6 (9.8)		30 (82)	
1976	20.2 (11.1)		26 (81)	
1977	26.3 (12.5)		10 (92)	
1978	20.8 (12.1)		14 (80)	
1979	20.6 (10.1)	22.6 (11.7)	3 (85)	17 (82)
1980	21.9 (11.0)		358 (78)	
1981	23.2 (12.2)		3 (66)	
1982	21.0 (9.7)		26 (83)	
1983	22.2 (10.5)		21 (77)	
1984	18.6 (8.5)		25 (72)	
1985	23.3 (13.5)		11 (75)	
1986	22.0 (10.6)		23 (84)	
1987	24.9 (12.0)		350 (80)	
1988	24.9 (11.9)		12 (86)	
1989	22.3 (9.2)	22.5 (11.1)	24 (82)	13 (79)
1990	19.3 (11.6)		6 (75)	
1991	23.2 (12.5)		21 (80)	
1992	21.8 (11.2)		5 (82)	
1993	25.1 (12.6)		346 (71)	
1994	23.8 (11.4)		17 (79)	
1995	20.5 (11.8)	22.2 (11.9)	9 (88)	8 (80)
25-Year	22.5 (11.5)		13 (81)	

Wind analysis was also conducted on decadal, yearly and seasonal time scales. The decadal analysis showed that the predominant wind direction during storm events, along with the wind speed, was similar for the three decades (Table 6.5). These values agreed well with the wind direction for all 25

years. As with the previous analysis, both wind speed and direction had large standard deviations associated with their average values, indicating that there were large variations in these variables over the decades. This suggests that the large variation in wind direction computed using all 25 years was not based on decadal variations, but could be a product of yearly variations.

Analysis of the wind direction was also completed on a yearly basis. This analysis indicated that the mean values for wind direction and wind speed were similar to that found for the other two analyzes. From Table 6.5, it can be seen that the wind direction varied considerably when precipitation was occurring, varying from 30° in 1975 to 346° in 1993.

Seasonal analysis was conducted to determine if the predominant wind direction varied with the seasons. The seasons were determined arbitrarily, based on the conditions in the area. Winter consisted of the months November to March, inclusive and was the largest seasons. The spring season was composed of April and May, while June to August formed the summer season. The remaining months were classified as the autumn season.

Results indicate that while wind direction was large during the summer months (Table 6.6.), the predominant wind direction did not significantly vary. The seasonal averages were also similar to the 25-year average. The large variation attached to the average wind direction indicates that the variation in wind direction during storm events was predominantly on a storm event basis. There were no patterns in the seasons analysis, as with the yearly and decadenal analyses, that may explain the variation over the 25-year time period.

The analysis of the predominant wind direction during storm events did suggest that the direction of anisotropy observed for the directional variograms of snow distribution is a product of the wind direction. The large variation in

Table 6.6. Seasonal averages of wind speed and direction. Values in brackets repesent the standard deviations associated with the variable.

Season	Wind Speed (km/hr)	Wind Direction (°)
Summer - 1970s	22.8 (10.7)	22 (78)
1980s	21.7 (9.7)	24 (73)
1990s	21.9 (9.6)	17 (75)
25-year	22.1 (10.0)	21 (76)
Autumn - 1970s	24.5 (12.3)	20 (90)
1980s	24.5 (12.3)	22 (85)
1990s	22.7 (11.9)	1 (84)
25-year	23.9 (12.2)	14 (86)
Spring - 1970s	21.8 (11.8)	3 (85)
1980s	20.8 (9.9)	6 (76)
1990s	19.6 (10.8)	8 (81)
25-year	20.7 (10.8)	6 (81)
Winter - 1970s	21.2 (12.0)	19 (78)
1980s	22.5 (11.6)	2 (81)
1990s	23.8 (14.0)	1 (82)
25-year	22.5 (12.5)	14 (80)

wind direction may also explain the variation in anisotropy directions and the fact that the snow drifts varied within and between sites.

This chapter explored the modeling of the snow distribution patterns over three different sea ice catchments (first-year, multiyear, and rubble sea ice), as opposed to examining snow depths. Single depth measurements are not as important to understanding processes operating within an icescape as the interrelationship between those values. A relatively new statistical technique known as the variogram was used to model the distribution patterns. This method takes into account the spatial dependence of sampling points, and models the spatial continuity of the snow depth. A review of the construction and analysis for this statistical technique was also presented in this chapter.

The variogram models constructed showed that for the three different ice catchments a different model was obtained, illustrating the appropriateness of the variograms in the modeling of the snow distribution patterns. The analysis of the directional variograms indicated that anisotropy was present in all the sample sites. This anisotropy was correlated with the predominant wind direction during storm events for the Resolute area. These models of the snow distribution can be applied to the quantification of the light penetration through the ice and snow layers in the Arctic. The application of the variogram models is investigated in the next chapter.

CHAPTER 7:

APPLICATION OF THE MODELS FOR SNOW DISTRIBUTION PATTERNS.

This chapter examines the research methods and results and discussion concerning the application of the models for the spatial distribution of snow on sea ice. In this chapter, the light penetrations through the three ice classes; first-year, multiyear and rubble sea ice, are examined and compared. Also the differentiation of the ice types from SAR images is performed. The first section introduces the techniques used to classify a SAR image, as well as to produce maps of snow and ice thickness values and the amount of light penetration through these layers. Section 2 of this chapter will present the results of the calculation of light penetration and ice discrimination.

7.1. RESEARCH METHODS.

7.1.1. Grey-level co-occurrence matrix method.

At present there is available both tonal (first-order) and textural (second-order) information for the discrimination of ice classes in SAR imagery. Studies have used the difference in tone between first-year and multiyear sea ice as a

method of classification for these ice types (Kwok et al., 1992; Nystuen and Garcia, 1992; Shuchman et al., 1989, Lynden et al., 1984). In these studies, maximum-likelihood or discriminant clustering types of classification are used to statistically separate the sea ice classes. However, these methods are only able to differentiate between first-year and multiyear sea ice. New ice is not distinguishable from FYI and land is not distinguishable from MYI. Also, different surfaces with similar scattering properties are not separable (i.e. rough FYI versus smooth FYI) (Barber, 1989). Therefore, grey tone has proven not to be effective in the discrimination of sea ice types in SAR imagery.

Due to the poor results obtained with tonal information, research had changed focus to more complex representations of texture, namely second-order texture measures. The difference between first-order and second-order approaches is that in the latter, the statistical relationship between each SAR resolution cell and its neighbor is used as a measure of the spatial information (Barber et al., 1993). A number of approaches to second-order texture measures exist. These approaches include statistical, stochastic, structural and frequency domain analysis (Barber and LeDrew, 1991). Statistical approaches, including the GLCM method, is based on the grey level probability density functions (pdf) which is "computed as the conditional joint probability of pairs of pixel grey levels in a local area of the image" (Barber and LeDrew, 1991). The basic assumption of stochastic approaches is that a particular statistical method (i.e. Markov Chains) is the basis for probabilistically estimating the texture fields. The third approach, the structural approach, makes use of the notion of texture primitive (Connors and Harlow, 1980a). The frequency domain analysis uses the frequency domain on the power spectra of the image to separate different textures within an image (Connors and Harlow, 1980b). Barber and LeDrew (1991) presents a detailed description of the various approaches.

With the large number of approaches available for the classification of sea ice types in SAR imagery, a comparative study of the various techniques was conducted that would outline the best method. Weszka et al. (1976), Connors and Harlow (1980b) and Barber et al. (1993) conducted rigorous studies on the effectiveness of a number of different approaches available for discrimination of various features from SAR imagery. Both of these studies found that the most effective method was the GLCM approach. The comparative analysis by Barber et al. (1993) was computed based on sea ice texture fields, which makes the results of the study of particular importance to this thesis. Based on these findings, the GLCM method was used to differentiate sea ice types in this thesis.

The Grey Level Co-Occurrence Matrix (GLCM) method used to differentiate sea ice types from SAR imagery was first developed by Haralick et al. (1973). This method produces a square matrix of dimension N which "provides the conditional joint probabilities of all pairwise combinations of pixels within a computational window" (Barber et al., 1993). The entries in the matrix represent the probability of occurrence of grey levels at two pixels dependent on the interpixel sampling distance (δ) and the orientation (α). This can be expressed algebraically as (Haralick et al., 1973):

$$\sum_{i=1}^{N}\sum_{j=1}^{N} C_{ij}^{2}$$

$$\Pr(x) = \left\{ C_{ij} | \delta, \alpha \right\} \tag{7.1}$$

$$C_{ij} = \frac{P_{ij}}{\sum_{i,j=1}^{N} P_{ij}} \tag{7.2}$$

where P is the frequency of occurrence of grey levels i and j and N refers to the total number of pixel pairs. The number of pixels pairs is dependent on the size

of the computational window.

The orientation and the interpixel sampling distance are two important parameters in the calculation of the GLCM. Orientation is defined as the direction in the image at which the probabilities of combinations of pixels are determined. Four directions are commonly used in the calculation of the GLCMs. The orientation α=0° is considered parallel to the look direction of the sensor. The interpixel sampling distance is similar to the lag distance in variogram analysis. This parameter refers to the separation distance between two pixels. For instance, in a GLCM analysis, if δ=3 and α=90° then the computation of the probability of grey levels would be calculated for pixels that were three pixels apart and oriented 90° to each other.

The texture structure of an image relates to the GLCM. In an image that is considered texture-poor or homogeneous in texture, the transition between different grey levels is not frequent and most of the adjacent pixels will have similar grey levels. This results in large values along the diagonal or near-diagonal entries of the GLCM matrix. When an image is texture-rich or heterogeneous in texture, the opposite occurs. There is a large probability that adjacent pixels will have dissimilar grey levels resulting in frequent transitions between high and low grey levels. This will in turn cause large values in the off-diagonal entries in the matrix. A coarser texture will produce a GLCM with a large cluster of probabilities, while finer textures will produce smaller clusters in the matrix. Tone in the image is measured by movement up and down the diagonal.

A number of statistical measures, known as texture statistics, can be derived from the matrix. Each statistic is defined as a single spatial measure that characterizes the texture information found in the image. These texture statistics are considered point estimates because they each provide a measure

of the total information content of the GLCM (Barber et al., 1993). Evaluation of each texture statistic, alone or in a number of combinations, provides the discriminability of the sea ice types. Five texture statistics were used in this research.

1. Uniformity (unif.)

$$\sum_{i=1}^{N}\sum_{j=1}^{N} C_{ij}^{2} \tag{7.3}$$

This texture statistic is primarily influenced by the high values in the matrix, such that large values in the GLCM will produce large uniformity values. Highly homogeneous areas will have high uniformity values.

2. Entropy (entr.)

$$-\sum_{i=1}^{N}\sum_{j=1}^{N} C_{ij} \log C_{ij} \tag{7.4}$$

This statistic is a measure that quantifies disorder in an image. An image with texture that is highly disordered (i.e. heterogeneous texture image) will have large entropy values.

3. Dissimilarity (diss.)

$$\sum_{i=1}^{N}\sum_{j=1}^{N} C_{ij}|(i-j)| \tag{7.5}$$

This is a measure of dissimilarity in grey levels for a given orientation and interpixel sampling distance. The more dissimilar the grey levels are, the larger the dissimilarity value. This statistic is sensitive to grey level spatial variability and tone of the image (Barber et al., 1993).

4. Contrast (cont)

$$\sum_{i=1}^{N}\sum_{j=1}^{N} C_{ij}(i-j)^{2} \tag{7.6}$$

This texture statistic is also known as the inertia statistic in the literature. It can be considered a measure of the contrast between grey levels (Shokr, 1989). Off-diagonal values found within the matrix highly influence the contrast statistic.

High contrast values indicate a heterogeneous image.

5. Correlation (corr.)

$$\sum_{i=1}^{N}\sum_{j=1}^{N}\frac{(i-\mu_x)(j-\mu_y)C_{ij}}{\sigma_x\sigma_y} \qquad (7.7)$$

where μ_x and μ_y refer to the mean of row i and j respectively and σ_x and σ_y represent the standard deviation of row i and j respectively. This measure is sensitive to the correlation between grey levels. High correlation values suggest that the image is heterogeneous in texture.

Once the five texture statistics were computed for the different subscenes, linear discriminant analysis (LDA) was executed to determine which combination of texture statistics would best differentiate or maximize discrimination of sea ice types in a SAR image. LDA has been commonly used in the literature to assess the contribution of several variables to classification precision (Blom et al., 1987; Schwaller, 1987; Steiner et al., 1971) and for the assessment of a set of variables to classification agreement (Barber and LeDrew, 1989; Franklin et al., 1989; Kershaw, 1987).

In this thesis, LDA was used to assess which set of the five texture statistics maximizes discrimination of sea ice types. If no environmental factor (i.e. texture statistic) is able to distinguish the ice classes, LDA produces a discriminant function (z) which is a linear combination of the environmental factors. The discriminant function is then able to distinguish the different ice classes (Ludwig and Reynolds, 1988). The linear transformation maximizes the inter- and intra-class variation over the different ice classes. The inter- versus intra-class variation is maximized by the first function (z_1). The second function (z_2) maximizes the F ratio. The important limitation is that z_2 is statistically orthogonal to z_1 (Barber and LeDrew, 1989).

Besides the two discriminant functions, output from LDA includes the

relative percent contribution of each variable to discrimination as well as the Mahalanobis multivariate distance measure (D2). The Mahalanobis distance measure is computed to measure the multivariate distance between each pair or group of variables and is thus used for class assignment. An F ratio is used to test the statistical significance of each pair or group of texture statistic (Ludwig and Reynolds, 1988). LDA uses each of these parameters to compare each ice type to another type in a pairwise fashion and displays the relationships between the ice classes in discriminant space. These plots provide information on the magnitude of class separation as a function of the texture statistics.

Contingency tables were tabulated for classification accuracies based on the different combinations of texture statistics. Each contingency table listed the number of sites correctly, as well as incorrectly, classified as a certain ice type by the linear discriminant analysis of the combination of texture statistics specified. From this table, a classification agreement was determined by dividing the number of correctly classified sites by the total number of sites. A comparison of the classification accuracies determined which combination of texture statistics best discriminated the sea ice types in SAR imagery.

7.1.2. Kriging.

In order to obtain snow depth and ice thickness values for areas not sampled within the sampling grid, a geostatistical method known as kriging was used. Kriging is an extension of the variogram, in that the kriging method interpolates depth and thickness values between sampling locations using the semivariance of the variograms. Kriging is considered a linear, unbiased, least-squares spatial interpolation method whose objective is the use a number of close data observations to estimation the value of the regionalized variable at a

location not sampled (Carr, 1995).

In this procedure, the data points are multiplied by a weight and the sum of these products is the best estimate for the unknown point. The semivariance function, or the variogram, is used to determine the weights needed to define the contribution of each sampled point to the interpolation (Villard and Maurer, 1996). Data points closer to the unknown point contribute most to the interpolation. The accuracy of the kriging estimates therefore depends primarily on the goodness of the computed variograms.

This method is unbiased because it has as an underlying assumption that the sum of the weights used for interpolation is one, such that:

$$\sum_{i=1}^{N} \lambda_i = 1 \qquad (7.8)$$

where N is the number of closest data points, and λ is the weight. Weights are chosen to minimize the variance of the observation error, or error variance.

Kriging estimates are examples of weighted averages of nearby samples:

$$v^* = \sum_{i=1}^{N} \lambda_i v_i \qquad (7.9)$$

where v^* is the interpolated value being estimated, v_i (i=1,2,3,...n) is the vector of values at the nearby locations, and λ_i (i=1,2,3,...n) is the vector of corresponding weights to be used in averaging these values. Isaaks and Srivastava (1989) and Carr (1995) provide further details on this process.

There is a higher degree of uncertainty associated with the predicated values at the boundary of the sampling grids. At these locations, the standard

errors associated with the kriging predictions tend to be the highest, resulting in a larger uncertainty. The reason for these large error values is because these areas are poorly sampled and data points are few and at a greater distance.

For this study, kriging was used to interpolate the snow and ice thickness depths at a 1 m interval for a 100 m x 100 m matrix. This method was done for one site on each ice catchment that represented the ice type and produced 10,000 snow and ice values for each ice type.

7.1.3. PAR Transmittance Model.

The kriged snow and ice maps for first-year, multiyear and rubble sea ice were used to estimate the amount of photosynthetically active radiation (PAR) that is transmitted through these layers to the underlying ocean. PAR is the waveband between 0.4 μm and 0.7 μm, and encompasses the blue and red bands of the visible portion of the electromagnetic spectrum. Algal pigments, especially chlorophyll, absorb the radiation within this waveband and use it to create organic compounds essential for life. Thus, this waveband is at the core of the photosynthetic process.

In order to calculate the amount of PAR transmitted through the snow and ice layers, a FORTRAN-based two-stream radiative transfer model was utilized. This model was supplied by D. Perovich at the CRREL research laboratory. The depth and layer type of snow and ice at each position are the primary inputs for the model. For the purpose of this study, the snow layer was defined as a cold, dry snow layer, while first-year sea ice was defined as cold blue ice and multiyear and rubble sea ice as white ice interior. For each location the number of layers, sky conditions, contribution to albedo from specular reflection, as well as the incident irradiance and the number of wavelengths must also be

specified. For all three ice catchments, a clear sky was used with an incident irradiance of 1 W/m^2. For snow covered sea ice, the contribution to albedo was considered zero.

The model uses the inputs to calculate, among other outputs, the incident radiation, albedo values and transmittance through the snow and ice layers for each location. These outputs are calculated for 61 wavelengths, between 0.4 μm and 1.0 μm, at an interval of 0.01 μm. Therefore, the sum of the transmittance for the wavelengths between 0.4 μm and 0.7 μm was considered the transmittance of PAR for a particular location. For each ice type, the amount of PAR that was transmitted through the snow and ice was calculated at every 1 m for a 100 m x 100 m matrix, producing 10,000 values for each ice type. These values can than be used to examine the spatial variability of PAR transmittance for first-year, multiyear and rubble sea ice.

7.2 RESULTS AND DISCUSSION.

7.2.1 Classification of Ice Types.

Classification of ice types using the GLCM method was done to allow for a regional examination of distribution patterns. Table 7.1 lists the classification accuracies in descending order for different combinations of texture statistics. (Appendix E lists the classification accuracies for all possible combination of texture statistics, as well as the contingency tables associated with the combinations.) The combination of uniformity-dissimilarity-entropy provided the best classification agreement, with an agreement just below 80%. This finding is in agreement with that of Barber et al. (1993), which found that the combination of uniformity - dissimilarity - entropy provided a classification of

Table 7.1. Classification accuracies for best seven combinations of texture statistics.

GLCM Statistics	Classification Agreement
Unif-Entro-Diss	79%
Unif-Entro-Corr-Cont	76%
Unif-Entro-Diss-Cont-Corr	76%
Unif-Entor-Diss-Cont	74%
Unif-Entro-Cont	73%
Unif-Entro-Diss-Corr	73%

Note: Unif = uniformity, Entro = entropy, Diss = dissimilarity, Corr = correlation, and Cont = continuity.

between 83% and 89%. This combination was one of the best available for the classification of the three ice types. The accuracies decreased as the combinations of statistics changed. No single statistic adequately classified the three ice classes individually (Appendix E).

An examination of the contingency table for uniformity-dissimilarity-entropy combination suggests that both FYI and MYI were misclassified predominantly as the next irregular ice type (Table 7.2). For instance, seven out of the eight misclassified FYI sites were classified as MYI. The same was found for MYI. This was a result of more irregular topography within the ice class being used as a site for classification. The RI misclassified sites were classified as MYI. These misclassified sites were generally more homogenous than the others and more closely resembled MYI sites, in terms of texture.

Table 7.2. Contingency table for the combination of uniformity-dissimilarity-entropy texture statistics for the three ice types.

	FYI	MYI	RI	
FYI	22	7	1	30
MYI	1	23	6	30
RI	1	3	26	30
	24	33	33	**79%**

Rubble sea ice had a classification agreement of 87%, greater than both FYI and MYI (Table 7.2). The high classification would indicate that the combination of uniformity-dissimilarity-entropy was an excellent classifier for this ice type. This high agreement was a result of the rubble sea ice subareas being more dissimilar in texture to both multiyear and first-year sea ice types.

7.2.2 Interpolation of Snow and Ice Thickness.

Figures 7.1 to 7.3 illustrate the kriged snow and ice surface plots for three sites sampled on the various sea ice catchments (FYI01, MYI01, and RI02, respectively). For first-year sea ice, the ice thickness was assumed to be constant and thus the surface plot for this ice catchment is uniform (Figure 7.1). The snow distribution on this ice catchment was rather uniform with a periodicity, forming dunes or sastrugi. This pattern is a result of the flat underlying ice and the lack of any large uplifted pieces that act as a catalyst for snow drifting.

The pattern of snow distribution for multiyear and rubble sea ice is a product of the underlying ice topography. Areas with thick ice cover, such as hummocks/uplifted ice pieces (areas of light color on Figures 7.2 and 7.3) generally had a shallow, if any snow cover (areas of dark color). This is a result of these areas being swept clear of snow by wind. The large pieces/hummocks will act as an element to catch the snow . Drifting around the elements will be in the direction of the predominant wind direction. Kriging produced adequate interpolated snow and ice thickness values based on the variogram models, which can be used to estimate the transmittance of PAR.

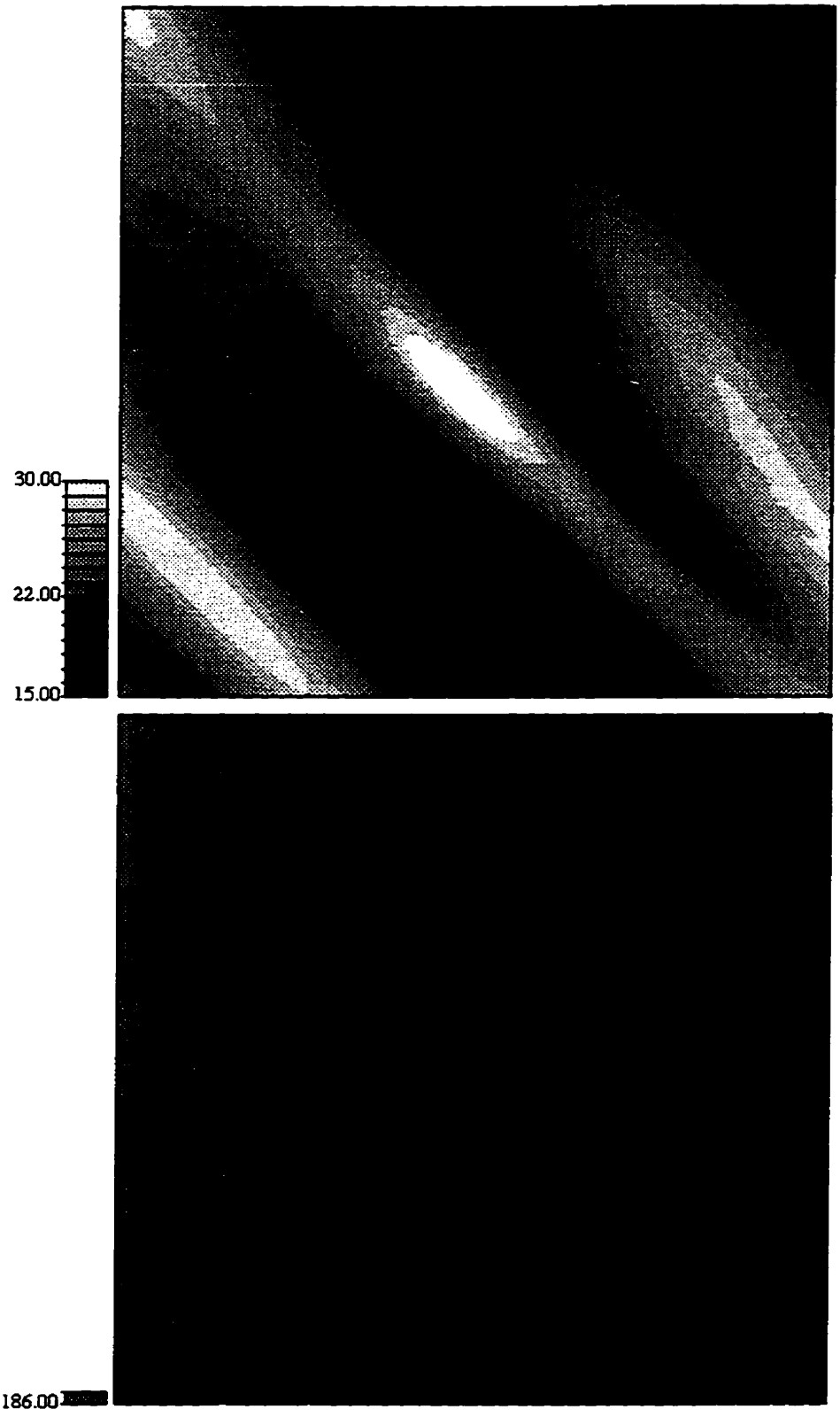

Figure 7.1. Surface plots of snow (top plot) and sea ice (bottom plot) thickness distribution over first-year sea ice (FYI01). Values are in centimeters.

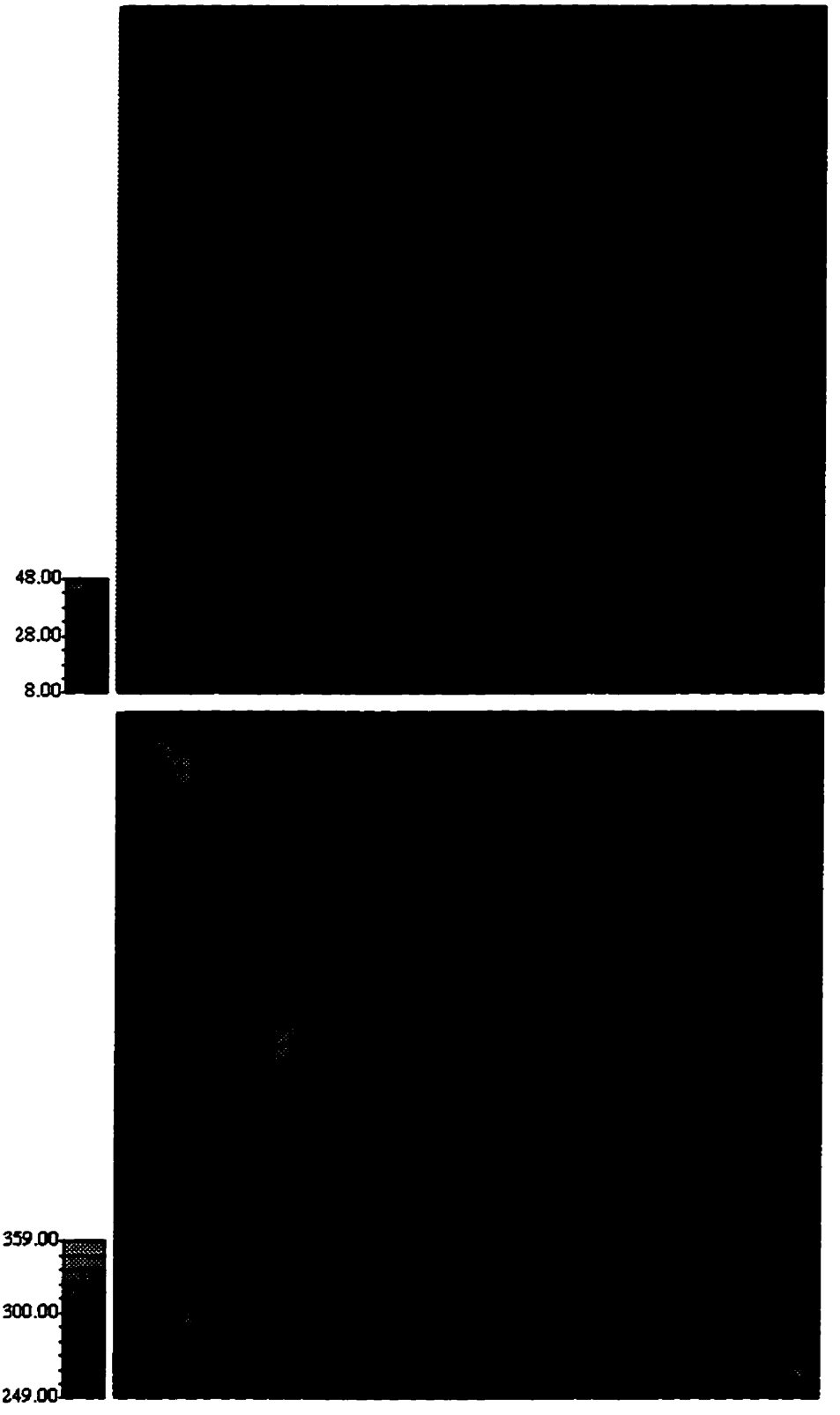

Figure 7.2. Surface plots of snow (top plot) and sea ice (bottom plot) thickness distribution over first-year sea ice (MYI01). Values are in centimeters.

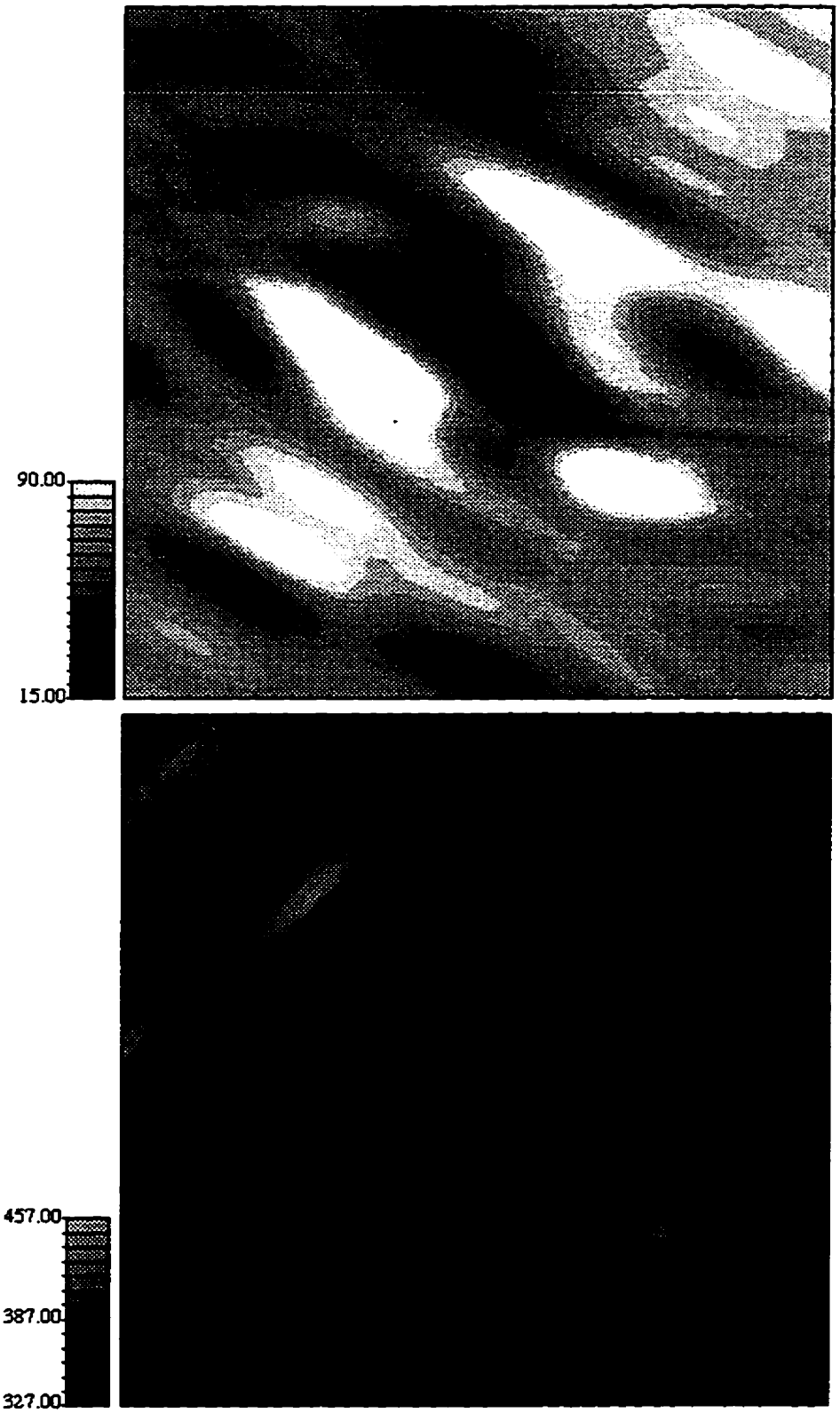

Figure 7.3. Surface plots of snow (top plot) and sea ice (bottom plot) thickness distribution over first-year sea ice (RI02). Values are in centimeters.

7.2.3 PAR Transmittance.

A useful application of the modeling of snow distribution patterns is the determination and examination of the transmittance of radiation through the ice snow layers, especially the photosynthetically active radiation. The model used in this thesis calculated the average transmittance through snow and ice for FYI as 2.21e-04 uE/m^2s, while for MYI the average transmittance was 5.75e-5 uE/m^2s and 2.49e-07 uE/m^2s. A general finding that can be concluded from this is that as the topography becomes more irregular, the amount of PAR that was transmitted became less, decreasing by at least an order of magnitude. This decrease in PAR transmittance is primarily a result of the affects ice topography has on the snow distribution patterns.

There was also a greater range in the transmittance values for RI catchment, compared to the other two ice types. This larger range was to be expected because the snow and ice depth variation was also greatest for this ice type. This variation in transmittance is illustrated in Figures 7.4, 7.5 and 7.6. It is evident for these plots that all three ice types showed a variation in PAR transmittance, however the variation was greater for the RI catchment.

In comparing the surface plots of snow distribution and PAR transmittance, two important but related features are evident. First, the two surface plots resemble each other in terms of distribution patterns. The resemblence between the snow distribution and PAR transmittance plots is evident for all three ice catchments. The second feature, in comparing these plots is that in areas with a thick snow cover, the amount of PAR that is transmitted through the snow and ice is inversely proportional to the depth of snow. For instance, in areas with a thick snow cover (i.e. light color areas in Figures 7.1 to 7.3) a lesser amount of PAR is able to transmit (i.e. darker areas

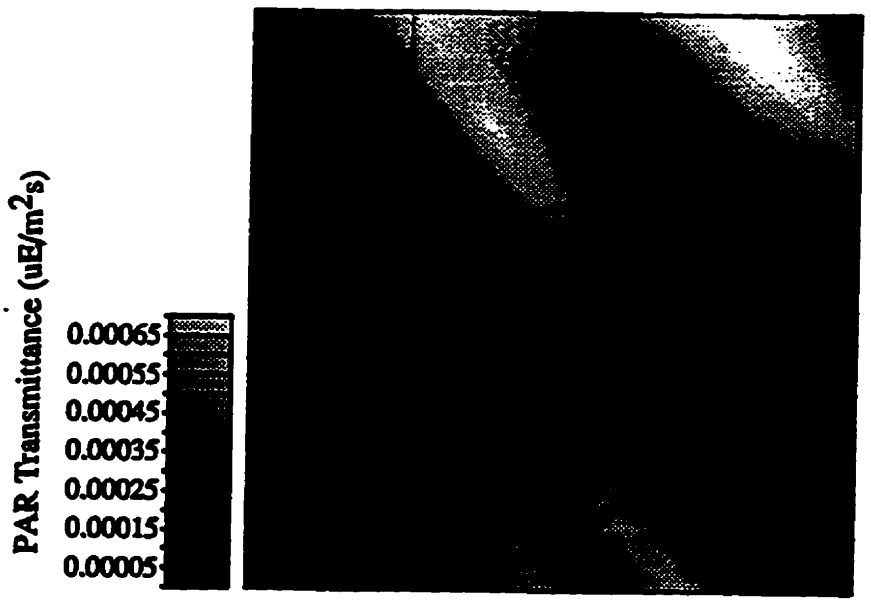

Figure 7.4. Surface plot of PAR transmittance through snow and ice on FYI catchment.

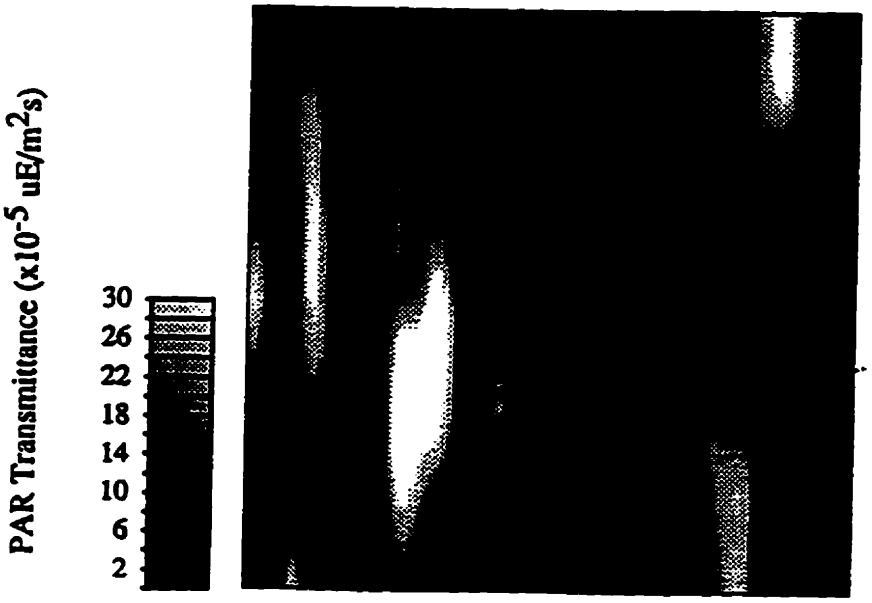

Figure 7.5. Surface plot of PAR transmittance through snow and ice on MYI catchment.

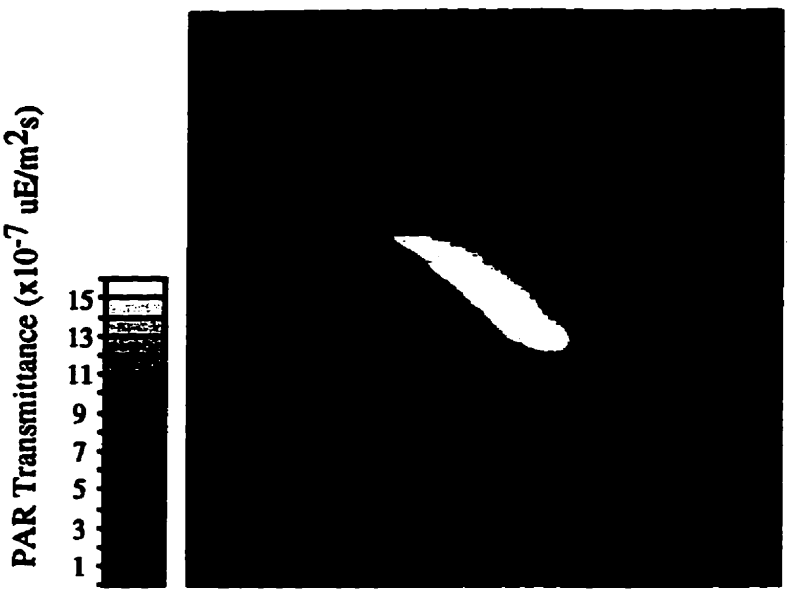

Figure 7.6. Surface plot of PAR transmittance through snow and ice on RI catchment..

in Figures 7.4 to 7.6). This pattern is apparent for all three ice catchments. There does not exist the same apparent similarity between the plots of PAR transmittance and ice thickness distribution. This lack of similarity illustrates the important effects or control the snow distribution has on the transmittance of PAR through the marine cryosphere.

As well, this application illustrates the importance of modelling the snow distribution patterns, as opposed to only the snow depth. If a uniform snow cover was assumed for the 100 m x 100 m grid, the PAR penetration would have also been uniform over first-year sea ice. Over the other ice topographies, the PAR penetration would have been considerably different. This difference in the PAR penetration plots would have produced erroneous values. Therefore, as was stated earlier, generalizing the snow distibution by using a single snow depth value would result in inaccurate estimates of PAR transmission. These plots illustrate the useful application of the snow distribution models estimated

using the variogram technique.

To illustrate the importance of snow distribution, the PAR penetration through the snow and ice layers is estimated using two different snow distribution patterns over smooth first-year sea ice. The first distribution pattern (case A) assumed that the maximum snow depth was equal to 35 cm. A minimum snow depth of 35 cm was the assumption for the second case (case B). A depth of 35 cm was used because it best represented the snow depth observed in the study area. Using these two cases, the snow distribution patterns were estimated and then the PAR transmittance was measured using the two-stream radiative transfer model.

The results indicate that the snow distribution patterns play an important role in the amount of PAR transmitted. The average transmission of PAR for case A (2.37e-03 uE/m^2s) is greater than that for case B (3.41e-06 uE/m^2s). This is to be expected because of the exponential decay of PAR transmittance associated with increasing snow depth.

The standard deviations associated with the PAR transmission for the two cases illustrate the importance of snow distribution. For case A, the standard deviation is 8.123e-03, while for case B the standard deviation is 4.71e-06, a three order of magnitude change. The smaller standard deviation associated with the second case indicated that the variation in PAR transmission was not as large as that observed for case A. The variation difference between cases is illustrated in Figure 7.7. Dark areas in these figures illustrate a greater penetration of PAR. Figure 7.7a illustrates the transmission of PAR for case A, while the transmission of PAR for case B is illustrated in Figure 7.7b. With a greater snow depth (case B) the variation in PAR is not substantial, compared to a smaller snow depth (case A). This variation difference illustrates the importance of snow distribution on the PAR transmission.

a. CASE A

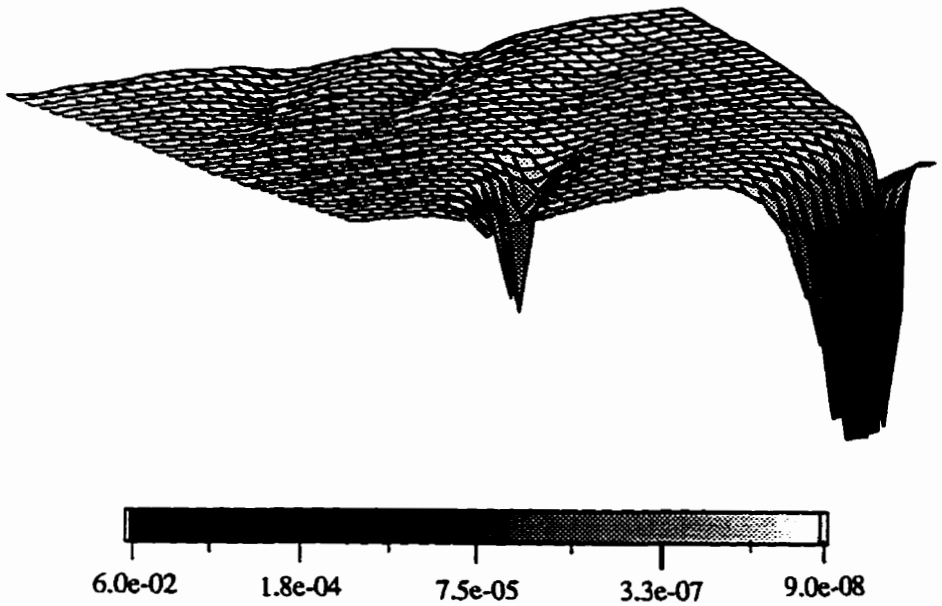

b. CASE B

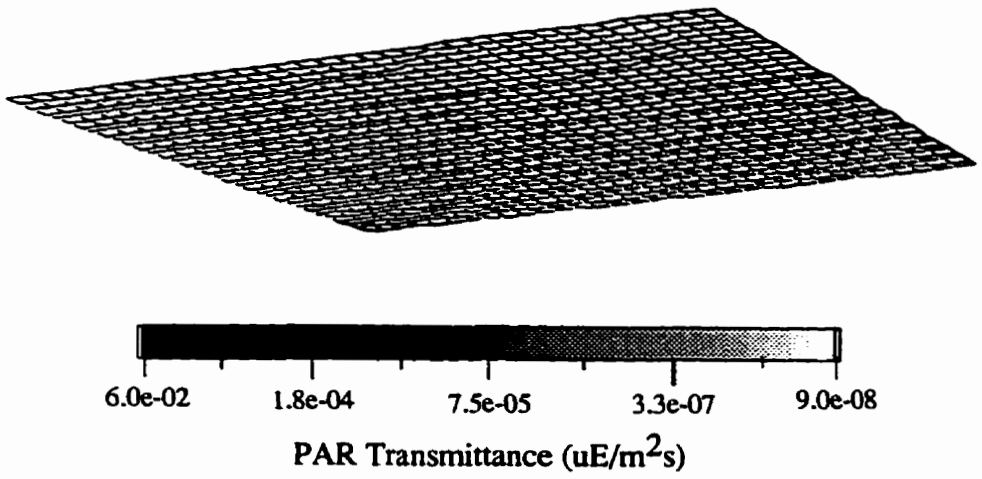

Figure 7.7. PAR transmission over smooth first-year sea ice using two different snow distribution patterns, a. maximum snow depth of 35 cm, b. minimum snow depth of 35 cm.

The second objective of this thesis, discussed in this chapter, illustrated the practical application of modeling the snow distribution patterns over various types of sea ice, as well as the importance of snow distribution. The application illustrated the effective utilization of snow distribution patterns in the determination of the PAR transmittance for an area of first-year, multiyear and rubble sea ice. The first part of this chapter was the segmentation of a SAR image based on the three ice classes using a GLCM method. Based on this classification, snow and ice distribution maps could be produced using variograms and kriging methods on a more regional scale. Kriging, as outlined in the second section of this thesis, was an effective method for interpolating snow and ice thickness values within an area based on the variogram models. The final section of this chapter implemented these distribution maps for the production of PAR transmittance plots. These plots illustrated the spatial variability of the transmittance of this waveband over the three ice catchments in the Canadian Arctic. Comparing two different snow distribution patterns over smooth first-year sea ice was also done to show the importance of the snow distribution on the PAR penetration.

CHAPTER 8:

CONCLUSIONS.

In this thesis, variograms have been shown to be an effective statistical technique for quantifying the spatial patterns of snow on three different sea ice catchments, as well as applying these models to the estimation of the spatial distribution of PAR transmittance. Parameters of the variogram were shown to have the utility in the interpretation of the physical mechanisms responsible for the observed distribution patterns. Findings illustrate that the surface topography of the different types of sea ice is a major factor determining the variogram model, or combination of models, that would best describe the spatial continuity of the snow distribution. The results further indicate that for first-year sea ice, the most appropriate variogram model consisted of a combination of the wave model and the gaussian model. This combination of models was due to the regular periodicity in snow drifts on the smooth first-year sea ice. For the more irregular sea ice topography, characteristic of multiyear and rubble sea ice, a gaussian model, either alone or in combination with a spherical model, produced the best statistical fit. The ability of the variogram to use different theoretical models suggests that this method is able to differentiate the snow distribution patterns for the three ice catchments with good success.

Between sites within each ice catchment, the various variogram

parameters differ considerably. This variation suggests that there are differences in the snow distribution patterns between locations within the three ice types. Any models developed that may attempt to represent the spatial patterns of snow distribution must take this variation into account. Representing the variation of these parameters in the model may be done using classical statistical techniques, such as the average of the parameters.

The three ice type catchments studied in this thesis exhibited geometric anisotropy. The direction of geometric anisotropy was similar for FYI and MYI catchments. The direction was oriented in the NE-SW direction. This direction is a result of the predominant wind direction during storm events in the area. Only one of the rubble sea ice sites had a geometric anisotropy direction similar to that found in the other sea ice types. The geometric anisotropy found in the other rubble site was oriented perpendicular to the predominant wind direction.

The snow distribution patterns modeled for the three ice catchments can be applied to examine a number of climatological and biological relationships. This thesis examined the transmittance of photosynthetically active radiation through the snow and ice layers. Findings indicated that as the snow thickness increases, the amount of PAR that was transmitted decreased. The spatial patterns of PAR transmittance closely resembled those of the snow distribution, illustrating the importance of snow distribution to the transmittance of PAR. This application showed the importance of the snow distribution, as opposed to snow depth, to the processes operating within the marine cryosphere.

Related to this objective was the segmentation of ice types from SAR imagery based on a GLCM method. This segmentation was done to allow the modeled snow distribution patterns, as well as the transmittance of PAR, to be used on a more regional scale. Findings indicated that the combination of three texture statistics (uniformity-dissimilarity-entropy) provided a classification

agreement of just under 80%. Therefore these three texture statistics can be used in a supervised classification scheme to segregate the ice types.

This work has several limitations which limit the findings, both geographically and temporally. First, only two years of data from a very small area of the Canadian Arctic were acquired and modeled to determine the distribution patterns. Additional work needs to be completed with a greater temporal (i.e. number of years) and spatial range (i.e. number of sampling locations). This additional work would be done in order to reduce the spatially and temporally derived biases present in the findings.

The second limitation deals with the difference in the sampling interval from 1995 to 1996. As was shown, this difference produced different models that best described the spatial continuity in the data set for MYI sites. This fact results in the possibility of different variogram models fitting the same site. If the sampling interval is reduced, for instance, certain features will not appear in the variogram and thus will be excluded in the modeling. The nugget variance, however give a good indication of the overall performance of the variogram model, and as such will suggest the exclusion of any features.

These limitations will also have implications on the PAR transmittance estimates produced in the second objective of this thesis. Because the radiative model used in estimating PAR is dependent on snow and ice thickness, inadequate modeling of the snow distribution patterns would result in inaccurate estimates of transmittance. However, there is no reason to assume that the distribution patterns of snow were modeled inaccurately. The elimination of these limitations should only enhance the applicability of the snow distribution models to the estimation of PAR transmittance.

This work is considered a first attempt at modeling the snow distribution patterns over various ice catchments. A logical extension of this work is to

quantify the spatial patterns of snow cover over various other types of sea ice (i.e. new ice, second year ice, etc.). This could improve the range of variability in the parameters associated with the variogram by examining these ice types individually as opposed to incorporating them into a generic ice class. As was already stated, future workers may want to evaluate these models in different geographical and seasonal conditions. The models may be used to examine the temporal change in snow depth through the autumn-winter-spring season transitions. The relationship between snow distribution and melt pond formation in the spring/summer seasons can also be examined using the variogram model.

The variogram models of snow distribution derived in this thesis can also be used to examine the relationship between snow distribution and climatological or biological properties of the marine cryosphere. For instance, the relationship between snow depth distribution and sea ice growth and decay could be examined using the variogram models. Another application of the variogram models is to study on a more regional scale the influences of snow distribution on hydrospheric and photosynthetic processes within ice covered oceans. The second objective of this thesis presented one such application, however many others exist, such as estimating the amount of chlorophyll production or the location of ringed seals.

REFERENCES

Aagaard, K., J.H. Swift and E.C. Carmack. 1985. Thermohaline circulation in the arctic mediterranean seas. Journal of Geophysical Research, Vol. 90, no. C3, 4833-4846.

Aagaard, K. and E.C. Carmack. 1989. The role of sea ice and other fresh water in the arctic circulation. Journal of Geophysical Research, Vol. 94, no. C10, 14,485-14,498.

Adams, W.P. 1976. Areal differentiation of snow cover in East Central Ontario. Water Resources Research, Vol. 12, no. 6, 1226-1234.

Adams, W.P. 1981. Chapter 10: Snow and ice on lakes. In: D.M. Gray and D.H. Male (eds.) Handbook of Snow - Principles, Processes, Management and Use. Toronto: Pergamon Press Canada Ltd., 437-474.

Ahmed, S., S. Sankaran and C.P. Gupta. 1995. Variographic analysis of some hydrogeological parameters: Use of geological soft data. Journal of Environmental Hydrology, Vol. 13, no. 2.

ASCE Task Committee on Geostatistical Techniques. 1990. Review of geostatistics in geohydrology. II: Applications. Journal of Hydraulic Engineering, Vol. 116, no. 5, 633-658.

Barber, D.G. 1989. Texture measures for SAR sea ice discrimination: an evaluation of univariate statistical distributions. Earth Observations Lab Technical Report Series, ISTS-EOL-TR89-005. Department of Geography, University of Waterloo, Ontario. 56p.

Barber, D.G. and E.F. LeDrew. 1989. Multivariate analysis texture statistics for SAR sea ice discrimination. Proceedings of the International Geoscience and Remote Sensing Society, Vancouver, B.C., Vol. 2, 759-762.

Barber, D.G. and E.F. LeDrew. 1991. SAR sea ice discrimination using texture statistics: a multivariate approach. Photogrammetric Engineering and Remote Sensing, Vol. 57, no. 4, 385-395.

Barber, D.G., D.D. Johnson and E.F. LeDrew. 1991. Measuring climatic state variables from SAR images of sea ice: The SIMS SAR validation site in Lancaster Sound. Arctic, Vol. 44, Supp. 1, 108-121.

Barber, D.G., M.E. Shokr, R.A. Fernandes, E.D. Soulis, D.G. Flett and E.F. LeDrew. 1993. A comparison of second-order classifiers for SAR sea ice discrimination. Photogrammetric Engineering and Remote Sensing, Vol. 59, no. 9, 1397-1408.

Barber, D.G., S.P. Reddan and E.F. LeDrew. 1995a. Statistical characterization of the geophysical and electrical properties of snow on landfast first-year sea ice. Journal of Geophysical Research, Vol. 100, 2673-2686.

Barber, D.G., T.N. Papakyriakou, E.F. LeDrew and M.E. Shokr. 1995b. An examination of the relation between the spring period evolution of the scattering coefficient (σ°) and radiative fluxes over land fast sea-ice. International Journal of Remote Sensing, Vol. 16, no. 17, 3343-3363.

Barry, R.G. 1983. Arctic ocean ice and climate: perspectives on a century of polar research. Annals of the Association of American Geographers, Vol. 73, no. 4, 485-501.

Berry, M.O. 1981. Chapter 2: Snow and climate. In: D.M. Gray and D.H. Male (eds.) Handbook of Snow - Principles, Processes, Management and Use. Toronto: Pergamon Press Canada Ltd., 32-59.

Blom, R.G., L.R. Schenck and R.E. Alley. 1987. What are the best radar wavelengths, incidence angles, and polarizations for discrimination among lava flows and sedimentary rock? A statistical approach. IEEE Transactions on Geoscience and Remote Sensing, vol. 25, no. 2, 208-213.

Blöschl, G., R. Kirnbauer and D. Gutknecht. 1991. Distributed snowmelt simulations in an alpine catchment: I. Model evaluation on the basis of snow cover patterns. Water Resources Research, Vol. 27, no. 12, 3171-3179.

Brown, R.D. and P. Cote. 1992. Interannual variability of landfast ice thickness in the Canadian High Arctic, 1950-1989. Arctic, Vol. 45, no. 3, 273-284.

Brun, E., Y. Durand, E. Martin and L. Braun. 1994. Snow modelling as an efficient tool to simulate snow cover evolution at different spatial scales. Snow and Ice Covers: Interactions with the Atmosphere and Ecosystems, IAHS Publ. no. 223, 163-174.

Burgess, T.M. and R. Webster. 1980. Optimal interpolation and isarithmic mapping of soil properties: I. The semivariogram and punctual kriging. Journal of Soil Science, Vol. 31, 315-331.

Burkard, M.B., H.R. Whiteley, H.O Schroeter and J.R. Donald. 1991. Snow depth/area relationships for various landscape units in Southwestern Ontario. Proceedings of the 48th Eastern Snow Conference, 51-65.

Burn, D.H. and S. Ray. 1989. Spatial analysis of snowpack data. In: C. Maksimovic and M. Radojkovic (eds.) Computational Modelling and Experimental Methods in Hydraulics (Hydrocomp '89), New York: Elsevier Applied Science. 475-483.

Carr, J.R. 1995. Numerical Analysis for the Geological Sciences. New Jersey: Prentice Hall. 583 p.

Carr, J.R., and C.E Glass. 1989. Use of geostatistics for accurate mapping of earthquake ground motion. Geophysical Journal, Vol. 97, 31-40.

Cess, R.D., G.L. Potter, M.-H. Zhang, J.-P. Blanchet, S. Chalita, R. Colman, D.A. Dazlinch, A.D. Del Genio, V. Dymnikov, V. Galin, D. Jerrett, E. Keup, A.A. Lacis, H. LeTreut, X.-Z. Liang, J.-F. Mahfouf, B.J. McAvaney, V.P. Meleshko, J.F.B. Mitchell, J.-J. Morcrette, P.M. Norris, D.A. Randall, L. Rikus, E. Roeckner, J.-F. Royer, U. Schlese, D.A. Sheinin, J.M. Slingo, A.P. Sokolov, K.E. Taylor, W.M. Washington, R.T. Wetherald, I. Yagai. 1991. Interpretation of snow-climate feedback as produced by 17 general circulation models. Science, Vol. 253, 888-892.

Champigny, N. and M. Armstrong. 1993. Geostatistics for the estimation of gold deposits. Mineralium Deposita, Vol. 28, 279-282.

Chellemi, D.O., K.G. Rohrbach, R.S. Yost and R.M. Sonoda. 1988. Analysis of the spatial pattern of plant pathogens and diseased plants using geostatistics. Phytopathology, Vol. 78, no.2, 221-226.

Clark, I. 1979. Practical Geostatistics. London: Elsevier Applied Science Publisher Ltd., 126 p.

Cohen, W. B., T. A. Spies and G. A. Bradshaw. 1990. Semivariograms of digital imagery for analysis of conifer canopy structure. Remote Sensing of Environment, Vol. 34, 167-178.

Connors, R.W. and C.A. Harlow. 1980a. Toward a structural textural analyzer based on statistical methods. Computer Graphics and Image Processing, Vol. 12, 224-256.

Connors, R.W. and C.A. Harlow. 1980b. A theoretical comparison of texture algorithms. IEEE Transactions on Pattern Analysis and Machine Intelligence, Vol. PAMI-2, no. 3, 204-222.

Cressie, N. A. C. 1989. Geostatistics. The American Statistician, Vol. 43, no. 4, 197-202.

Cressie, N. A. C. 1993. Statistics for Spatial Data. New York: John Wiley and Sons. 900 p.

Crocker, G. 1992. Observations of the snowcover on sea ice in the Gulf of Bothnia. International Journal of Remote Sensing, Vol. 13, no. 13, 2433-2446.

Curran, P.J. 1988. The semivariogram in remote sensing: an introduction. Remote Sensing of Environment, Vol. 24, 493-507.

Daugharty, D.A. and R.B.B. Dickison. 1982. Snow cover distribution in forested and deforested landscapes in New Brunswick, Canada. Proceedings of the 39th Annual Eastern Snow Conference, 10-19.

Davies, T.D. 1994. Snow cover-atmosphere interactions. Snow and Ice Covers: Interactions with the Atmosphere and Ecosystems, IAHS Publ. no. 223, 3-13.

DeAbreu, R.A., J. Key, J.A. Maslanik, M.C. Serreze and E.F. LeDrew. 1994. Comparison of in situ and AVHRR-derived broadband albedo over arctic sea ice. Arctic, Vol. 47, no. 3, 288-297.

Delhomme, J.P. 1979. Spatial variability and uncertainty in groundwater flow parameters: A geostatistical approach. Water Resources Research, Vol. 15, no. 2, 269-280.

de Montmollin, F.A., R.J. Olivier, R.G. Simard and F. Zwahlen. 1980. Evaluation of a precipitation map using a smoothed elevation-precipitation relationship and optimal estimates (Kriging). Nordic Hydrology, Vol. 11, 113-120.

Derksen, C. 1995. Section 3.1: Microclimatology. In: Misurak, K.M, C.P. Derksen, D.G. Barber and E.F. LeDrew. SIMMS '95 Data Report. Earth Observation Laboratory Technical Report, ISTS-EOL-SIMS-TR-95-003.

Dickinson, W.T. and H.R. Whiteley. 1972. A sampling scheme for shallow snowpacks. Bulletin of the International Association of Hydrological Sciences, Vol. 17, 247-258.

Donald, W. 1994. Geostatistics for mapping weeds, with a Canada thistle (*Cirscum cirvense*) patch as a case study. Weed Science, Vol. 42, 648-657.

Donald, J.R., E.D. Soulis, N. Kouwen and A. Pietroniro. 1995. A land cover-based snow cover representation for distributed hydrologic models. Water Resources Research, Vol. 31, no. 4, 995-1009.

Eicken, H., M.A. Lange, H-W. Hubberten and P. Wadhams. 1994. Characteristics and distribution patterns of snow and meteoric ice in the Weddell Sea and their contribution to the mass balance of sea ice. Annales Geophysicae, Vol. 12, 80-93.

Eicken, H., H. Fischer and P. Lemke. 1995. Effects of the snow cover on Antarctic sea ice and potential modulation on its response to climate change. Annals of Glaciology, Vol. 21, 369-376.

Elder, K., J. Dozier and J. Michaelsen. 1991. Snow accumulation and distribution in an alpine watershed. Water Resources Research, Vol. 27, no. 7, 1541-1552.

Evans, B.M., D.A. Walker, C.S. Benson, E.A. Nordstrand and G.W. Petersen. 1989. Spatial interrelationships between terrain, snow distribution and vegetation patterns at an arctic foothills site in Alaska. Holarctic Ecology, Vol. 12, 270-278.

Flato, G.M. and R.D. Brown. 1996. Variability and climate sensitivity of landfast Arctic sea ice. Journal of Geophysical Research, Vol. 101, no. C10, 25767-25777.

Franklin, S.E., D.R. Peddle and J.E. Moulton. 1989. Spectral/geomorphometric discrimination and mapping of terrain: a study in Gros Morne National Park. Canadian Journal of Remote Sensing, Vol. 15, no. 1, 28-42.

French, H.M. and O. Slaymaker. 1993. Chapter 1: Canada's Cold Land Mass. In: H.M. French and O. Slaymaker (eds.) Canada's Cold Environments. Montreal-Kingston: McGill-Queen's University Press, 3-28.

Furgal, C.M., S. Innes and K.M. Kovacs. 1996. Characteristics of ringed seal, *Phoca hispida*, subnivean structures and breeding habitat and their effects on predation. Canadian Journal of Zoology, Vol. 74, 858-874.

Golding, D.L. and R.H. Swanson. 1986. Snow distribution patterns in clearings and adjacent forest. Water Resources Research, Vol. 22, no. 13, 1931-1940.

González-Gurriarán, E., J. Freire and L. Fernández. 1993. Geostatistical analysis of spatial distribution of *Liocaranus depurator*, *Macropipus tuberculatus* and *Polybuis henslowii* (Crustacea Brachyura) over the Galician Continental Shelf (NW Spain). Marine Biology, Vol. 115, 453-461.

Goodison, B.E. 1981. Compatibility of Canadian snowfall and snow cover data. Water Resources Research, Vol. 17, no. 4. 893-900.

Guillard, J., D. Gerdeaux, G. Brun and R. Chappaz. 1992. The use of geostatistics to analyze data from an echo-integration survey of fish stock in Lake Sainte-Croix. Fisheries Research, Vol. 13, 395-406.

Hallikainen, M. and F.T. Ulaby. 1986. Dielectric and scattering behaviour of snow at microwave frequencies. Proceedings of International Geoscience and Remote Sensing Society Symposium, 87-91.

Halvorson, J.J., J.L. Smith, H. Bolton Jr. and R.E. Rossi. 1995. Evaluating shrub-associated spatial patterns of soil properties in a shrub-steppe ecosystem using multiple-variable geostatistics. Soil Science Society of America Journal, Vol. 59, 1476-1487.

Hamilton, W.L. and J. F. Lahey. 1982. A mountain snowcover model for Crater Lake National Park Oregon and vicinity. Physical Geography, Vol. 3, no. 1, 83-95.

Hammill, M.O. and T.G. Smith. 1989. Factors affecting the distribution and abundance of ringed seal structures in Barrow Strait, Northwest Territories. Canadian Journal of Zoology, Vol. 67, 2212-2219.

Hammill, M.O. and T.G. Smith. 1991. The role of predation in the ecology of the ringed seal in Barrow Strait, Northwest Territories, Canada. Mar. Mammal. Sci., 7, 123-135.

Haralick, R.M., K. Shanmugan and I. Dinstein. 1973. Textural features for image classification. IEEE Transactions on Systems, Man, and Cybernetics, Vol. SMC-3, no. 6, 610-621.

Heacock, T. and J. Lewis. 1989. A review of microwave remote sensing of snow. Proceedings of the 46th Annual Eastern Snow Conference, 287-291.

Herzfeld, U.C. 1993. A method for seafloor classification using directional variograms, demonstrated for data from the Western Flank of the Mid-Atlantic Ridge. Mathematical Geology, Vol. 25, no. 7, 901-924.

Hibler, W.D. and J. Zhang. 1995. On the effects of sea-ice dynamics on oceanic thermohaline circulation. Annals of Glaciology, Vol. 21.

Hohn, M.E. 1988. Geostatistics and Petroleum Geology. New York: Van Nostrand Reinhold. 257p.

Holmes, Q.A., D.R. Nuesch and R.A. Shuchman. 1984. Textural analysis and real-time classification of sea-ice types using digital SAR data. IEEE Transactions on Geoscience and Remote Sensing, Vol. GE-22, no. 2, 113-120.

Holt, B., R. Kwok and E. Rignor. 1989. Ice classification algorithm development and verification for the Alaska SAR Facility using aircraft imagery. Proceedings of the International Geoscience and Remote Sensing Society, Vancouver, B.C., Vol. 2, 751-754.

Hosang, J. and K. Dettwiler. 1991. Evaluation of a water equivalent of snow cover map in a small catchment area using a geostatistical approach. Hydrological Processes, Vol. 5, 283-290.

Isaaks, E.H. and R.M Srivastava. 1989. An Introduction to Applied Geostatistics. New York: Oxford University Press. 552p.

Jackson, R.B. and M.M. Caldwell. 1993. The scale of nutrient heterogeneity around individual plants and its quantification with geostatistics. Ecology, Vol. 74, no. 2, 612-614.

Johannessen, O.M., M. Miles and E. Bjorgo. 1995. Decreases in Arctic sea ice extent and area, 1978-1994. Nature, (in press).

Journel, A.G. and C.J. Huijbregts. 1978. Mining Geostatistics. New York: Academic Press, 600 p.

Kemp, W.P., T.M. Kalans and W.F. Quimby. 1989. Rangeland grasshopper (*Orthoptera: Acrididae*) spatial variability: macroscale population assessment. Journal of Economic Entomology, Vol. 82, no. 5, 1270-1276.

Kershaw, C.D. 1987. Discrimination problems for satellite images. International Journal of Remote Sensing, Vol. 8, no. 9, 1377-1383.

Kind, R.J. 1981. Chapter 8: Snow Drifting. In: D.M. Gray and D.H. Male (eds.) Handbook of Snow- Principles, Processes, Management and Use. Toronto: Pergamon Press Canada Ltd., 338-359.

Kind, R.J. 1986. Snowdrifting: A review of modelling methods. Cold Regions Science and Technology, Vol. 12, 217-228.

Kind, R.J. 1990. Mechanisms of aeolian transport of snow and sand. Journal of Wind Engineering and Industrial Aerodynamics, Vol. 36, 855-866.

Kopanev, I.D. 1976. Probability estimate of snow-cover depth distribution. Soviet Hydrology: Selected Papers, Vol. 15, no. 4, 281-287.

Kotlyakov, V.M. and M.G. Grosswald. 1990. Interaction of sea ice, snow and glaciers with the atmosphere and ocean. Polar Geography and Geology, Vol. 14, no. 1, 3-248.

Kovacs, A. and R.M. Morey. 1978. Radar anisotropy of sea ice due to preferred azimuth orientation of the horizontal c-axis of ice crystals. Journal of Geophysical Research, Vol. 83, no. 12, 171-201.

Kuz'min, P.O. 1960. Snowcover and Snow Reserves (in Russian). Leningrad, USSR: Gidrometeorologicheskoe Izdatel'stvo. (English translation, Washington D.C. National Science Foundation, 1963).

Kwok, R., E. Rignot, B. Holt and R.G. Onstott. 1992. Identification of sea ice types in spaceborne synthetic aperture radar data. Journal of Geophysical Research, Vol. 97, no. C2, 2391-2402.

Lange, M.A. and H. Eicken. 1991. The sea ice thickness distribution in the northwestern Weddell Sea. Journal of Geophysical Research, Vol. 96, no. C3, 4821-4837.

Langham, E.J. 1981. Chapter 7: Physics and properties of snowcover. In: D.M. Gray and D.H. Male (eds.) Handbook of Snow - Principles, Processes, Management and Use. Toronto: Pergamon Press Canada Ltd., 275-337.

Lecoustre, R., D. Fargette, C. Fauquet and P. de Reffye. 1989. Analysis and mapping of the spatial spread of African cassava mosaic virus using geostatistics and the kriging technique. Phytopathology, Vol. 79, 913-920.

Ledley, T.S. 1988. A coupled energy balance climate-sea ice model: impact of sea ice and leads on climate. Journal of Geophysical Research, Vol. 93, no. D12, 15919-15932.

Ledley, T.S. 1991. Snow on sea ice: competing effects in shaping climate. Journal of Geophysical Research, Vol. 96, no. D9, 17195-17208.

Ledley, T.S. 1993. Variations in snow on sea ice: a mechanism for producing climate variations. Journal of Geophysical Research, Vol. 98, no. D6, 10401-10410.

LeDrew, E.F., D.G. Barber, T Agnew and D. Dunlop. 1992. Canadian Sea Ice Atlas from Microwave Remotely Sensed Imagery: July 1987 to June 1990. Climatological Studies Number 44, 80 p.

LeDrew, E.F. 1993. Chapter 11: Climate Variability, Change and Sensitivity. In: H.M. French and O. Slaymaker (eds.) Canada's Cold Environments, Montreal-Kingston: McGill-Queen's University Press, 271-290.

LeDrew, E.F. and D.G. Barber. 1994. The SIMMS Program: A study of change and variability within the marine cryosphere. Arctic, Vol. 47, no. 3, 256-264.

Lewis, E.L. 1982. Chapter 2: The Arctic Ocean: water masses and energy exchanges. In: L. Rey (ed) The Arctic Ocean: The Hydrographic Environment and the Fate of Pollutants. New York: John Wiley and Son.

Liebhold, A.M., X. Zhang, M.E. Hohn, J.S. Elkinton, M. Ticehurst, G.L. Benzon and R.W. Campbell. 1991. Geostatistical analysis of gypsy moth (*Lepidoptera: Lymantriidae*) egg mass populations. Environmental Entomology, Vol. 20, no. 5, 1407-1417.

Liebhold, A.M., R.E. Rossi and W.P. Kemp. 1993. Geostatistics and geographical information systems in applied insect ecology. Annual Review of Entomology, Vol. 38, 303-327.

Ludwig, J.A. and J.F. Reynolds. 1988. Statistical Ecology. New York: John Wiley and Son. 337 p.

Lynch-Stieglitz, M. 1994. The development and validation of a simple snow model for the GISS GCM. Journal of Climate, Vol. 7, 1842-1855.

Lynden, J.D., B.A. Burns, and A.L. Maffett. 1984. Characterization of sea ice types using synthetic aperture radar. IEEE Transactions on Geoscience and Remote Sensing, GE-22(5), 431-439.

Lytle, V.I. and S.F. Ackley. 1996. Heat flux through sea ice in the western Weddell Sea: Convective and conductive transfer processes. Journal of Geophysical Research, Vol. 101, no. C4, 8853-8868.

Marshall, S., J.O. Roads and G. Glatzmaier. 1994. Snow hydrology in a general circulation model. Journal of Climate, Vol. 7, 1251-1269.

Martinez-Cob, A. and R.H. Cuenca. 1992. Influence of elevation on regional evapotranspiration using multivariate geostatistics for various climatic regions in Oregon. Journal of Hydrology, Vol. 136, 353-380.

Massom, R.A., M.R. Drinkwater and C. Haas. 1997. Winter snow cover on sea ice in the Weddell Sea. Journal of Geophysical Research, Vol. 102, no, C1, 1101-1117.

Matheron, G. 1963. Principles of Geostatistics. Economic Geology, Vol. 58, 1246-1266.

Maykut, G.A. and N. Untersteiner. 1971. Some results from a time-dependent thermodynamic model of sea ice. Journal of Geophysical Research, Vol. 76, no. 6, 1550-1575.

Maykut, G.A. 1978. Energy exchange over young sea ice in the central Arctic. Journal of Geophysical Research, Vol. 83, no. C7, 3646-3658.

Maykut, G.A. 1986. Chapter 5: The surface heat and mass balance. In: N. Untersteiner (ed.) Geophysics of Sea Ice. Dordrecht: Martinus Nijhoff Publ., 395-463.

McBratney, A.B. and R. Webster. 1986. Choosing functions for semivariograms of soil properties and fitting them to sampling estimates. Journal of Soil Science, Vol. 37, 617-639.

McKay, G.A. and D.M. Gray. 1981. Chapter 5: The distribution of snowcover. In: D.M. Gray and D.H. Male (eds.) Handbook of Snow - Principles, Processes, Management and Use. Toronto: Pergamon Press Canada Ltd., 153-190.

McLaren, I.A. 1958. The Economics of Seals in the Eastern Canadian Arctic. Fisheries Research Board of Canada, Arctic Unit Circular, 11, 94 p.

McLellan, H.J. 1965. Elements of Physical Oceanography. Toronto: Pergamon Press Canada Ltd., 151 p.

Midgarden, D.G., R.R. Youngman and S.J. Fleischer. 1993. Spatial analysis of counts of western corn rootworm (Cloeoptera: chrysomelidae) adults on yellow sticky traps in corn: geostatistics and dispersion indices. Environmental Entomology, Vol. 22, no. 5, 1124-1133.

Miesch, A.T. 1975. Variograms and variance components in geochemistry and ore evaluation. Geological Society of America Memoir, Vol. 142, 333-340.

Monestiez, P., M. Goulard and G. Charmet. 1994. Geostatistics for spatial genetic structures: study of wild populations of perennial ryegrass. Theor. Appl. Genet., Vol. 88, 33-41.

Morey, R.M., A. Kovacs and G.F.N. Cox. 1984. Electromagnetic properties of sea ice. Cold Regions Science and Technology, Vol. 9, 53-75.

Norrish, N.I. and G.H. Blackwell. 1987. A mine operator's implementation of geostatistics. CIM Bulletin, Vol. 80, no. 899, 103-112.

Nystuen, J.A. and F.W. Garcia Jr. 1992. Sea ice classification using SAR backscatter statistics. IEEE Transactions on Geoscience and Remote Sensing, Vol. GE-30, no. 3, 502-509.

Oliver, M.A. and R. Webster. 1986. Semivariograms for modelling the spatial pattern of landform and soil properties. Earth Surface Processes and Landforms, Vol. 11, 491-504.

Oliver, M.A. and R. Webster. 1987. The elucidation of soil pattern in the Wyre Forest of the West Midlands, England: II spatial distribution. Journal of Soil Science, Vol. 38, 293-307.

Pan, G. 1995. Practical issues of geostatistical reserve estimation in the mining industry. CIM Bulletin, Vol. 88, no. 993, 31-37.

Pannatier, Y. 1996. Variowin: Software for Spatial Data Analysis in 2D. New York: Springer-Verlag, 91 p.

Patch, J.R. 1981. Effects of forest cover on snow cover distribution in the Nashwaak experimental watershed project. Proceedings of the 38th Annual Eastern Snow Conference, 76-87.

Pelletier, D. and A.M. Parma. 1994. Spatial distribution of Pacific halibut (Hippoglossus stenolepis): an application of geostatistics to longline survey data. Canadian Journal of Fisheries and Aquatic Sciences, Vol. 51, 1506-1518.

Perovich, D.K., A.J. Gow and W.B. Tucker. 1988. Physical properties of snow and ice in the winter marginal ice zone of Fram Strait. Proceedings of International Geoscience and Remote Sensing Society Symposium. 1119-1123.

Petitgas, P. 1993. Geostatistics for fish stock assessment: a review and an acoustic application. ICES Journal of Marine Sciences, Vol. 50, 285-298.

Phillips, D.L., J. Dolph and D. Marks. 1992. A comparison of geostatistical procedures for spatial analysis of precipitation in mountainous terrain. Agricultural and Forest Meteorology, Vol. 58, 119-141.

Pike, D.G. and H.E. Welch. 1990. Spatial and temporal distribution of sub-ice macrofauna in the Barrow Strait area, Northwest Territories. Canadian Journal of Fisheries and Aquatic Sciences, Vol. 47, 81-91.

Rachner, M. and H. Matthäus. 1986. Project SNOW: operational estimation of snowcover development in the mountains of the German Democratic Republic. Modelling Snowmelt-Induced Processes, IAHS Publ. no. 155, 71-82.

Randall, D.A., R.D. Cess, J.P. Blanchet, S. Chalita, R. Colman, D.A. Dazlich, A.D. Del Genio, E. Keup, A. Lacis, H. LeTreut, X.-Z. Liang, B.J. McAvaney, J.F. Mahfouf, V.P. Meleschko, J.-J. Morcrette, P.M. Norris, G.L. Potter, L. Rikus, E. Roeckner, J.F. Royer, U. Schlese, D.A. Sheinin, A.P. Sokolov, K.E. Taylor, R.T. Wetherald, I. Yagai and M.-H. Zhang. 1994. Analysis of snow feedbacks in 14 general circulation models. Journal of Geophysical Research, Vol. 99, no. D10, 20,757-20,771.

Robinson, D.A., K.F. Dewey and R.R. Heim. 1993. Global snow cover monitoring; an update. Bulletin of American Meteorological Society, Vol. 74, 1689-1696.

Rossi, R.E., D.J. Mulla, A.G. Journel and E.H. Franz. 1992. Geostatistical tools for modelling and interpreting ecological spatial dependence. Ecological Monographs, Vol. 62, no. 2, 277-314.

Royle, A., I. Clark, P.I. Brooker, H. Parker, A. Journel, J.M. Rendu, R. Sandefur, D.C. Grant and P. Mousset-Jones. 1980. Geostatistics. New York: McGraw-Hill Inc., 168 p.

Rundels, B. 1995. The thermohaline circulation of the Arctic Ocean and the Greenland Sea. Philosophical Transactions of the Royal Society of London (A), Vol. 352, 287-299.

Sambles, K.M., A. Harrison, M.G. Anderson and T. Pangburn. 1990. A prototype physically-based model for the prediction of the spatial distribution of snowcover. Proceedings of the 47th Annual Eastern Snow Conference, 109-119.

Schlesinger, M.E. and J.F.B. Mitchell. 1987. Climate model simulation of the equilibrium climatic response to increased carbon dioxide. Review of Geophysics, Vol. 25, 760-798.

Schotzko, D.J. and L.E. O'Keeffe. 1989. Geostatistical description of the spatial distribution of *Lygus hesperus* (Heteroptera: Miridae) in lentils. Journal of Economic Entomology, Vol. 82, no. 5, 1277-1288.

Schotzko, D.J. and C.M. Smith. 1991. Effects of host plant on the between-plant spatial distribution of Russian wheat aphid (Homoptera: aphididae). Journal of Economic Entomology, Vol. 84, no. 6, 1725-1734.

Schroeter, H.O. and H.R. Whiteley. 1986. Distribution of snow cover as influenced by landscape unites in southwestern Ontario. Proceedings of the 43rd Annual Eastern Snow Conference, 32-44.

Schroeter, H.O. and H.R. Whiteley. 1987. Application of a snow accumulation-ablation model for areal distribution of shallow ephemeral snowpacks. Proceedings of the 44th Annual Eastern Snow Conference, 129-143.

Schroeter, H.O., D.K Boyd and H.R. Whiteley. 1991. Area snow accumulation-ablation model (ASAAM): Experience of real-time use in southwestern Ontario. Proceedings of the 48th Annual Eastern Snow Conference, 25-38.

Schwaller, M.R. 1987. A geobotanical investigation based on linear discriminant and profile analyses of airborne thematic mapper simulation data. Remote Sensing of the Environment, Vol. 23, 23-34.

Shanmugan, K.S., V. Narayanan, V.S. Frost, J.A. Stiles and J.C. Holtzman. 1981. Textural features for radar image analysis. IEEE Transactions on Geoscience and Remote Sensing, Vol. GE-19, no. 3, 153-181.

Shuchman, R.A., C.C. Wackeman, A.L. Maffett, R.G. Onstott and L.L. Sutherland. 1989. The discrimination of sea ice types using SAR backscatter statistics. Proceedings of the International Geoscience and Remote Sensing Society, Ann Arbor, Michigan, Vol. 2, 1131-1133.

Shokr, M.E. 1989. Texture measures for sea-ice classification from radar images. Proceedings of the International Geoscience and Remote Sensing Society, Vancouver, B.C., Vol. 2, 763-768.

Shokr, M.E. 1991. Evaluation of second-order texture parameters for sea ice classification from radar images. Journal of Geophysical Research, Vol. 96, no. C6, 10625-10640.

Singleton, R.A., B.C. Straits and M. Miller Straits. 1993. Approaches to Social Research (2nd ed.). New York: Oxford University Press. 510 p.

Smith T.G. and I. Sterling. 1975. The breeding habitat of the ringed seal (*Phoca hispida*). The birth lair and associated structures. Canadian Journal of Zoology, Vol. 53, 966-981.

Smith, T.G. 1987. The Ringed Seal, *Phoca hispida*, of the Canadian Western Arctic. Canadian Bulletin of Fisheries and Aquatic Sciences, Vol. 219, 81p.

Sommerfeld, R.A., R.C. Bales and A. Mast. 1994. Spatial statistics of snowmelt flow data from lysimeters and aerial photos. Geophysical Research Letters, Vol. 21, no. 25, 2821-2824.

Steffen, K. and F. Müller. 1977. Local snow distribution on Axel Heiberg Island, Canada: an empirical method of extrapolation from snow-course data on White Glacier. Geographica Helvetica, Vol. 32, no.4, 195-202.

Steffuhn, H., and G.E. Dyck. 1973. Estimating true basin snowcover. In: Advanced Concepts and Techniques in the Study of Snow and Ice Resources, Washington, D.C.: National Academy of Sciences, U.S. International Hydrological Decade, 314-328.

Steiner, D., K. Baumberger and J. Maurer. 1971. Computer-processing and classification of multivariate information from remote sensing imagery. A review of the methodology as applied to a sample of agricultural crops. Sixth International Symposium on Remote Sensing of the Environment, Ann Arbor, Michigan, 895-907.

Tucker, W.B., A.J. Glow and W.F. Weeks. 1987. Physical properties of summer sea ice in the Fram Strait. Journal of Geophysical Research, Vol. 92, no. C7, 6787-6803.

Tucker, W.B., D.K. Perovich, A.J. Gow, W.F. Weeks and M. Drinkwater. 1992. Chapter 2: Physical properties of sea ice relevant to remote sensing. In: F.D. Carsey (ed.) Microwave Remote Sensing of Sea Ice. Washington: American Geophysical Union, 9-28.

Ulaby, F.T., F. Kouyate, B. Brisco and T.H.L. Williams. 1986. Textural information in SAR images. IEEE Transactions on Geoscience and Remote Sensing, Vol. GE-24, no. 2, 235-245.

Ujihashi, Y., N. Takase, H. Ishida and E. Hibobe. 1994. Distributed snow cover model for a mountainous basin. Snow and Ice Covers: Interactions with the Atmosphere and Ecosystems, IAHS Publ. no. 223, 153-162.

Villard, M.-A. and B.A. Maurer. 1996. Geostatistics as a tool for examining hypothesized declines in migratory birds. Ecology, Vol. 77, no. 1, 59-68.

Welch, H.E. and M.A. Bergmann. 1989. Seasonal development of ice algae and its prediction from environmental factors near Resolute, N.W.T., Canada. Canadian Journal of Fisheries and Aquatic Sciences, Vol. 46, 1793-1804.

Welch, H.E. 1991. Comparisons between lakes and seas during the arctic winter. Arctic and Alpine Research, Vol.23, no. 1, 11-23.

Welch, H.E., M.A. Bergmann, T.D. Siferd and P.S. Amarualik. 1991. Seasonal development of ice algae near Chesterfield Inlet, N.W.T., Canada. Canadian Journal of Fisheries and Aquatic Sciences, Vol. 48, 2395-2402.

Weszka, J.S., C.R. Dyer and A. Rosenfeld. 1976. A comparative study of texture measures for terrain classification. IEEE Transactions on Systems, Man and Cybernetics, Vol. 6, no. 4, 269-285.

Woodcock, C.E., A.H. Strahler and D.L.B. Jupp. 1988a. The use of variograms in remote sensing: I. Scene models and simulated images. Remote Sensing of Environment, Vol. 25, 323-348.

Woodcock, C.E., A.H. Strahler and D.L.B. Jupp. 1988b. The use of variograms in remote sensing: II. Real digital images. Remote Sensing of Environment, Vol. 25, 349-379.

Worby, A.P., M.O. Jeffries, W.F. Weeks, K. Morris and R. Jaña. 1996. The thickness distribution of sea ice and snow cover during late winter in the Bellingshausen and Amundsen Seas, Antarctica. Journal of Geophysical Research, Vol. 101, no. C12, 28441-28455.

Yang, J. and J.D. Neelin. 1993. Sea-ice interaction with the thermohaline circulation. Geophysical Research Letters, Vol. 20, no. 2, 217-220.

APPENDIX A:

PRELIMINARY DATA ANALYSIS

Table A1. Descriptive statistics for snow depth, sampled at each individual site. An 'S' with the sample name indicates a site sampled during 1995.

	FYI01	FYI02	FYI03	FYI04	FYI05	SFYI01	SFYI02	SFYI03
mean (cm)	23.5	21.6	36.4	29.5	35.6	11.0	20.8	51.4
stnd. dev.	7.5	6.8	7.4	7.2	7.6	6.7	11.1	21.6
min.	7.0	4.0	5.0	16.0	20.0	2.0	2.0	5.0
max.	51.0	43.0	55.0	56.0	58.0	33.0	63.0	110.0
count	505	485	485	485	485	240	125	121

	MYI01	MYI02	MYI03	MYI04	SMYI01		RI01	RI02
mean (cm)	25.1	46.3	36.1	34.4	21.2		37.0	69.6
stnd. dev.	16.1	20.9	18.5	19.3	16.9		25.0	32.6
min.	0	1.0	0	0	0		0	1.0
max.	79.0	131.0	112.0	91.0	67.0		79.0	139.0
count	485	485	485	485	117		485	485

Table A2. Ice surface topography values sampled at each individual site for multiyear and rubble sea ice. An 'S' with the sample name indicates a site sampled during 1995.

	MYI01	MYI02	MYI03	MYI04	SMYI01	Average
mean (cm)	287.2	207.6	265.8	317.5	291.7	269.3
stnd. dev.	26.6	20.2	26.5	32.5	27.37	48.5
min.	240.8	178.2	229.6	266.4	250.0	
max.	380.2	330.5	397.3	464.0	374.5	
count	445	468	468	468	116	2433

	RI01	RI02	Average
mean (cm)	245.6	363.9	305.1
stnd. dev.	25.9	30.9	65.7
min.	163.5	304.7	
max.	401.0	492.5	
count	463	468	931

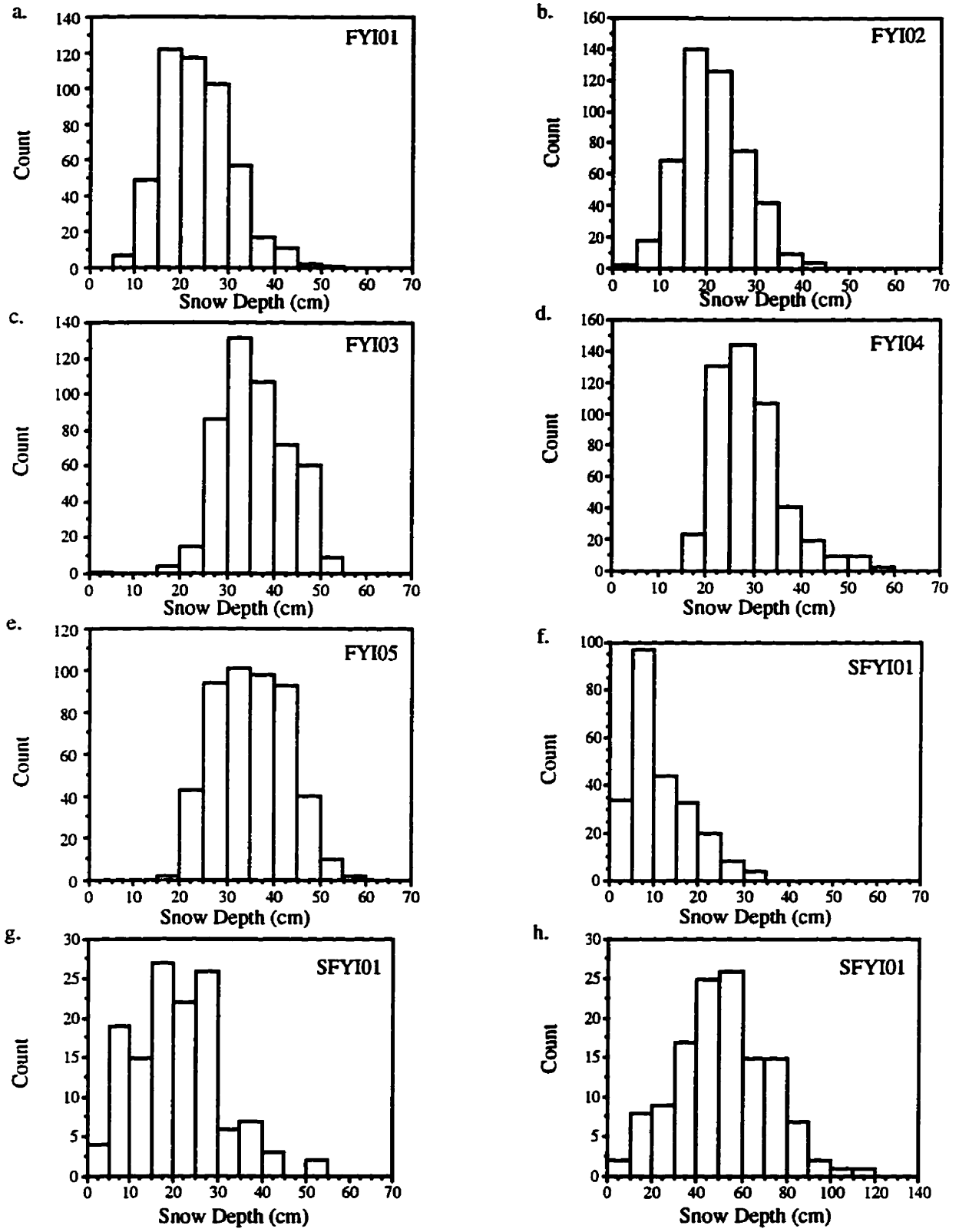

Figure A1. Histograms of the snow depth sampled for eight first-year sea ice sites.

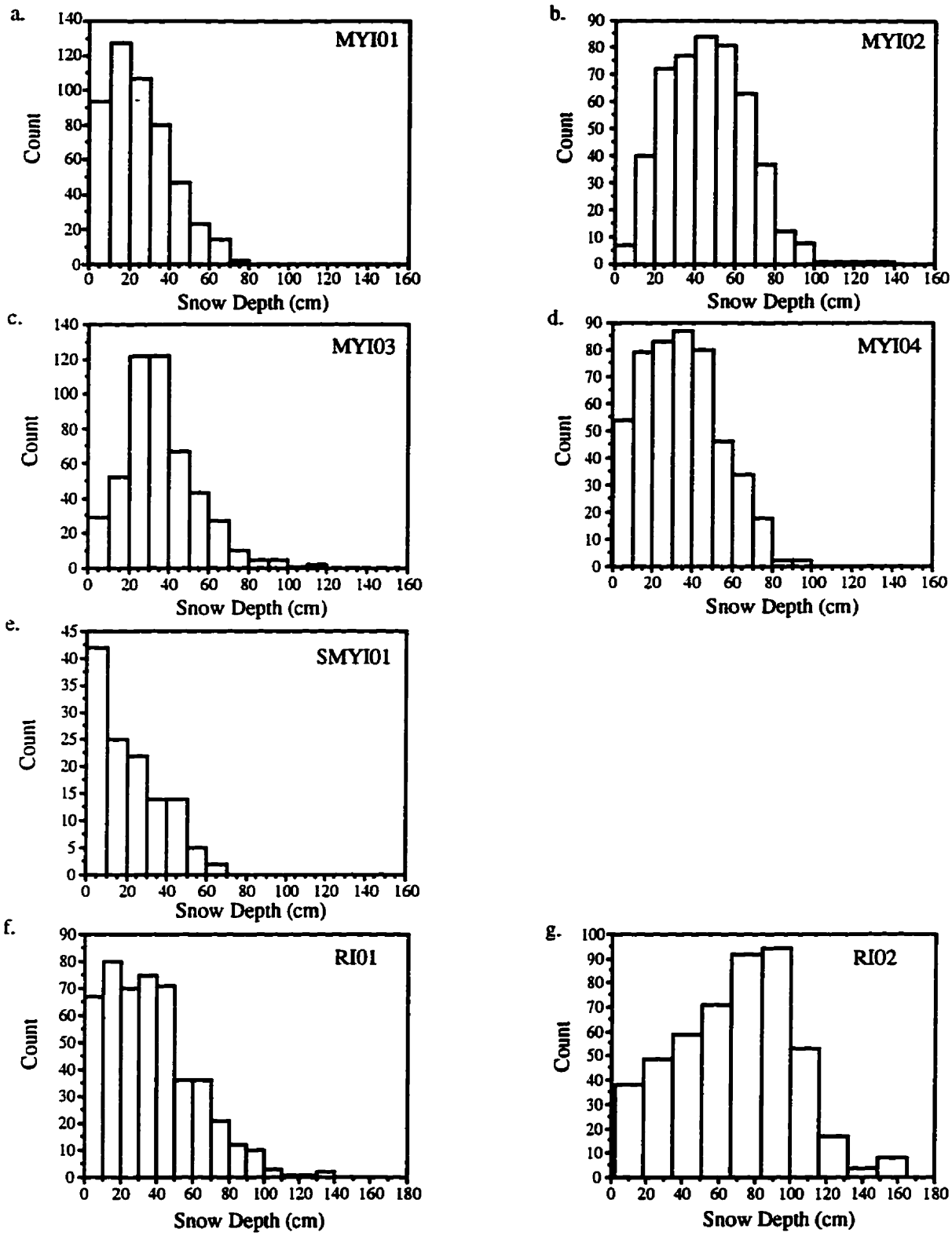

Figure A2. Histograms of snow depth sampled on five multi-year and two rubble sea ice sites.

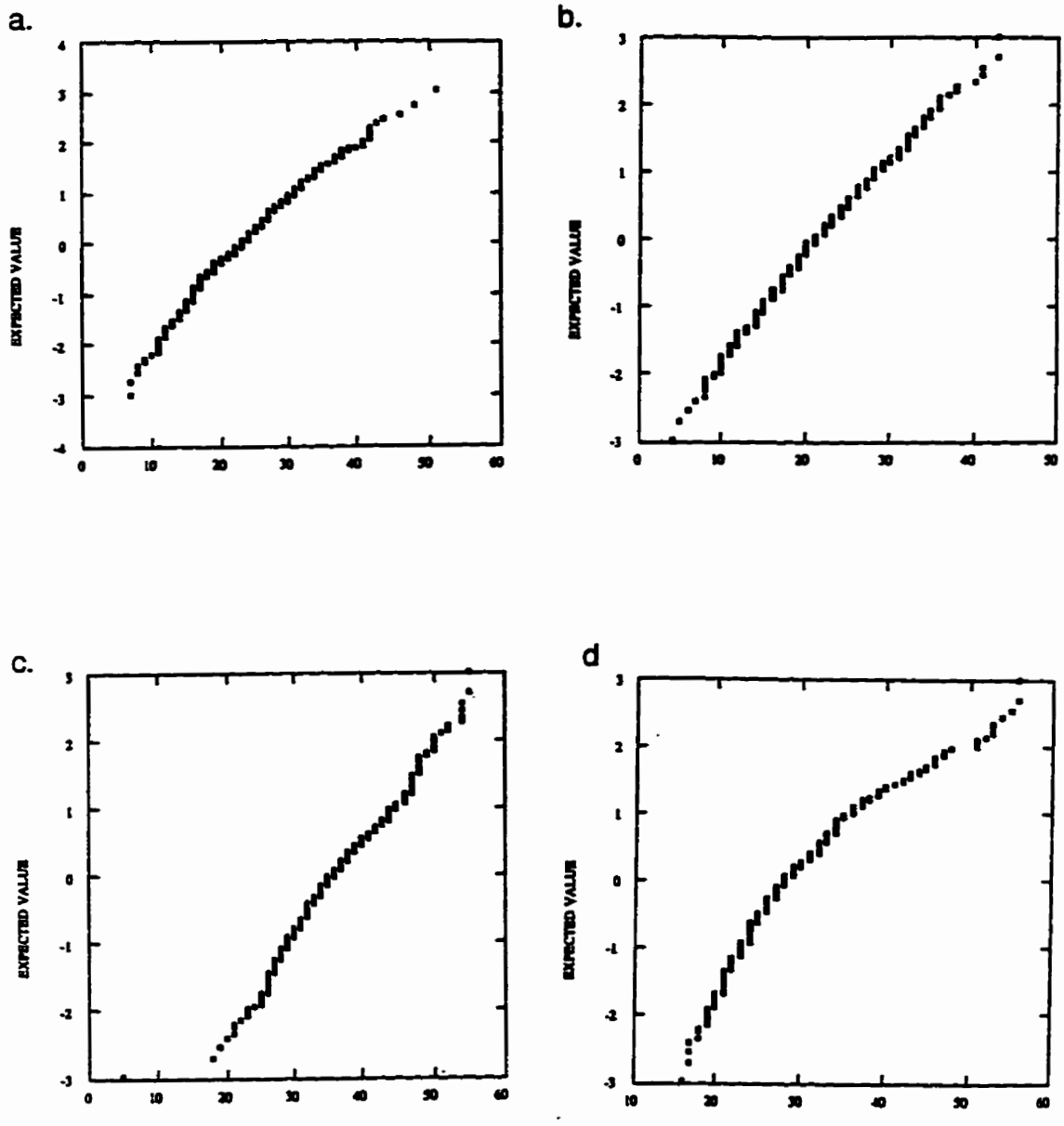

Figure A3. Normal probability plots for the 8 first-year sea ice sites; a. FYI01, b. FYI02, c. FYI03, d. FYI04, e. FYI05, f. SFYI01, g. SFYI02, and h. SFYI03.

e.

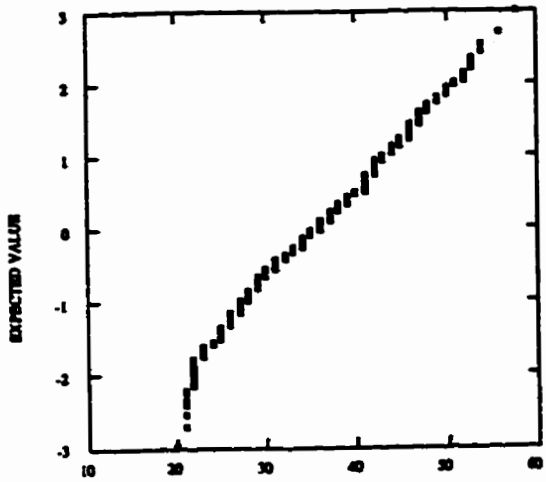

f.

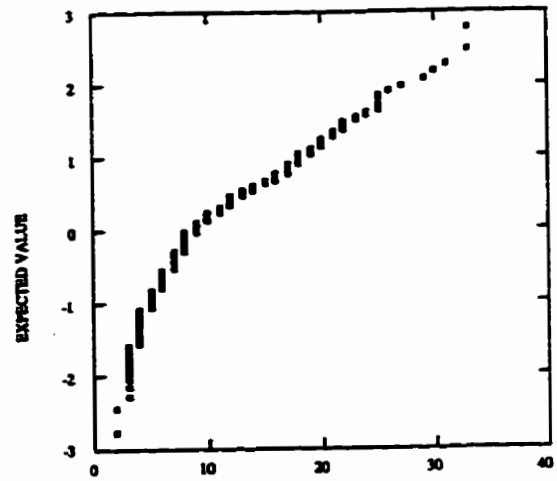

g.

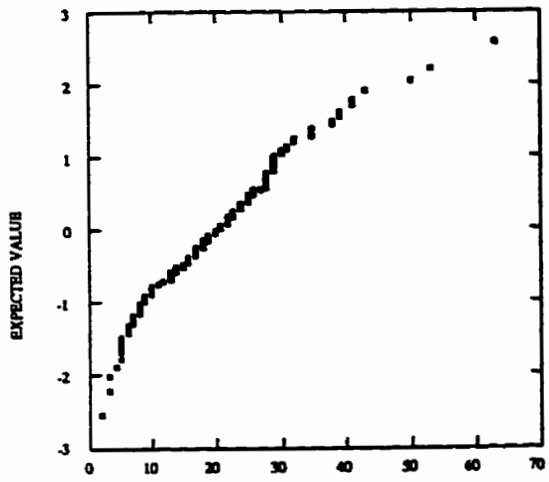

h.

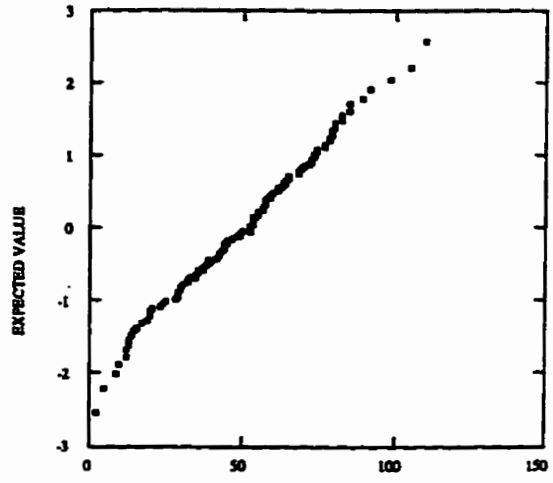

Figure A3. con't.

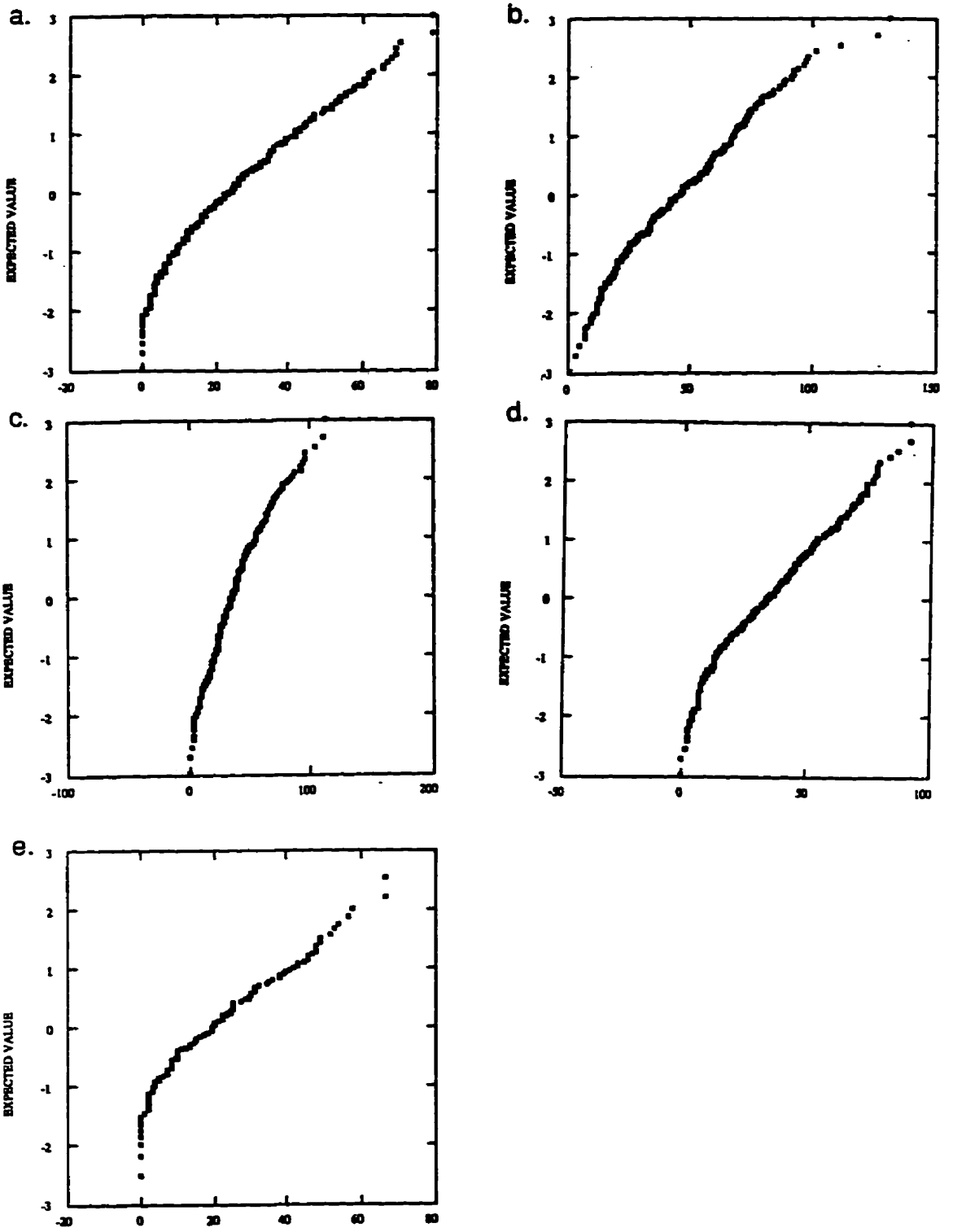

Figure A4. Normal probability plots for the 5 multi-year sea ice sites; a. MYI01, b. MYI02, c. MYI03, d. MYI04, e. SMYI01.

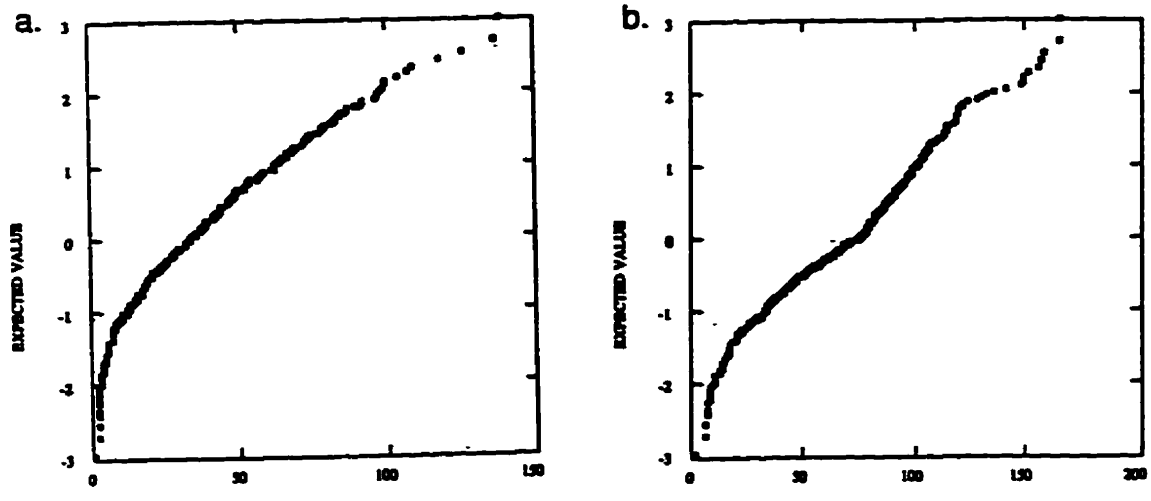

Figure A5. Normal probability plots for the 2 rubble sea ice sties; a. RI01 and b. RI02.

APPENDIX B:

H-SCATTERPLOTS

a).

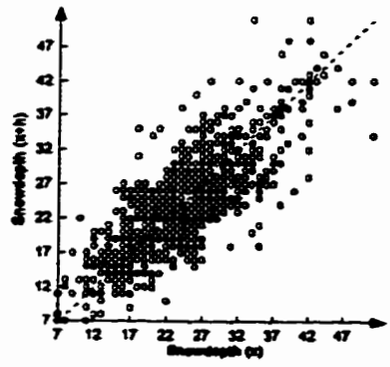

b).

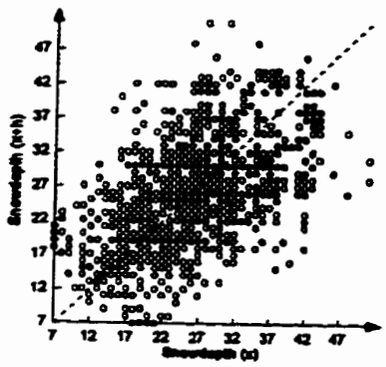

c).

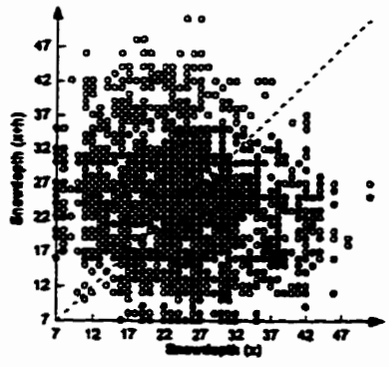

Figure B1. H-scatterplots for FYI01; a). h-scatterplot for lag 1, b). h-scatterplot for lag 4, and c). h-scatterplot for lag 13.

a).

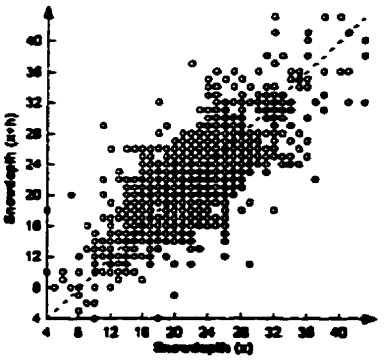

b).

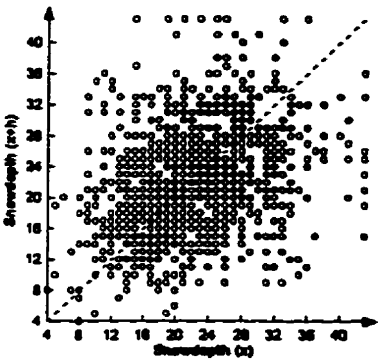

c).

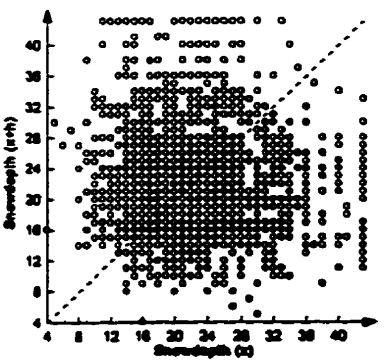

Figure B2. H-scatterplots for FYI02; a). h-scatterplot for lag 1, b). h-scatterplot for lag 4, and c). h-scatterplot for lag 13.

a).

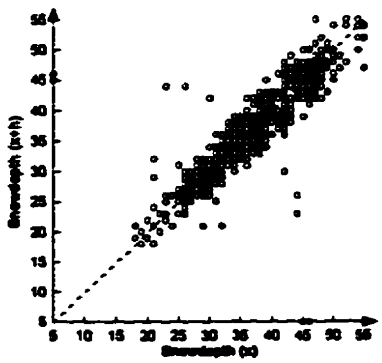

b).

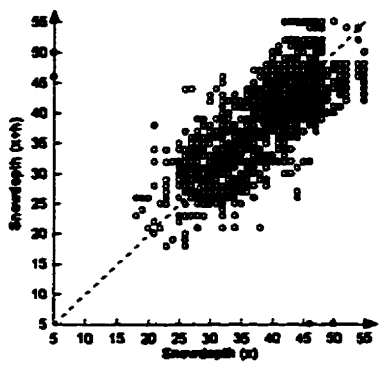

c).

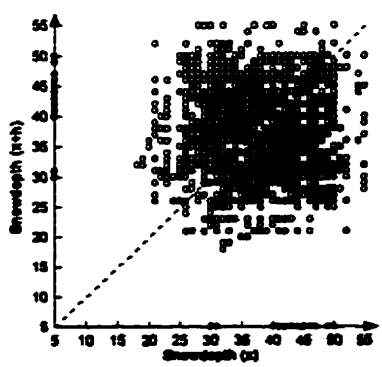

Figure B3. H-scatterplots for FYI03; a). h-scatterplot for lag 1, b). h-scatterplot for lag 4, and c). h-scatterplot for lag 13.

a).

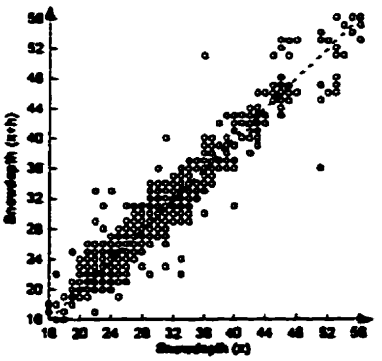

b).

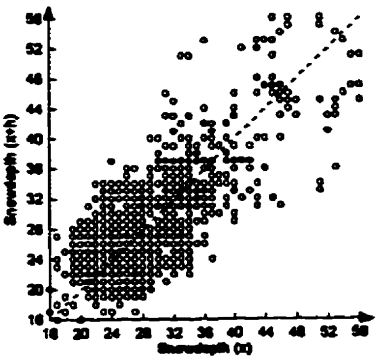

c).

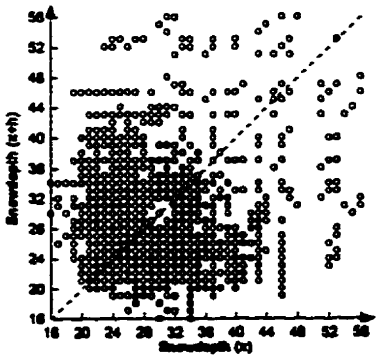

Figure B4. H-scatterplots for FYI04; a). h-scatterplot for lag 1, b). h-scatterplot for lag 4, and c). h-scatterplot for lag 13.

a).

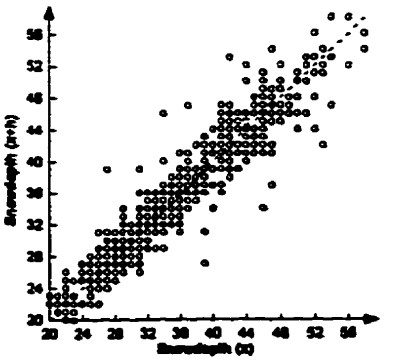

b).

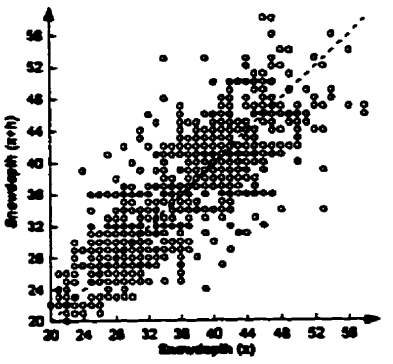

c).

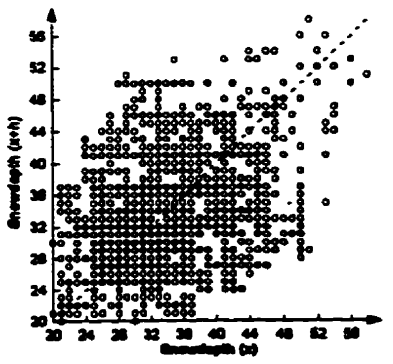

Figure B5. H-scatterplots for FYI05; a). h-scatterplot for lag 1, b). h-scatterplot for lag 4, and c). h-scatterplot for lag 13.

a).

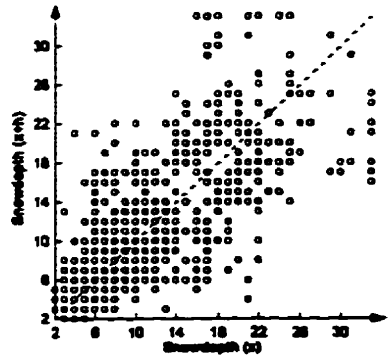

b).

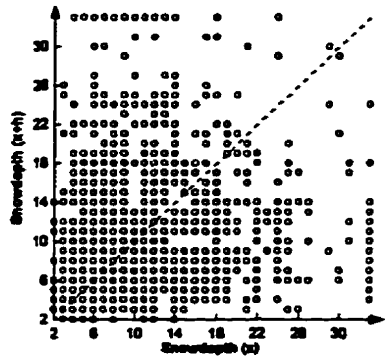

c).

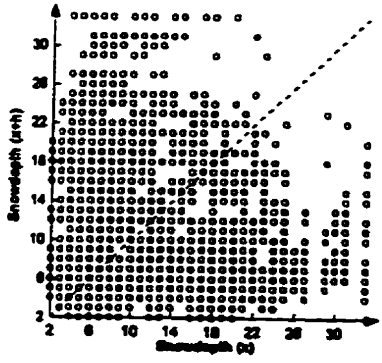

Figure B6. H-scatterplots for SFYI01; a). h-scatterplot for lag 1, b). h-scatterplot for lag 4, and c). h-scatterplot for lag 13.

a).

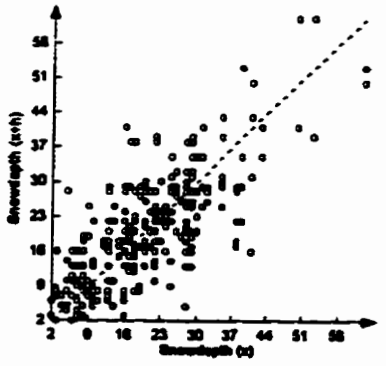

b).

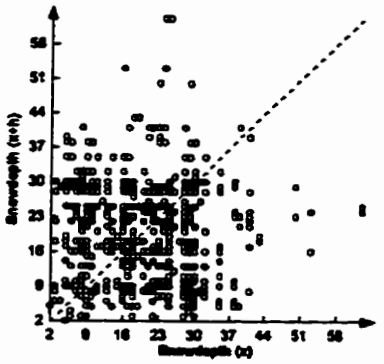

c).

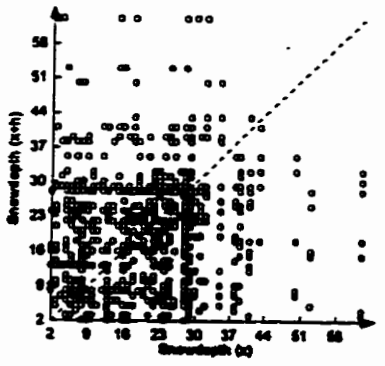

Figure B7. H-scatterplots for SFYI02; a). h-scatterplot for lag 1, b). h-scatterplot for lag 4, and c). h-scatterplot for lag 13.

a).

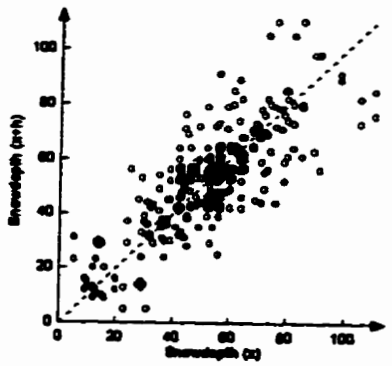

b).

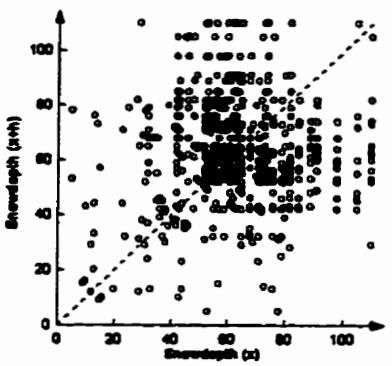

c).

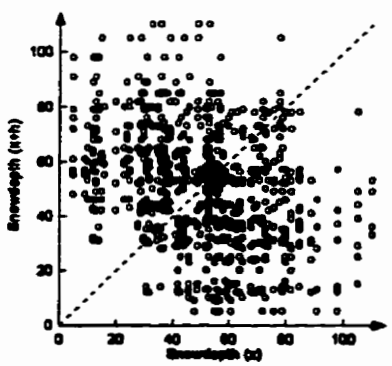

Figure B8. H-scatterplots for SFYI03; a). h-scatterplot for lag 1, b). h-scatterplot for lag 4, and c). h-scatterplot for lag 13.

a).

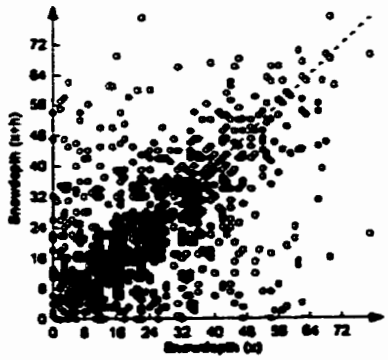

b).

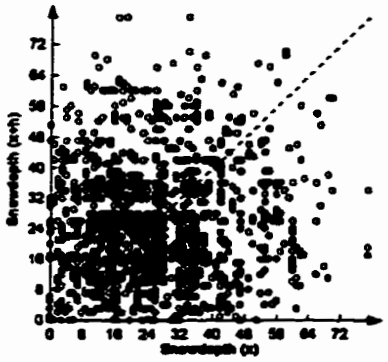

c).

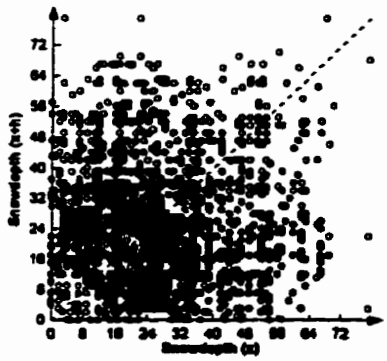

Figure B9. H-scatterplots for MYI01; a). h-scatterplot for lag 1, b). h-scatterplot for lag 4, and c). h-scatterplot for lag 13.

a).

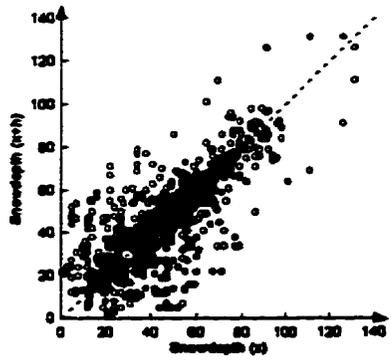

b).

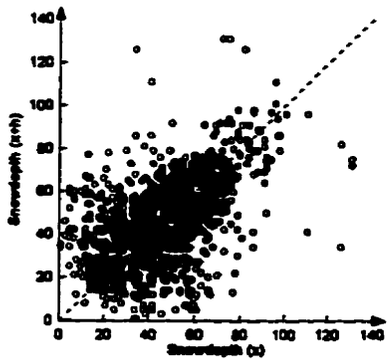

c).

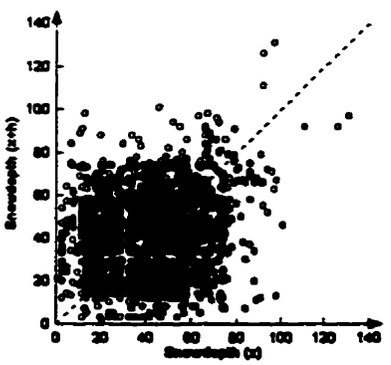

Figure B10. H-scatterplots for MYI02; a). h-scatterplot for lag 1, b). h-scatterplot for lag 4, and c). h-scatterplot for lag 13.

a).

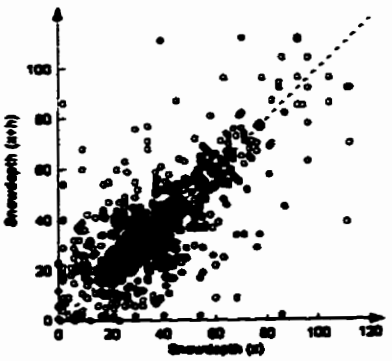

b).

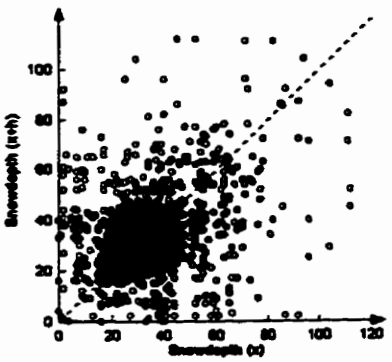

c).

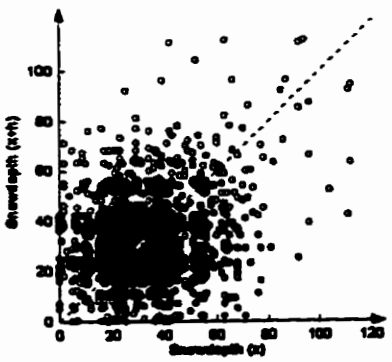

Figure B11. H-scatterplots for MYI03; a). h-scatterplot for lag 1, b). h-scatterplot for lag 4, and c). h-scatterplot for lag 13.

a).

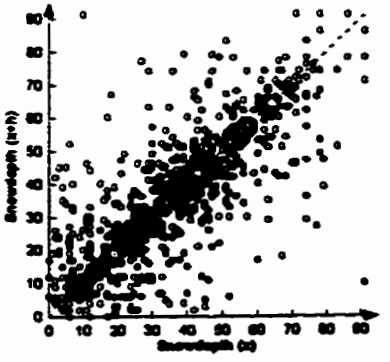

b).

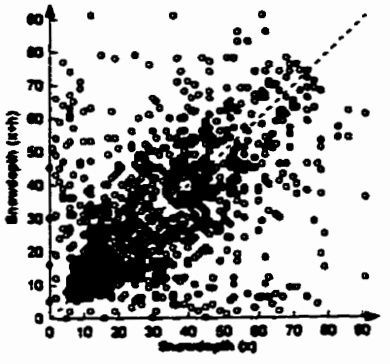

c).

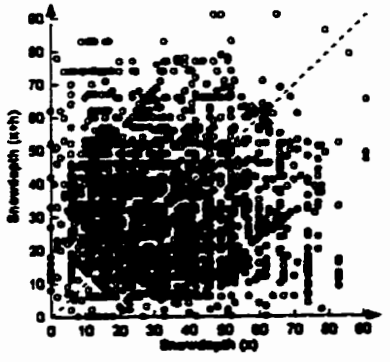

Figure B12. H-scatterplots for MYI04; a). h-scatterplot for lag 1, b). h-scatterplot for lag 4, and c). h-scatterplot for lag 13.

a).

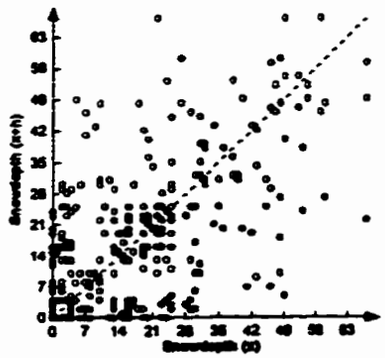

b).

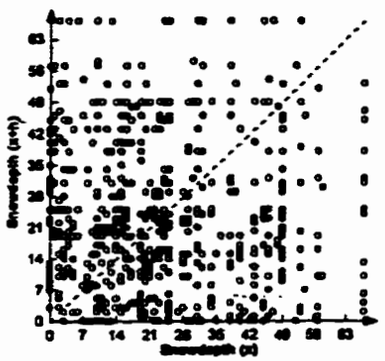

c).

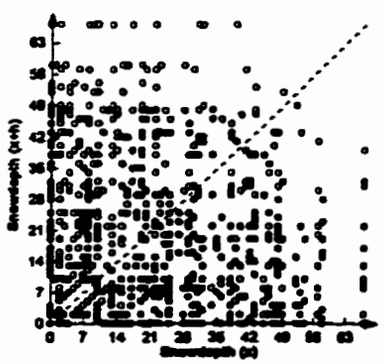

Figure B13. H-scatterplots for SMYI01; a). h-scatterplot for lag 1, b). h-scatterplot for lag 4, and c). h-scatterplot for lag 13.

a).

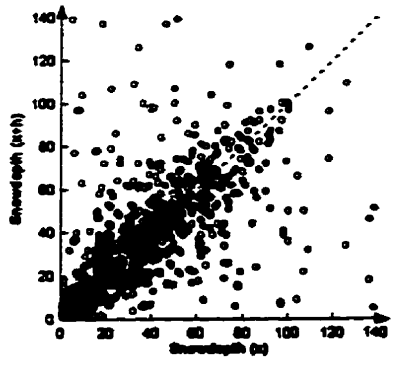

b).

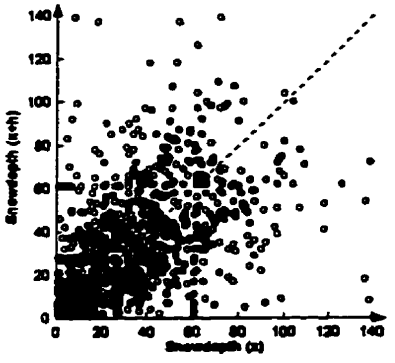

c).

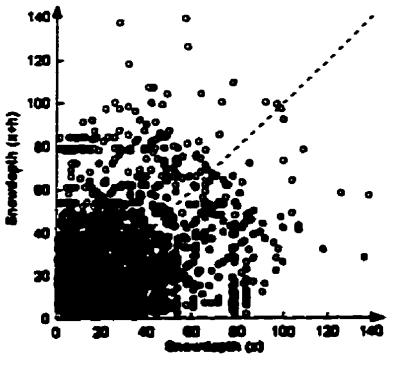

Figure B14. H-scatterplots for RI01; a). h-scatterplot for lag 1, b). h-scatterplot for lag 4, and c). h-scatterplot for lag 13.

a).

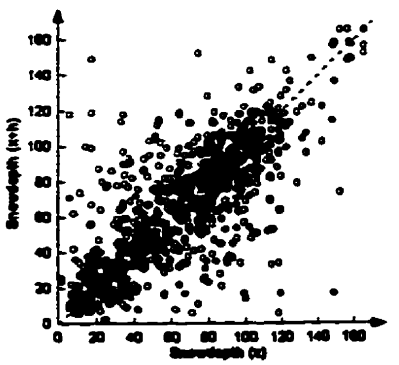

b).

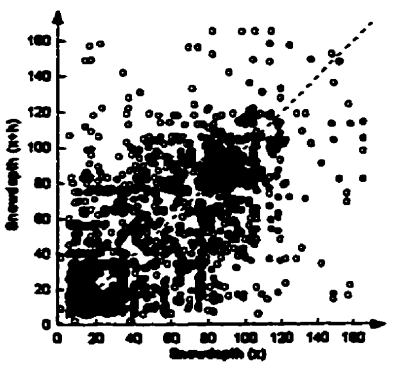

c).

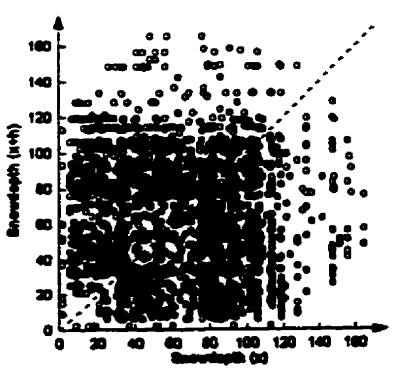

Figure B15. H-scatterplots for RI02; a). h-scatterplot for lag 1, b). h-scatterplot for lag 4, and c). h-scatterplot for lag 13.

APPENDIX C:

OMNIDIRECTIONAL VARIOGRAMS

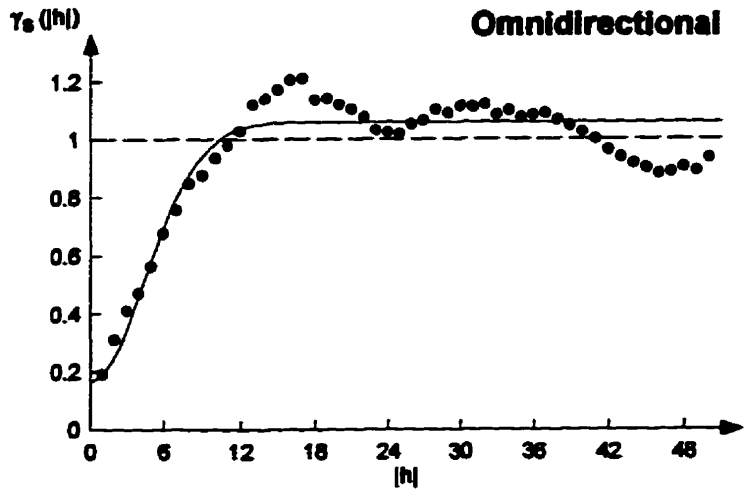

Figure C1. Omnidirectional variogram for FYI01.

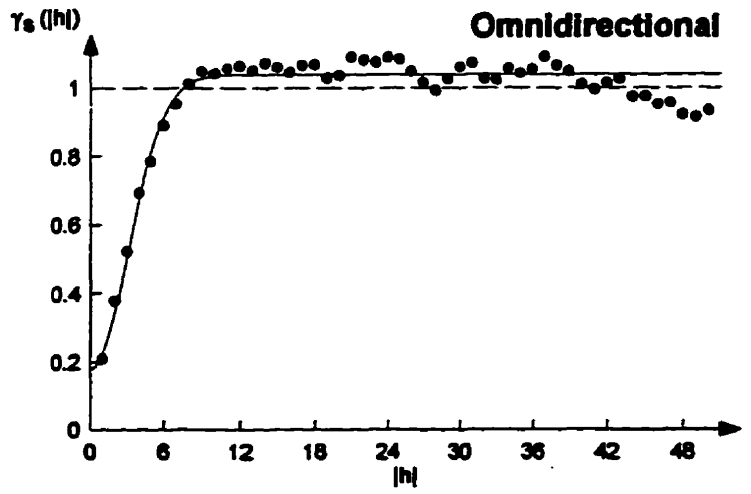

Figure C2. Omnidirectional variogram for FYI02.

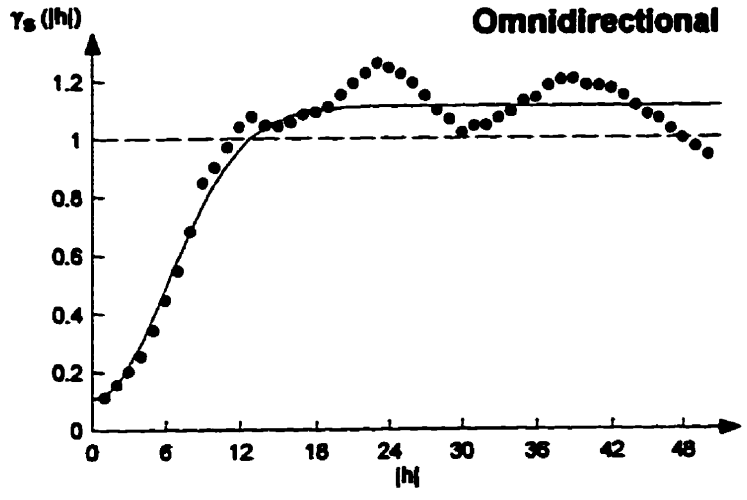

Figure C3. Omnidirectional variogram for FYI03.

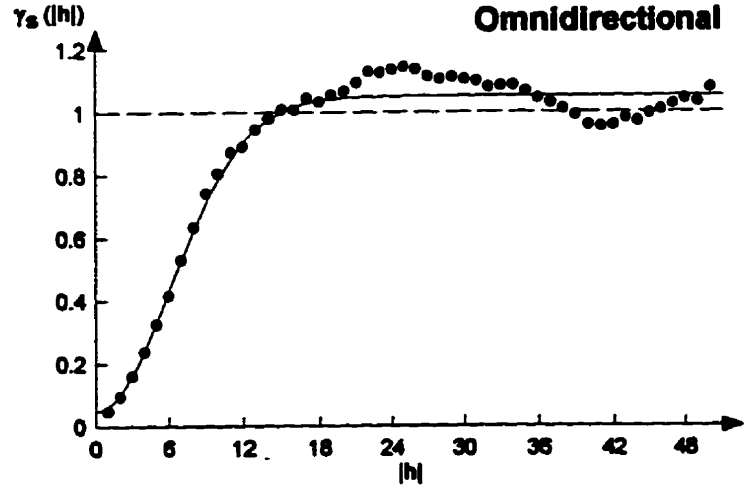

Figure C4. Omnidirectional variogram for FYI04.

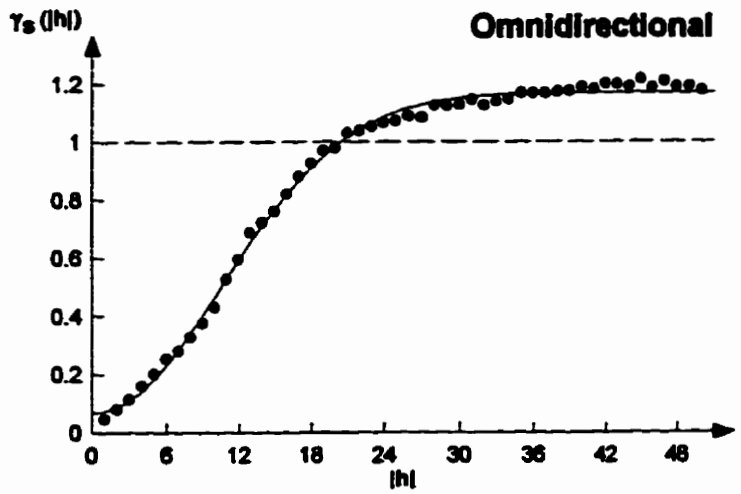

Figure C5. Omnidirectional variogram for FYI05.

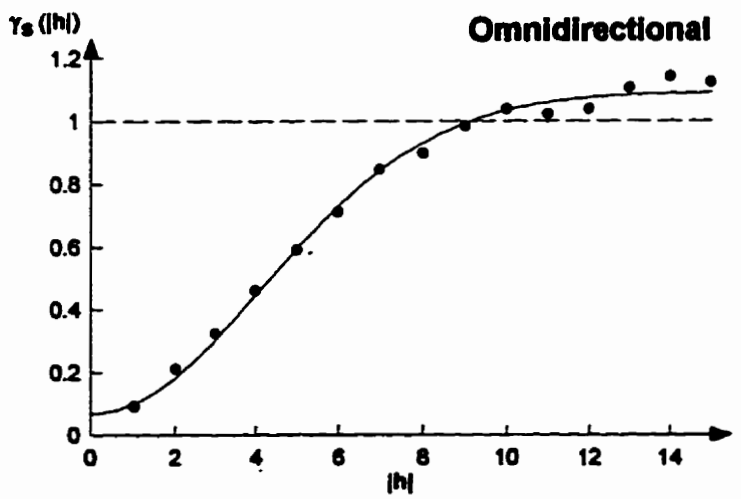

Figure C6. Omnidirectional variogram for SFYI01.

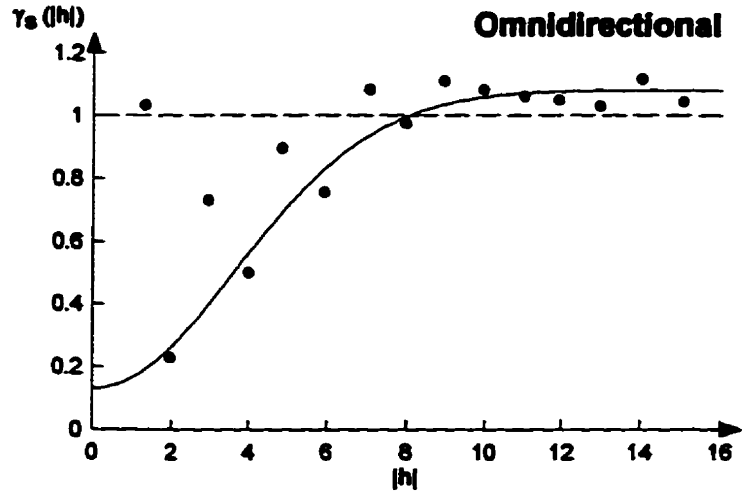

Figure C7. Omnidirectional variogram for SFYI02.

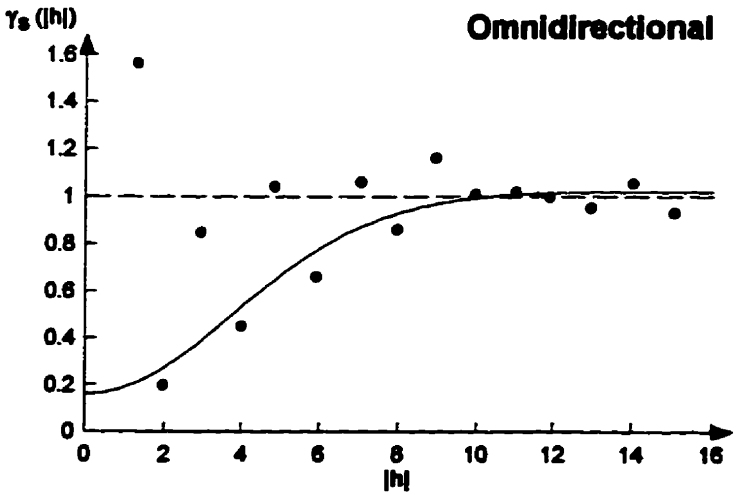

Figure C8. Omnidirectional variogram for SFYI03.

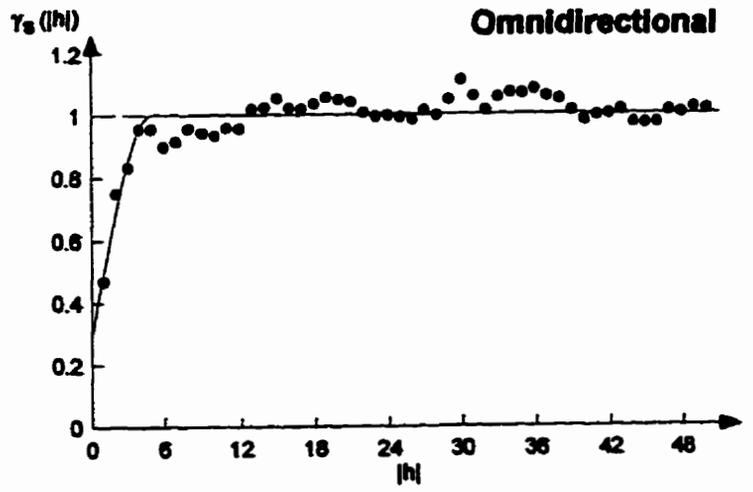

Figure C9. Omnidirectional variogram for MYI01.

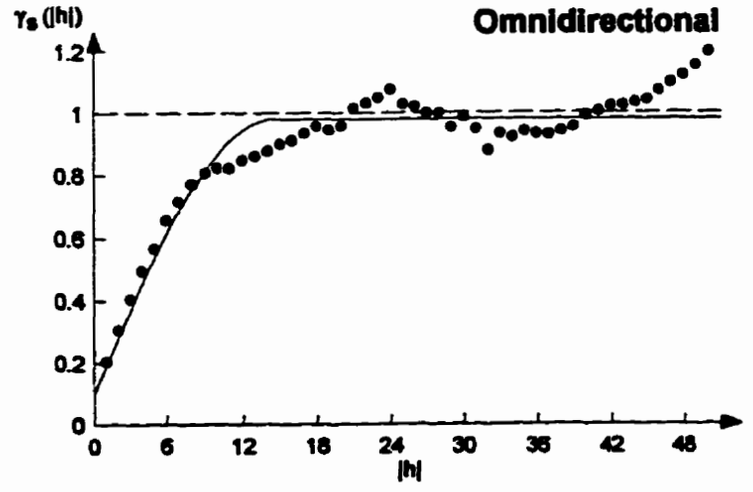

Figure C10. Omnidirectional variogram for MYI02.

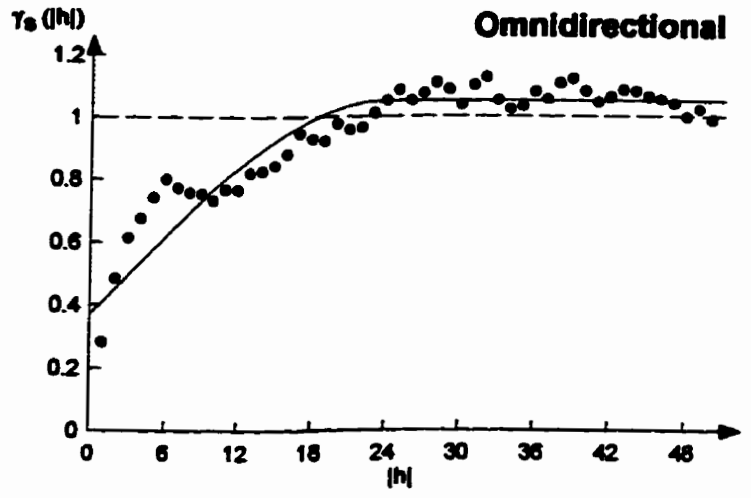

Figure C11. Omnidirectional variogram for MYI03.

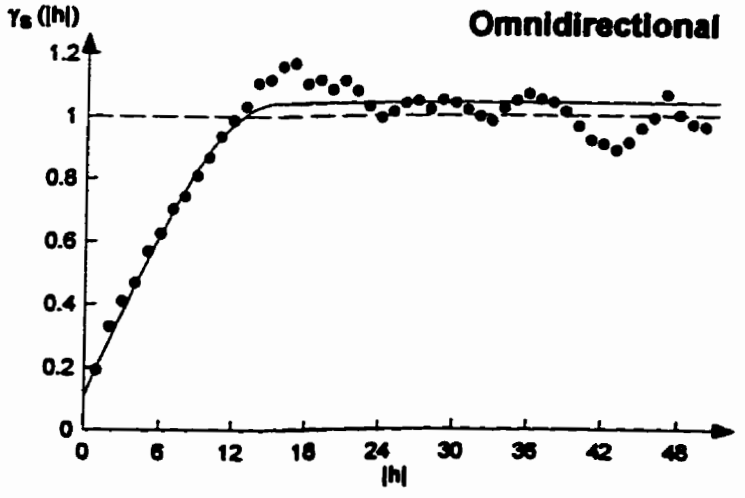

Figure C12. Omnidirectional variogram for MYI04.

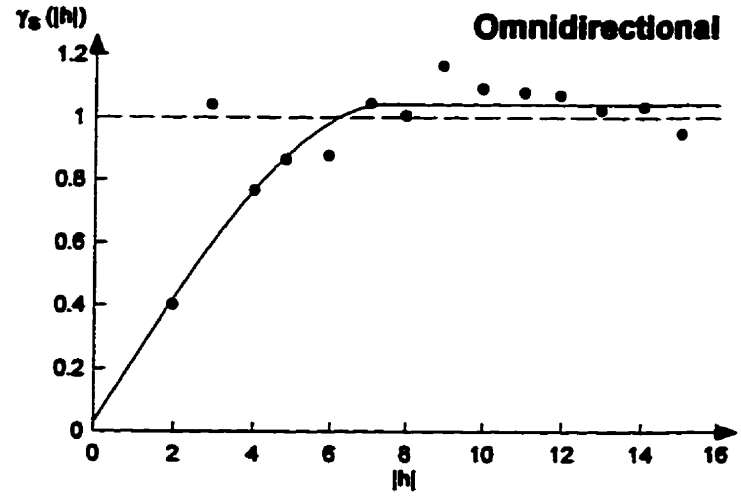

Figure C13. Omnidirectional variogram for SMYI01.

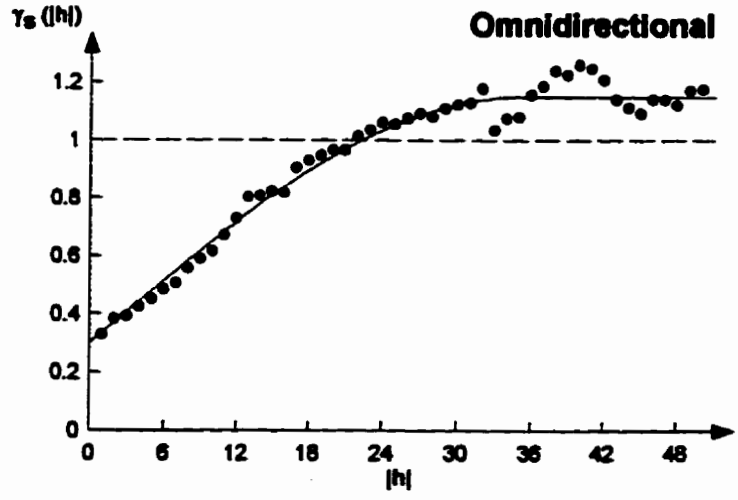

Figure C14. Omnidirectional variogram for RI01.

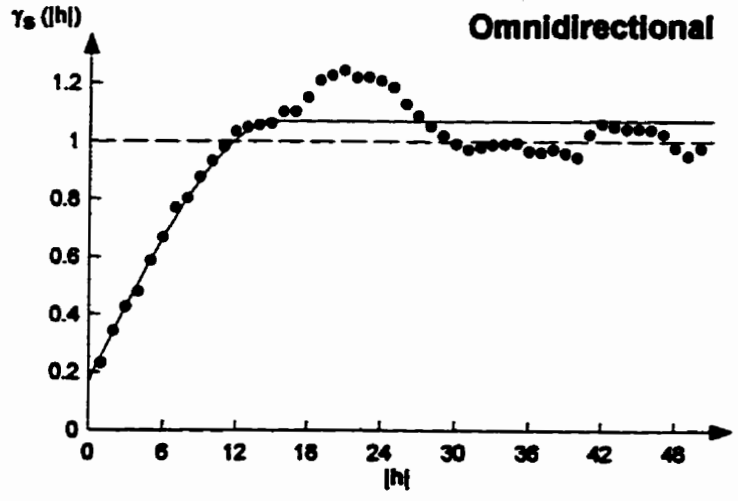

Figure C15. Omnidirectional variogram for RI02.

APPENDIX D:

DIRECTIONAL VARIOGRAMS

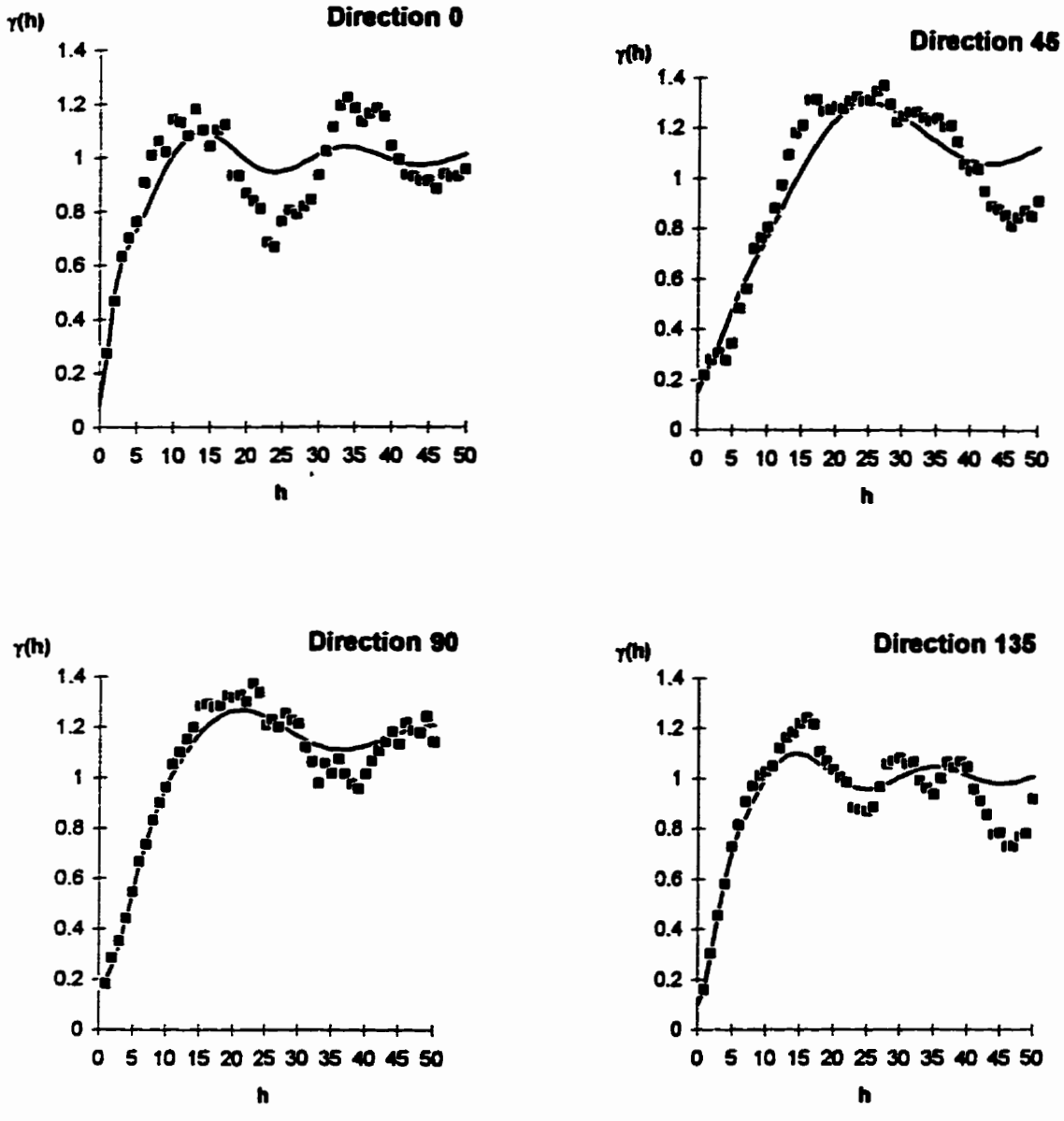

Figure D1. Directional variograms for FYI01.

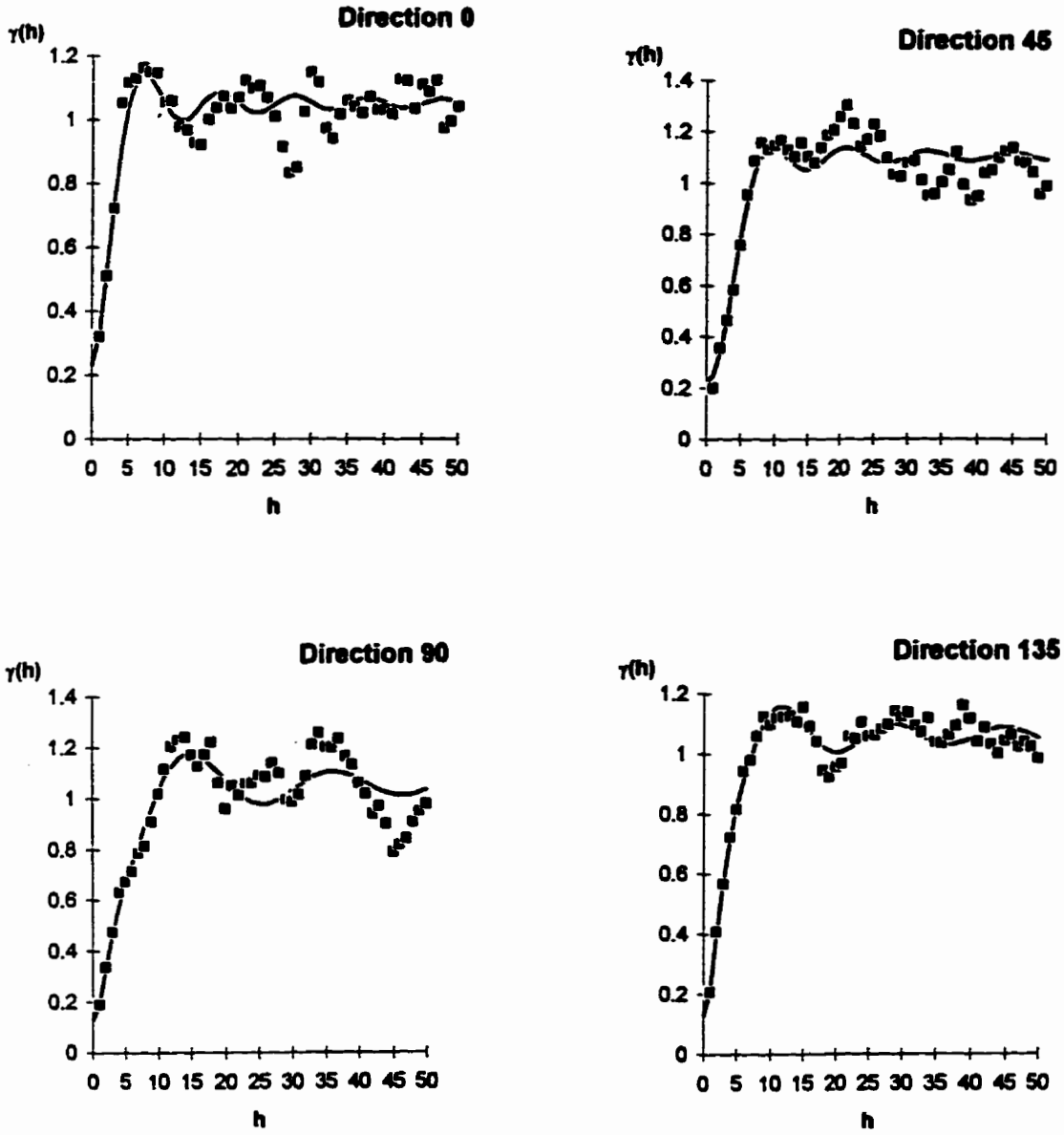

Figure D2. Directional variograms for FYI02.

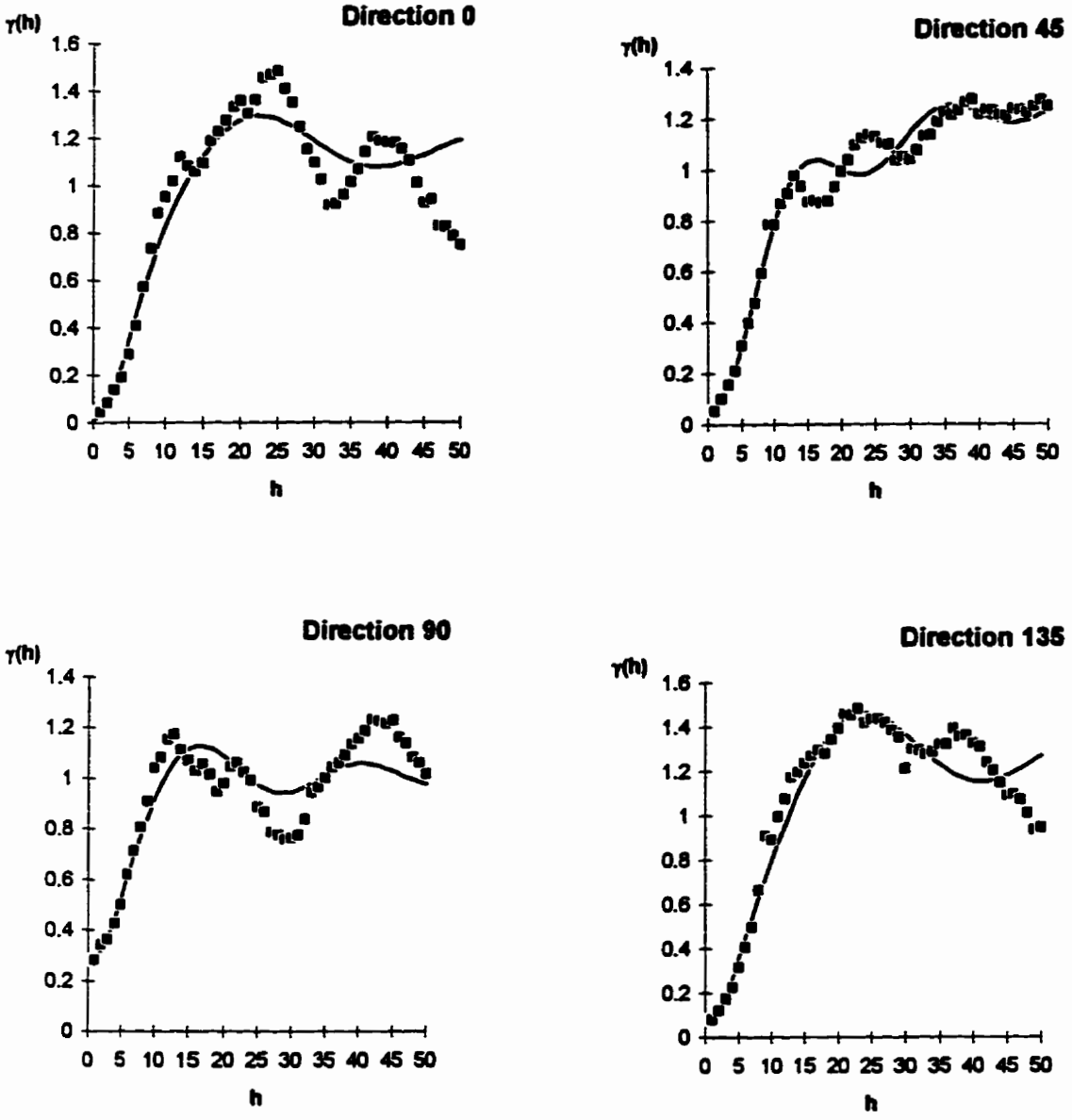

Figure D3. Directional variograms for FYI03.

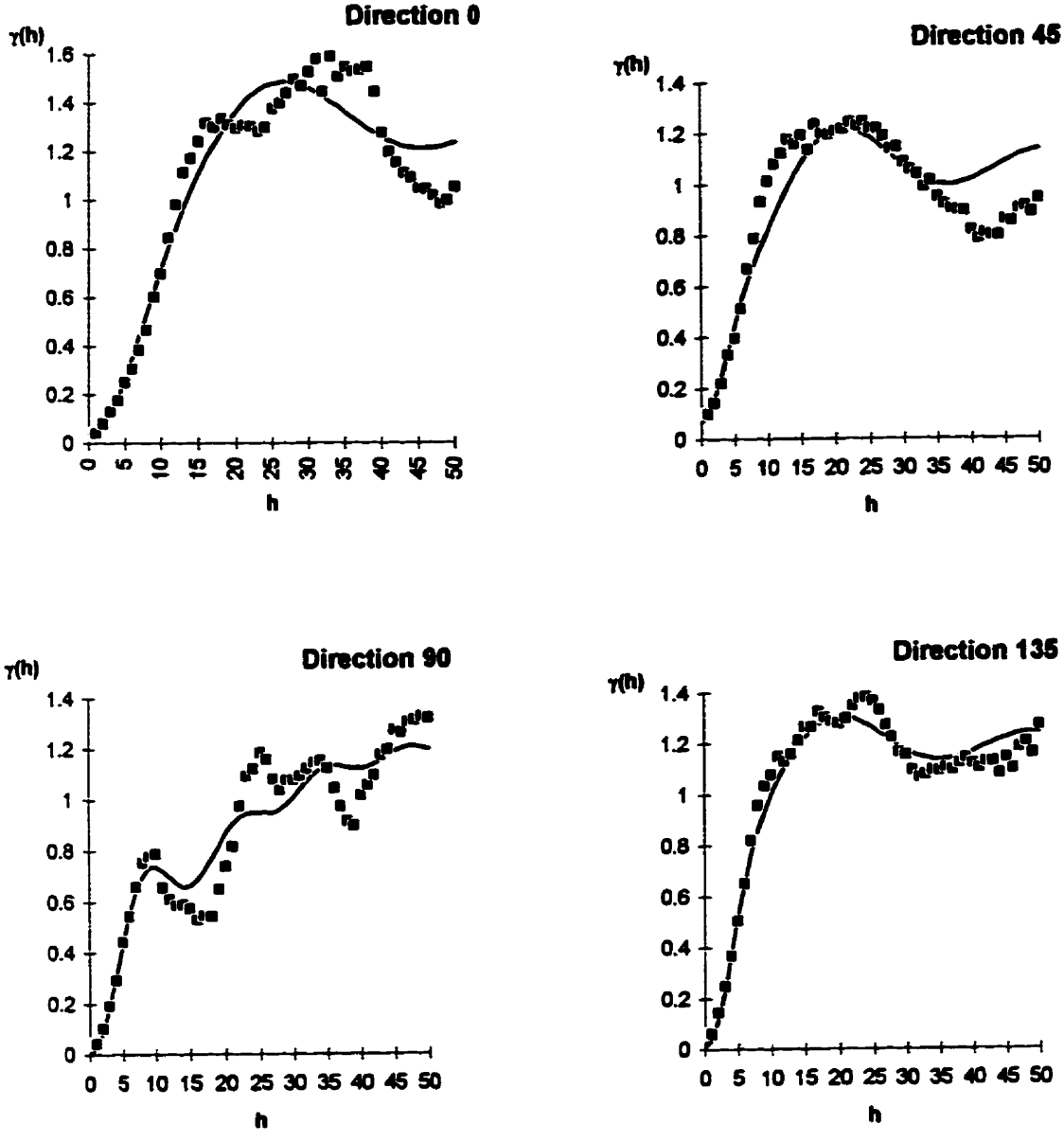

Figure D4. Directional variograms for FYI04.

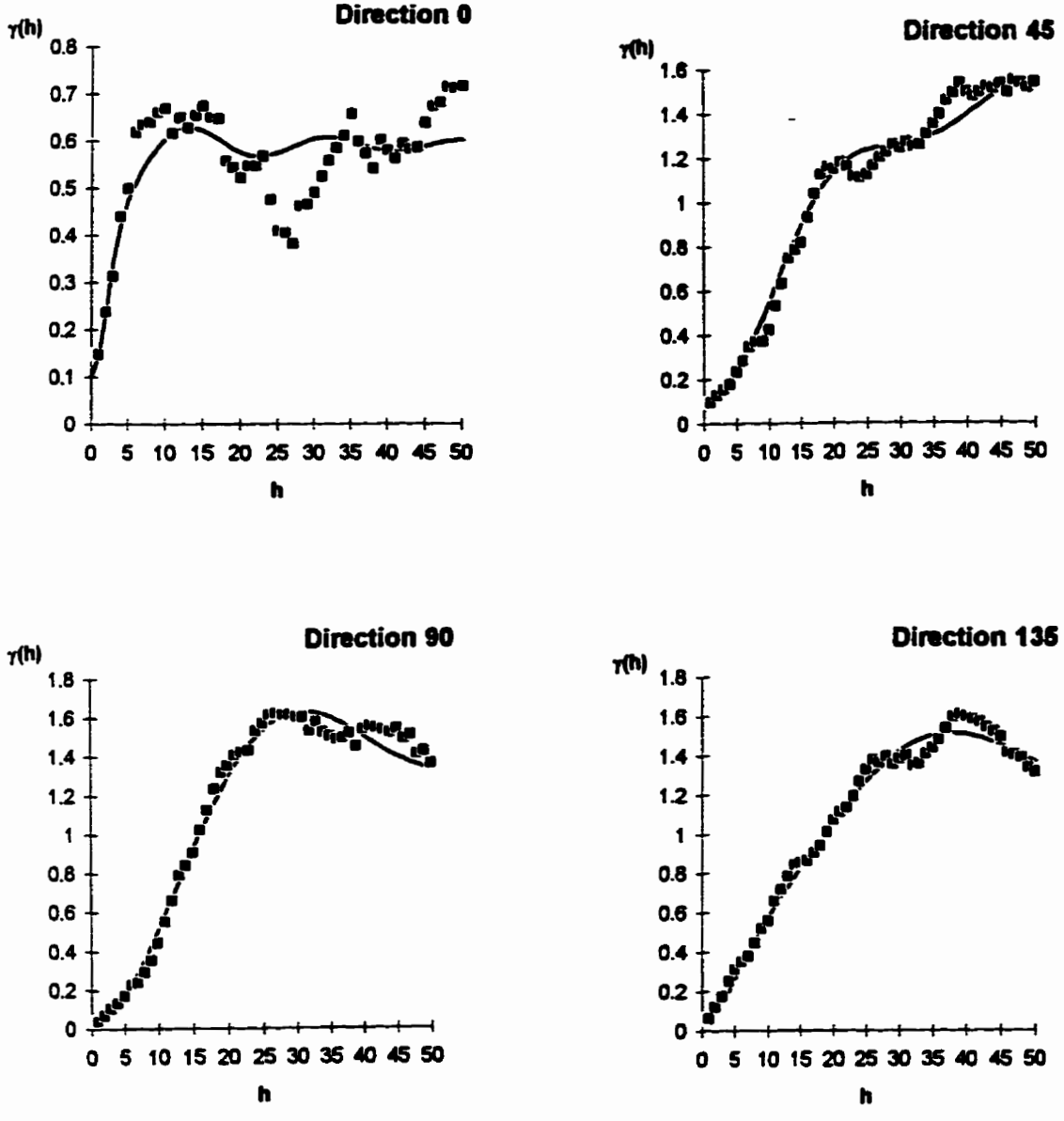

Figure D5. Directional variograms for FY105.

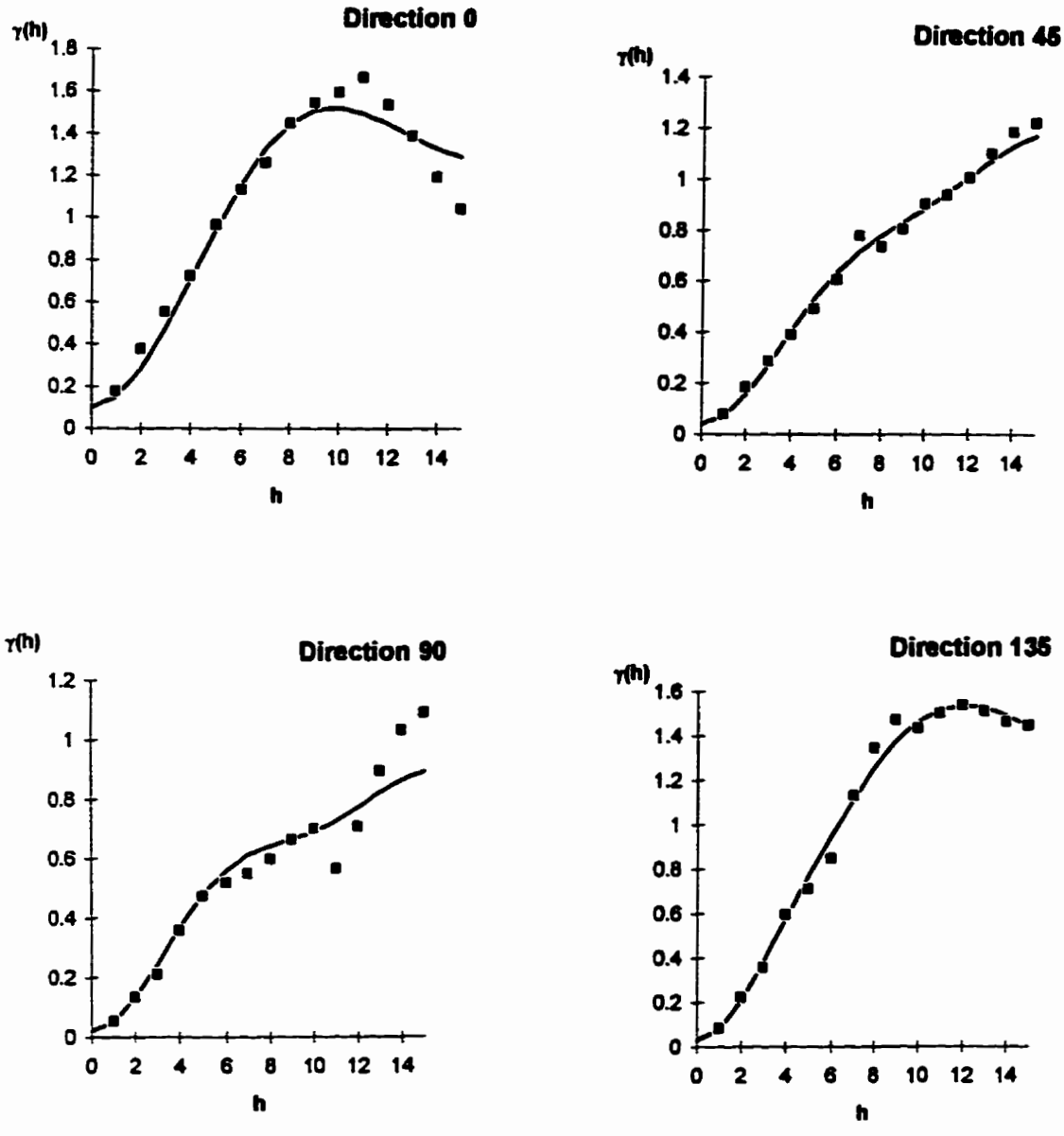

Figure D6. Directional variograms for SFYI01.

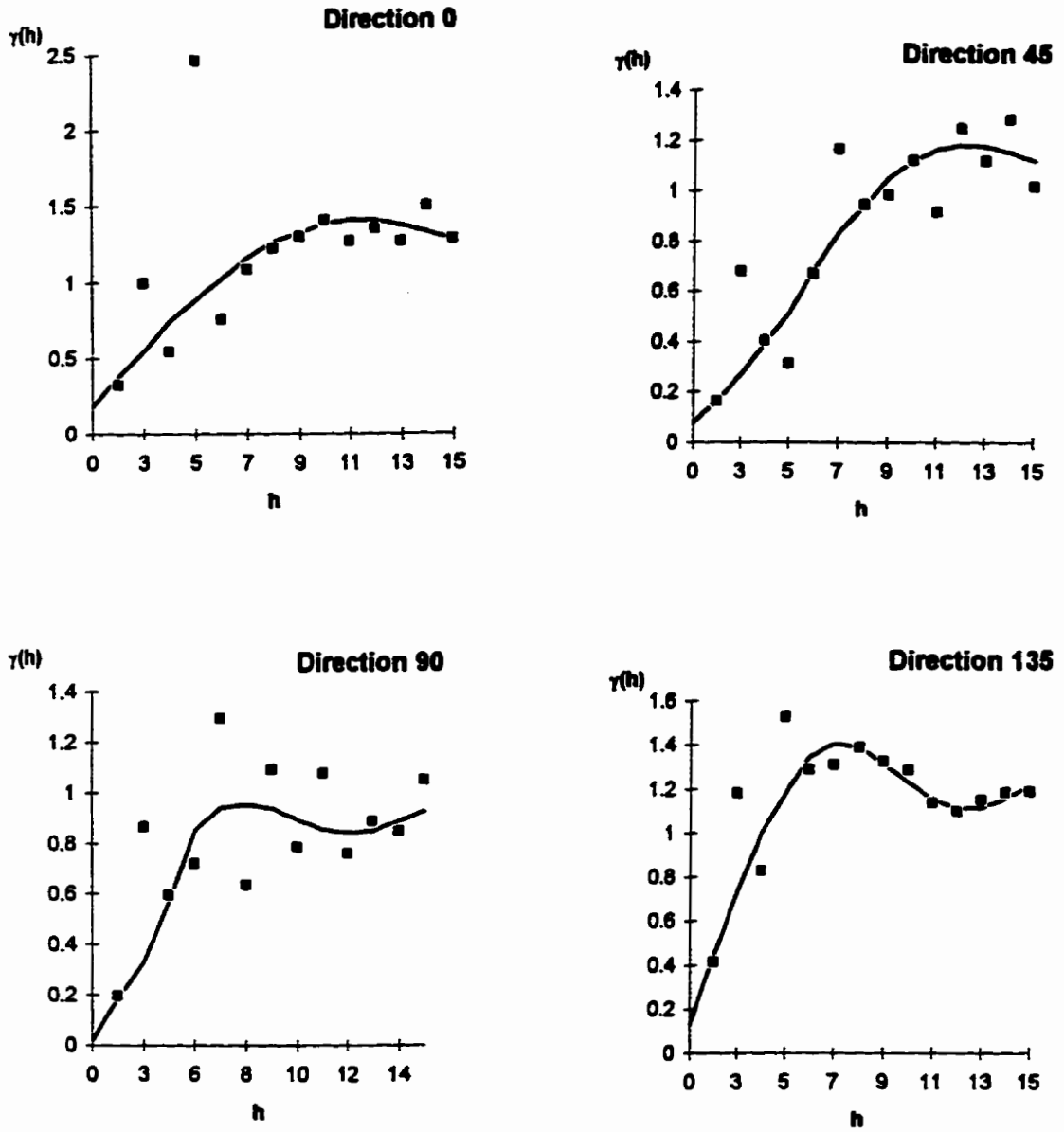

Figure D7. Directional variograms for SFYI02.

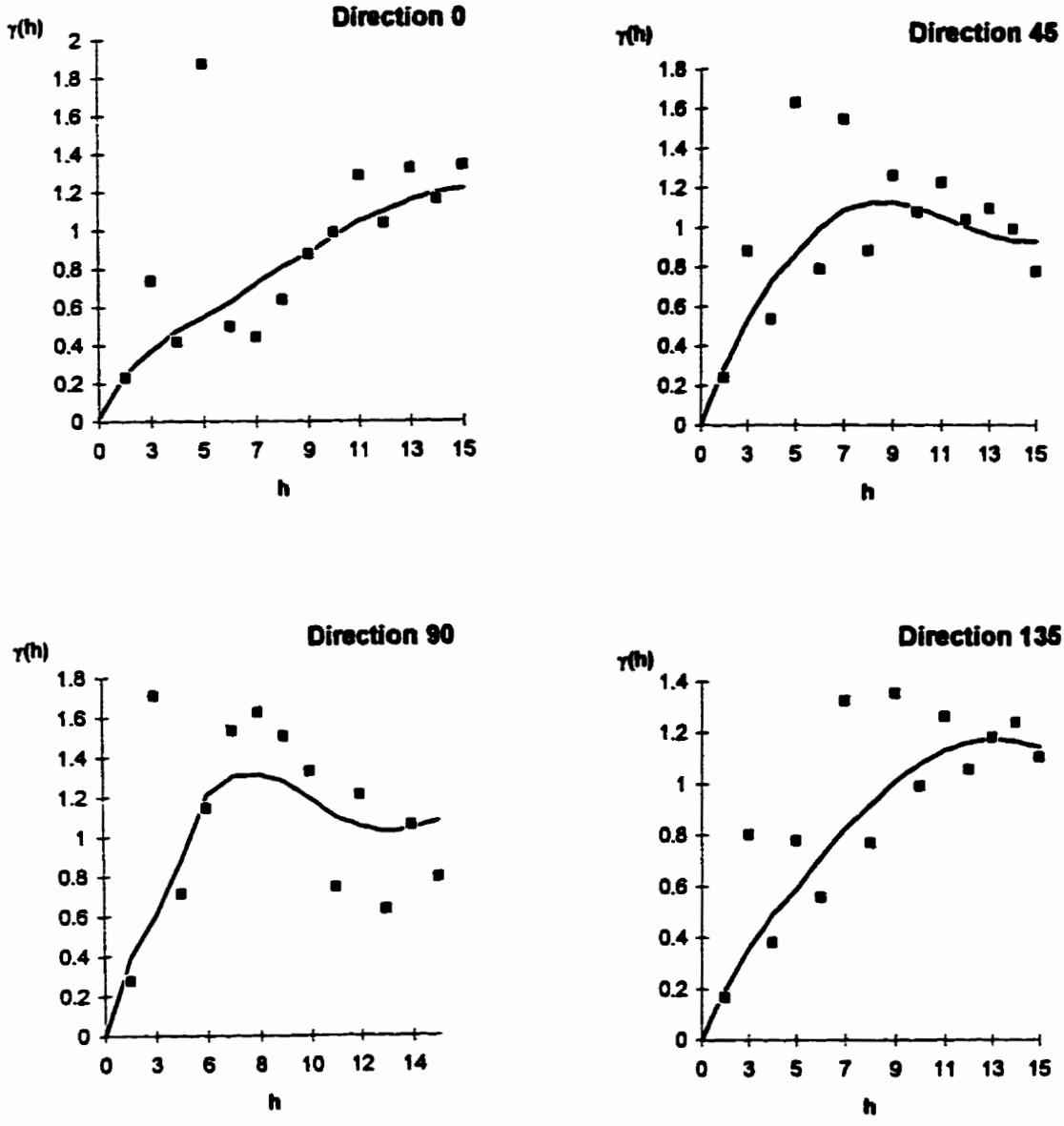

Figure D8. Directional variograms for SFYI03.

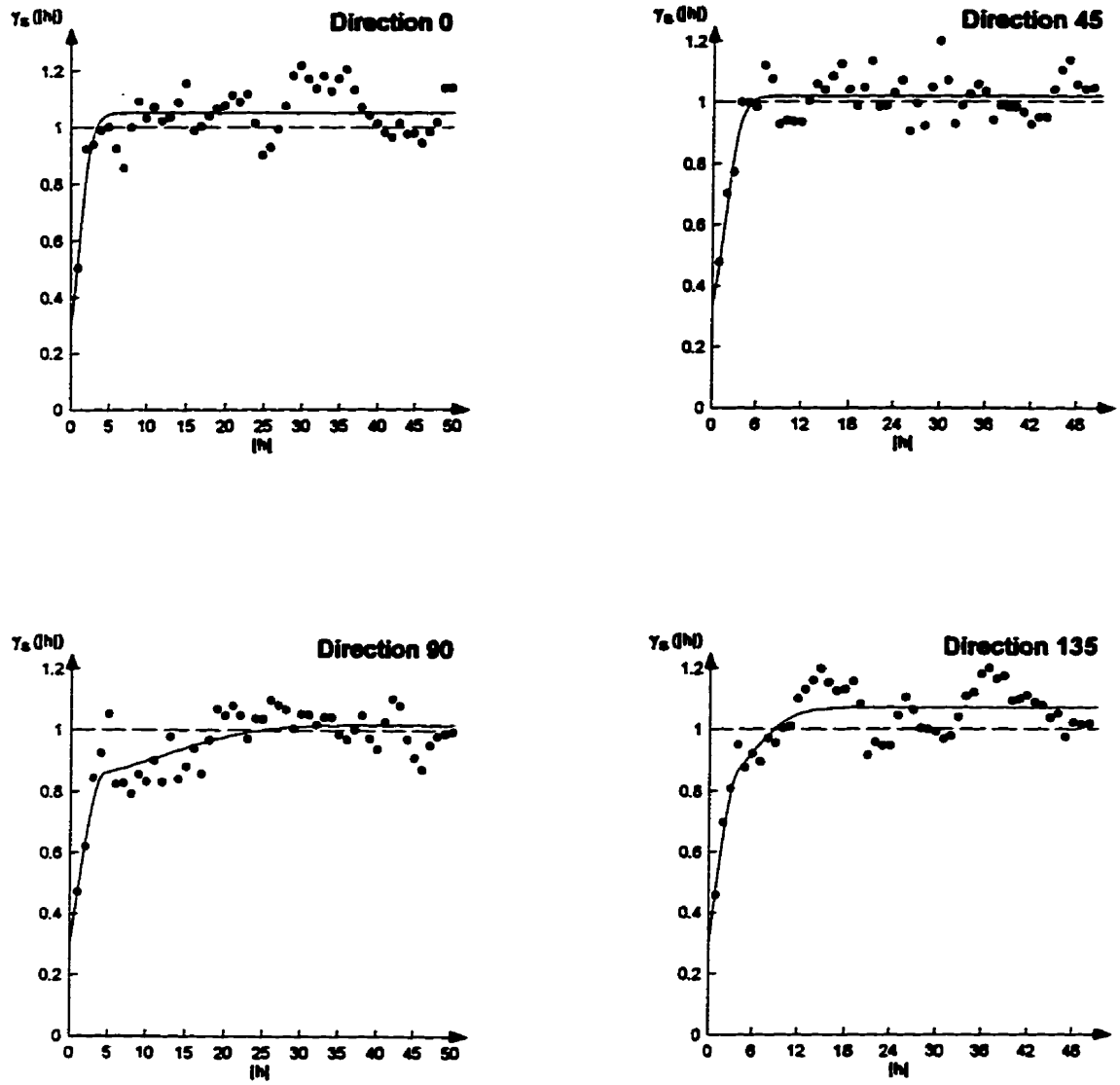

Figure D9. Directional variograms for MYI01.

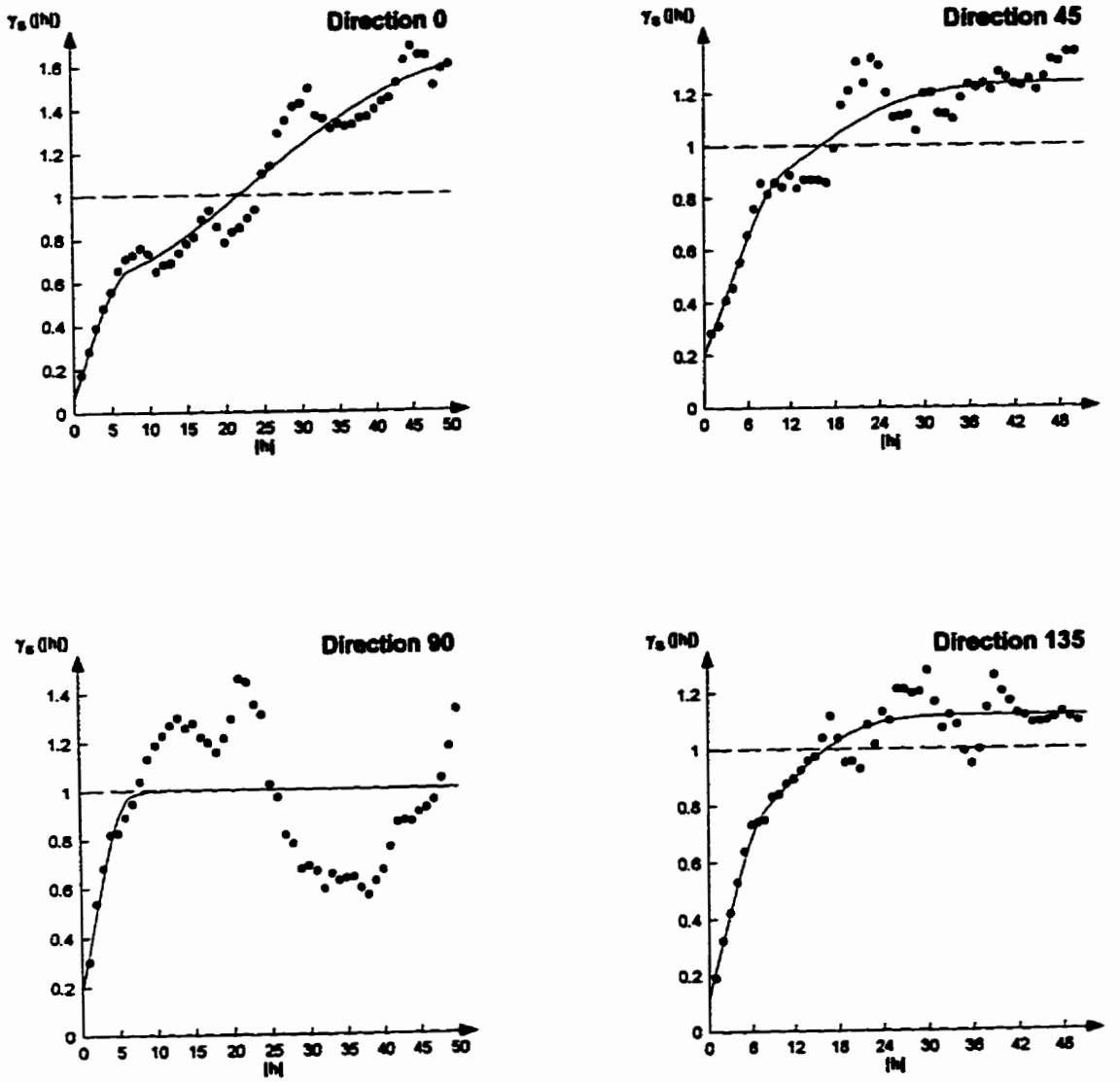

Figure D10. Directional variograms for MYI02.

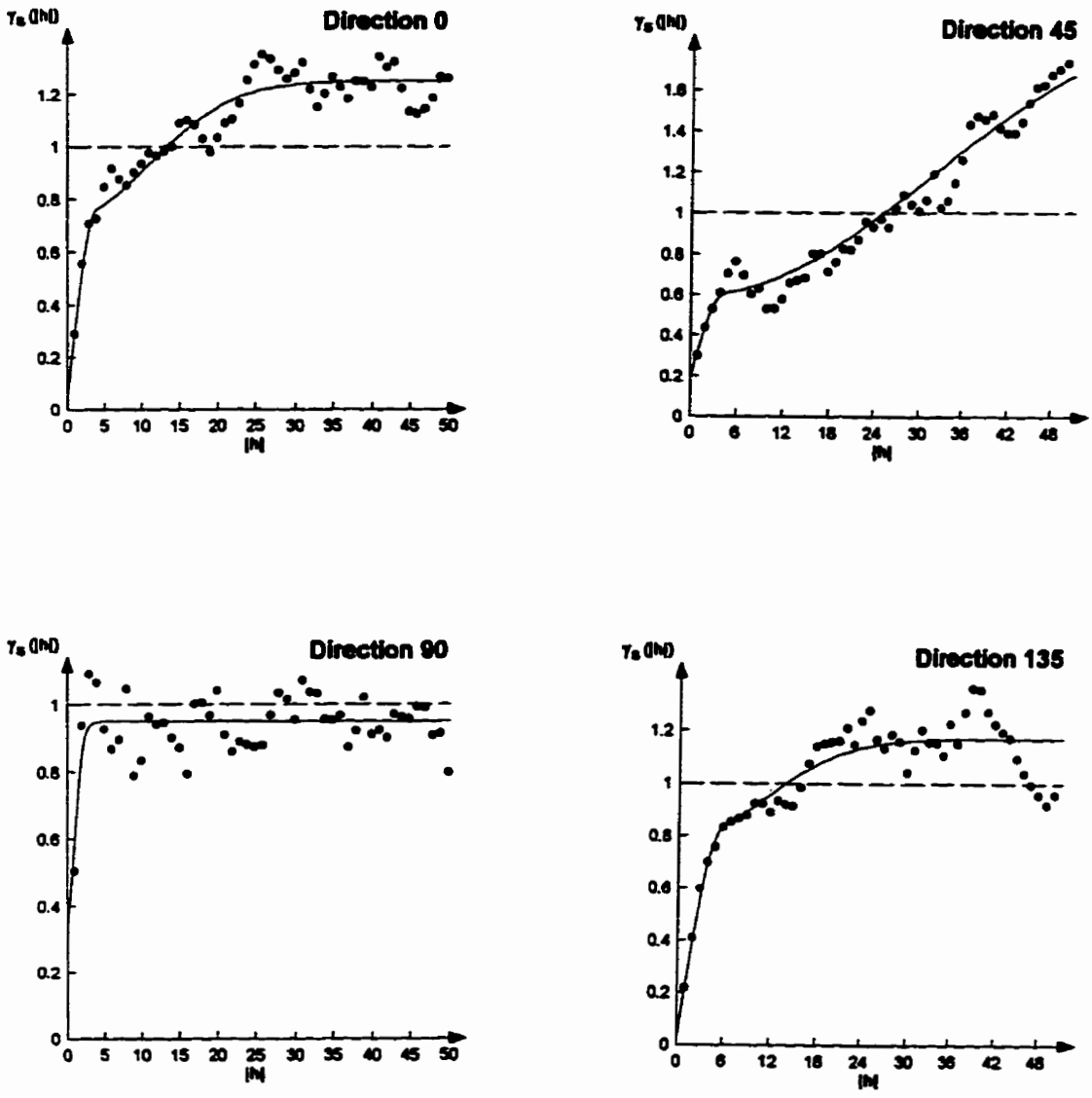

Figure D11. Directional variograms for MYI03.

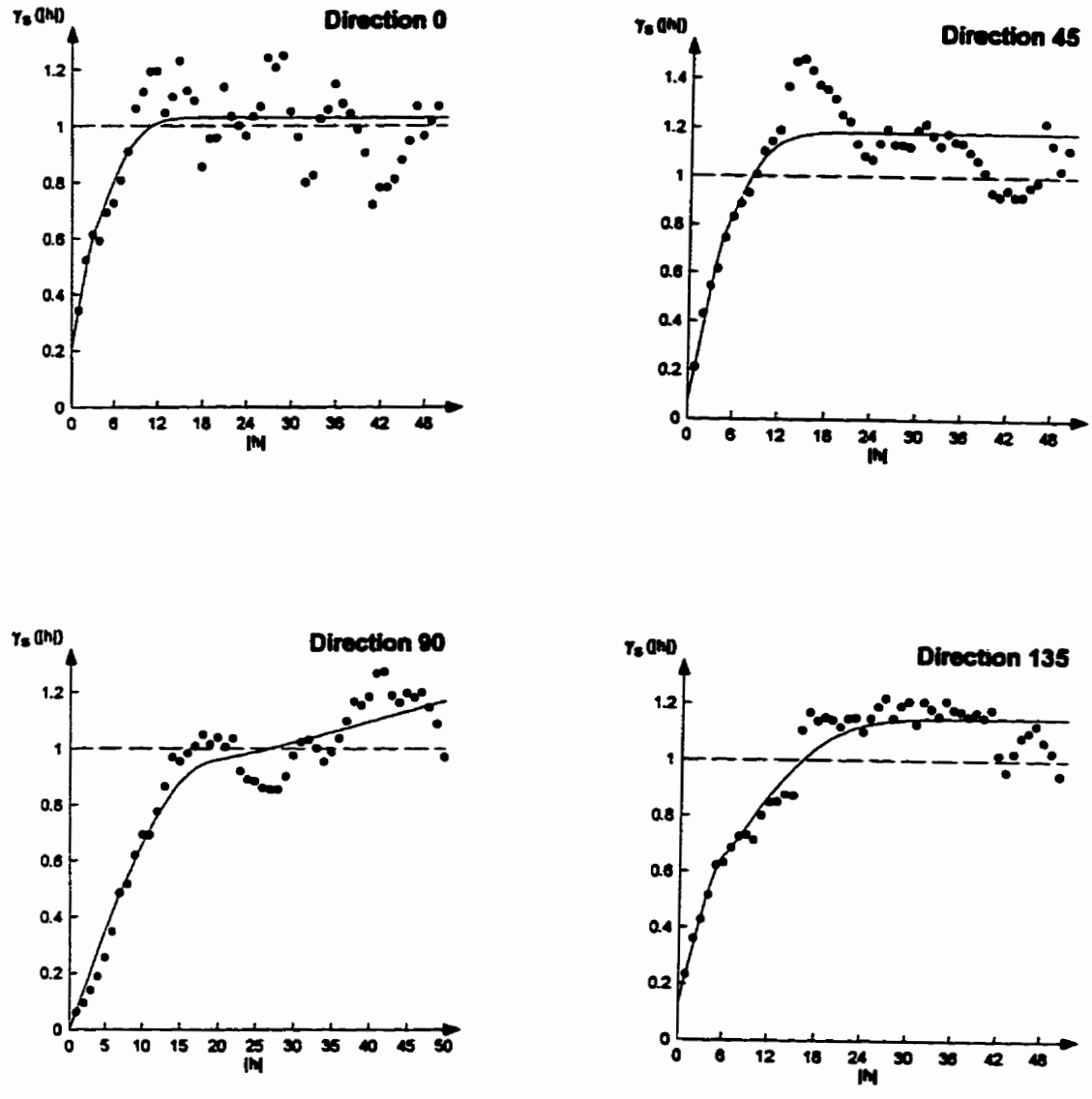

Figure D12. Directional variograms for MYI04.

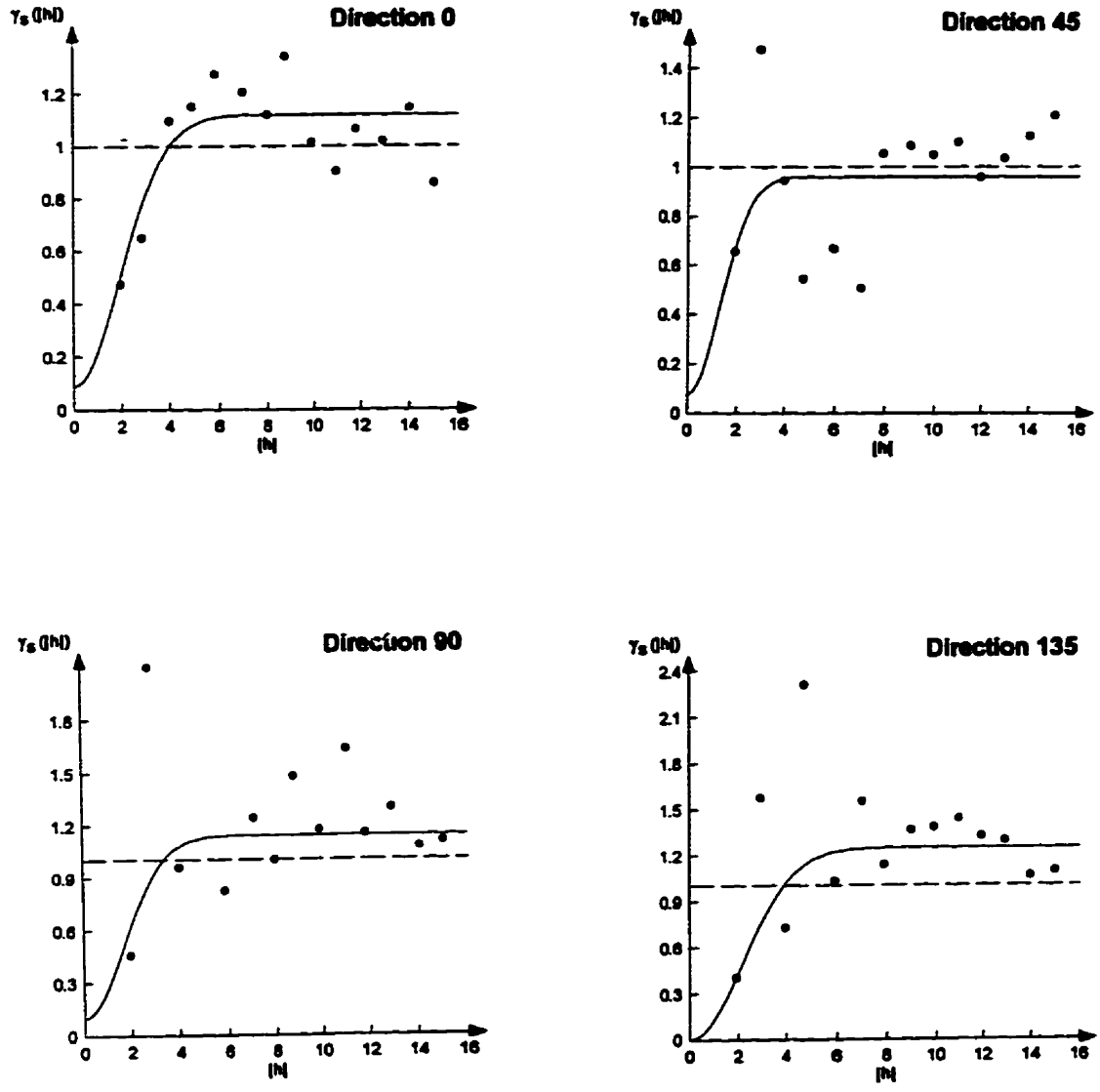

Figure D13. Directional variograms for SMYI01.

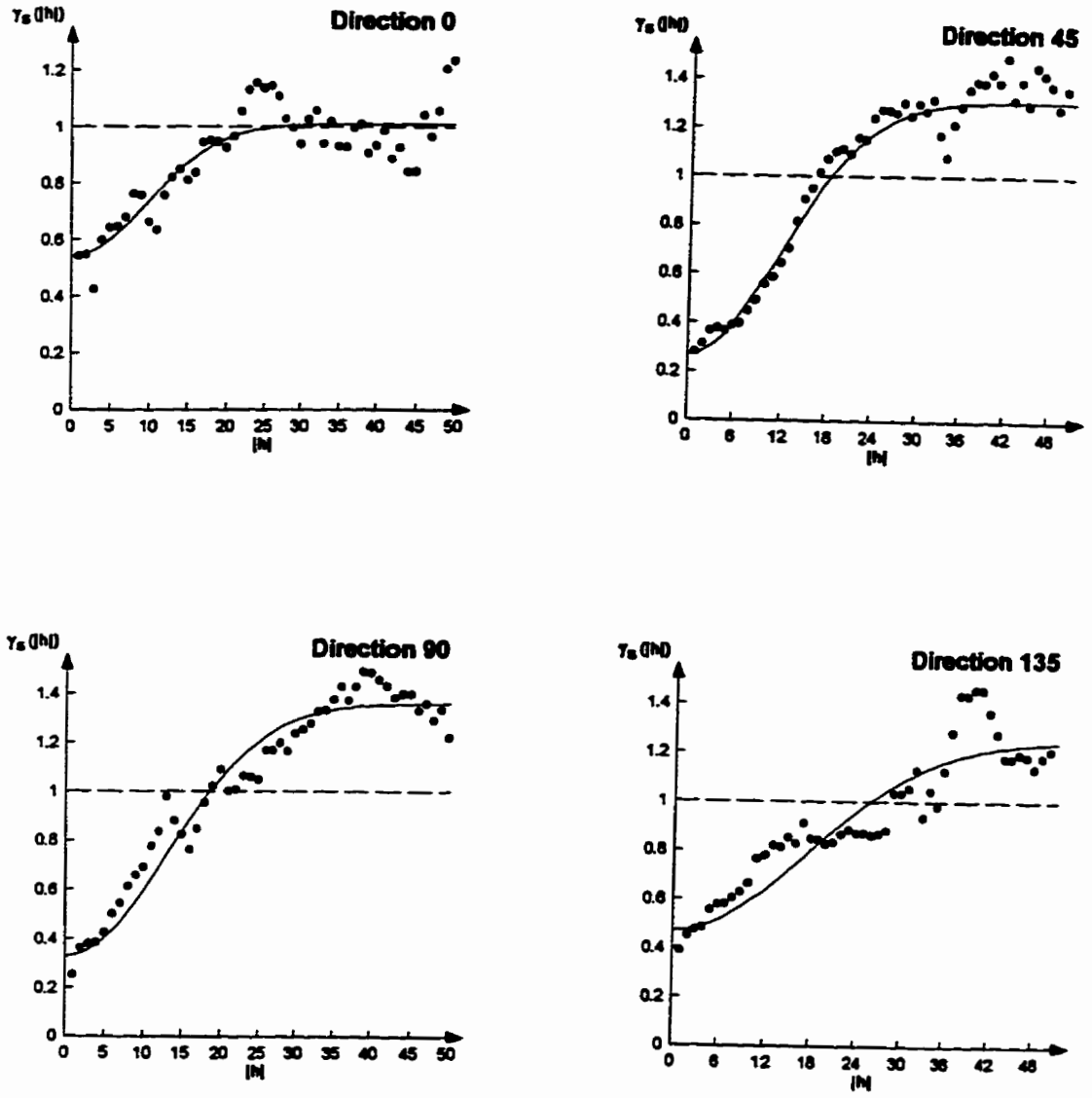

Figure D14. Directional variograms for RI01.

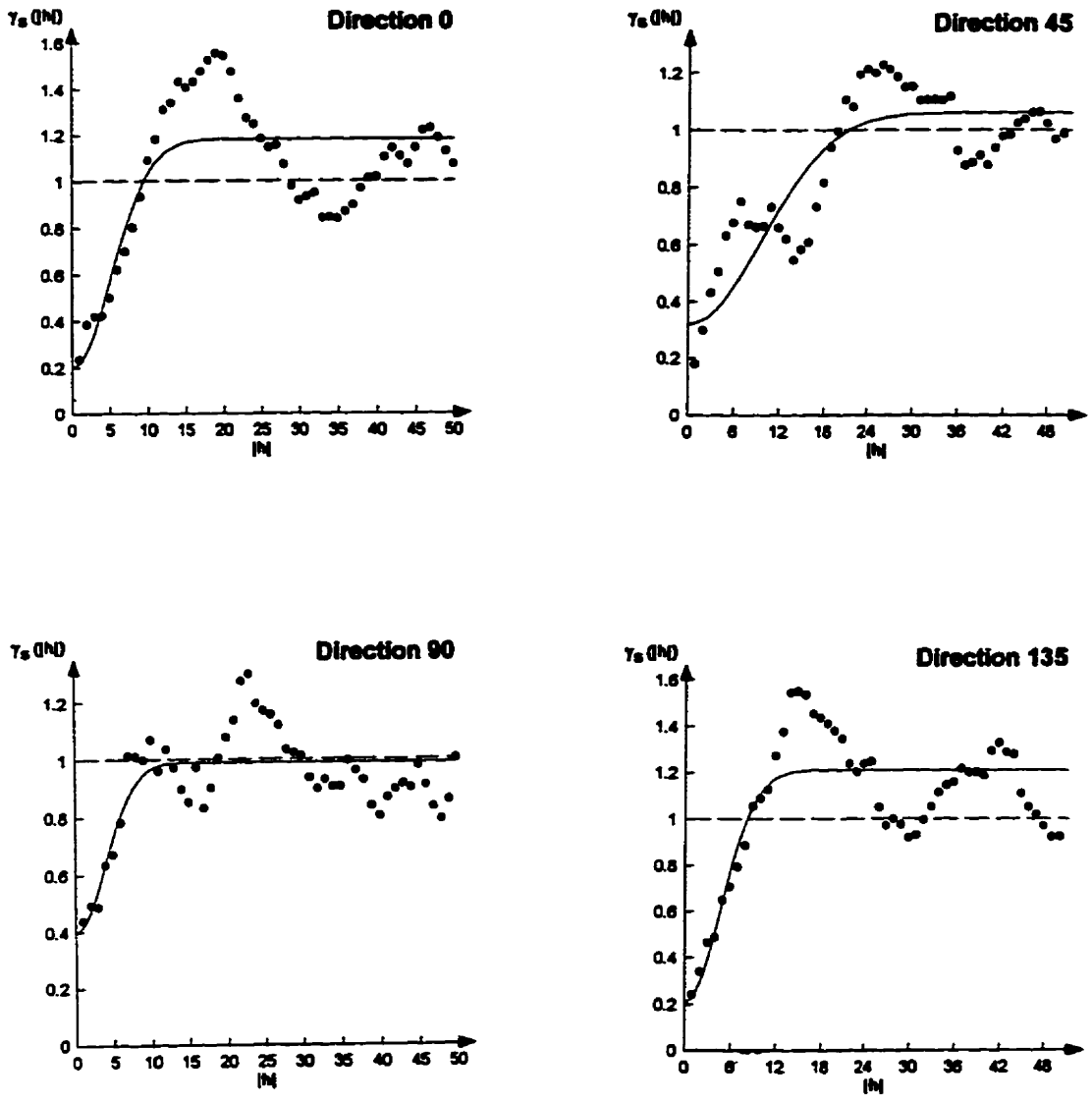

Figure D15. Directional variograms for RI02.

APPENDIX E:

GLCM STATISTICS AND CONTINGENCY TABLES

Table E1. GLCM statistics for 30 first-year sea ice training sites.

	01 FYI	02 FYI	03 FYI	04 FYI	05 FYI	06 FYI
Unif.	0.12	0.17	0.14	0.15	0.13	0.11
Corr.	0.13	0.14	0.08	-0.05	-0.02	0.13
Entro.	1.00	0.88	0.92	0.91	0.97	1.04
Diss.	1.08	0.79	0.91	0.96	1.90	1.17
Cont.	2.13	1.21	1.52	1.61	2.02	2.35
	07 FYI	08 FYI	09 FYI	10 FYI	11 FYI	12 FYI
Unif.	0.13	0.14	0.20	0.14	0.18	0.17
Corr.	0.01	0.22	0.11	0.30	0.91	0.07
Entro.	0.96	0.93	0.79	0.97	0.86	0.87
Diss.	1.08	0.89	0.66	0.99	0.87	0.83
Cont.	1.92	1.51	0.85	1.86	1.45	1.44
	13 FYI	14 FYI	15 FYI	16 FYI	17 FYI	18 FYI
Unif.	0.17	0.13	0.15	0.15	0.14	0.15
Corr.	0.06	-0.01	0.08	0.14	0.19	0.05
Entro.	0.85	0.97	0.92	0.91	0.96	0.91
Diss.	0.78	1.08	0.99	0.88	1.05	0.93
Cont.	1.13	2.05	1.65	1.35	1.94	1.61
	19 FYI	20 FYI	21 FYI	22 FYI	23 FYI	24 FYI
Unif.	0.15	0.13	0.12	0.12	0.12	0.12
Corr.	0.22	0.03	0.01	-0.01	0.07	0.09
Entro.	0.94	0.97	0.99	0.99	0.98	1.00
Diss.	1.00	1.11	1.10	1.14	1.01	1.02
Cont.	2.16	2.11	2.16	2.24	1.90	1.88
	25 FYI	26 FYI	27 FYI	28 FYI	29 FYI	30 FYI
Unif.	0.12	0.14	0.16	0.16	0.17	0.13
Corr.	-0.08	0.06	0.01	0.06	0.07	-0.02
Entro.	0.98	0.95	0.90	0.89	0.85	0.97
Diss.	1.13	0.96	0.94	0.90	0.80	1.09
Cont.	2.10	1.72	1.83	1.54	1.16	1.98

Table E2. GLCM statistics for the 30 multiyear sea ice training sites.

	01 MYI	02 MYI	03 MYI	04 MYI	05 MYI	06 MYI
Unif.	0.13	0.11	0.13	0.12	0.13	0.12
Corr.	0.13	-0.02	0.03	0.06	0.14	0.09
Entro.	0.95	1.02	0.97	0.99	0.97	1.01
Diss.	0.94	1.18	1.00	1.11	1.00	1.10
Cont.	1.63	2.40	1.77	2.06	1.80	2.03
	07 MYI	08 MYI	09 MYI	10 MYI	11 MYI	12 MYI
Unif.	0.14	0.12	0.10	0.13	0.13	0.14
Corr.	0.14	0.01	0.06	0.04	0.08	0.04
Entro.	0.96	0.98	1.04	0.95	0.97	0.94
Diss.	0.92	1.12	1.16	1.02	0.99	1.02
Cont.	0.54	2.08	2.28	1.85	1.78	1.80
	13 MYI	14 MYI	15 MYI	16 MYI	17 MYI	18 MYI
Unif.	0.13	0.13	0.12	0.13	0.11	0.11
Corr.	0.05	0.7	-0.03	0.20	0.19	0.10
Entro.	0.94	0.96	0.98	0.98	1.04	1.04
Diss.	0.99	0.99	1.15	0.93	1.07	1.25
Cont.	1.67	1.73	2.10	1.67	2.05	2.59
	19 MYI	20 MYI	21 MYI	22 MYI	23 MYI	24 MYI
Unif.	0.13	0.12	0.11	0.13	0.12	0.11
Corr.	0.05	-0.01	0.15	0.07	-0.04	0.05
Entro.	0.97	1.00	1.03	0.98	0.99	1.01
Diss.	1.02	1.13	1.11	0.96	1.17	1.12
Cont.	1.83	2.08	2.14	1.72	2.19	2.06
	25 MYI	26 MYI	27 MYI	28 MYI	29 MYI	30 MYI
Unif.	0.11	0.13	0.13	0.10	0.11	0.12
Corr.	0.18	0.07	0.08	0.10	-0.03	0.17
Entro.	1.04	0.97	0.96	1.06	1.01	1.00
Diss.	1.16	1.03	0.97	1.25	1.13	1.00
Cont.	2.45	1.76	1.67	2.77	2.12	1.93

Table E3. GLCM statistics for the 30 rubble sea ice training sites.

	01 RI	02 RI	03 RI	04 RI	05 RI	06 RI
Unif.	0.09	0.09	0.10	0.09	0.09	0.08
Corr.	0.37	0.24	0.27	0.25	0.08	0.30
Entro.	1.10	1.10	1.08	1.11	1.12	1.13
Diss.	1.26	1.39	1.29	1.62	1.54	1.38
Cont.	2.78	3.20	3.19	4.58	4.06	3.10
	07 RI	08 RI	09 RI	10 RI	11 RI	12 RI
Unif.	0.11	0.11	0.15	0.10	0.11	0.11
Corr.	0.21	0.16	0.12	0.10	0.17	0.02
Entro.	1.05	1.03	0.90	1.08	1.02	1.02
Diss.	1.24	1.20	0.92	1.33	1.13	1.19
Cont.	2.69	2.60	1.47	3.02	2.12	2.34
	13 RI	14 RI	15 RI	16 RI	17 RI	18 RI
Unif.	0.10	0.11	0.10	0.10	0.11	0.09
Corr.	0.17	0.12	0.17	0.06	0.13	0.21
Entro.	1.06	1.02	1.05	1.06	1.04	1.11
Diss.	1.18	1.11	1.20	1.34	1.18	1.33
Cont.	2.26	2.19	2.69	3.18	2.38	2.93
	19 RI	20 RI	21 RI	22 RI	23 RI	24 RI
Unif.	0.10	0.12	0.12	0.11	0.10	0.08
Corr.	0.17	0.09	0.22	0.09	0.16	0.11
Entro.	1.08	1.00	1.02	1.03	1.07	1.13
Diss.	1.27	1.09	1.05	1.17	1.26	1.46
Cont.	2.91	2.07	2.11	2.36	2.73	3.45
	25 RI	26 RI	27 RI	28 RI	29 RI	30 RI
Unif.	0.11	0.11	0.09	0.10	0.11	0.09
Corr.	0.08	0.12	0.15	0.30	0.11	0.22
Entro.	1.02	1.03	1.10	1.08	1.03	1.10
Diss.	1.17	1.11	1.41	1.24	1.15	1.21
Cont.	2.25	2.18	3.28	2.84	2.24	2.44

Table E4. Contingency tables for all GLCM statistic combinations.

Unif.

	FYI	MYI	RI	
FYI	17	12	1	30
MYI	2	19	9	30
RI	1	2	27	30
	20	33	37	53%

Corr.

	FYI	MYI	RI	
FYI	4	19	7	30
MYI	4	19	7	30
RI	9	4	17	30
	17	42	31	44%

Entro.

	FYI	MYI	RI	
FYI	18	11	1	30
MYI	7	17	6	30
RI	1	6	23	30
	26	34	30	64%

Diss.

	FYI	MYI	RI	
FYI	19	9	2	30
MYI	15	9	6	30
RI	1	6	23	30
	35	24	31	57%

Cont.

	FYI	MYI	RI	
FYI	16	14	0	30
MYI	14	12	4	30
RI	1	9	20	30
	31	35	24	53%

Unif., Entro.

	FYI	MYI	RI	
FYI	2	28	0	30
MYI	0	30	0	30
RI	0	28	2	30
	2	86	2	38%

Unif., Diss.

	FYI	MYI	RI	
FYI	6	23	1	30
MYI	0	30	0	30
RI	0	22	8	30
	6	75	9	49%

Unif., Corr.

	FYI	MYI	RI	
FYI	16	12	2	30
MYI	8	21	1	30
RI	0	20	10	30
	24	53	13	52%

Unif., Cont.

	FYI	MYI	RI	
FYI	6	24	0	30
MYI	0	29	1	30
RI	0	13	17	30
	6	66	18	58%

Entro., Diss.

	FYI	MYI	RI	
FYI	0	29	1	30
MYI	0	30	0	30
RI	0	30	0	30
	0	89	1	33%

Entro. Corr.

	FYI	MYI	RI	
FYI	5	15	10	30
MYI	1	19	10	30
RI	9	19	2	30
	15	53	22	29%

Entro., Cont.

	FYI	MYI	RI	
FYI	0	30	0	30
MYI	0	30	0	30
RI	0	28	2	30
	0	88	2	36%

Diss., Corr.

	FYI	MYI	RI	
FYI	7	13	10	30
MYI	2	20	8	30
RI	6	21	3	30
	15	54	21	33%

Diss., Cont.

	FYI	MYI	RI	
FYI	1	29	0	30
MYI	0	30	0	30
RI	0	29	1	30
	1	88	1	36%

Corr., Cont

	FYI	MYI	RI	
FYI	8	12	10	30
MYI	3	19	8	30
RI	4	19	7	30
	15	40	25	38%

Unif., Entro., Diss.

	FYI	MYI	RI	
FYI	22	7	1	30
MYI	1	23	6	30
RI	1	3	26	30
	24	33	33	79%

Unif., Entro., Corr.

	FYI	MYI	RI	
FYI	17	12	1	30
MYI	3	21	6	30
RI	1	4	25	30
	21	37	32	70%

Unif., Entro., Cont.

	FYI	MYI	RI	
FYI	20	10	0	30
MYI	1	25	4	30
RI	1	8	21	30
	22	43	25	73%

Unif., Diss., Corr.

	FYI	MYI	RI	
FYI	16	11	3	30
MYI	11	13	6	30
RI	1	8	21	30
	38	32	30	62%

Unif., Diss., Cont.

	FYI	MYI	RI	
FYI	17	12	1	30
MYI	11	14	5	30
RI	1	9	20	30
	29	35	26	57%

Unif., Corr., Cont.

	FYI	MYI	RI	
FYI	17	12	1	30
MYI	12	15	3	30
RI	1	9	20	30
	30	36	24	58%

Entro., Diss., Corr.

	FYI	MYI	RI	
FYI	6	19	5	30
MYI	7	20	3	30
RI	6	3	21	30
	19	42	29	52%

Entro. Cont., Diss.

	FYI	MYI	RI	
FYI	16	13	1	30
MYI	13	13	4	30
RI	1	12	17	30
	40	38	22	51%

Entro., Corr., Cont.

	FYI	MYI	RI	
FYI	15	13	2	30
MYI	13	14	3	30
RI	4	7	19	30
	32	34	24	53%

Diss., Corr., Cont

	FYI	MYI	RI	
FYI	15	14	1	30
MYI	10	17	3	30
RI	3	8	19	30
	28	39	23	57%

Unif., Entro., Diss., Cont.

	FYI	MYI	RI	
FYI	22	8	0	30
MYI	1	25	4	30
RI	1	9	20	30
	24	42	24	74%

Entro. Diss., Corr., Cont.

	FYI	MYI	RI	
FYI	12	16	2	30
MYI	8	19	3	30
RI	4	7	19	30
	24	42	24	56%

All Statistics

	FYI	MYI	RI	
FYI	22	7	1	30
MYI	1	26	3	30
RI	1	9	20	30
	24	42	24	76%

Unif., Entro., Diss., Corr.

	FYI	MYI	RI	
FYI	20	9	1	30
MYI	1	23	6	30
RI	1	6	23	30
	22	38	30	73%

Unif., Diss., Corr., Cont.

	FYI	MYI	RI	
FYI	17	12	1	30
MYI	11	16	3	30
RI	1	9	20	30
	29	37	24	59%

Unif., Entro., Corr., Cont.

	FYI	MYI	RI	
FYI	22	7	1	30
MYI	1	26	3	30
RI	1	9	20	30
	24	42	24	76%